Geocryology (Permafrost) Course at the University of Alaska Fairbanks

T.E. Osterkamp
Geophysical Institute, University of Alaska Fairbanks

Early years

Professor Ebb Rice developed a course on Arctic Engineering during the 1960s at the University of Alaska Fairbanks. This course was the inspiration for a series of courses in engineering and science dealing with snow, ice, and permafrost. A course on the physics of ice was developed by Professor T.E. Osterkamp in 1970 and taught during the early 1970s. This was followed by a series of separate special topics courses on snow, ice, and permafrost.

These special topics courses evolved into Physics 643 (Physical properties of snow, ice, and permafrost) taught in 1974, Physics 693 (Physical properties of sea ice) taught in 1975, and Physics 693 (Permafrost: Physical properties and processes) taught in 1976.

Eventually, these courses evolved into separate courses on snow and ice (Professor Benson), glaciers (Professor Harrison), sea ice (Professor Osterkamp), and permafrost (Professor Osterkamp). Professor Weeks took over the sea ice course when he came to the university in the mid-1980s. The permafrost course was taught for the second time in 1979 through the Department of Geology and Geophysics, and I taught it every other year since then until 1997, when I retired. Professor Romanovsky has taught the course since then using my course notes as a basis.

Nature of the course

From the beginning, the permafrost course was seen primarily as a materials science course about permafrost, its physical properties, and physical processes occurring within it. It was designed to provide students with the necessary scientific background to understand and study permafrost. Materials science courses bring together a number of disciplines (physics, chemistry, geophysics, geology, engineering) to study a single material. A relatively large amount of background information had to be provided because there was an unusual diversity of student preparation and because the selected topics were often not covered in previous courses.

The course was designed for science and engineering students at the advanced undergraduate and beginning graduate student level and for research personnel with specialties in other areas. Minimum preparation for the course included mathematics at the level of ordinary differential equations and at least senior standing in the sciences or engineering. Topics included soil physics, especially thermodynamics; thermal, electrical, and mechanical properties; and heat and mass flow processes, particularly those related to freezing and thawing. Solved problems and applications from the fields of engineering, mining, geology, environmental physics and geophysics were used to illustrate the course material. The course material was developed primarily from published papers. A fairly comprehensive literature survey was provided as a guide to additional reading.

Problems were developed for the purposes of providing exposure to additional topics, to illustrate certain points, and to allow the students to test their understanding of the material. The table of contents is reproduced below.

PERMAFROST: PROPERTIES AND PROCESSES*

T. E. Osterkamp

Table of Contents

I have most of my lecture notes for the course transcribed and will have a few CDs available for people who are teaching courses on permafrost.

Potential Use of Rock Glaciers as Mountain Permafrost Indicators in Yukon Territory, Canada

Amaris Page
Department of Geography, University of Ottawa, Ottawa, Canada
Antoni Lewkowicz
Department of Geography, University of Ottawa, Ottawa, Canada
Panya Lipovsky
Yukon Geological Survey, Whitehorse, Canada
Jeff Bond
Yukon Geological Survey, Whitehorse, Canada

Introduction

Analysis of the distribution of active rock glaciers is widely accepted as a way to establish the lower boundary of mountain permafrost. Rock glaciers have been used in this capacity for modeling probable permafrost distribution, mainly in Europe (e.g., Imhof 1996, Lambiel & Reynard 2001, Frauenfelder 2005, Etzelmüller et al. 2007, Fukui et al. 2007, and others). All of these models have examined permafrost distribution over relatively small areas.

We are beginning a similar project in Canada's Yukon Territory. A key difference from previous research is the spatial extent over which the study is being conducted. Currently the distribution of rock glaciers and their activity status are being examined in the southern half of the territory, an area of approximately 250,000 km^2.

A second difference between this and the European research is that in North America, rock glacier distribution may represent only the lower limit of *high elevation* permafrost. Permafrost also occurs in lower elevation valley bottoms due to a combination of temperature inversions due to cold air drainage (Lewkowicz & Ednie, 2004), and ecological interactions associated with surface hydrology. This situation does not occur in Europe, where rock glacier distribution can be used to model the full extent of permafrost in mountainous areas.

Our broad goal is to use the distribution of rock glaciers as an independent means of testing mountain permafrost probability models. This abstract focuses on potential sources of information and current knowledge of rock glacier distribution.

Methodology

Rock glacier location data for this research will be derived mainly from the Yukon Geological Survey's surficial geology maps (see Fig. 1 for map coverage). Rock glacier origins and activity status will be determined by examining their morphology on aerial photographs and remotely sensed imagery. Rock glaciers will be classified as active, inactive, or relict. Their distribution will be assessed at various scales and the usefulness of the rock glaciers for determining probable permafrost distribution in southern Yukon will be evaluated. A sub-sample of the rock glacier population will be visited and their origins and activity status verified in the field.

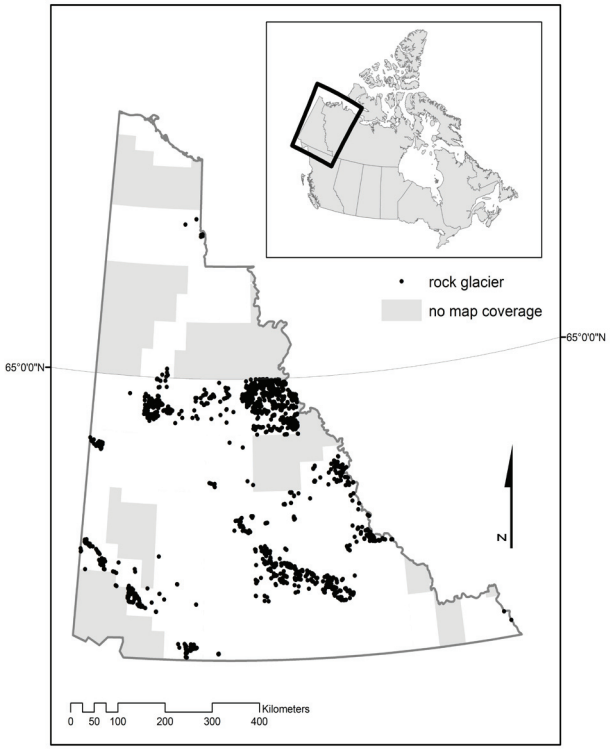

Figure 1. Study area showing surficial geology map coverage (white) and distribution of known rock glaciers (black dots) in the Yukon Territory. According to Heginbottom et al. (1995) discontinuous permafrost becomes continuous at about 64°45′N in this region.

Approximately 1650 individual rock glaciers have been identified to date on maps at scales of 1:25,000 to 1:250,000, which cover roughly 75% of the Territory south of 65°N (the zones of discontinuous permafrost in the Yukon). Verification that the complete population has been mapped will be undertaken for selected areas using aerial photographs. An indication that the maps may not show all the features, possibly because of differences in scale, is that Sloan and Dyke (1998) state that more than 1100 rock glaciers are present in the Selwyn Mountains alone.

Rock glacier density, elevation, and aspect will be compared in different parts of the Territory. Figure 1 shows that there is considerable variation in density with most rock glaciers concentrated in the NW- to SE-trending Selwyn Mountains, Pelly Mountains and Kluane Ranges. Densities in these areas can reach 1 rock glacier per 4 km^2. Extraction of other

parameters, such as orientation, elevation and dimensions, is in progress. Variability in these will be examined, and the possibility of their correlation with climate factors will be studied. From this it is expected that trends in high elevation permafrost distribution will be evident.

Depending on the outcome of the assessment described above, the rock glacier inventory may provide the basis for a permafrost distribution model, or it may be used to verify the results of other models such as those being produced by BTS investigations (Lewkowicz & Ednie 2004, Lewkowicz & Bonnaventure 2008, Bonnaventure & Lewkowicz in review).

Implications

This research is expected to produce the first rock glacier inventory for the southern Yukon, and may additionally be used to create the first permafrost probability map based on geomorphic indicators in the same region. Large-scale permafrost distribution mapping has thus far been carried out using only very general interpolation between existing climate stations with only qualitative consideration of topography (Heginbottom et al. 1995). This project aims to compare methods, improve accuracy, and develop a means of including topographic effects in Canadian permafrost mapping.

Acknowledgments

This research is being funded by the Canadian Foundation for Climate and Atmospheric Sciences.

References

Bonnaventure, P.P. & Lewkowicz, A.G. (in review). Mountain permafrost probability mapping using the BTS method in two climatically dissimilar locations, northwest Canada. *Canadian Journal of Earth Sciences*.

Etzelmüller, B., Farbrot, H., Gudmundsson, Á., Humlum, O., Tveito, O.E. & Björnsson, H. 2007. The regional distribution of mountain permafrost in Iceland. *Permafrost and Periglacial Processes* 18(2): 185-199.

Frauenfelder, R. 2005. *Regional-scale Modeling of the Occurrence and Dynamics of Rockglaciers and the Distribution of Paleopermafrost*. Schriftenreihe Physische Geographie Glaziologie und Geomorphodynamik, 45, Geographisches Institut der Universität Zürich; Zürich.

Fukui, K., Fujii, Y., Mikhailov, N., Ostantin, O. & Iwahana, G. 2007. The lower limit of mountain permafrost in the Russian Altai Mountains. *Permafrost and Periglacial Processes* 18(2): 129-136.

Heginbottom, J.A., Dubreuil, M.A. & Harker, P.T. 1995. Canada – Permafrost. 1:7,500,000 scale map. *National Atlas of Canada* (5th ed.). Natural Resources Canada.

Imhof, M. 1996. Modelling and verification of the permafrost distribution in the Bernese Alps (Western Switzerland). *Permafrost and Periglacial Processes* 7(3): 267-280.

Lambiel, C. & Reynard, E. 2001. Regional modelling of present, past and future potential distribution of discontinuous permafrost based on a rock glacier inventory in the Bagnes-Hérémence area (Western Swiss Alps). *Norsk Geografisk Tidsskrift – Norwegian Journal of Geography*, 55(4): 219-223.

Lewkowicz, A. & Bonnaventure, P.P. 2008. Interchangeability of mountain permafrost probability models. *Permafrost and Periglacial Processes* 19(1): in press.

Lewkowicz, A. & Ednie, M. 2004. Probability mapping of mountain permafrost using the BTS method, Wolf Creek, Yukon Territory, Canada. *Permafrost and Periglacial Processes* 15(1): 67-80.

Sloan, V. & Dyke, L. 1998. Decadal and millennial velocities of rock glaciers, Selwyn Mountains, Canada. *Geografiska Annaler*, 80A(3-4): 237-249.

Soil Carbon Distribution in the Alaska Arctic Coastal Plain

Erik Pullman
University of Alaska Anchorage, Kachemak Bay Campus, 533 East Pioneer Ave., Homer, AK 99603
M. Torre Jorgenson
ABR, Inc. – Environmental Research and Services, P.O. Box 80410, Fairbanks, AK 99708
Yuri Shur
University of Alaska Fairbanks, Civil and Environmental Engineering, P.O. Box 755900, Fairbanks, AK 99775

Introduction

The accumulation of soil carbon in arctic soils represents a globally significant sink of atmospheric carbon that is both formed and maintained by development and accretion of permafrost. Much of this near-surface carbon currently sequestered in permafrost can be incorporated into the active layer through surface disturbance (Pullman et al. 2007) and thermokarst processes related to climate change (Jorgenson et al. 2006). Most recent estimates sample only the active layers or top 100 cm of soil (however, see Bockheim & Hinkel 2007) or are based on samples taken from a limited number of geomorphological terrains.

In this study, we have used a landscape-classification approach to sampling in an area of the North Slope Coastal Plain of Alaska covering 850 km^2 (Fig. 1). The terrain units, surface forms, and vegetation communities of the landscape in this area were classified through aerial photo interpretation and extensive field surveys. Samples for soil carbon were distributed across the major terrain types identified across the study area. Total soil carbon results for each terrain unit were then applied to the terrain map and a total carbon inventory was calculated for the study area.

Methods

Sample collection

Soil cores were collected during the summer in 2001–2003 in the NPR-A area. An intact soil plug was removed down to permafrost. Intact 3-inch (7.5 cm) soil cores in permafrost were collected using a specially-designed soil corer attached to a portable power head. At each location, we attempted to core into the underlying sand sheet and locate sediments with less than 10% visible ice. We postulate that this may represent the syngenetic/epigenetic boundary within the existing permafrost. At each soil pit, soil stratigraphy, texture, and color were described from the intact, frozen soil core. Cryogenic structures were described according to Shur and Jorgenson (1998). Visual ice content was estimated for each stratigraphic section. Soil textures were grouped into lithofacies classes based on similarities on particle size distribution and depositional patterns (Pullman et al. 2007). Frozen soil samples were taken every 10–20 cm (within stratigraphic sections) along the entire length of the core. Sample volumes were measured in the field by taking three measures of core length (at equidistant intervals around the circumference) and three measures of core circumference (at the ends and midpoint of the core length). Unfrozen core material was removed prior to measurement. Mean length and circumference values were used to calculate the cylindrical core volume. Core samples were then placed in labeled ziplock freezer bags for transport. A total of 47 cores and bank exposures were included in this analysis, with total sample depths ranging from 1.8 to 4 m. Most cores extended to 2.7 m.

Field samples were weighed and thawed at room temperature. Excess water was decanted off the sample once all solids had settled to the bottom of the sample bag. Soils were oven-dried to a constant weight at 60°C. A subsample of the homogenized dried soil was submitted for total carbon and nitrogen analysis to the Palmer Soils Laboratory (Palmer, Alaska).

Soil carbon calculations

Soil carbon content was calculated for each stratigraphic section within individual cores, and then summed over 100 cm and 200 cm. Stratigraphic sections that extended through the 100 cm and 200 cm depths were split for the purposes of calculating total carbon for these specific depths. Since we did not sample every stratigraphic section of every core, estimates of the carbon content in unsampled sections were made to obtain total carbon stocks for each core. A stratigraphic method was used to reduce variability that could be introduced by a length-weighted mean method. In this study a total of 612 stratigraphic sections were identified in 46 cores. Of these sections, 476 were sampled for %C content. Measurements on a majority of these sections (400) were made for sample volume, excess ice volume, dry soil density, and water content. Using data from the sampled stratigraphic sections, we were able to calculate mean carbon contents for stratigraphic sections that were missing data for either % carbon, dry density, or both. For stratigraphic sections missing % carbon measures, we used the mean %C of the section's lithofacies class (Table 1). For sections missing dry density measures, sample dry density was calculated using a regression of dry density based on %C of active layer samples multiplied by the % excess ice (from the visual field estimate). For the minority of stratigraphic sections with neither density nor %C measures, we used a value of both %C and dry density, based on calculated means of the appropriate lithofacies class.

Mean carbon stocks for each terrain type were applied to the terrain map of the study area to show the spatial distribution of carbon in the active layer, top 1 m, and top 2 m of soil across the study area to produce a distribution pattern of total

carbon in terrestrial areas of the landscape Terrain types that were not samples include water bodies (lakes, ponds, rivers, and streams) and some of the less-common terrain types.

Results and Discussion

Overall, older surfaces with less-active depositional environments had the largest soil carbon stocks (Fig. 1). Mean accumulation of surface organic material was least in ice-poor thaw basin margins (8.0 cm), eolian inactive sands (11.3 cm), and alluvial-marine deposits (11.1 cm), and greatest in ice-rich thaw basin centers (32.2 cm) and margins (48.8 cm).

Carbon stocks were greatest in alluvial-marine deposits and thaw basin centers, and lowest in eolian inactive sands and basin margins. A general trend of increasing soil organic carbon with decreasing depositional activity was seen across the study area. Soil carbon stocks were lowest in riverine terrain units (active riverbeds, active overbank, and inactive overbank deposits) and highest in thaw basin and and alluvial-marine deposits. In riverine terrains, mean (± s.d.) carbon stocks in the top 1 m of soil ranged from a low of 10.2 ± 7.8 kg C/m² in meander active riverbed deposits to 20.0 ± 2 kg C/m² in delta inactive overbank deposits. In thaw basin terrains, the range was 37.8 ± 3.9 kg C/m² in ice-poor margin deposits to 41.7 ± 13.4 kg C/m² in ice-rich center deposits. Alluvial-marine deposits, which experience minimal deposition or erosional activity, had the highest soil carbon stocks (58.2 ± 16.5 kg C/m²). When calculated in the top 2 m, large increases in carbon stocks were seen in all terrain units (Fig. 1). These data represent conservative estimates of total soil carbon stocks, because additional soil carbon may be present beyond our sampling depths, especially in ice-rich thaw basin centers and alluvial-marine terrains. Our estimates of carbon stocks fall into the range of other recently published accounts (Ping et al. 2002, Bockheim & Hinkel 2007) of carbon stocks in the top 1 m (Ping et al. 2002) and 2 m (Bockheim & Hinkel 2007) of soil on the Arctic Coastal Plain. However, this study includes a wider variety of terrain types and includes carbon-poor soil types that have not been previously sampled.

Soil organic carbon data for sampled terrain units were combined with an existing terrain unit map of a portion of the Western Beaufort Coastal Plain to produce a distribution map of soil organic carbon. As additional terrain unit maps in this area become available, we plan to expand the carbon distribution map and generate a regional soil carbon estimate based on the current dataset. Based on previous soil surveys in the area, this data can be applied to approximately 7000 km² of the Beaufort Coastal Plain. In addition, this data can be combined with thaw settlement estimates across the same area to identify terrain units where sequestered carbon may be incorporated into the active layer under the conditions of a warmer climate or human disturbance.

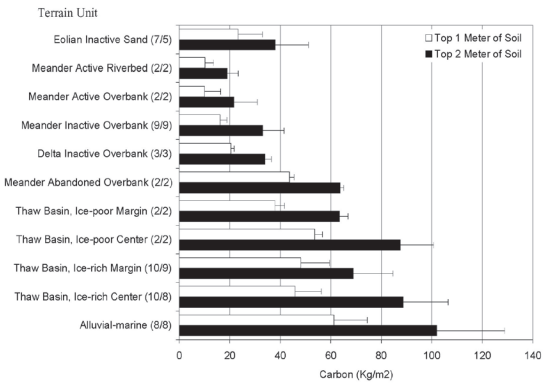

Figure 1. Mean carbon content of soils in common terrain units of the Arctic Coastal Plain, Alaska. Error bars represent standard deviation and numbers in parenthesis show the sample size (number of cores) used to calculate 1 m and 2 m soil organic carbon.

Acknowledgments

This research was funded by ConocoPhillips Alaska, Inc. and managed by Caryn Rae, Senior Biological Consultant. John Shook, Tim Cater, Gerald Frost, Luke Mcdonagh, and Jennifer Mitchell assisted with the fieldwork and soil processing.

References

Bockheim, J.G. & Hinkel, K.M. 2007. The importance of "deep" organic carbon in permafrost-affected soils of Arctic Alaska. *Soil Science Society of America Journal* 71: 1889-1892.

Jorgenson, M.T., Shur, Y. & Pullman, E.R. 2006. Abrupt increase in permafrost degradation in Arctic Alaska. *Geophysical Research Letters* 33: L022503.

Ping, C.L., Michaelson, G.J., Kimble, J.M. & Everett, L. 2002. Chap. 47. Soil organic carbon stores in Alaska. In: R. Lal, J.M. Kimble, & R. Follet (eds.), *Agricultural Practices and Policies of Carbon Sequestration in Soils*. CRC Press LLC, 485-494.

Pullman, E.R., Jorgenson, M.T., and Shur, Y. 2007. Thaw settlement in soils of the Arctic Coastal Plain, Alaska. *Arctic, Antarctic, and Alpine Research*, 39: 468-476.

Shur, Y. & Jorgenson, M.T. 1998. Cryostructure development on the floodplain of the Colville River Delta, Northern Alaska. *Proceedings of the Seventh International Conference on Permafrost, Yellowknife, Canada*: 993-999.

The 2007 "Anaktuvuk River" Tundra Fire on the Arctic Slope of Alaska: A New Phenomenon?

Charles Racine
U.S. Army Cold Regions Research Laboratory (Retired), 219 E. King Street, Edenton, NC 27932, USA
Randi Jandt
Bureau of Land Management, Alaska Fire Service, Fort Wainwright, AK 99703, USA

Introduction

A 1000 km^2 (256,000 acres) tundra fire started by lightning, burned from mid-July to early October 2007, and drew national attention as the largest Alaskan wildfire of the year and the largest North Slope tundra fire in recorded history. It burned from 68.7° to 69.5°N latitude (-150.5° longitude) in the east-central North Slope foothills just south of the Colville River. It doubled the known acres burned north of 68° since records have been kept by Alaska Fire Service (around 1950). As with the melting of Arctic Ocean ice and the expansion of shrubs across the tundra, there has been speculation about whether large fires in arctic tundra are more evidence of climate warming in the north (*Anchorage Daily News*, Sept 28, 2007). The objective of this paper is to place this fire and tundra fires in general in the historical context of wildfire in Alaska.

We used published reports and an online spatial database (afsmaps.blm.gov) of fires between 1956 and 2007 to analyze the extent of tundra fires north and west of tree line. The database shows the latitude-longitude of fire starts, area burned, date of detection, and date when declared out, and displays perimeters of larger fires (>400 ha).

Inferences about the longer term tundra fire regime can be made from pollen and charcoal in lake bottom sediments and suggest that burning increased coincident with the transition from herb tundra to shrub tundra about 13.3 to 14.3 ka BP (Higuera et al. 2008). However, it is noteworthy that fossil charcoal in lake sediments or other paleo-evidence of fire *north* of the Brooks Range is generally lacking for the past 5000 years.

Tundra fire locations

Figure 1 shows all recorded tundra fires (1956–2007) north of 68°N. The AR (Anaktuvuk River) fire is outlined in the right center of the map west of the Alaska Pipeline. Several tundra fires are concentrated along the Noatak River (west side of map) near 68°N, but only 10 recorded fires including the AR fire have been reported north of 69° on the North Slope. Tundra fires occur almost annually north and west of tree line in the Seward Peninsula and the Noatak River Valley, where they are much more common than on the North Slope. Larger tundra fires in these three regions are listed in Table 1.

Of the 10 tundra fires reported north of 69°, four others were >400 ha, occurring in 1993 and 1977 on the western Arctic Slope (Fig. 1, Table 1). Prior to 2007, no large tundra fires had occurred on the east side of the North Slope. One other large tundra fire (Sagavanirktok), in addition to the AR fire, occurred in this area in 2007 (just east of the Alaska Pipeline, Fig. 1).

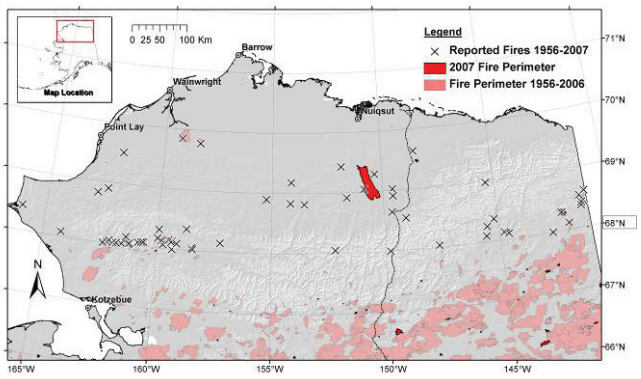

Figure 1. Map of northern Alaska showing locations of all reported fires from 1956–2007 north of 66°N latitude. The *X*s mostly denote smaller tundra fires (<400 ha) north of 68°. The Anaktuvuk River fire is strongly shaded, and the perimeters of large forest fires south of the Brooks Range are lightly shaded.

Tundra fire size

Only one other tundra fire—in 1977 in the central Seward Peninsula—was as large (1,000 km^2) as the AR fire (Table 1). The second largest fire on the North Slope was 330 km^2. Most tundra fires are small (<400 ha), particularly in comparison with boreal forest fires, which can cover 2000 to 6000 km^2 or more (Kasischke et al. 2002). Some of these forest fires are outlined in Figure 1. Racine et al. (1985) analyzed tundra fire size in the Noatak watershed showing that, of 79 fires between 1956 and 1983, almost half were less than 10 ha in size.

As surface or ground fires, tundra fires are easily stopped by rivers and streams and can be more easily extinguished by small rain or fog events or even nightly humidity. Tundra fire flame lengths are typically 2–8 m compared with 15–30 m in black spruce crown fires. Therefore, firebrand production and spotting potential across natural firebreaks are much reduced. The AR fire was confined between the Itkillik and Nanushuk Rivers, but burned a long distance (70 km) from north to south between these two rivers.

Tundra fire timing

The AR fire was started by lightning on July 16, and was declared out on October 6. No other tundra fires are known to have burned this long (almost 3 months) and late into the fall, although the nearby 2007 Sagavanirktok fire, about 90 km northeast of the AR fire, began on September 7, and

burned to October 9 (Table 1). The AR fire initially remained fairly small and was even thought to be "out" in early August, but roared back to life during record warmth and drought in early September and burned to October 5, when the area was blanketed by snow. The other large tundra fire of the same size at Imuruk Lake in the Seward Peninsula (Table 1) burned for over two months from July 9 to September 12. It has been proposed that late-season fires would burn deeper and would be more severe because the active layer deepens, allowing deeper drying of the organic mat.

The AR fire was the largest fire of the 2007 Alaska fire season. The largest fire year on record was 2004 when 6.5 million acres burned statewide, but only a few minor tundra fires were recorded. The year 1977 appears to be the only large Alaska fire year (ranked sixth), when there were both extensive large tundra and boreal forest fires. A total of 2.5 million acres burned with about 0.7 million acres (2800 km^2) resulting from tundra fires in the Seward Peninsula and Noatak River regions (Table 1).

Implications for permafrost

Tundra wildfire results in warmer soil temperatures and initially deeper thaw for several years following fire. Thawing is the result of (1) the removal of all or a portion of the insulating organic soil layer, (2) lowered surface albedo, (3) increased soil moisture, and (4) a longer thaw period as a result of earlier snowmelt and delayed fall freeze-back (Liljedahl et al. 2007).

Table 1. Characteristics of some large tundra fires in three regions of Alaska north and west of tree line.

Fire Name	Year Dates	Fire Size (km^2)	Lat.	Long.
North Slope	1956–2007	2113		
Anaktuvuk	2007 7/16–10/5	1000	69.3	150.5
Sagavanirktok	2007 9/7–10/9	13	69.5	148.3
B678	1993 7/22–8/18	330	69.9	159.1
B480	1993 7/3–8/17	67	69.8	158 2
Kokolik R.	1977 7/26–8/7	46	69.5	161.8
Seward Penin.	1956–2007	5229		
Imuruk Lake	1977 7/9–9/12	1000	65.5	163.0
Niagra Ck.	1997 7/22–9/25	300	65.5	164.5
Coffee Creek	1971 6/29–7/22	210	65.3	164.6
Chicago Ck.	1990 8/8–9/11	220	66.0	162.2
Wagon Wheel	1977 7/9–8/5	180	65.0	162 8
Noatak River	1956–2007	1881		
Mission Lowland	1977 7/15–8/18	458	67.5	162.5
Uvgoon	1999 6/26–8/3	354	67.8	162.7
Noatak Canyon	1977 6/24–7/4	121	68.0	161 7

On flat terrain, thaw depths generally return to pre-fire levels within 10 to 25 years (Racine et al. 2004). However, where slopes are steep, as on river banks and back slopes, tundra fires have been observed to cause subsidence, massive thaw, erosion, and even exposure of ice wedges. Where permafrost is "warm" or discontinuous, as on the Seward Peninsula, the effects of tundra fire on permafrost may be greater (Liljedahl et al. 2007, Racine et al. 1983).

Discussion

By far most wildfire in Alaska occurs in the Interior boreal forests between the Brooks Range and the Alaska Range, where an average of 2869 km^2 burned annually from 1960 to 2000 (Kasischke et al. 2002). Boreal forest fires of 1000 km are not uncommon. Total tundra area burned from 1956 to 2007 is largest for the Seward Peninsula (5229 km^2) (Table 1). The total for the North Slope (2113 km^2) is strongly influenced by the one 1000 km^2 AR fire.

Clearly the factors that determine the frequency and extent of tundra fires are different from those that control boreal forest fire. Lightning frequency, climate, and fuels are different north and west of tree line. Tundra fires are likely more climate-driven than fuel-driven. In the fall of 2007, a large temperature anomaly (10°C warmer than usual) and sunny dry weather along the Arctic Coast possibly associated with an ice-free Arctic Ocean was reported at the December 2007 AGU meeting (arcus.org/press/).

However, the expansion and increase in shrubs predicted and measured in the Alaskan Arctic may also affect the tundra fire regime (Higuera et al. 2008). Separating the effects of climate change and warming from those of fire disturbance and succession remains a major problem, in part because changes in vegetation and disturbance regime are linked.

References

Higuera, P.E. et al. 2008. Frequent fires in ancient shrub tundra: implications of paleorecords for arctic environmental change. *PLoS ONE* 3(3).

Kasischke, E.S., Williams, D. & Barry, D. 2002. Analysis of the patterns of large fires in the boreal forest region of Alaska. *Int. J. of Wildland Fire* 11:131-144.

Liljedahl, A. et al. 2007. Physical short-term changes after a tussock tundra fire, Seward Peninsula, Alaska. *J. Geophys. Res., Earth Surface* 112: doi:10.1029.

Racine, C. et al. 1985. Tundra fire regimes in the Noatak River Watershed, Alaska: 1956–83. *Arctic* 38: 194-200.

Racine, C. et al. 1983. Permafrost thaw associated with tundra fires in NW Alaska. *Proceedings of the 4th Internatl. Conf. on Permafrost. Nat. Academy Press,* 1024-1028.

Racine, C. et al. 2004. Tundra fire and vegetation change along a hillslope on the Seward Peninsula, Alaska, USA. *Arctic, Antarctic and Alpine Res.* 36: 1-10.

Ice Wedge Thermal Regime in Northern Victoria Land, Antarctica

Rossana Raffi
Department of Earth Sciences, "La Sapienza" University, Roma, Italy
Simone Sega
Department of Earth Sciences, "La Sapienza" University, Roma, Italy

Introduction

A study on the ice wedge thermal regime in northern Victoria Land, Antarctica, was conducted by installing dataloggers at three selected sites. Two of the sites are located in the Terra Nova Bay area, near Baker Rocks (74°12′27″S, 164°50′01″E, 11 m a.s.l.) and Boomerang Glacier (74°30′13″S, 163°50′10″E, 874 m a.s.l.). The third site is located near Mount Jackman (72°23′07″S, 163°10′49″E, 1326 m a.s.l.) in the Freyberg Mountains (Fig. 1).

Testo Testor 171-4 dataloggers, equipped with NTC sensors (±0.2 accuracy), were installed in the Terra Nova Bay sites. At the Mount Jackman site PT100 sensors (±0.1 accuracy) mounted on a Campbell CR1000-XT datalogger were used. In each installation, four sensors took hourly temperatures of the air, the ice wedge top and bottom, and the ground surface. The air temperature was measured at a height of 180 cm above the ground at Baker Rocks, 110 cm at Boomerang Glacier, and 155 cm at Mount Jackman. The ground surface temperature was measured at a depth of 2 cm. The ice wedge top and bottom were measured, respectively, at a depth of 50 cm and 133 cm at Baker Rocks, 38 cm and 83 cm at Boomerang Glacier, and 35 cm and 85 cm at Mount Jackman.

Data were collected during the period from 1 February 2004 to 31 December 2006 at Baker Rocks and Boomerang Glacier, and from 1 February 2006 to 31 December 2006 at Mount Jackman (Fig. 2).

The purpose of the study was to provide new data on the ice wedge thermal regime, and to verify if thermal conditions at the sites can trigger ice wedge cracking.

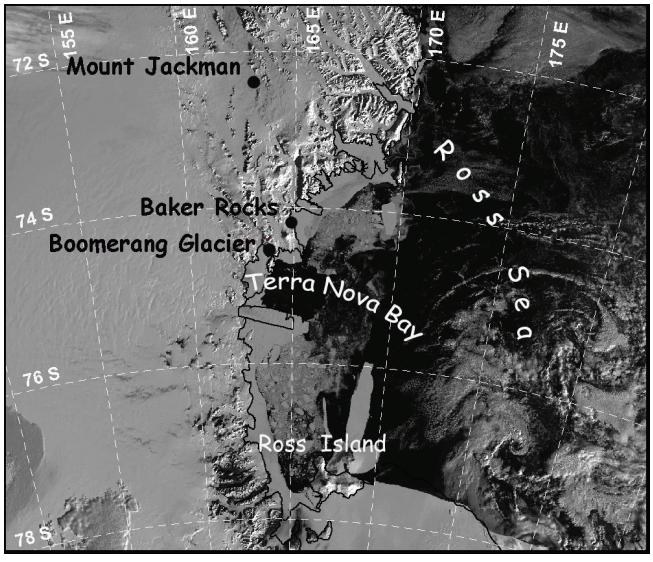

Figure 1. Location of the study sites. Satellite image by Italian Antarctic National Research Program.

Ice Wedge Thermal Regime

Air temperature

The mean annual air temperature (MAAT) during the period from 1 February 2004 to 31 January 2006 was -21.1°C at Baker Rocks and -16.3°C at Boomerang Glacier. The mean air temperature, calculated over 11 months, was -23.3°C at Mount Jackman.

According to Burn (1990), ice wedge cracking is primarily controlled by the winter temperature regime. During the winters of 2004, 2005, and 2006, the mean air temperatures, calculated from April to September, were -25.5°C, -28.4°C, and -28.8°C, respectively, at Baker Rocks, Boomerang Glacier, and Mount Jackman. The lowest monthly mean air temperatures most often occurred in May and July (Fig. 2), with lows below -45°C at Baker Rocks and Boomerang Glacier, and -50°C at Mount Jackman. Moreover, frequent, large temperature fluctuations occurred throughout the winter seasons, with either sharp drops or rapid increases in air temperatures.

In the Arctic, the correlation between sharp air temperature drop, ground cooling rate and ice wedge cracking was fully documented by the field studies of different authors (i.e., Mackay 1993, Allard & Kasper 1998, Fortier & Allard 2005). According to the authors, atmospheric cooling events of major amplitude were taken into account, and their mean values were calculated. Applying this method at the study sites revealed that mean air temperature drops of 18°C, 16.6°C, and 19.3°C, over mean periods of 33.3 hours, 47.7 hours, and 26 hours, at mean air cooling rates of -2.1°C/h, -0.4°C/h and -0.7°C/h, occurred, respectively, at Baker Rocks, Boomerang Glacier, and Mount Jackman. These

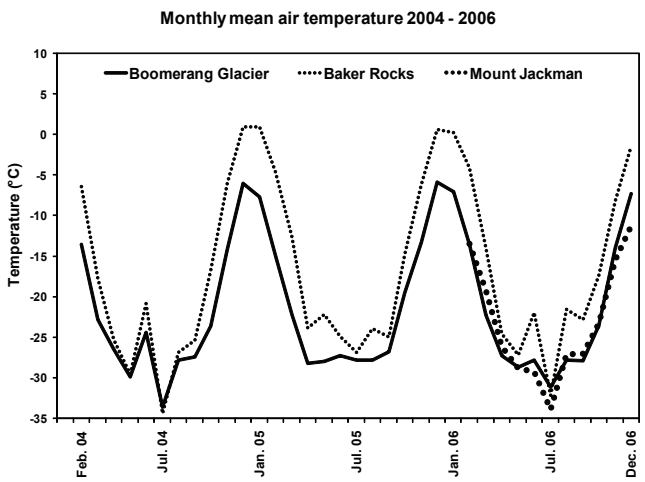

Figure 2. Monthly mean air temperature for 2004–2006 at the ice wedge polygon sites: Baker Rocks (11 m a.s.l.), Boomerng Glacier (874 m a.s.l.), and Mount Jackman (1326 m a.s.l.).

values exceed the 4-day temperature drop rate of 1.8°C/d, reported by Mackay (1993), which favored ice wedge cracking on the western Arctic coast. They also exceed the mean drops of 7.9°C, over mean periods of 18 hours, at a mean air cooling rate of -0.5°C/h measured before cracking events by Fortier and Allard (2005), at Bylot Island in the eastern Canadian Arctic Archipelago.

Ground temperature

The mean annual ground surface temperature (MAGST) was -17.1°C at Baker Rocks and -20.4°C at Boomerang Glacier. The mean ground surface temperature, over an 11-month period, was -22.4°C at Mount Jackman.

During winter seasons the mean ground surface temperature (MGST) was -28.6°C at Baker Rocks, -29.8°C at Boomerang Glacier, and -33.1°C at Mount Jackman. Temperatures with lows below -40°C were recorded at all sites.

The mean annual temperature of the top of the ice wedge was -15.3°C at Baker Rocks, -20.2°C at Boomerang Glacier. A mean value of -21.3°C was recorded at Mount Jackman over an 11-month period. During the winter months, ice wedge top temperatures were consistently below -20°C at Baker Rocks (mean value -21.7°C) and Boomerang Glacier (mean value -26.8°C), and below -25°C at Mount Jackman (mean value -28.4°C).

The ground surface thermal regime closely follows that of the air, with similar large and rapid fluctuations in temperature. Mean ground cooling rates (MGCR) of -28.6°C/d, -4.8°C/d, and -12.4°C/d at the surface, and of -0.4°C/d, -0.5°C/d, and -1.3°C/d at the ice wedge tops were obtained, respectively, at Baker Rocks, Boomerang Glacier, and Mount Jackman. These rates exceed the MGCR before frost-cracking episodes of -0.3°C/d at the surface and -0.2°C/d at the permafrost table, reported by Fortier & Allard (2005).

Discussion

The analysis of the thermal regime at the ice wedge polygon sites revealed that, in winter, the temperatures of the air and on the tops of the ice wedges fell below -30°C and -20°C, respectively. These values exceed the limits at which thermal-contraction cracking is known to occur in the Arctic (Lachenbruch 1966, Allard & Kasper 1998, Fortier & Allard 2005). Comparison of the cooling rates of the air and ground with those measured by Mackay (1993) and Fortier & Allard (2005) at the time of cracking events shows that thermal conditions at the study sites are more severe than those identified in the Arctic areas, and they most likely can trigger ice wedge cracking. This is also supported by the existence of open cracks observed, both in the ice wedges discussed in this article and in many others excavated during summer field surveys in northern Victoria Land (Raffi 2003).

At present, no field data of snow cover are available; however, we can infer that there was no thick snow cover at the three sites because throughout winter seasons, the daily ground surface temperatures were almost always lower than the daily air temperatures. When the opposite occurred, daily ground surface temperatures only remained higher than the air temperature for very brief periods (from a few hours to a few days), and then quickly decreased. The strong katabatic winds, with gusts reaching speeds of more than 200 km/h in winter, prevent snow accumulation and its insulating effect on the ground.

Acknowledgments

This research was carried out within the Italian Antarctic National Research Program. Thanks are due to Dr. R. Bono, CNR-ISSIA of Genova, I, and to Dr. U. Gentili, Climate Project, ENEA, Roma, I, for the field maintenance of the thermometric stations.

References

Allard, M. & Kasper, J.N. 1998. Temperature conditions for ice-wedge cracking: field measurements from Salluit, northern Québec. In: A.G. Lewkowicz & M. Allard (eds.), *Proceedings of the Seventh International Permafrost Conference, Yellowknife, Canada, June 23-27, 1998*. Centre d'études nordiques, Québec: Université Laval, Collection Nordicana 57: 5-12.

Burn, C.R. 1990. Implications for palaeoenvironmental reconstruction of recent ice-wedge development at Mayo, Yukon Territory. *Permafrost and Periglacial Processes* 1(1): 3-14.

Fortier, D. & Allard, M. 2005. Frost-cracking conditions, Bylot Island, Eastern Canadian Arctic Archipelago. *Permafrost and Periglacial Processes* 16(2): 145-161.

Lachenbruch, A.H. 1966. Contraction theory of ice-wedge polygons: a qualitative discussion. *Proceedings of the First International Permafrost Conference, Lafayette, Indiana, November 11-15, 1963*. Washington, DC: National Academy of Sciences-National Research Council, publication no. 1287: 63-71.

Mackay, J.R. 1993. Air temperature, snow cover, creep of frozen ground, and the time of ice-wedge cracking, western Arctic coast. *Canadian Journal of Earth Sciences* 30: 1720-1729.

Raffi, R. 2003. Ice wedges in the Terra Nova Bay region (northern Victoria Land, Antarctica). Distribution and morphological features. *Terra Antartica Reports* 8: 143-148.

Soil Thermal and UV Radiation Monitoring on a Maritime Antarctic Permafrost Area by Means of REMS (Rover Environmental Monitoring Station-Mars Science Laboratory) Sensors

M. Ramos
Department of Physics, University of Alcalá, Spain
J. Gómez, E. Sebastian, J. Martín, C. Armiens
Astrobiological Center (INTA-CSIC), Spain
J.J. Blanco
Department of Physics, University of Alcalá, Spain
M.A. de Pablo
Department of Geology, University of Alcalá, Spain
D. Tomé
Department of Physics, University of Alcalá, Spain

Introduction

The present climatic characteristics of Mars induce the extensive presence of permafrost areas in this lonely planet (Carr 2006). Therefore, environmental parameters that are included in Martian rover missions are the focus for monitoring thermal characteristics and soil surface evolution in order to understand the active layer thickness and the energy balance between the soil and the atmosphere.

On the other hand, the intensity of the incoming UV radiation on the soil level is a key parameter of Mars habitability. Nevertheless, Mars conditions are quite different to those observed on the Earth's surface. On Earth, a deep ozone absorption band centered at 2550Å prevents most of the UV radiation from reaching the surface, whereas on Mars, at least in low latitudes and in summer at high latitudes, the full solar flux at wavelengths greater than 1900Å falls unattenuated onto the surface.

The REMS (Rover Environmental Monitoring Station) is an environmental station designed by the Centro de Astrobiología (Spain) with the collaboration of national and international partners (CRISA/EADS, UPC and FMI), which is part of the payload of the MSL (Mars Science Laboratory) NASA mission to Mars (http://mars.jpl.nasa.gov/msl/overview/).

This mission is expected to be launched in the final months of 2009, and mainly consists of a rover with a complete set of scientific instruments; the rover will carry the biggest, most advanced suite of instruments for scientific studies ever sent to the Martian surface.

Five sensors compose the REMS instrument: ground (GT-REMS) and air temperatures, wind speed and direction, pressure, humidity and ultraviolet radiation (UV-REMS). It also includes all the electronics and software required by sensor read out, signal conditioning and data transmission to the rover. Wind vector, air temperature, and humidity and ground temperature sensors are located in small booms which are attached to the rover mast, while the ultraviolet sensor is on the rover deck and pressure inside the rover body and connected with external ambient by a small opening (see Fig. 1).

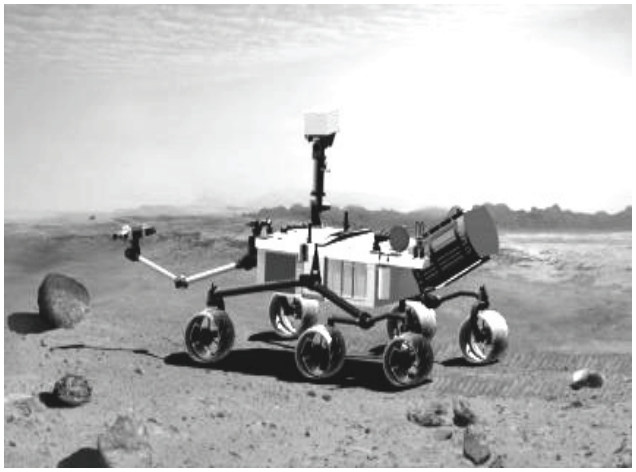

Figure 1. Mars Science Laboratory rover (MSL).

MSL is the third rover generation sent to Mars and is the first time that a rover is equipped with an environmental station to characterize the local micrometeorology and its effect on soil surface, as well the first time that ultraviolet radiation at surface level will be recorded.

Antarctic field test

In the 2007–08 Spanish Antarctic program, our scientific team has included a field test related to the REMS sensor and its behavior on permafrost areas in the surroundings of the Spanish Antarctic Stations (SAS) that are built on Livingston and Deception Islands (Maritime Antarctica).

Livingston and Deception Islands are located in the sub-Antarctic South Shetland Archipelago at (62°39′S; 60°21′W and 62°43′S, 60°57′W). The climate at sea level is cold oceanic, with frequent summer rainfall in low areas and a moderate annual temperature range. The climate reflects the strong influence of the circum-Antarctic low-pressure system (King et al. 2003).

Data from different stations on King George Island (South Shetland Archipelago) show the mean annual air temperature (MAAT) to be approximately -1.6°C near sea level and the annual precipitation to be about 500 mm.

Permafrost in the South Shetland Islands is widespread

above the Holocene raised beaches (ca. 30 m a.s.l.) (Serrano & López-Martinez. 2000). Meteorological and geophysical data indicate, however, that environmental conditions in the islands are marginal for the maintenance of permafrost (Hauck et al. 2007).

Instruments and Methods

A simplified model of the REMS GT and UV sensors are part of the experiment deployed on Antarctica. The model tries to reproduce the conditions measurement of REMS on Mars.

This experiment is composed of some standard meteorological sensors and the photodiodes and thermopiles corresponding to the REMS model (Table 1). All the sensors are mounted on a 1.8 m mast and include a Pt100 air temperature with solar protection shield at the top of the mast and a Kipp and Zonnen CNR1 net radiometer for measuring infrared (CG3) and solar short wave (CM3) radiation at 1.5 m high. REMS GT and UV sensors and its amplification box are at 0.7 m high, and finally two Pt100 sensors are in close contact with the soil surface in the angle of view of the GT-REMS thermopiles.

In the case of the GT-REMS sensor, the model uses the first two bands of REMS thermopiles (8–14 μm and 16–20 μm), and their physical disposition is essentially similar to the flight model. The thermopiles have been previously calibrated using a similar setup to the one described in the REMS calibration plan. Finally, the internal thermopile temperature sensors RTD are also sampled in order to recover the IR energy coming out from the ground surface.

For the UV-REMS sensor the Antarctic experience used only the bands A, B, and C, and contrary to those used in REMS rover (Vazquez et al. 2007). The sensor output signals are sampled by the datalogger model Squirrel 1250 of the company Grant with a general sample period of 5 min, which is the result of averaging samples every minute.

Experiment Objectives

Finally the main objectives of this experience are the following:

1. To compare the soil thermal evolution, measured directly with a good soil thermal contact Pt100 thermoresistences, with the temperature register by means of the GT-REMS thermopiles installed in a mast.

Table 1. Expected signals and system resolution.

Channel	*Range*	*Expected signal*	*Resolution*
UV-A	335-395nm	50μW/cm^2	30nW/cm^2
UV-B	280-325 nm	10μW/cm^2	24nW/cm^2
UV-C	220-275 nm	100nW/cm^2	1,2 nW/cm^2
GT-A	8-14μm	±20ºC	0.012ºC
GT-B	16-20μm	±20ºC	0.061ºC
CG3	5–50 μm	+250 W/m^2	5 W/m^2
CM3	305–2800 nm	1000 W/m^2	5 W/m^2
Pt100		±20ºC	0.015 ºC

2. To analyze the active layer thermal behavior and its effect on the soil surface temperature on a well-known site where we are measuring thermal and mechanical evolution of the active layer by means of CALM (Circumpolar Active Layer Monitoring) protocol (Ramos & Vieira 2003, Ramos et al. 2007).
3. To develop a method that allows us to obtain, with only soil surface and atmosphere temperature data, information about the thermal active layer regime on the surface of Mars.
4. To check the UV-REMS response under Antarctic conditions by registering the UV radiation incoming on soil surface by means of three sensors in the range of A, B, and C spectral bands.

References

Carr, M. 2006. *The Surface of Mars*. Cambridge: Cambridge University Press, 307 pp.

Hauck, C. Vieira, G. Gruber, S. Blanco, J. & Ramos, M. 2007. Geophysical identification of permafrost in Livingston Island, maritime Antarctica. *J. Geophys. Res.* 112: F02S19, doi:10.1029/2006JF000544.

King, J.C. Turner, J. Marchall, G.J., Connolley, W.M. & Lachlan-Cope, T.A. 2003. Antarctic Peninsula variability and its causes as revealed by analysis of instrumental records, in Antarctic Peninsula climate variability. In: E. Domack et al. (eds.), *Antarctic Research Series* AGU 79: 17-30.

Ramos, M. & Vieira, G. 2003. Active layer and permafrost monitoring in Livingston Island, Antarctic. First results from 2000 to 2001. In: M. Phillips, S.M. Springman & L. Arenson (eds.), *Proceedings of the Eighth International Conference on Permafrost, Balkema Publishers, Lisse, Zurich*: 929-933.

Ramos, M., Vieira, G., Gruber, S., Blanco, J.J., Hauck, C., Hidalgo, M.A., Tomé, D., Neves, M. & Trindade, A. 2007. Permafrost and active layer monitoring in the Maritime Antarctic: Preliminary results from CALM sites on Livingston and Deception Islands. *U.S. Geological Survey and The National Academies, USGS OF-2007-1047, Short Research Paper 070*, doi:10.3133/of2007-1047.srp070.

Serrano, E. & López-Martínez, J. 2000. Rock glaciers in the South Shetland Islands, Western Antarctica, *Geomorphology* 35: 145-162.

Vázquez, L. Zorzano, M.P. & Jiménez, S. 2007. Spectral Information Retrieval from Integrated Broadband Photodiode Martian Ultraviolet Measurements, *Optics Letters* 32(17): 2596-2598.

Characterizing Polar Landscapes from Multispectral and Hyperspectral Imagery

Justin L. Rich
State University of New York at Buffalo, Department of Geology, Buffalo, New York, USA
Bea Csatho
State University of New York at Buffalo, Department of Geology, Buffalo, New York, USA
Erzsébet Merényi
Rice University, Department of Electrical and Computer Engineering, Houston, Texas, USA
Brian Bue
Rice University, Department of Electrical and Computer Engineering, Houston, Texas, USA
Chien-Lu Ping
University of Alaska Fairbanks, School of Natural Resources and Agricultural Sciences, Fairbanks, Alaska, USA
Lynn Everett
The Ohio State University, Byrd Polar Research Center, Columbus, Ohio, USA

Introduction

There is a physically based, conceptual understanding of many of the significant interactions that impact permafrost-affected soils. Our observationally based knowledge however, is inadequate in many cases to quantify these interactions or to predict their net impact. To pursue key goals, such as understanding the response of permafrost-affected soil systems to global environmental changes and their role in the carbon balance, and to transform our conceptual understanding of these processes into quantitative knowledge, it is necessary to acquire geographically diverse sets of fundamental observations at high spatial and often temporal resolution. The main goal of the research presented here is to characterize permafrost-affected landscapes by using multispectral and hyperspectral imagery.

Approach

The sheer amount and the heterogeneity of datasets (e.g., LIDAR, stereo imagery, multispectral, hyperspectral, and SAR imagery) make joint interpretation (fusion) a daunting task. Here remote sensing, pattern recognition, and landscape analysis techniques are combined for the delineation of soil landscape units and geomorphic features and for inferring the physical properties and composition of the surface from a fused dataset consisting of an Advanced Land Imager (ALI), Landsat +ETM (ETM) or Landsat TM (TM) scene, and topographic data with its derivative products.

Exploration of the relationship between the mapped surface units and permafrost conditions on the North Slope of Alaska (Fig. 1) has been undertaken. Since the depth of the permafrost manifests in the active layer on a variety of scales, we apply texture-based, object-oriented multiresolution soft classifications. This allowed for integration of multiple data types within the same surface unit through the use of a region-based segmentation algorithm based on data values and shape properties (Darwish et al. 2003). It is recognized that this type of analysis will lend itself to better characterization of complex landscape units and processes than a pixel-based approach and can help to alleviate traditional spatial analysis quandaries, such as the modifiable aerial unit problem (Burnett & Blaschke 2003) or the effects of hard classifications.

Nonstandard advanced Neural Network architectures to attack tasks, such as the determination of the relevant merits of the data components, have also been utilized. Pixel-level fusion, where the measured values from all experiments for a given location (image pixel) are used as one stack-vector serving as the signature of the material at that location, has been applied. Here, one particular challenge is to determine the relative contributions of the data from the various measurements.

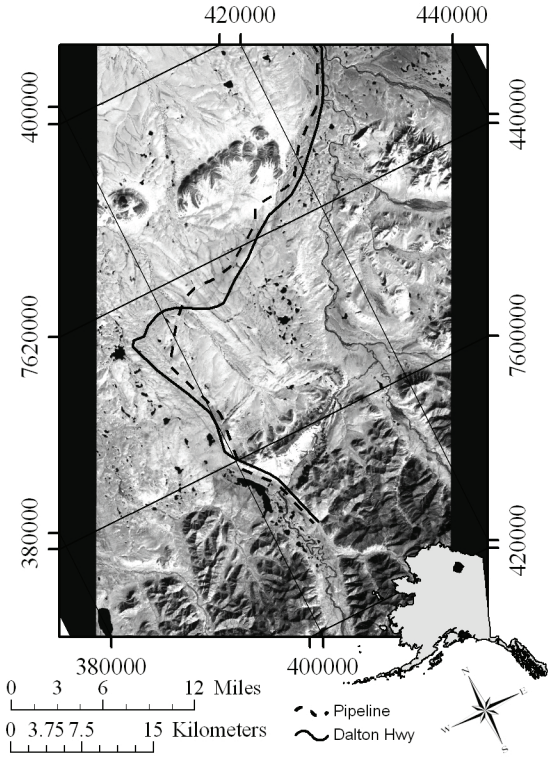

Figure 1. The area of interest in the region of Toolik Lake, Alaska. The location of the Dalton Highway and the Trans Alaska Pipeline are also included for reference.

Results

An example illustrating the concept, from the North Slope of Alaska, using TM, ETM and ALI data, in conjunction with topographic data to develop our object-based model has been undertaken. This analysis was conducted by first processing the data within ENVI (by ITT visual information solutions) to retrieve surface reflectance values and to register the datasets into a common reference system. The results were then imported into Definiens Pro (by Definiens AG) for segmentation and classification based on known surface units such as moist acidic tundra or moist nonacidic tundra (~18 classes total). The results of this segmentation appear to produce objects that correspond well to what has previously been established; however, further work is needed in characterizing class definitions.

By using self-organized manifold learning (SOMs, an unsupervised Artificial Neural Network paradigm), we also clustered a 9-band multispectral image from the ALI instrument. Details of this technique, capabilities, and former analyses are summarized in Merényi et al. (2007) and references therein. We separated 30 different vegetative, soil, and landscape units along the Dalton Highway in the Toolik Lake area. These include various water bodies with different sediment loads, glacial ice, snow, a variety of soils and vegetation. Detailed interpretation is ongoing. This unsupervised segmentation serves to support a detailed supervised classification.

Point-source soils (pedon) data and field spectrometry data have also been acquired at different units to provide ground truth for the satellite image interpretation.

Conclusions and Future Work

Previous studies conducted have utilized datasets that were largely moderate spatial and low spectra resolution. This study is employing datasets that are also moderate spatial resolution, but will be reinforced with high spectral resolution data, resulting in a more accurate assessment of the surface materials and increased confidence in the model. Additionally, by implementing a segmentation of the datasets, it is possible to utilize textual and contextual information that can be lost in pixel-based classifications (Blaschke & Strobl 2001). This type of processing also allows for a more automated processing scheme that can facilitate an efficient temporal study and produce datasets that have undergone the same processing steps with little room for human error. This decreases the amount of time it takes to run an analysis and increases confidence in the model. Preliminary results have shown that image segmentation through a texture-based, object-oriented approach yields landscape unit geometries that appear to correlate well with previously conducted aerial photograph analysis undertaken in the region (Walker 1996).

Field spectral measurements, collected over major land-cover types, indicate that the spectral differences between different landscape units are often minor. Based on high-dimensional intricate signatures, hyperspectral data could provide material discrimination, even in cases of many classes with potentially subtle spectral distinctions. Exploitation of these types of data is a great challenge in itself, both for discovery (unsupervised clustering) and for mapping known species (supervised classification). Fused with other data, this challenge increases. Analysis of hyperspectral imagery resides in our long-term goals, and we hope to report on those at a later date.

Acknowledgments

EM is partially supported by the AISRP (grant NNG05GA94G) of NASA's SMD. BB is supported by NASA GSRP graduate fellowship NNX0AR79H. BC and JR are supported by NASA's ICESat program.

References

Blaschke, T. & Strobl, J. 2001. What's wrong with pixels? Some recent developments interfacing remote sensing and GIS. *GIS Zeitschrift fur Geoinformationssystme* 6(11): 12-17.

Burnett, C. & Blaschke, T. 1994. A multi-scale segmentation/object relationship modeling methodology for landscape analysis. *Ecological Modeling* 31: 737-747.

Darwish, A. et al. 2003. Image Segmentation for the Purpose Of Object-Based Classification. *Geoscience and Remote Sensing Symposium, 2003. IGARSS '03. Proceedings. 2003 IEEE International* 3: 2039-2041.

Merényi, E., Farrand, W.H., Brown, R.H., Villmann, Th. & Fyfe, C. 2007. Information extraction and knowledge discovery from high-dimensional and high-volume complex data sets through precision manifold learning, *Proc. NASA Science Technology Conference (NSTC2007)*, College *Park, Maryland, June 19–21, 2007*: 11pp. ISBN 0-9785223-2-X.

Walker, D.A. 1996. GIS data from the Alaska North Slope. *National Snow and Ice Data Center (Digital Media)*. Accessed 3-15-07.

Contribution of Terrestrial Laser Scanning for Studying the Creep of Mountain Permafrost

François Riff
Geographic Institute of Lausanne University
Christophe Lambiel
Geographic Institute of Lausanne University
Thierry Oppikofer
Institute of Geomatics and Risk Analysis, University of Lausanne

Introduction

Up to now, differential GPS and triangulation using theodolite were the most used terrestrial techniques for measuring the creep of permanently frozen sediment bodies. Recently, the studies of Bauer et al. (2003) and Bodin (2007) demonstrated that terrestrial laser scanning (TLS) offers good opportunities to provide precise measurements on mountain permafrost creep.

This abstract presents positive results of TLS measurements carried out on two permafrost-related creeping landforms located in the Swiss Alps: the tiny Lac des Vaux rock glacier, located in a wider complex slope, and on the Col des Gentianes push moraine (cf. Lambiel 2006). First, the two principal stages of the methodology (data acquisition and treatment) will be presented.

Data Acquisition

TLS is based on the contactless and reflectorless acquisition of a XYZ point cloud of the topography using a time-of-flight principle. The TLS data acquisition stage is relatively quick and easy. However, two recurrent problems were identified using the Optech ILRIS 3D in alpine periglacial landforms:

- The localization of ideal viewpoints is crucial in order to avoid occlusion and too far distances to the object. At a distance shorter than 100 m and with a point cloud resolution better than 5 cm, we were able to identify every object in a unique way. This allows the observation of the movement of the matrix and the bigger blocks. Beyond a distance of about 300 m and a resolution higher than 10 cm, this advantage is lost, but measurement of mass movement is still possible.
- No points can be obtained from snow-covered surfaces, since snow does not reflect the TLS signal.

Data Treatment

The longest stage in the TLS methodology is data treatment with the Polyworks™ software. The raw TLS point clouds need to be cleaned from unwanted objects, unified to a single point cloud and finally georeferenced using GPS points. Sequential TLS point clouds, or TLS time-series, enable the calculation of relative differences, which are related to slope movements (e.g., Oppikofer et al. in review). Positive differences (yellow to red colors in Figs. 1, 2) are related to advances or elevation increases of the creep, while negative differences (blue to pink colors in Figs. 1, 2) are signs of mass loss or depletion.

In addition, the following operations can be carried out:

- Precise volume calculation by creation of parallel cross-sections or use of 3D point clouds.
- Creation of movement vectors by point pair identification. However, using real time kinematics GPS to obtain this kind of information is more practical, faster and more precise than the TLS, but provides only information on selected monitoring points.
- Easy integration of the results in a GIS, since all information is georeferenced.

Results

Lac des Vaux rock glacier

In the upper part of the rock glacier, a distinct blue area (1) indicates a loss of elevation of about 35 cm (Fig. 1). Directly below (2), the light green to yellow colors correspond to positive values, which indicate a general slight increase (5–15 cm) in elevation. Several big blocks even show a positive displacement of about 50 cm. In the lower part (3), the increase in elevation is a bit lower. The GPS data indicates slightly larger displacements.

According to geomorphologic evidence, the successive loss (1) and gain (2-3) in elevation may be the result of

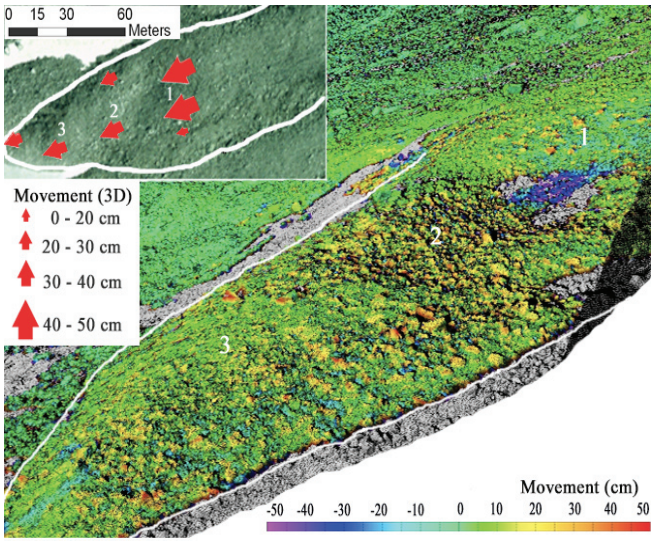

Figure 1. Topographic evolution of the Lac des Vaux rock glacier between 19 July and 16 October 2007, represented with a 50 cm scale. Top left are represented the D-GPS movements extrapolated between the same dates.

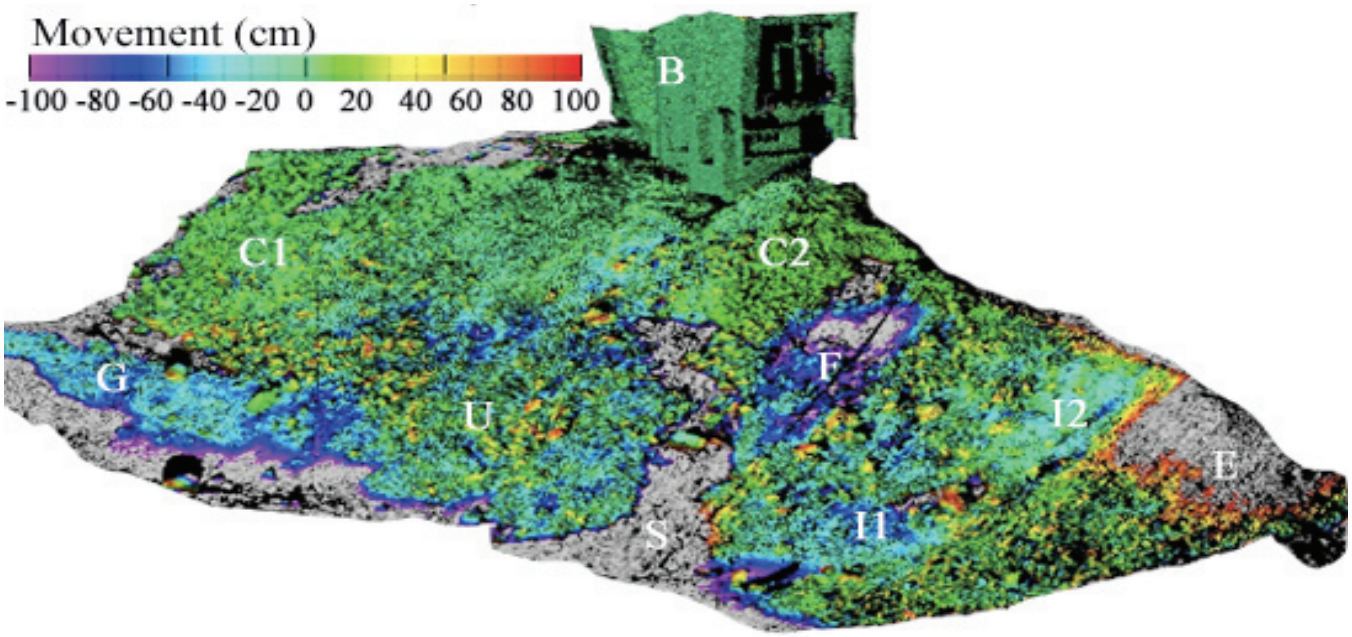

Figure 2. Topographic evolution of the northeast and central parts of the "Col des Gentianes" push moraine between 19 July and 16 October 2007 represented with a 100 cm scale.

a landslide-like development process, as evidenced in destabilized rock glaciers (see Roer et al. 2008). The upper area (1) corresponds to a scar, whereas the lower area (2-3) is the place of a rapid accumulation of materials, with higher destabilization of metric blocks.

Col des Gentianes push moraine

According to geoelectrical measurements and direct observations, the ice content in the moraine is locally important (Lambiel 2006). Generally speaking, all the moraine displays more or less marked movements (Fig. 2). For instance, we can recognize accumulation of materials below a scar (U), a scar of debris flow (F) above an area without any data because of the presence of snow at the time of the first survey (S) and settlement of the moraine due to dead ice melting (I1, I2). C1 and C2 areas are more stable, even if a slight movement (creep) can be observed. The debris-covered glacier at the foot of the moraine is clearly visible (G); (E) is the result of excavation work; and finally, the data confirms the building stability (B).

Discussion and Conclusion

The comparison TLS point clouds evidenced different processes in both investigated landforms, like, for example, permafrost creep, sliding, and settlement due to melting of massive ice. The measurements revealed also that the movement of metric blocks is more important than the displacement of smaller elements, like small rocks and the matrix. Thus, we can conclude that the creeping velocities measured with D-GPS may be slightly overestimated, since, with this technique, large boulders are normally chosen.

Regarding the accuracy of the TLS method, the mean error on sequential TLS point cloud comparisons can be estimated to about 3 cm. This is in the same order of magnitude than with D-GPS. According to the high resolution and precision of the data, the TLS appears to be an efficient technique for studying the creep of mountain permafrost.

References

Bauer, A., Paar, G. & Kaufmann, V. 2003. Terrestrial laser scanning for rock glacier monitoring. *Proceedings of the Eighth International Conference on Permafrost, Zürich, Switzerland, June 2003, 1*: 55-60.

Bodin, X. 2008. Géodynamique du pergélisol de montagne: fonctionnement, distribution et évolution récente. L'exemple du massif du Combeynot (Hautes Alpes*)*. *Thesis. University of Paris-Diderot* (Paris 7), 274 pp.

Lambiel, C. 2006. Le pergélisol dans les terrains sédimentaires à forte déclivité: distribution, régime thermique et instabilités. *Thèse, Université de Lausanne, Institut de Géographie, coll. "Travaux et Recherches"* No. 33: 260 pp.

Oppikofer, T., Jaboyedoff, M. & Keusen, H.-R. In review. Terrestrial laser scanner monitoring of the 2006 Eiger rockslide in the Swiss Alps. *Nature Geosciences*.

Roer, I., Avian, M., Delaloye, R., Lambiel, C., Haeberli, W., Kääb, A. & Kaufmann, V. 2008. Observations and considerations on collapsing active rockglaciers in the Alps. *Proceedings of the Ninth International Conference on Permafrost, Fairbanks, Alaska, 29 June–3 July 2008*.

Extensive Secondary Chaos Formation in Chryse Chaos and Simud Valles, Mars

J. Alexis. P. Rodriguez
Planetary Science Institute, 1700 E. Ft. Lowell Rd., Suite 106, Tucson, Arizona, USA
Ken L. Tanaka
Astrogeology Team, U.S. Geological Survey, Flagstaff, Arizona, USA
Jeffrey S. Kargel
Hydrology & Water Resources, University of Arizona, Tucson, Arizona, USA
David Crown
Planetary Science Institute, 1700 E. Ft. Lowell Rd., Suite 106, Tucson, Arizona, USA
Daniel C. Berman
Planetary Science Institute, 1700 E. Ft. Lowell Rd., Suite 106, Tucson, Arizona, USA

Introduction

The southern circum-Chryse region along the highland-lowland boundary of Mars displays the planet's largest and most complex assemblage of interconnected canyons and channels. The geologic history of this region is key to the understanding of the evolution of crustal volatile release as well as of the nature of the largest condensed surface fluid flows on the planet. Here, large plateau zones have undergone collapse, forming low-lying depressions floored by broken-up and morphologically diverse blocks.

These collapsed terrains, traditionally referred to as chaotic terrains, commonly occur in close spatial association with Martian outflow channels. Martian chaotic terrains and outflow channels have been intensively studied since the 1970s. The consensus is that chaotic terrains represent zones where aquifer destabilization led to ground collapse and to the rapid release of vast amounts of fluids at the surface, which subsequently carved the outflow channels (Sharp 1973). Impact crater densities and geologic relations indicate that both the chaotic terrains and the outflow channels formed during the Late Hesperian Epoch (Scott & Tanaka 1986). An obvious implication of this hypothesis is that the formation of chaotic terrains necessarily pre-dated, but was penecontemporaneous with, the excavation of their associated outflow channels.

Yet, some chaotic terrains formed within the floors of outflow channels, and thus must post-date the excavation of the channel floors they modify. These chaotic terrains, known as secondary chaotic terrains, have been previously described as occurring in the higher outflow channel floors (Rodriguez et al. 2005) . Here, we present a synthesis of the morphologic attributes of a secondary chaotic terrain known as Chryse Chaos that apparently destroyed the southern reaches of the lower outflow channel system of Simud Valles (Fig. 1).

Morphology of Chryse Chaos

Chryse Chaos is located along the lower outflow channel floor of Simud Valles. Its maximum length and width are 700 km and 270 km, respectively, and its surface area is ~0.12 million km^2. Yet, the floor of Chryse Chaos is located a mere ~200 m below adjacent channel floors. Chryse Chaos exhibits a large population of knobs, which are locally closely spaced into clusters (zones outlined by yellow line in Fig. 1b).

The northern margin of Chryse Chaos consists of a prominent break in slope (black, teethed line in Fig. 1b). Our mapping shows that no channels cut down to the chaos floor level and extend north from this break in slope, which forms the downstream margin of the chaotic terrain, suggesting that the formation of Chryse Chaos was not associated with generation of catastrophic floods. In addition, we have not identified any landforms indicative of water ponding such as equipotential terraces (shorelines) along the margins of the

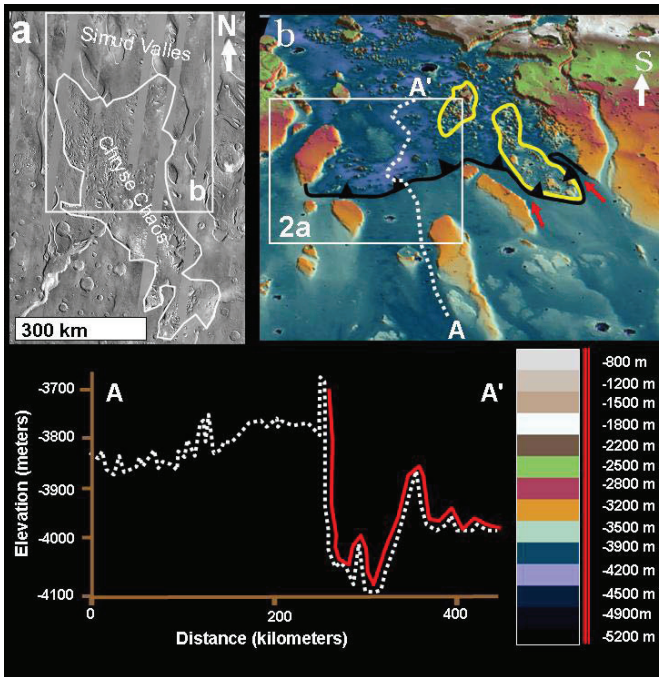

Figure 1. (a) View of Chryse Chaos (part of THEMIS IR mosaic centered at -10.06°N; 322.31°E). (b) View of northern margin of Chryse Chaos. Perspective view of MOLA-based shaded DEM (128 pixels/degree) centered at 13.81°N; 321.15°E and related elevation profile (A-A'). The hachured line shows the location of the break in slope that marks the northern margin of Chryse Chaos. The yellow lines outline collapsed mesas, one of which is flanked by two erosional channels (red arrows). Shown is the location of Fig. 2a.

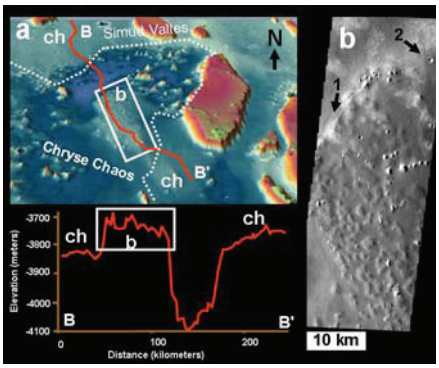

Figure 2. (a) Perspective view of MOLA-based shaded DEM (128 pixels/degree) of the northeastern part of Chryse Chaos (margins marked by white dots) and elevation profile (B-B'). The white box (location of panel b) shows a bulge within the chaos floor, the surface of which is at a higher elevation than proximal channel floors (ch). (b) Close-up of bulge within Chryse Chaos. In the northern margin of the bulge, a graben (arrow 1) transitions into a fractured terrain (arrow 2). (part of THEMIS VIS V19110016 centered at 13.78°N; 322.06°E.

chaotic terrain or of the surrounding high-standing blocks within it, suggesting that bodies of water never ponded within (or, if shorelines formed, they were subsequently destroyed during chaos formation).

A bulge in northeastern Chryse Chaos rises above outflow channel floors both in the regional upslope and downslope directions (see profile in Fig. 2). Nevertheless, its surface does not display surface flow features; instead it has a hilly texture. Its northern margin is marked by a distinct graben and some fracturing (Fig. 2b).

Interpretative Synthesis

To the best of our knowledge, Chryse Chaos is the largest secondary chaotic terrain on Mars and, unlike most chaotic terrains in southern circum-Chryse, its morphology is not diagnostic of flood release and is consistent with a total absence of aqueous fluid emissions.

Location and shape of precursor aquifer

Assuming that (1) the Simud Valles lower outflow channel floor consists of debris flow deposits (Rodriguez et al. 2006) and that (2) Chryse Chaos formed by substrate regional volatile depletion, then an aquifer must have existed within the debris flow deposits and/or within the channel floor materials located at their base. If the maximum dimensions of this aquifer correspond to the extent of Chryse Chaos, then the formational history of this secondary chaotic terrain may be related to:

(a) Deflation of volatile-rich lenses within debris flow deposits: The lower floor of Simud Valles/Chryse Chaos likely consists of sedimentary deposits emplaced by multistage debris flows produced by catastrophic collapse events originating within Ganges, Eos, and Capri Chasmata (Rodriguez et al. 2006). Rodriguez et al. (2006) proposed that instabilities within individual debris flows may have resulted in multiple surges leading to the generation of volatile-depleted and volatile-enriched pulses. Consequently, the lower channel floor within Simud Valles may consist of a mosaic of volatile-poor and volatile-rich geologic materials. Thus, regional volatile deflation of volatile-rich materials may have resulted in, or contributed to, the formation of Chryse Chaos.

(b) Deflation of an aquifer underlying debris flow deposits: Debris flows associated with lower outflow channel activity may have eroded into and then buried an aquifer. Volatile depletion of this putative aquifer could have led to resurfacing of the overlying geologic materials and the generation of Chryse Chaos.

Chaos formation does not appear to have led to the generation of floods, suggesting that its pre-existing aquifer was not under a significant hydraulic head. This can be explained by the fact that the channel floors of Simud Valles form an almost equipotential surface, and as a consequence the aquifer's maximum potentiometric level would correspond to its upper boundary (located at the base of the debris flow deposits).

A case for diapiritic activity

The northern margin of the bulge located in the northeastern part of Chryse Chaos (Fig. 2) displays a graben in close proximity to a cluster of surface fractures, which is indicative of surface extension. Whereas the northern part of the bulge has a smooth texture, its southern part displays extensive surface pitting (Fig. 2b). Moreover, hills appear to be more closely spaced in the southern part of the bulge, where their long axes are aligned parallel to the margin of the bulge (Fig. 2). Assuming that the transition between the smooth hilly zone and the pitted hilly zone is not related to differences in mantle compositional properties, then a difference in the distribution of surface stress could account for this contact. A likely geologic scenario is that the bulge represents the uplifted surface of a large, rising diapir, and that at least some of the hills forming its surface may be the result of undulations along the top of the diapiric plume.

References

Rodriguez, J.A.P. et al. 2005. Outflow channel sources, reactivation, and chaos formation, Xanthe Terra, Mars. *Icarus* 175: 36-57.

Rodriguez, J.A.P. et al. 2006. Headward growth of chasmata by volatile outbursts, collapse, and drainage: Evidence from Ganges chaos, Mars. *Geophys. Res. Lett.* 33: L18203.

Scott, D.H. & Tanaka, K.L. 1986. *Geologic Map of the Western Equatorial Region of Mars*. U.S. Geol. Surv. Misc. Invest. Ser., Map I-1802-A.

Sharp, R.P. 1973. Mars: Troughed Terrain. *J. Geophys. Res.* 78: 4063-83.

Development of Soil Databases on the Territory of Permafrost-Affected Regions in Russia

D.I. Rukhovich, N.I. Belousova, P.V. Koroleva, E.V. Vil'chevskaya, L.G. Kolesnikova
V.V. Dokuchaev Soil Science Institute, Russian Academy of Agricultural Sciences, Moscow, Russia

Soil mapping in Russia has a rich and long history. Since the time of Dokuchaev, a system of soil maps of the country on different scales has been developed. The soil maps in Russia are compiled on very different scales: from the 1:10,000 scale for separate farms to small-scale maps (1:16 M) included in the national atlases.

Soil maps on the scale of 1:1 M and smaller are available for the whole territory of Russia. The 1:1 M state soil map is currently at the stage of its finalization and updating. Both the legends to separate pages of the map and the soil polygons are being updated. Soil maps on the scale of 1:4 M and smaller give the general picture of soil distribution in the country. The number of soil polygons on such maps is relatively small; these maps do not correlate well with the topographic bases and the materials of remote sensing (satellite imagery). The 1:2.5 M map occupies a transitional position in this series of soil maps of Russia. There are 35,000 soil polygons on this map and 305 mapping units in the legend, including 205 soil units and 100 names of different soil combinations (soil complexes).

Traditionally, soil maps for the territory of Russia are published with legends and special explanatory notes. However, these valuable reference materials usually do not contain quantitative information on the soil properties. A thorough study of soil classification systems applied on the maps of different years makes it possible to judge the geographic distribution of soils, but does not allow quantitative calculations and the development of special maps, for example, the maps of soil acidity or the maps of carbon reserves. The absence of quantitative soil characteristics lowers the efficiency of digital versions of soil maps on the territory of Russia. The creation of the geographic information system on Russian soils supplied with necessary attribute databases on the soil properties is one of the challenges for soil geography in Russia.

The soil databases have to include information on the soil profile horizonation and characteristic depths of soil horizons. Thus, podzolic soils are characterized by the following horizonation: O-A2-A2/Bt-Bt-BtC-C. The O horizon O is thin (5–10 cm), slightly decomposed leaf litter; the eluvial horizon A2 is a light-textured horizon with platy structure and very variable (5–50 cm) thickness. The transitional eluvial-illuvial whitish/brown horizon A2/Bt turns into the dark-brown or brown illuvial horizon Bt of 35–55 cm in thickness. The Bt horizon has a heavier texture than the A2 A2/Bt horizons and clear illuviation features in the form of clay coatings. It gradually turns via the BtC horizon into the parent rock C at a depth of 300–350 cm. Quantitative characteristics of the soil properties should be given for every genetic horizon. At present, it is feasible to perform this work on the basis of the "Soil Map of the Russian Federation" on the 1:2.5 M scale (Fridland et. al. 1988, Fig. 1).

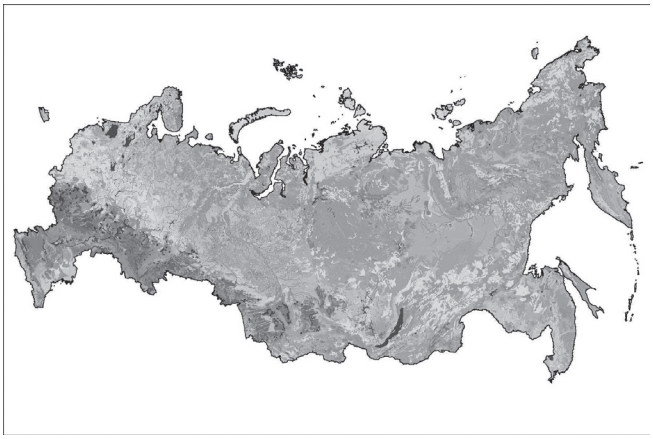

Figure 1. "Soil Map of the Russian Federation," 1:2.5 M scale.

Figure 2. Agroclimatic zoning of Russia.

The unified legend to this map is supplied with information on the horizonation of 205 soil units shown on the map. The legend to the map also contains information on the soil texture and on the character of parent materials. The textural part of the legend consists of 30 units. A given soil unit can be found on parent materials of different geneses and textures. On average, there are three texture classes corresponding to the given soil units. A combination "soil name + texture" gives us about 600 different soils shown on the map. The same genetic unit of soil developed from the parent materials of different textures normally has different quantitative characteristics of its properties, including the thickness of soil horizons, the humus content, base saturation, etc.

Each of the 600 combinations "genetic soil name + soil texture" has its own spatial distribution. Its properties vary in dependence on the particular climatic and geobotanic conditions. The character of climatic conditions can he judged from the special map of climatic zoning of Russia.

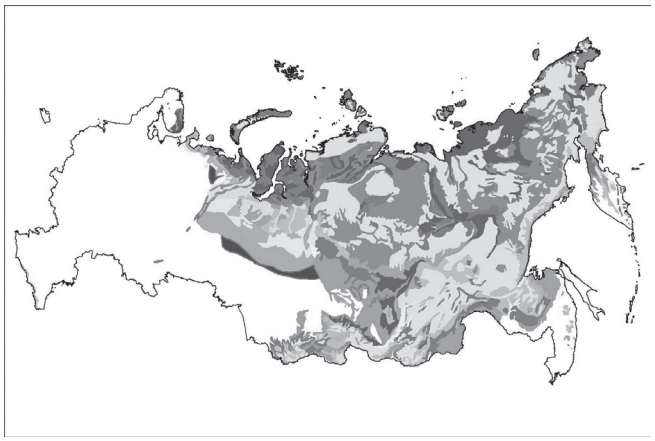

Figure 3. Permafrost distribution in Russia.

Figure 4. Area for which the soil database is being developed.

To reflect the natural variability in soil characteristics, the attribute database to the map should contain information on the range of variation of the particular soil properties. Thus, as a first approximation, the database is developed for 205 soil units in the legend. Then, it has to be refined, and the ranges of variation in the particular soil properties should be reduced with due account for the parent materials and bioclimatic conditions (natural zones). A digitized version of the "Map of the Agroclimatic Zoning of Russia" (Shahshko et. al. 1984) is shown in Figure 2.

One of the factors taken into account in the natural climatic zoning of Russia is the presence of permafrost. The map of permafrost distribution (Brown et al. 1997, Fig. 3) generally corresponds to the natural climatic zoning of Russia, though there are significant differences between the two maps in some regions.

At present, the attribute database to the "Soil Map of the Russian Federation" is being developed in the Dokuchaev Soil Science Institute; particular attention is paid to the territory of Siberia and the Far East of the country (Fig. 4). About 90% of the territory, for which this database is developed, lies within the permafrost zone of Russia.

The database includes information on the soil profiles within the particular combination of major factors: "genetic soil name + soil texture (parent material) + bioclimatic zone." The following information is included in the description of particular soil horizons: thickness, acidity, humus content, exchange capacity, etc. It is important that the soil database (Table 1), corrected for the particular provinces and parent materials from which a given soil is developed (with Podburs [Spodosols] as an example), gives us more adequate information on the values of the particular soil properties.

Table 1.

Natural and agricultural units	Parent rocks	Horizon	Humus content, %
Values from the database for the soil map on the 1:2.5 M scale			
Not differentiated by natural and agricultural zones and parent rocks		O1	21.3–73.0
		Bh	0.2–5.3
		BhC	0.2–2.1
Values from the corrected database			
North Siberia mountain region	acid metamorphic and igneous rocks	O1	60.0
		Bh	2.3
		BhC	1.5
	sandstone	O1	50.0
		Bh	2.0
		BhC	1.5
South Siberian mountain region	acid metamorphic and igneous rocks	O1	50.0
		Bh	3.2
		BhC	2.0

References

Brown, J., Ferrians, O.J., Jr., Heginbottom, J.A. & Melnikov, E.S. 1997. *Circum-Arctic Map of Permafrost and Ground-Ice Conditions*. Reston, VA, USA: U.S. Geological Survey, Circum-Pacific Map Series, CP-45 (ISBN 0-607-88745-1).

Fridland, V.M. (ed.) 1988. *Soil Map of the Russian Soviet Federative Socialistic Republic.* Scale of 1:2.5 M. Moscow, Russia: Central Administration for Geodesy and Cartography (GUGK), 16 sheets (in Russian).

Shashko, D.I., Gaydamaka, E.I., Kashtanov, A.N. et al. (eds.) 1984. *Natural and Agricultural Zoning of Lands of the U.S.S.R.* Map on a Scale of 1:8 M. Moscow, Russia: Central Administration for Geodesy and Cartography (GUGK) (in Russian).

Helical Piles for Power Transmission Lines: Case Study in Northern Manitoba, Canada

Mohammed Sakr
Almita Manufacturing Ltd., Ponoka, Alberta, Canada

Introduction

Helical piles have been used with great success to support power transmission lines. This is mainly due to the fact that helical piles offer significantly higher uplift resistance compared to other deep foundation options combined with their ease in installation in remote areas with relatively small equipment. Moreover helical piles can be loaded immediately after installation. This paper summarizes a case study for helical pile foundations supporting power transmission line located in Northern Manitoba, Canada, in which the site conditions, pile installation, and performance of foundations are described.

Subsurface Statigraphy

Pile load tests were carried out in two different soil conditions including either soft to firm clay or stiff high plastic clay with silt varves that extended along the entire embedded depth of piles. The groundwater level was measured at the existing ground surface. The undrained shear strength parameters obtained from undrained compression (CIUC) triaxial tests are summarized in Table 1. Residual undrained shear strength values were used to estimate the axial capacities of helical piles.

Screw Pile Configuration

Four pile load tests were carried out, including two compression and two uplift load tests. The helical pile configurations used for the pile load test program consisted of two piles with triple helixes spaced at either 2.5D or 3D, where D is the helix diameter, for guy anchors (i.e., to resist uplift loads) and two piles with either triple or four helixes for tower support (i.e., to support compression loads). Helical pile configurations are summarized in Table 2.

Table 1. Soil design parameters.

Soil Type	Undrained Shear Strength, C_u (kPa)	
	Peak	Residual
Soft to firm clay	30	18
Stiff clay	60	30

Pile Installation and Test Setup

The helical piles tested in this study were manufactured and installed by ALMITA Manufacturing Ltd. of Ponoka, Alberta. Helical piles were installed through the use of mechanical torque applied at the pile head. Torque applied at the pile head during pile installation was continuously recorded, and penetration depth was measured. Final measured torque at the end of pile installation and total embedment depths are also summarized in Table 2. The maximum torque measured during installation for triple helix and four helix piles C1 and C2 installed in stiff clay and soft to firm clay were similar. However, the maximum torque for guy anchor, T2, was higher than that of T1 by about 15% due to higher spacing ratio. The embedment depth for triple helix pile was 7.5 m, while the embedment depth for four helix pile was 10.8 m. For guy anchors, the embedment depths were 7.9 m for both piles.

Typical pile load test setup consisted of two reaction piles and a test pile. The reaction piles were positioned at

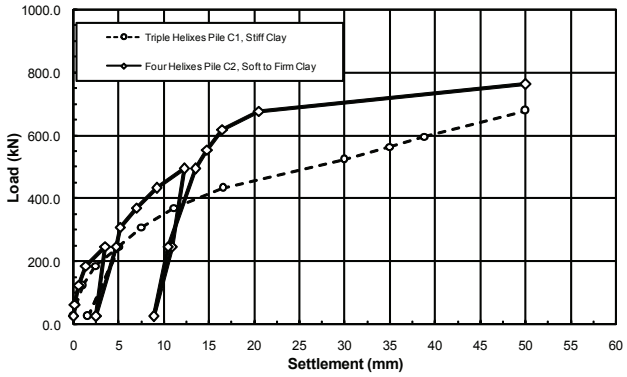

Figure 1. Load vs. settlement curves for axial compression load tests.

Table 2. Summary of pile installation.

Pile No	Pile Configuration		Test Type	Soil Type	Installation Torque kN.m (ft.lbs)	Embedment Depth m
	(Dia. (m) ×Length (m) × No. of helixes × Helix thickness (mm) × Helixes Dia. (m)	Spacing between helixes (m)				
C1	Triple helixes (0.324 × 8.5 × 3× 25.4× 0.813)	2.134	Compression	Stiff clay	94.9 (70,000)	7.5
T1	Triple helixes (0.219 × 8.5 × 3× 19× 0.711)	1.778	Uplift	Stiff clay	52.9 (39,000)	7.9
C2	Four helixes (0.324 × 11.6 × 4× 25.4× 0.864)	2.286	Compression	Soft to firm	94.9 (70,000)	10.8
T2	Triple helixes (0.219 × 8.5 × 3× 19× 0.711)	2.134	Uplift	Soft to firm	61.0 (45,000)	7.9

spacing of 6 m (about 4 helix diameter from the tested pile). Axial pile load tests were conducted according to the ASTM D-1143 Quick Load Test Method for Piles under Static Axial Compressive Load and ASTM D-3689 Quick Load Test Method for Piles under Static Axial Tensile Load. Loads were applied in increments of approximately 10% of the estimated pile capacity in 10-minute time intervals.

Load Test Results

Axial compressive pile capacities

The results of compressive load tests are presented in Figure 1 in the form of load settlement curves. It can be noted from Figure 1 that load settlements were linear at the initial part of the load-settlement curve up to a settlement of about 3 mm and corresponding loads of about 200 kN. At higher settlement levels, piles showed a nonlinear load-settlement followed by plunging failure at settlement of about 50 mm and corresponding loads of 677 kN and 772 kN for piles C1 and C2, respectively. The ultimate compressive load capacities for piles C1 and C2 are presented in Table 3. Cycles were carried out at loads of about 245 kN, and 490 kN indicated that the effect of cyclic loading had a minor effect on the response.

It is noted from Figure 1 that pile C2 with four helixes installed in stiff clay offered higher resistance compared to pile C1 with triple helixes installed in soft to firm clay. This behaviour suggested that the cylindrical shear failure mechanism is mobilized. In cylindrical shear failure mechanism, the load at pile head is resisted by three components including the skin friction along the shaft, the developed cylindrical shear resistance between the helixes, and the surrounding soil and end bearing of the bottom helix (for compression load tests) or the top helix(for uplift load tests). For pile C2 with four helixes, the cylindrical shear resistance component was considerably higher than that of pile C1 with triple helixes due to the larger surface area.

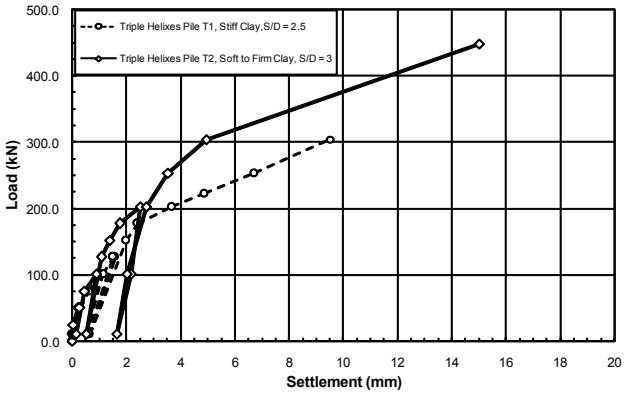

Figure 2. Load vs. displacement curves for axial tension (uplift) load tests.

Table 3. Pile load test results.

Pile No	Soil Conditions	Ultimate Pile Capacity (Q_{ult}) kN	Ultimate Settlement mm
Compression Test Results			
C1	Stiff clay	677	50
C2	Soft to firm	772	50
Tension (Uplift) Test Results			
T1	Stiff clay	370	15
T2	Soft to firm	445	15

Axial tension (uplift) pile capacity

The results of tensile (uplift) load tests are presented in Figure 2 in the form of load displacement curves for piles T1 and T2. Both piles had the same configurations, except pile T1 installed in stiff clay had a triple helixes spaced at 2.5D (1.77 m), where D is the diameter of the helix, while pile T2 installed in soft clay helixes were spaced at 3D (2.134 m). It can be seen from Figure 2 that load displacement curves for both piles were linear at the initial part of the uplift load up to a settlement of about 1 mm and load of about 100 kN. It should be noted that pile T1 installed in stiff clay showed softer response manifested by the larger displacement at the same load level compared to pile T2. However at higher displacement levels, the load-displacement curves were highly nonlinear, and pile T2 reached a plunging failure of about 445 kN at displacement level of about 15 mm (i.e., 2.5% of the helix diameter). The uplift load test for pile T1 was stopped at a load level of about 300 kN, while pile T2 was tested till failure. The ultimate capacity of pile T1 was extrapolated based on the shape of load-displacement curve, and the results are presented in Table 3.

Conclusions

The results of the axial compression and tension load tests performed in soft to firm or stiff clays demonstrated the suitability of helical pile foundations for the power transmission lines in Northern Manitoba. The results of the load testing program confirmed that the helical pile is a viable deep foundation option for construction of power transmission towers in remote areas and demonstrated their advantages.

The results of the full-scale load tests are also used to validate the theoretical model used for helical pile design installed in soft and stiff high plastic clays. The results indicated that the cylindrical shear failure mechanism controls the behavior of helical piles with spacing ratio up to 3 installed in clay materials.

References

ASTM D 1143-81. 1981. Standard Test Method for Piles Under Static Axial Compressive Load (Reapproved 1994). *Annual Book of ASTM Standards* 1997, Vol. 04.08: 95-105.

ASTM D 3689-90. 1990. Standard Test Method for Individual Piles Under Static Axial Tensile Load; (Reapproved 1995). *Annual Book of ASTM Standard,* 1997, Vol. 04.08: 366-375.

Mountain Permafrost Parameters Simulated by Regional Climate Models

Nadine Salzmann
National Center for Atmospheric Research (NCAR/ISSE), Boulder, CO, USA
Christian Hauck
Institute for Meteorology and Climate Research, Karlsruhe Institute of Technology (KIT), Germany
Linda O. Mearns
National Center for Atmospheric Research (NCAR/ISSE), Boulder, CO, USA

Introduction

Permafrost as a thermal phenomenon is strongly affected by the changes in the atmospheric condition (Haeberli & Beniston 1998). However, for a significant time of the year the seasonal snow cover decouples the ground from the atmosphere and thus considerably influences the ground thermal regime (Zhang 2005). As a consequence, permafrost conditions are affected by climatic change twofold: directly by changes in the atmospheric condition, and indirectly by the changes in the duration and dynamics of the seasonal snow cover. The sensitivity of permafrost on these two interacting variables is not clear in detail so far, and neither is how the atmosphere and thus also the seasonal snow cover will change.

Snow accumulation and snowmelt in mountain topography have nonuniform and high spatial variability mainly caused by the local topography, which interacts among others with atmospheric stability, precipitation, moisture distribution, radiation, wind and avalanches. Measuring and modeling of snow parameters in complex mountain topography is thus a challenging task. Among the most promising tools to simulate climate variables in mountain areas are Regional Climate Models (Leung & Qian 2003). Due to their higher spatial resolution compared to GCM, they better resolve the atmospheric dynamics caused by the heterogeneous surfaces such as mountain topographies. The benefits of using RCM simulations for permafrost modeling in complex high mountain topography have been demonstrated by Salzmann et al. 2007a,b. However, the performance of snow representation in RCMs related to permafrost has not been validated in detail so far and most likely differs for different regions and models.

With large projects such as NARCCAP in North America or PRUDENCE and ENSEMBLES in Europe, there is now increasing RCM output available for further use by the impact community. However, the performance of these model outputs must be proven for specific applications because model performance is not simply transferable between variables and regions.

This study aims at investigating the performance of RCMs to simulate seasonal snow cover in mountain environments, with regard on further modeling of subsurface processes.

Study Site and Data

Study site

We focus on a relatively small area (about 500 km2) in the Colorado Rocky Mountains—the Upper Colorado River Basin (UCRB). This basin is surrounded by some of the highest peaks of the Rocky Mountains. Because the streamflow of this area is a major contributor to the Colorado River's annual run off, this area is relatively well equipped with snow measurement stations (see next section).

Data

All RCM simulations used in this study have been performed within the North American Regional Climate Change Program NARCCAP (http://www.narccap.ucar.edu/). Here, we analyze only NCEP-Reanalyses driven runs, since they allow us to compare the RCM output directly with observations. They are all run with a grid spacing of 50 km and cover the UCRB by 10 grid boxes. The following RCM simulations are used here:

- ECPC (Experimental Climate Prediction Center): Scripps Institution of Oceanography, La Jolla, CA, USA.
- MRCC (Modèle Régional Canadien du Climat): Ouranos Consortium, Montreal (Quebec), Canada.
- RegCM3 (REGional Climate Model): UC Santa Cruz, ITCP, USA.

The *observations* we use are point measurement from SNOTEL stations. There are 45 stations located in the UCRB, many of them providing data since 1981.

In addition to the SNOTEL data, we use high-resolution reanalyses (NARR; North American Regional Reanalyses) for comparison purposes. NARR has a grid spacing of 32 km and covers UCRB by 26 grid boxes. NARR data are supposed to be especially valuable for hydrological studies.

First Analysis

We have analyzed the total volume of accumulated precipitation for the individual grid boxes and the average of all grid boxes covering the UCRB. The RCM outputs were compared to SNOTEL and NARR data. The total volume of accumulated precipitation and their temporal distribution showed overall good agreement.

We also compared the 2 m air temperature. The NARCCAP runs simulated generally higher air temperature than NARR, and particularly than SNOTEL.

The results for the annual snow cycles for two time periods are shown in the following Figures. Most obvious are the deviations between NARCCAP (and NARR!) and SNOTEL. Some of these deviations can certainly be explained by grid elevation differences between NARCCAP and SNOTEL, which is also apparent from air temperature, where

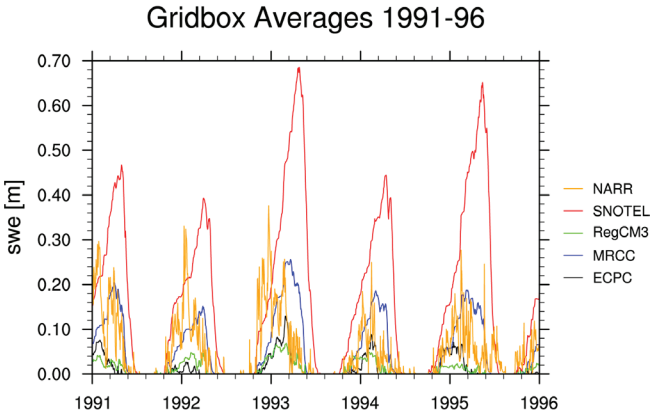

Figure 1.

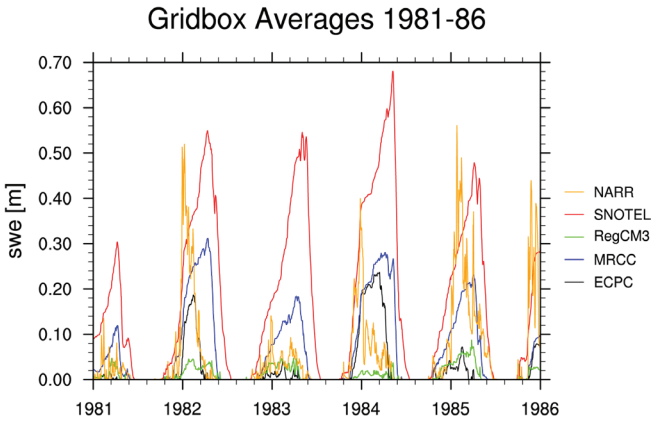

Figure 2.

SNOTEL overall shows lowest temperatures. Furthermore, the SNOTEL sites are generally located where the snow pack lasts long. Therefore, it can be assumed that SNOTEL observations slightly overestimate SWE relatively to the average of SWE over the whole region of the UCRB. Also, RegCM3 produces small SWE values in each year, which partly can be explained by the too-high air temperature that is simulated by RegCM3 (not shown).

Perspectives

For permafrost, among the most significant parameters of the seasonal snow cover are the timing and duration of significant snow depth. Therefore, in a next step, we will compare the duration of the seasonal snow cover and try to associate the deviations to model intern explanations (e.g., air temperature). Furthermore, we will apply the time series of the RCM simulations as input for a water/heat-coupled soil model (COUP; Janson & Karlberg 2004) to simulate ground surface temperatures, which are not provided by the NARCCAP outputs. Similar analyses are planned for the Schilthorn area in the Swiss Alps with RCM simulations from the PRUDENCE and ENSEMBLES projects.

Acknowledgments

This study is financially supported by the Swiss National Science Foundation's program for prospect researcher.

We acknowledge the NARCCAP modeling groups for providing us preliminary simulation results.

NARR data are provided by the NOAA/OAR/ESRL PSD, Boulder, Colorado, USA, http://www.cdc.noaa.gov/

SNOTEL data are provided by Natural Resources Conservation Service, United States Department of Agriculture.

References

Haeberli, W. & Beniston, M. 1998. Climate change and its impact on glaciers and permafrost in the Alps. *Ambio* 27(4): 258-265.

Jansson, P.-E. & Karlberg, L. 2004. *Coupled Heat and Mass Transfer Model for Soil-Plant-Atmosphere Systems*. Stockholm: Royal Institute of Technolgy, Dept. of Civl and Environmental Engineering, 435 pp.

Leung, L.R. & Qian, Y. 2003. The sensitivity of precipitation and snowpack simulations to model resolution via nesting in regions of complex terrain. *J. Hydrometerology* 4: 1025-1043.

Salzmann, N., Frei, C., Vidale, P.L. & Hoelzle, M. 2007a. The application of Regional Climate Model output for the simulation of high-mountain permafrost scenarios. *Global and Planetary Change* 56: 188-202, doi:10.1016/j.gloplacha.2006.07.006.

Salzmann, N., Noetzli, J., Hauck, C., Gruber, S., Hoelzle, M. & Haeberli, W. 2007b. Ground-surface temperature scenarios in complex high-mountain topographies based on Regional Climate Model results. *Journal of Geophysical Research–Earth Surface* 112: F02S12, doi:10.1029/2006JF000527.

Zhang, T. 2005. Influence of the seasonal snow cover on the ground thermal regime: an overview. *Rev. Geophys*. 43: RG4002, doi:10.1029/2004RG000157.

Permafrost Dynamics and Landscape Changes in a Subarctic Peat Plateau, Northern Sweden

A.B.K. Sannel
Department of Physical Geography and Quaternary Geology, Stockholm University, Sweden
P. Kuhry
Department of Physical Geography and Quaternary Geology, Stockholm University, Sweden

Introduction

Perennially frozen peatlands in subarctic regions are sensitive to a warming climate, since permafrost temperatures are close to the 0°C mean annual isotherm. Few monitoring studies have been performed of permafrost dynamics in subarctic peatlands because of their often remote location, the expensive logistics, and the harsh field conditions.

Rapid and extensive permafrost thawing in bogs and mixed mires underlain by permafrost in northern Sweden has been recorded by Christensen et al. (2004). Zuidhoff (2002) conclude that in palsas block erosion, thermokarst and wind erosion are the most important degradational processes involved in the decay. Sollid & Sørbel (1974) found that where frozen palsa plateaus are in direct contact with water, the permafrost core is undermined, causing cracks in the peat. The peat then slips sideways, creating a steep erosion edge. This edge gradually works its way in towards the central part of the palsa.

In a modeling study from Russia, Mazhitova et al. (2004) suggest a 20–30 cm deepening of the active layer in peat plateaus until 2080 as a result of future global warming. It is not only the air temperature that affects the thaw depth; precipitation, snow depth, the ice content in the ground, and other hydrogeological conditions are also important factors for the active layer distribution (Oberman & Mazhitova 2001). Long-term ecosystem monitoring is important for predicting the behaviour of subarctic peatlands under the expected future warmer and wetter climate conditions.

Aim, Methods, and Study Area

The main objective of this project is to study local climate and ground dynamics in a subarctic peat plateau/thermokarst lake complex in order to get a better understanding of how these permafrost peatlands will respond to climate change. Which factors and mechanisms cause the collapse of peat plateaus into thermokarst lakes? Why does the erosion occur only in certain parts of the peat plateau and along certain parts of the thermokarst lake shoreline? How sensitive are these ecosystems to global warming? At the peat plateau/thermokarst lake complex in Tavvavuoma (68°28′N, 20°54′E), northern Sweden, permafrost temperature and landscape dynamics are studied through monitoring of ground temperatures, meteorological data, and snow depth (since 2005), and a time series analysis of aerial photographs and satellite images (from 1963 to 2003). On the peat plateau, snow depth and ground temperatures down to 2 m depth are recorded at 9 different microsites; on the peat plateau, at the eroding edge of the peat plateau, in the thermokarst lake, and in a nearby non-permafrost fen (Fig. 1, 2, 3). A 20 m deep borehole for ground temperature measurements is planned. Air temperature, precipitation, and wind data are recorded on top of the plateau. Snow depth is monitored by using a stationary digital camera that records one image per day.

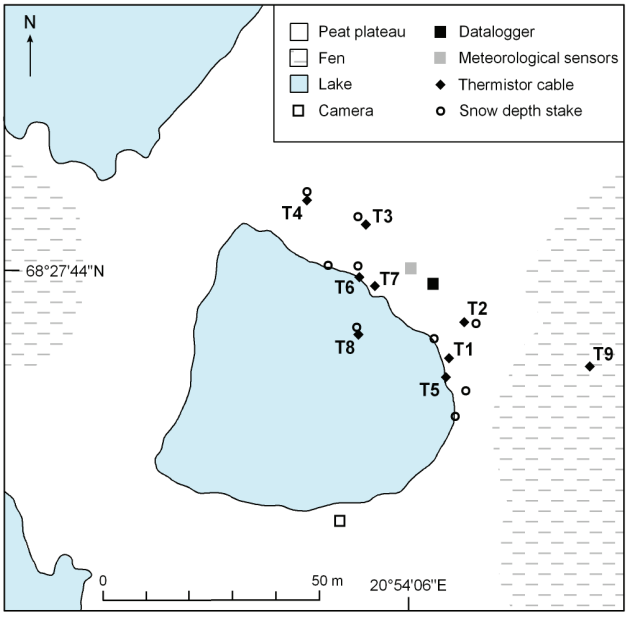

Figure 1. Map showing the location of thermistor cables and snow depth stakes at the monitoring site in Tavvavuoma.

Preliminary Results and Discussion

A comparison of panchromatic aerial photographs with a recent IKONOS image shows that, on a landscape level, major thermokarst drainage has occurred between 1963 and 2003. Along the present thermokarst lake shorelines, field observations show that erosion is active. Ground subsidence of up to 11 cm in 2 years has been observed along the shoreline, whereas the central parts of the monitored peat plateau surface appear to remain stable. The monitoring data are indicating that the permafrost in the peat plateau is thawing out, probably due to recent warming. On the central, dry peat plateau sites, the ground temperatures below 1 m depth are just below 0°C, implying that the peat plateau will be very sensitive to any further increase in temperature. Winter observations indicate very thin snow cover at the top of the peat plateau compared to the edges and in the thermokarst depressions, showing the importance of snow distribution for the permafrost (Fig. 4).

Figure 2. The peat plateau/thermokarst lake complex with monitoring equipment.

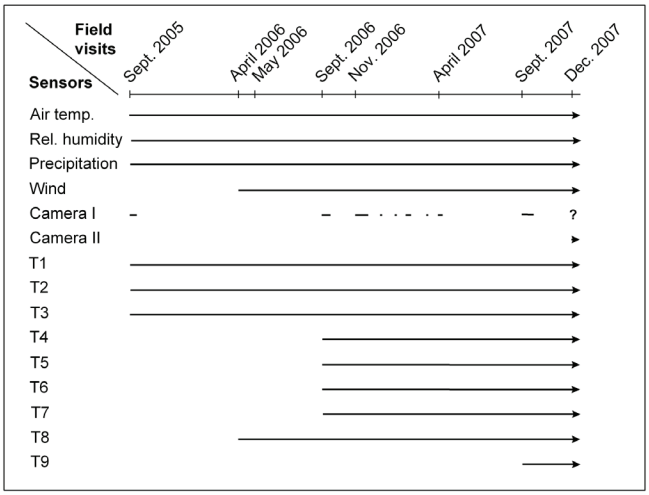

Figure 3. Ongoing monitoring activities at the peat plateau/thermokarst lake complex in Tavvavuoma. Thermistor cables T1 and T5–T7 have thermistors at 2 cm, 10 cm, 25 cm, 50 cm, and 100 cm depth. Thermistor cables T2–T4 and T9 also have thermistors at 150 cm and 200 cm depth. T8 has thermistors located 70 cm, 110 cm, 150 cm, 190 cm, and 230 cm below the lake sediment surface (for location of the thermistor cables, see Fig. 1a).

Warmer temperatures as well as increased precipitation in the winter can cause thawing of the permafrost, resulting in collapse of the peat plateau and increased methane emissions from thermokarst lakes. However, thawing of the permafrost can also result in drainage of thermokarst lakes and renewed peat accumulation.

Acknowledgments

Financial support has been achieved by the Göran Gustafsson Foundation, Foundation Lars Hiertas Minne, Helge Ax:son Johnson Foundation and Swedish Society for Anthropology and Geography. Thanks also to Prof. Peter Jansson at Stockholm University!

Figure 4. Snow distribution at the edge of the thermokarst lake and on top of the peat plateau, December 2007.

References

Christensen, T.R., Johansson, T., Åkerman, H.J., Mastepanov, M., Malmer, N., Friborg, T., Crill, P. & Svensson, B.H. 2004. Thawing sub-arctic permafrost: Effects on vegetation and methane emissions. *Geophysical Research Letters* 31: L04501, doi:10.1029/2003GLO18680.

Mazhitova, G., Karstkarel, N., Oberman, N., Romanovsky, V. & Kuhry, P. 2004. Permafrost and infrastructure in the Usa Basin (northeast European Russia): Possible impacts of global warming. *Ambio* 33(6): 289-294.

Oberman, N.G. & Mazhitova, G.G. 2001. Permafrost dynamics in the north-east of European Russia at the end of the 20th century. *Norsk Geografisk Tidsskrift* 55: 241-244.

Sollid, J.L. & Sørbel, L. 1974. Palsa bogs at Haugtjørnin, Dovrefjell, South Norway. *Norsk Geografisk Tidsskrift* 28: 53-60.

Zuidhoff, F.S. 2002. Recent decay of a single palsa in relation to weather conditions between 1996 and 2000 in Laivadalen, northern Sweden. *Geografiska Annaler* 84A(2): 103-111.

Variable Peat Accumulation Rates in Stable Subarctic Peat Plateaus, West-Central Canada

A.B.K. Sannel
Department of Physical Geography and Quaternary Geology, Stockholm University, Sweden
P. Kuhry
Department of Physical Geography and Quaternary Geology, Stockholm University, Sweden

Introduction

Peatland ecosystems located in the boreal forest and tundra biomes contain a large and significant pool of soil organic carbon. The carbon storage in boreal and subarctic peat deposits is approximately 455 Pg C, representing one-third of the total world pool of soil carbon (Gorham 1991).

As a result of global warming, the highest increases in temperature are predicted to take place at high northern latitudes. For most permafrost regions a reduction in permafrost area and an increase in thaw depth are expected (ACIA 2004, IPCC 2007). Permafrost peatlands are sensitive ecosystems expected to respond rapidly to changes in climate. Since perennially frozen peatlands in the sporadic and discontinuous permafrost zones are already near thawing, they are most sensitive to climate changes (Tarnocai 2006). Climate warming may affect permafrost peatlands in many ways: permafrost degradation, formation of thaw lakes, increased thaw depth, drier peat surfaces, changes in carbon accumulation, methane emissions, plant communities, hydrology, and fire frequency (e.g., Gorham 1991, Zoltai 1995, ACIA 2004).

An increased knowledge of permafrost conditions and carbon accumulation rates in subarctic permafrost peatlands throughout the Holocene is important for understanding how these ecosystems might respond to the predicted future climate changes.

Aim, Study Area, and Methods

The aim of this study is to better understand the long-term carbon dynamics in subarctic peat plateaus in relation to vegetation and permafrost conditions.

Selwyn Lake and Ennadai Lake are located within the low subarctic ecoclimatic region in west-central Canada, where the climate is characterized by very cold winters and short, warm summers (Fig. 1).

The peat profile SL1 (59º53′N, 104º12′W) was collected in the discontinuous permafrost zone from a treed peat plateau bog calving into Selwyn Lake (Fig. 2). The peat profile EL1 (60º50′N, 101º33′W) was collected in the continuous permafrost zone from a polygonal peat plateau on the western shore of a small lake located 1 km west of Ennadai Lake (Fig. 3).

In both peat profiles (SL1 and EL1), vegetation succession and high-resolution peat and carbon accumulation rates have been studied through plant macrofossil analyses and extensive AMS radiocarbon dating. Bulk densities were measured throughout the profiles as well as carbon (C) and nitrogen (N) content.

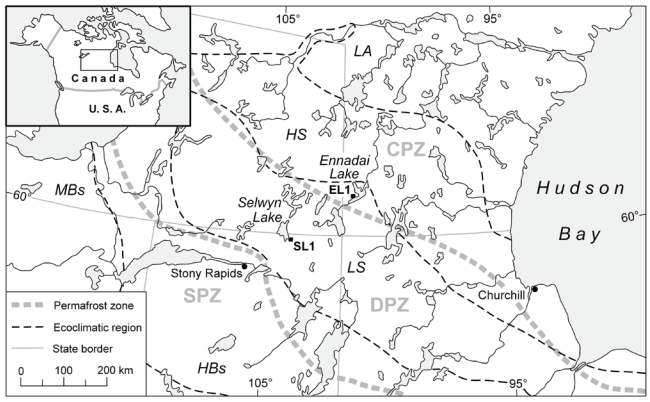

Figure 1. Location of Selwyn Lake and Ennadai Lake, permafrost zonation, and ecoclimatic regions in west-central Canada. CPZ = continuous permafrost zone, DPZ = discontinuous permafrost zone and SPZ = sporadic permafrost zone (after Zoltai 1995). LA = low arctic, HS = high subarctic, LS = low subarctic, HBs = subhumid high boreal and MBs = subhumid mid-boreal ecoclimatic region (after Ecoregions Working Group 1989).

Figure 2. The collection site of peat profile SL1 at a forested peat plateau calving into Selwyn Lake (Photo: © P. Kuhry).

Results and Discussion

Peat formation at the two sites began around 6600–5900 cal yr BP, and permafrost conditions have prevailed in the peat plateaus since permafrost aggradation occurred between 5600–4500 cal yr BP (Sannel & Kuhry in press). An important characteristic of these peat plateaus are the alternating layers of *Sphagnum fuscum* and rootlet peat layers. *Sphagnum* stages represent slightly more moist surface conditions than rootlet stages, which mainly contain roots, *Picea* needles, and leaves from ericaceous shrubs. The long-term peat and carbon accumulation rates for both the studied peat profiles are 0.30–0.31 mm/yr and 12.5–12.7

Figure 3. The collection site of peat profile EL1 at a polygonal peat plateau near Ennadai Lake (Photo: © P. Kuhry).

gC/m^2yr, which is coherent with previously reported data from subarctic Canadian peatlands by Tarnocai (1988) and Gorham (1991).

Extensive radiocarbon dating of the peat profile SL1 shows that accumulation rates are variable over time and that abrupt shifts in accumulation rates occur when the vegetation composition in the peat changes. Vertical peat growth is generally 4–5 times higher in *Sphagnum* peat than in rootlet peat. Also, the net carbon accumulation is 3–4 times higher in *Sphagnum* peat. The lowest accumulation rates are recorded in rootlet layers that have been subjected to fires. *Sphagnum* peat represents 78% of the peat profile height, but only 44% of the time since the peatland was formed (Sannel & Kuhry submitted).

In both EL1 and SL1, C/N ratios in *Sphagnum* peat are relatively high (around 90–140) and remain rather stable throughout most of the profiles, indicating that the organic material that has been incorporated into the permafrost has a low degree of decomposition (Sannel & Kuhry submitted). Persistently dry surfaces as a result of stable permafrost conditions since the peat plateaus developed suggest that these peatlands have been negligible as methane sources throughout their history. Therefore, generally they have represented a negative net radiative climatic forcing over time. However in a future warmer climate, permafrost degradation may cause wetter surface conditions, formation of collapse scars, and thermokarst lakes, and turn these areas into methane sources.

Acknowledgments

Financial support has been given by the K&A Wallenberg Foundation, Ymer-80 Foundation, Royal Swedish Academy of Science, Ahlmann Foundation, Vice-President Central Research Fund, EU GLIMPSE project, and Swedish Research Council.

References

ACIA (Arctic Climate Impact Assessment). 2004. *Impacts of a Warming Arctic*, 1st ed. Cambridge University Press, 139 pp.

Ecoregions Working Group. 1989. *Ecoclimatic regions of Canada, First Approximation*. Ecological Land Classification Series, No. 23. Canada, Ottawa: Sustainable Development Branch, Wildlife Service, Environment, 118 pp.

Gorham, E. 1991. Northern peatlands – role in the carbon-cycle and probable responses to climatic warming. *Ecological Applications* 1(2): 182-195.

IPCC (Intergovernmental Panel on Climate Change). 2007. *Climate Change 2007: The Scientific Basis. Summary for Policymakers*. Geneva: IPCC Secretariat, 21 pp.

Sannel, A.B.K. & Kuhry, P. in press. Long-term stability of permafrost in subarctic peat plateaus, west-central Canada. *The Holocene* 18(4).

Sannel, A.B.K. & Kuhry, P. submitted. Peat growth and decay dynamics in subarctic peat plateaus, west-central Canada. *Boreas*.

Tarnocai, C. 1988. Wetlands in Canada: Distribution and characteristics. In: H.I. Schiff & L.A. Barrie (eds.), *Global change, Canadian Wetlands Study, Workshop Report and Research Plan*. York University, New York: Canadian Institute for Research in Atmospheric Chemistry, 21-25.

Tarnocai, C. 2006. The effect of climate change on carbon in Canadian peatlands. *Global and Planetary Change* 53(4): 222-232.

Zoltai, S.C. 1995. Permafrost distribution in peatlands of west-central Canada during the Holocene warm period 6000 years BP. *Geographie Physique et Quaternaire* 49(1): 45-54.

^{14}C Age of Fossil Wood Remains Buried by an Inactive Rock Glacier, Upper Ticino Area (Southern Swiss Alps)

Cristian Scapozza
Institute of Geography, University of Lausanne, Switzerland
Christophe Lambiel
Institute of Geography, University of Lausanne, Switzerland
Emmanuel Reynard
Institute of Geography, University of Lausanne, Switzerland
Marco Antognini
Natural History Museum of the Canton Ticino, Lugano, Switzerland
Philippe Schoeneich
Institute of Alpine Geography, University of Grenoble, France

Introduction

Within the framework of permafrost investigations in the Southern Swiss Alps of the Canton Ticino (see Scapozza & Reynard in press), eight fossil wood stem remains were found at a depth of 1 m below surface at the front of the Piancabella rock glacier (Fig. 1), situated in the Eastern part of the Blenio Valley (Lepontine Alps of the Ticino, Southern Switzerland).

Previously, ^{14}C datings of soils and moss buried by a rock glacier in the European Alps have been discussed, for example, by Mortara et al. (1992), Giraudi & Frezzotti (1997), Calderoni et al. (1998), Haeberli et al. (1999), and Dramis et al. (2003).

Site and Sampling

The Piancabella rock glacier (46°27′N, 9°01′E) has developed within a former east-facing glacial cirque from perennially frozen scree slopes at 2650–2460 m a.s.l. According to geomorphological observations and mapping, frequency-domain electromagnetic lateral mapping and 2D resistivity profiling (Geonics EM-16R and EM-31), direct current (DC) resistivity vertical soundings, thermal prospecting and space-borne radar interferometry analysis, Piancabella rock glacier is currently inactive (Scapozza 2008). The rock glacier surface is completely lacking of vascular plants.

Eight fossil wood stem remains were found beneath 1 m of coarse blocky sediments (Fig. 2). They were covered with sand and silt. The longest wood stem is 36 cm long and 6 cm large.

Radiocarbon Dating

Necessary preparation and pre-treatment of the sample material for radiocarbon dating was carried out by the ^{14}C laboratory of the Department of Geography at the University of Zurich (GIUZ). The dating itself was done by AMS (accelerator mass spectrometry) with the tandem accelerator of the Institute of Particle Physics at the Swiss Federal Institute of Technology Zurich (ETH).

Radiocarbon dating of the sample PIANCA2 gives a mean conventional ^{14}C age of 845 ± 50 y BP (UZ-5545/ETH-34417). Calibration of the radiocarbon dating, performed with the software OxCal 3.10 (Bronk Ramsey 2005) using the radiocarbon calibration curve IntCal04 (Reimer et al. 2004), gave, with statistical probability of 95.4%, an age of 1040–1280 cal AD (790 ± 120 cal BP).

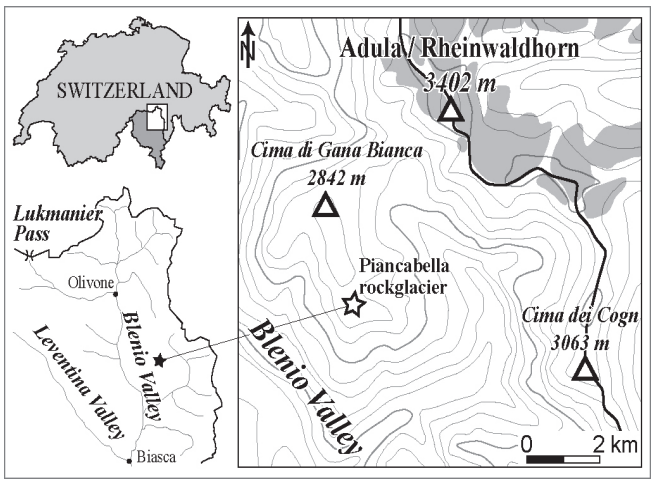

Figure 1. Geographical location of the Piancabella rock glacier.

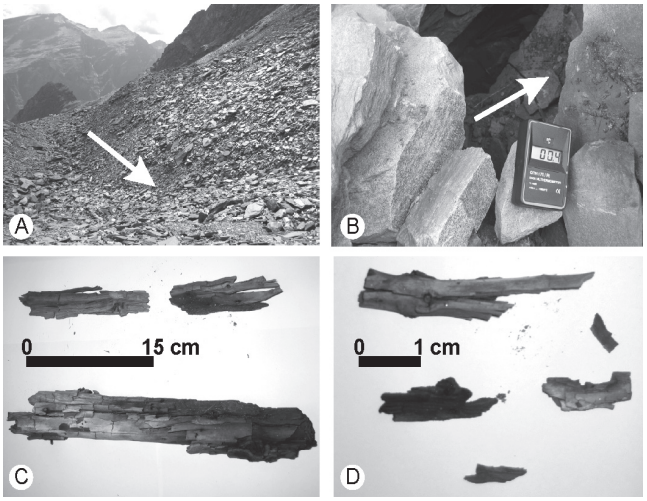

Figure 2. A–B: Sample site. C–D: Wood stem remains.

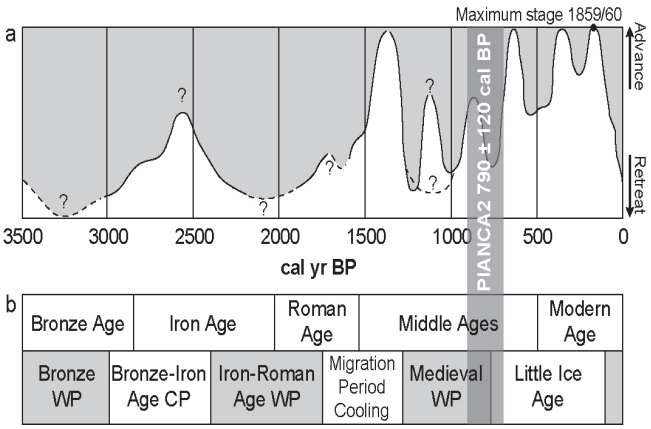

Figure 3. Comparison of the radiocarbon age of the sample PIANCA2 with (a) the Greater Aletsch glacier fluctuations in the last 3500 years, established by Holzhauser et al. (2005), and (b) the chronological and climatic framework of the Swiss Alps since the middle of the Bronze Age (Grosjean et al. 2007). WP: warm/dry; CP: cold/moist.

This age range corresponds to the end of the Medieval Climatic Optimum, a warm and dry period preceding the Little Ice Age cooling period (Grosjean et al. 2007). According to the Greater Aletsch glacier fluctuations established by Holzhauser et al. (2005), the period corresponds to a retreat phase of the alpine glaciers, with a front position similar to today (Fig. 3).

Discussion and Conclusions

Chronologic data suggest that the Piancabella rock glacier probably became inactive during the Medieval Climatic Optimum. The position of the wood remains at the front of the rock glacier confirms that it did not advance anymore after the Medieval Climatic Optimum. If we consider that climatic inactivation stops aggradation of ice in rock glacier permafrost, it confirms that ice within rock glaciers is probably several centuries old and by far predates recent climatic events such as the Little Ice Age, as it was pointed out by Haeberli et al. (1999).

Another hypothesis is possible. During the Medieval Climatic Optimum, the rock glacier front would have been several tens of meters higher in the slope. In this case, wood burial can be interpreted as the result of an advance or a reactivation of the Piancabella rock glacier during the Little Ice Age. Following these hypotheses, wood stems would have been exposed at the soil's surface for several decades before being buried.

The Piancabella rock glacier is currently situated close to the present regional lower limit of discontinuous permafrost (Scapozza 2008). It is, therefore, very difficult to determine which of the two hypotheses is likely realistic. Following the first hypothesis, ^{14}C dating of wood remains found at the front of the Piancabella inactive rock glacier could constitute the first absolute age determination of an alpine rock glacier inactivation.

References

Bronk Ramsey, C. 2005. *OxCal Program, v. 3.10*. Radiocarbon Accelerator Unit, University of Oxford.

Calderoni, G., Guglielmin, M. & Tellini, C. 1998. Radiocarbon dating and postglacial evolution, Upper Valtellina and Livignese Area (Sondrio, Central Italian Alps). *Permafrost and Periglacial Processes* 9: 275-284.

Dramis, F., Giraudi, C. & Guglielmin, M. 2003. Rock glacier distribution and paleoclimate in Italy. *Proceedings of the 8th International Conference on Permafrost, Zurich, Switzerland, July 21–25, 2003*: 199-204.

Giraudi, C. & Frezzotti, M. 1997. Late Pleistocene glacial events in the Central Apennine, Italy. *Quaternary Research* 483: 280-290.

Grosjean, M., Suter, P.J., Trachsel, M. & Wanner H. 2007. Ice-borne prehistoric finds in the Swiss Alps reflect Holocene glacier fluctuations. *Journal of Quaternary Science* 22: 203-207.

Haeberli, W., Kääb, A., Wagner, S., Vonder Mühll, D., Geissler, P., Haas, J.N., Glatzel-Mattheier, H. & Wagenbach, D. 1999. Pollen analysis and ^{14}C age of moss remains in a permafrost core recovered from the active rock glacier Murtèl-Corvatsch, Swiss Alps: geomorphological and glaciological implications. *Journal of Glaciology* 43: 1-8.

Holzhauser, H., Magny, M. & Zumbühl, H.J. 2005. Glacier and lake-level variations in west-central Europe over the last 3500 years. *The Holocene* 15: 789-801.

Mortara, G., Orombelli, G., Pelfini, M. & Tellini, C. 1992. Suoli e suoli sepolti olocenici per la datazione di eventi geomorfologici in ambiente alpino: alcuni esempi tratti da indagini preliminari in Val d'Aosta. *Il Quaternario* 52: 135-146.

Reimer, P.J., Baillie, M.G., Bard, E. & others, 2004. IntCal04 Terrestrial Radiocarbon Age Calibration, 0-26 cal kyr BP. *Radiocarbon* 46: 1029-1058.

Scapozza, C. 2008. *Contribution à l'étude géomorphologique et géophysique des environnements périglaciaires des Alpes Tessinoises orientales*. MSc Thesis, Inst. of Geography, Univ. of Lausanne. Published February 28, 2008, on http:/doc.rero.ch/

Scapozza, C. & Reynard, E. (in press). Rock glaciers e limite inferiore del permafrost discontinuo tra la Cima di Gana Bianca e la Cima di Piancabella (Val Blenio, TI). *Geologia Insubrica*.

Interactions Between Permafrost and the Carbon Cycle

Kevin Schaefer
National Snow and Ice Data Center, University of Colorado
Tingjun Zhang
National Snow and Ice Data Center, University of Colorado
Lixin Lu
Cooperative Institute for Research in Environmental Sciences, University of Colorado
Ian Baker
Department of Atmospheric Science, Colorado State University

Introduction

The net terrestrial carbon flux or Net Ecosystem Exchange (NEE) is the small difference between two large gross fluxes: R – GPP, where *R* is ecosystem respiration and *GPP* is Gross Primary Productivity or photosynthesis. GPP for plant growth removes CO_2 from the atmosphere; R, due to microbial decay of dead plant material, returns CO_2 to the atmosphere. A positive NEE indicates a net flux into the atmosphere, and a negative NEE indicates a net biological uptake of CO_2. Microbial decay is slow in permafrost regions due to low temperatures, resulting in a large buildup of organic material both in the active layer and the underlying permafrost. About 950 Gt of carbon (equivalent to current atmospheric CO_2) was frozen into permafrost during the last ice age, protected from decay and effectively removed from the active carbon cycle (Zimov et al. 2006).

Climate warming across the high northern latitudes has resulted in widespread permafrost degradation (Zhang et al. 2005). Future projections indicate a loss of ~90% of near surface permafrost by 2100 (Lawrence & Slater 2005). As the permafrost thaws, the frozen organic matter will decay, rapidly increasing atmospheric CO_2 in addition to anthropogenic emissions. To predict the fate of this frozen carbon, we must understand how snow cover, soil thermal regime, and soil freeze-thaw processes influence the carbon cycle in regions of permafrost.

To assess these interactions, we simulated permafrost and carbon cycle dynamics across the Northern Hemisphere using the Simple Biosphere Carnegie-Ames-Stanford Approach (SiBCASA) driven by the NCEP reanalysis at 2x2 degrees. Correlations between output model variables identified key relationships between simulated soil temperatures, active layers, photosynthetic uptake, respiration fluxes, and biomass.

SiBCASA computes surface energy and carbon fluxes at 15-minute time steps using the Community Land Model snow and soil models and the CASA biogeochemical model (Schaefer et al. 2008). To improve soil thermodynamics, we (1) added the Sturm et al. (1995) snow classifications to account for depth hoar effects on snow thermal properties; (2) added the effects of organic matter to soil properties to account for the insolating effect of peat; and (3) extended the soil model depth from 3.4 m to 15 m. To reach steady state, we ran three simulations from 1982 to 2007 (75 years total) using the final soil temperatures and soil moistures from one simulation as initial values to the next. We algebraically calculated steady state carbon pool sizes using time average decay rate constants.

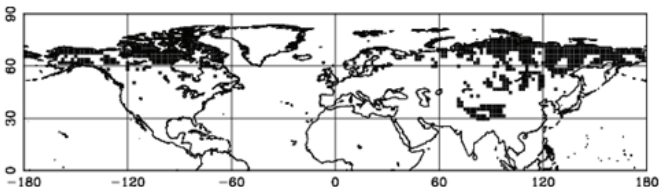

Figure 1. Simulated permafrost in Northern Hemisphere (black).

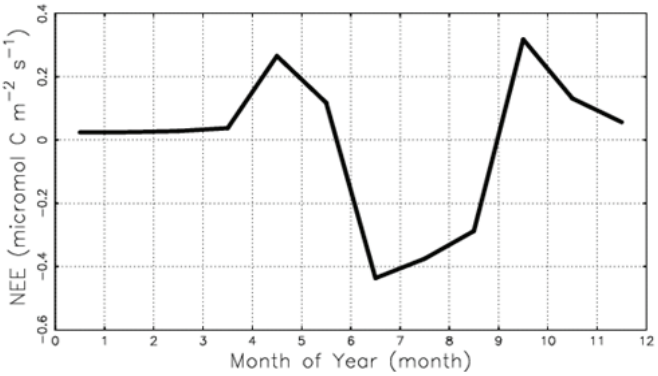

Figure 2. Seasonal cycle in simulated NEE at 70N and 120E.

Results

SiBCASA produced a fairly realistic permafrost distribution for the Northern Hemisphere (Fig. 1). The wave-like pattern in Siberia results from a similar pattern in NCEP precipitation, which is an artifact of the spectral representation of wind fields (Schaefer et al. 2004). Bands of heavy precipitation strongly insulate the soil in winter, resulting in warmer soil temperatures and preventing permafrost formation.

Figure 2 shows a typical seasonal cycle in NEE for a representative point in Siberia (70N, 120E). The NEE shown in Figure 2 is typical in both magnitude and seasonal variation for permafrost regions across both North America and Eurasia. Most permafrost areas are near steady state and the carbon fluxes balanced, meaning that NEE ~ 0 when averaged over several years. All GPP and nearly all R occur in the short arctic summer, peaking at about 6 μmol C m^{-2} s^{-1} in July. GPP is stronger than R in summer due to nearly

continuous daylight, resulting in net CO_2 uptake (negative NEE). In spring and fall, cooler temperatures and shorter days limit GPP, but not R, resulting in a net CO_2 release into the atmosphere (positive NEE). GPP shuts down in winter, but R can continue even in partially frozen soils; so we see positive, but weak NEE in winter.

Winter snow depths modulate the annual NEE cycle by influencing soil temperature and active layer depth. Deeper snows in winter insulate the soil, resulting in warmer soils in spring, which in turn results in deeper active layers the following summer. The timing of snowfall in fall is as important as snow depth: early snows in fall also result in warmer soils in winter and spring and a deeper active layer the following summer.

Winter snow depths affect GPP and R at different times of the year, producing a lopsided, time-delayed effect on the NEE seasonal cycle. Warmer soils and deeper active layers due to deeper winter snow increases R all year, but increase GPP only in late summer, when the active layer is deepest. Increased R due to warmer soil temperatures lead to increased NEE in spring and fall. In summer, increases in GPP overpower increases in R, resulting in increased CO_2 uptake (decrease in NEE).

Our results indicate a strong, time lagged response by the biosphere to changes in winter snow depth. Variations in snow depth in fall and early winter are effectively saved as variations in soil temperature, which in turn influences active layer depth the following summer. Through this memory of the soil temperature and active layer depth, winter snow depths effectively modulate biological fluxes throughout the following summer and fall.

Acknowledgments

This study was supported by the U.S. National Aeronautics and Space Administration (NASA) grant NNX06AE65G to the University of Colorado at Boulder.

References

Lawrence, D.M. & Slater, A.G. 2005. A projection of severe near-surface permafrost degradation during the 21st century, *Geophys. Res. Lett*. 32(24): doi:10.1029/2005GL025080.

Schaefer, K., Denning, A.S. & Leonard, O. 2004. The winter Arctic Oscillation and the timing of snowmelt in Europe. *Geophys. Res. Lett*. 31(22): Art. No. L22205.

Schaefer, K., Collatz, G.J., Tans, P., Denning, A.S., Baker, I., Berry, J., Prihodko, L., Suits, N. & Philpott, A 2008. The combined Simple Biosphere/Carnegie-Ames-Stanford Approach (SiBCASA) terrestrial carbon cycle model, *J. Geophys. Res*. (in press).

Sturm, M., Holgrem, J. & Liston, G.E. 1995. A seasonal snow cover classification system for local to global applications. *J. Clim*. 8(5): 1261-1283.

Zhang, T.J., Frauenfeld, O.W., Serreze, M.C., Etringer, A., Oelke, C., McCreight, J, Barry, R.G., Gilichinsky, D., Yang, D.Q., Ye, H.C., Ling, F. & Chudinova, S. 2005. Spatial and temporal variability in active layer thickness over the Russian Arctic drainage basin. *J. Geophys. Res.: Atmos.* 110(D16): Art. No. D16101.

Zimov, S.A., Schuur, E.A.G. & Chapin, F.S. 2006. Permafrost and the global carbon budget. *Science* 312(5780): 1612-1613.

Surface Offsets and *N*-Factors Across Altitudinal Tree Line, Wolf Creek Area, Yukon Territory, Canada

Emily A. Schultz
Department of Geography, University of Ottawa, Ottawa, Canada
Antoni G. Lewkowicz
Department of Geography, University of Ottawa, Ottawa, Canada

Introduction

Site-specific conditions that control ground heat flow and the surface temperature regime play an important role in determining permafrost occurrence in the discontinuous zone (Smith & Riseborough 2002). These include depth of snow, soil properties, and vegetation cover. As it is currently impractical to fully evaluate the effects of these variables on the energy balance in mountain basins, climate-permafrost relations must be simplified. One method that has recently been attempted is the TTOP model (Juliussen & Humlum 2007), which describes the relationship between the mean annual air temperature and the temperature at the top of permafrost in terms of the surface and thermal offsets (Smith & Riseborough 2002). Key components of this model are *n*-factors, which relate air and ground climate by establishing the ratio between air and surface freezing (winter) and thawing (summer) degree-days, thus summarizing the surface energy balance on a seasonal basis. Here we examine surface offsets and freezing and thawing *n*-factor variability at a number of sites through altitudinal tree line in the southern Yukon.

Study Area and Methods

Air and ground surface temperatures were measured hourly at 10 sites at elevations ranging from 1011–1640 m a.s.l. in and around the Wolf Creek research basin (60°32′N 135°13′W) near Whitehorse. This area is located within the sporadic discontinuous permafrost zone (Heginbottom et al. 1995), but permafrost is predicted to be extensive above 1400 m and continuous on mountain summits (Lewkowicz & Ednie 2004). The basin spans 3 major ecological zones that are mainly related to elevation: boreal forest at elevations below 1100 m, sub-alpine taiga/shrub tundra between 1100 m and 1500 m and alpine tundra above 1500 m (Francis et al. 1997). The measurement sites covered all 3 zones.

Instrumentation at each site consisted of an Onset Hobo Pro 8 datalogger equipped with an internal and external thermistor (accuracy of ±0.2°C). The body of each logger, containing an internal thermistor, was installed just below the ground surface while the external sensor was mounted within a solar radiation shield to measure air temperature at a height of 1.6 m.

Data presented here were collected from October 2003 to August 2006, comprising 3 freezing seasons and 2 thawing seasons. Data, collected at site on a palsa in the middle of the basin since April 2001, provide 2 additional freezing and 2 thawing seasons for analysis.

Snowpack development over the winter was tracked in 2005–06 using iButton miniature loggers, installed on stakes at 10–20 cm intervals (10, 20, 30, 40, 60 and 80 cm) at most of the logger sites. Temperatures were recorded by the iButtons sensors at 4-hour intervals. Differences in the temperature readings of iButtons above and below the snow were used to determine snow depths.

Results

Surface offsets

Surface offsets varied from 0.4° to 3.6°C (Table 1). Offsets for the forested and alpine tundra sites fall within the high and low parts of this range, respectively, while those measured at the sub-alpine taiga/shrub tundra sites cover almost the entire range. The smallest range in values was recorded at the forested sites (1.5°C), slightly smaller than at the alpine tundra sites (1.7°C), where snow accumulation is typically lowest.

Table 1. Surface offsets and *n*-factors at the study sites.

Site / Elevation (m)	Veg. Zone	Max. Snow Depth (2005–06)	Surface Offset (°C)	*nf*	*nt*
T2	boreal forest		2.9	0.29	
1011		70±9 cm	2.1	0.49	0.92
T3			3.6	0.12	
1145		70±9 cm	3.6	0.36	0.92
T4	sub-alpine taiga/shrub tundra		3.1	0.23	
1290		>80 cm	3.0	0.35	0.83
P9			3.8	0.39	-
			2.3	0.57	1.05
			3.0	0.45	1.08
1254			3.3	0.26	0.99
		50±9 cm	3.4	-	-
CR1			2.4	0.49	-
			2.7	0.36	0.91
1260		70±9 cm	2.4	0.56	0.92
CR2			2.8	0.40	-
			3.2	0.31	0.80
1271		50±9 cm	3.6	0.41	1.01
CR3			1.2	0.73	-
			1.0	-	0.95
1363		50±9 cm	2.2	0.55	-
CR4	alpine tundra		0.9	0.70	-
			1.4	0.52	0.86
1457		45±14 cm	2.1	0.51	0.87
CR5					
1495		-	0.4	-	-
Bowl					
1640		-	2.2	0.60	-

N-factors

Freezing factors (*nf*) over the study period ranged from 0.12 to 0.73 (Table 1). Figure 1 demonstrates that *nf* values exhibit a broad relationship with both elevation and vegetation. Values for the forested sites were all <0.40, ranging from 0.12 to 0.36, while those calculated for the tundra sites were all >0.50. Freezing factors for the sub-alpine taiga/shrub tundra zone point to the role of variable vegetation and snow cover close to and below tree line, with values ranging from 0.23 to 0.73 at these sites. Values of *nf* measured at individual sites exhibited significant interannual variability with increases of more than 0.20 at some sites between 2004–05 and 2005–06. Snow accumulation differences likely account for this pattern. Whitehorse recorded a maximum of 47 cm of snow on the ground in 2004–05, but a maximum of only 22 cm in 2005–06 (Environment Canada 2008).

Thawing factors (*nt*) ranged from 0.80 to 1.08, a much smaller range than for *nf* (Table 1). Values of *nt* calculated for the forested sites over the study period were both 0.92, slightly above those calculated for the tundra site (0.86 and 0.87). Sites where *nt* was greater than 1.0 were all situated above 1200 m, and all are located within the sub-alpine taiga/shrub tundra zone. Along the Mount Sima trail, there is a clear transition in *nt* associated with tree line, with thawing factors at the two forested sites (T2 and T3) nearly 0.10 higher than at the sub-alpine site (T4) in 2005.

Discussion and Conclusions

Our results support the findings of Karunaratne and Burn (2004) and the modeling of Smith and Riseborough (2002) that snow depth is the most important variable influencing *nf*, because the low thermal conductivity of snow restricts heat loss from the ground surface. *Nt* values are higher and vary less. They may relate to land cover as suggested by Klene et al. (2001) who obtained the highest values on bare ground and wet tundra sites. Similarly, Taylor (1995) calculated the highest values of *nt* at open sites and lowest at shaded sites, predominantly those located within the forest.

The relationship between surface offset, *n*-factors, elevation, and vegetation in the study area, therefore, demonstrates that trends previously identified in relation to latitudinal tree line also apply to the altitudinal tree line.

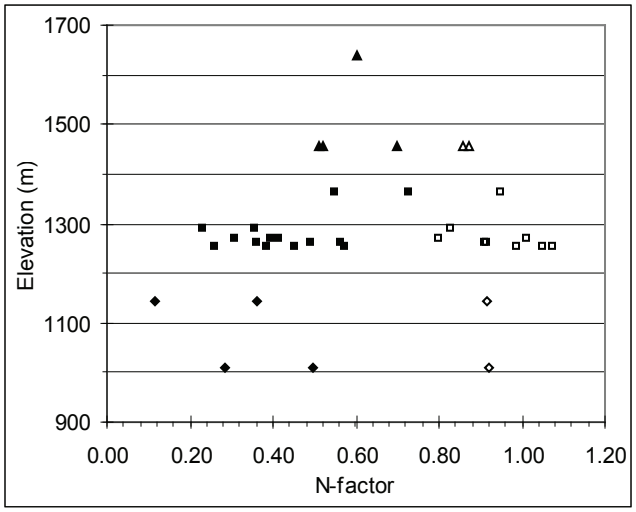

Figure 1. Relationship between elevation, vegetation and seasonal *n*-factors at the study sites (2001–2006). Freezing (filled) and thawing (outlined) factors are shown for the boreal forest (diamond), sub-alpine taiga (square) and alpine tundra (triangle) vegetation zones.

Acknowledgments

This research was supported financially by the Canadian Foundation for Climate and Atmospheric Sciences, NSERC, the Northern Scientific Training Program (INAC), the Geological Survey of Canada, and the Yukon Geological Survey. Logistical support was given by Water Resources Branch, Yukon Government. Field assistance was given by Jim Coates, Phil Bonnaventure, Pauline Favero, and Martina Knopp.

References

Environment Canada. 2008. National Climate Archive [online]. http://www.climate.weatheroffice.ec.gc.ca (Accessed February 9, 2008).

Francis, S., Smith, S. & Janowicz, R. 1997. Intégration des données et la zonation écologique du basin versant du ruisseau Wolf. In: J.W. Pomeroy & R.J. Granger (eds.), *Wolf Creek Research Basin: Hydrology, Ecology, Environment*. Saskatoon: National Water Research Institute, 97-104.

Heginbotton, J.A., Dubreuil, M.A. & Harker, P.T. 1995. Canada-Permafrost. In *National Atlas of Canada,* 5th ed. Ottawa: National Atlas Information Service, Natural Resources Canada. Plate 2.1 MCR 4177, 1:7,500,000.

Juliussen, H. & Humlum, O. 2007. Towards a TTOP Ground Temperature Model for Mountaneous Terrain in Central-Eastern Norway. *Permafrost and Periglacial Processes* 18: 161-184.

Karunaratne, K.C. & Burn, C.R. 2004. Relations between air and surface temperature in discontinuous permafrost terrain near Mayo, Yukon Territory. *Canadian Journal of Earth Sciences* 41: 1437-1451.

Klene, A.E., Nelson, F.E. & Shiklomanov, N.I. 2001. The n-factor in natural landscapes: variability of air and soil-surface temperatures, Kuparuk river basin, Alaska, USA. *Arctic*, *Antarctic and Alpine Research* 33: 140-148.

Lewkowicz, A.G. & Ednie, M. 2004. Probability mapping of mountain permafrost using the BTS method, Wolf Creek, Yukon Territory, Canada. *Permafrost and Periglacial Processes* 15(1): 67-80.

Smith, M.W. & Riseborough, D.W. 2002. Climate and limits of permafrost: A zonal analysis. *Permafrost and Periglacial Processes* 13: 1-15.

Taylor, A.E. 1995. Field measurements of n-factors for natural forest areas, Mackenzie Valley, Northwest Territories. *Current Research 1995-B,* Geological Survey of Canada, 89-98.

The Contribution of Old Carbon to Respiration from Alaskan Tundra Following Permafrost Thaw

Edward A.G. Schuur, Jason G. Vogel, K. Grace Crummer, Hanna Lee, Koushik Dutta
Department of Botany, University of Florida, Gainesville, FL 32601-8526, USA

Introduction

Up to 1670 Pg of soil carbon (C) has accumulated in high latitude ecosystems after the retreat of the last major ice sheets. This soil C has until now been largely protected from decomposition by cold temperature, water-logging, and permafrost. Recent studies suggest that, due to climate warming, these ecosystems may no longer be accumulating C, and in some cases may be losing stored C to the atmosphere. We hypothesize that sustained transfers of C to the atmosphere that could cause a significant positive feedback to climate change will come from old C, which forms the bulk of the soil pool.

Materials and Methods

Field sites

We used radiocarbon ($\Delta^{14}C$) measurements of carbon dioxide to detect the age of C respired from tussock tundra near Denali National Park, Alaska. These measurements were made in the Eight Mile Lake Watershed (63°52′42.1″N, 149°15′12.9″W) on the north slope of the Alaska Range. Ground temperature in a borehole has been monitored for several decades at this site, before and after the permafrost was observed to thaw (Osterkamp & Romanovsky 1999). In this watershed, our study has defined three sites that represent differing amounts of disturbance from permafrost thawing based on observations of the vegetation and the borehole measurements: (1) tussock tundra typical of arctic ecosystems, dominated by the sedge *Eriophorum vaginatum* and *Sphagnum spp* mosses (Minimal thaw); (2) a site near the borehole used for permafrost temperatures, where the vegetation composition has been shifting to include more shrub species, such as *Vaccinium uliginosum* and *Rubus chamaemorus* (Moderate thaw); and (3) a site located where permafrost melted more than several decades ago, now largely dominated by shrub species (Extensive thaw) (Schuur et al. 2007). These three sites are a natural experimental gradient representing the long-term effects of permafrost thawing on C loss. This thawing has occurred without any visible surface disturbance (i.e., fire) and is thought to be an effect of regional climate warming. We made radiocarbon measurements of ecosystem respiration, incubations of soil organic matter, and incubations of aboveground and belowground plant biomass to determine the age and isotopic value of C respired from these sites.

Radiocarbon field measurements

Ecosystem respiration $\Delta^{14}CO_2$ measurements were measured using a modified dynamic flow chamber system analogous to the system used for measuring ecosystem CO_2 fluxes. At monthly intervals during the growing season (May–September), dark, 10 L, plastic chambers were placed over collars in the soil surface. To remove background atmospheric air present when the chamber top is fit to the collar, the air stream is scrubbed with Ascarite. Carbon dioxide was scrubbed from the system at a rate similar to that of soil CO_2 efflux until 2–3 chamber volumes of air had passed through the scrubber, when the CO_2 remaining is almost exclusively soil-respired CO_2. The air stream was then diverted through a molecular sieve to quantitatively trap ~1.0 mg CO_2. In the laboratory, the molecular sieve traps were heated to 625°C to desorb CO_2. Carbon dioxide was then purified and analyzed for $\delta^{13}C$ and $\Delta^{14}C$.

Radiocarbon laboratory measurements

To estimate the contribution of plant respiration, surface litter, and deep, old soil C to surface $\Delta^{14}CO_2$ fluxes, we incubated these materials in the laboratory to determine the isotopic composition of evolved CO_2. We collected 2 replicate soil samples per site down to the mineral soil interface (typically the full August active layer depth) and separated the profiles into 5 depth increments (0–5, 5–15, 15–25, 25–35, 35+ cm). The final depth increment was variable because the total organic layer thickness varied among samples. All samples were split, large roots and stems removed, and the halves kept intact to preserve the soil structure. Soil core splits were incubated in separate glass jars at 3°C and 8°C to determine the temperature sensitivity (expressed as a Q_{10} value) for respiration from these soil. Rates of CO_2 production were then measured daily using an IRGA to monitor the change in CO_2 concentration in the incubation jar headspace over time. Jars were sealed and flushed with moist CO_2-free air when CO_2 concentrations exceed 1%. After 5 days of incubation in the laboratory, the jars were completely scrubbed with CO_2-free air, and respired $^{14}CO_2$ was allowed to accumulate and was then collected for $\Delta^{14}C$ analysis. Similar incubations were made of aboveground and belowground plant parts harvested from 5 x 5cm quadrats during the growing season.

Source partitioning

We estimated the relative contribution of the plant and soil components to the R_{eco} flux using the $\Delta^{14}C$ measurements and a standard statistical modeling approach. The laboratory soil incubations were combined into surface soil (top 2 horizons) and deep soil (lower 3 horizons) components by flux-weighting the soil incubations. To calculate a combined isotope respiration value for the surface and deep soil, the $\Delta^{14}C$ values for the layers that were combined were weighted by (1) the relative CO_2 flux on a per gram dry soil basis, (2)

Table 1. Fluxes and isotopes of carbon dioxide from laboratory incubations of soil organic layers at 15°C.

Site	Soil Layer cm	Carbon Flux μg C gdw^{-1} hr^{-1} (± SE)	Soil Mass $kgdw\ m^{-2}$ (± SE)	Average Summer Temperature ºC	$\Delta^{14}C$ ‰ (± SE)
Minimal	0-5	8.09 (4.21)	3.06 (0.76)	14.0	+101 (7)
	5-15	6.05 (2.14)	5.13 (1.90)	12.2	+96 (13)
	15-25	3.07 (1.64)	8.80 (0.79)	4.7	+53 (6)
	25-35	1.66 (0.23)	14.61 (3.14)	2.0	+48 (1)
	35+	1.26 (0.65)	181.86 (46.21)	0.6	-56 (66)
Moderate	0-5	7.65 (1.31)	3.80 (0.56)	14.0	+94 (11)
	5-15	3.47 (1.73)	5.49 (1.01)	12.2	+78 (23)
	15-25	3.16 (0.71)	10.06 (0.87)	4.7	+35 (10)
	25-35	1.18 (0.28)	17.37 (0.92)	2.0	+25 (4)
	35+	0.38 (0.18)	66.87 (19.27)	0.6	-32 (32)
Extensive	0-5	9.88 (3.38)	3.06 (0.76)	14.0	+101 (7)
	5-15	4.26 (2.00)	5.13 (1.90)	12.2	+96 (13)
	15-25	2.05 (1.01)	8.80 (0.79)	4.7	+53 (6)
	25-35	1.98 (0.58)	14.61 (3.14)	2.0	+48 (1)
	35+	0.46 (0.13)	181.86 (46.21)	0.6	-56 (66)

the relative amount of soil mass in the combined horizons, and (3) by the average field temperature for the horizons (this varied over the season). Plant respiration $\Delta^{14}C$ values measured over the growing season matched the atmospheric values in 2004 (data not shown), and were assumed to follow the atmospheric decline.

Total R_{eco} $\Delta^{14}CO_2$ flux is a combination of surface and deep soil respiration, along with plant respiration. Because there is no single solution that describes the contribution of 3 unknown sources with a single isotope tracer, a standard statistical approach yields a range of possible contributions of the component sources to R_{eco}. Of the sources (plant respiration, surface soil respiration, deep soil respiration), the contribution of the deep soil is the most clearly defined, as demonstrated by the smallest standard deviation and overall range. This is a result of the deep soil having a $\Delta^{14}C$ value furthest away from the $\Delta^{14}C$ value of R_{eco}, thus its contribution to the total is most constrained. While the deep soil C was the only source that could bring the R_{eco} $\Delta^{14}C$ value below that of the current atmosphere,
the $\Delta^{14}C$ values of plant respiration and surface soil respiration were more similar and thus could substitute for one another.

Results and Conclusions

Over the study period, ecosystem respiration radiocarbon values averaged from +35‰ to +95‰ in different months across sites. For soil incubations, surface soil radiocarbon was elevated relative both to ecosystem respiration and the current atmospheric radiocarbon value, demonstrating the significant contribution from C fixed over the past years to several decades (Table 1). The deeper soil, in contrast, had respiration isotope values that averaged below zero, reflecting the significant effect of radioactive decay on the isotope content of deeper soil layers. The plant and soil incubations were combined in a multisource mixing model to determine probable contributions from these different sources to ecosystem respiration. Deep soil respiration generally averaged between 5–15% of total ecosystem respiration, but reached as high as 40% in some months. When aggregated across the growing season, the two sites undergoing more disturbance from permafrost thaw had on average 2–3 times the loss of old, deep C as compared to the least disturbed site. From this isotope partitioning, we determined that the respiration of old C increases following permafrost thaw and contributes towards making these tundra ecosystems net sources of C to the atmosphere.

References

Osterkamp, T.E. & Romanovsky, V.E. 1999. Evidence for warming and thawing of discontinuous permafrost in Alaska. *Permafrost and Periglac. Process* 10: 17-37.

Schuur, E.A.G., Crummer, K.G., Vogel, J.G. & Mack, M.C. 2007. Plant species composition and productivity following permafrost thaw and thermokarst in Alaskan tundra. *Ecosystems* 10: 280-292.

Interactions Between Human Disturbance, Demographics of *Betula Fruticosa* Pall., and Permafrost in the Vitimskoye Upland, East Siberia

I.R. Sekulich
Institute of General and Experimental Biology SB RAS, Ulan-Ude, Russia

The demographic structure of plant coenopopulations is one of the basic estimation criteria of the modern state of species in coenosis, level of vital condition, degrees of their stability, and prospects of development (Harper 1992, Rabotnov 1978, 1985, Uranov 1960, 1975).

Our research was performed on the central part of the Vitimskoye upland, which is located in eastern Siberia (Fig. 1). It is large isolated area which is situated at the southern limit of continuous permafrost. The permafrost is the major ecological factor which determines character and distribution of vegetation here. Communities formed by low birches or birch-shrublands are the most widespread here.

The capacity of permafrost in the research area is from 50–250 m with temperature from 0 to -3°C; depth bedding of permafrost in birch-shrublands in August-September is about 1.0–1.6 m (Vtorushin & Pigareva 1996).

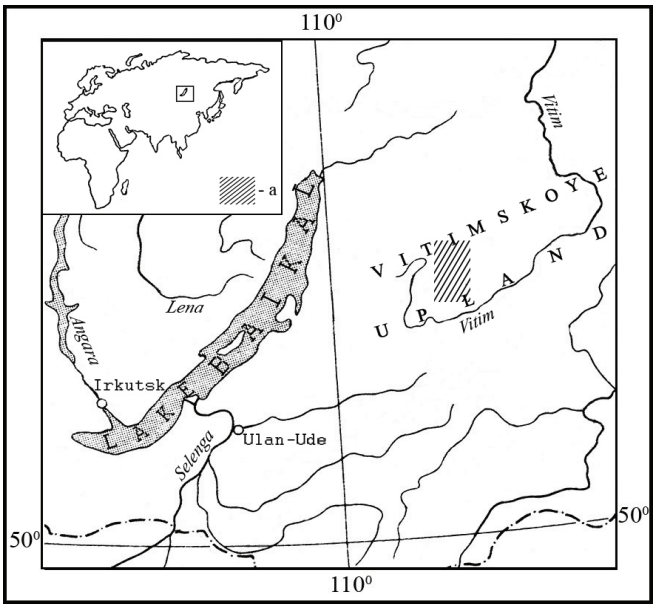

Figure 1. Map of location of researches area: a – research area.

Table 1. Age stages and age groups of the plants.

The age stages	The age groups	The letter code
latent	seed	sm
pre-generative	germ	pl
	juvenile	j
	immature	im
	virginile	v
generative	young generative	g_1
	mature generative	g_2
	old generative	g_3
post-generative	subsenile	ss
	senile	s

The object of our research is *Betula fruticosa* Pall. subsp. *montana* M. Schemberg, the basic dominant of birch-shrublands.

We studied changes of the demographic structure of the coenopopulations of *Betula fruticosa* on sites with partial destruction of vegetative cover as a result of the influence of track transport and pasturing. Research carried out was spent on the model area in 100 square meters on which continuously calculated individuals on age groups.

Rabotnov (1978) had divided the whole life cycle of plants into the following age stages and age groups, which are submitted in Table 1. The letter code of each age group has been offered by Uranov (1960).

The age level of the coenopopulations is estimated by the index of age (Δ) proposed by Uranov (1975) and by the index of effectiveness of the populations (ω) proposed by Zhivotovsky (2001). Values of Δ and ω were calculated by the following formulas:

$$\Delta = \sum n_i m_i \Big/ \sum n_i \quad (1)$$

$$\omega = \sum n_i e_i \Big/ \sum n_i \quad (2)$$

where n_i is the number of individuals of each age group; m_i is the coefficient of the age group, calculated by Uranov (1975); and e_i is the efficiency of plants of each age group, calculated by Zhivotovsky (2001).

Indexes Δ and ω varies from 0 to 1, and the highest value characterized the elder coenopopulation.

In estimating the degree of anthropogenic influence on the demographic spectrum of disturbed coenopopulations, it is necessary to compare them with a base spectrum, which is the modal characteristic of dynamic balance of coenopopulation (Smirnova 1987). The base spectrum coenopopulation *B. fruticosa* on the Vitimskoye upland is full-constituent, has one peak, with absolute maximum on old generative individuals.

It was marked two variants of modification of the demographic structure.

One of them shows an increase in the quantity of pregenerative individuals at the remaining high number of generative individuals. An age spectrum of such coenopopulations has two peaks. As an example, the age spectrum coenopopulation in the community of Multiherboso–Betuletum fruticosae is shown (Fig. 2). The community is situated near to a settlement along a highway and often is exposed to the influence of track-type vehicles.

At the unitary passage of the cross-country vehicle, according to mechanical influence, the integrity of the vegetative cover is broken. As a result of these disturbances,

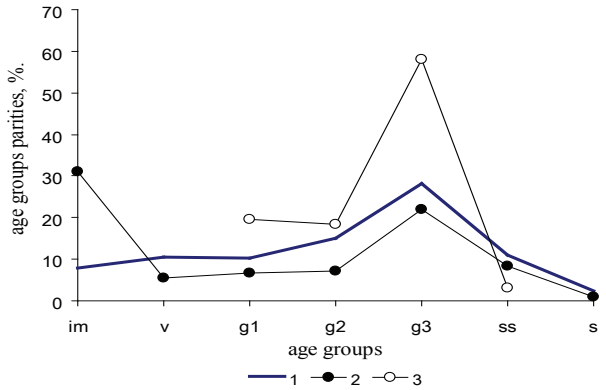

Figure 2. The age spectrums coenopopulations of *Betula fruticosa*. 1 – base spectrum; 2 – community of Multiherboso–Betuletum fruticosae; 3 – community of Kobresio–Betuletum fruticosae. Characteristics of age groups were explained above.

Table 2. The quantity, index of age (Δ) and index of effectiveness (ω) of anthropogenically disturbed coenopopulations of *Betula fruticosa*.

Community	Multiherboso-Betuletum fruticosae	Kobresio-Betuletum fruticosae
The general quantity, pcs./100 m^2	482.3 ± 17.2	23.3 ± 3.2
The quantity of age groups, pcs./100 m^2:		
j	89.4 ± 9.6	-
im	149.4±11.7	-
v	25.9±4.1	-
g_1	32.9±4.3	4.6 ±0.6
g_2	34.1±4.3	4.3 ± 0.5
g_3	105.9±6.4	13.7±2.4
ss	40.0 ±3.9	0.7 ±0.1
S	4.7 ±0.6	-
Δ	0.32	0.65
ω	0.43	0.81

gaps formed, which are the microecotope for renewal *B fruticosa.* There is a rejuvenation of the coenopopulation at the expense of the high number of young individuals (Table 2).

The short-term influence of transport does not effect adult individuals of *B. fruticosa* essentially. At multiple or constant impacts of track-type transports, the adult individuals finally perish, which leads to replacement of birch-shrublands on grassy communities of meadow. This leads to a change of hydrothermal condition of the soil, and the depth of seasonal thawing of permafrost and bogging, thermokarst can develop.

Another variant of anthropogenic changes of the demographic structure occurs with pasturing. As a result of trampling and pasturing, the young individuals of *B. fruticosa* disappear from the structure of the community together with grassy plants. The coenopopulation is presented by old-age plants. The community of Kobresio–Betuletum fruticosae, located on an abrupt slope, can be an example of such kind of coenopopulation. The age spectrum here has one peak, but it is not full-constituent and presented by old individuals (Fig. 2). The number of individuals of *B. fruticosa* in this coenopopulation is low (Table 2).

The low indexes Δ and ω of coenopopulation of *B. fruticosa* occurring in the community of Multiherboso–Betuletum fruticosae shows its invasive character and is considered as young according to "delta-omega" classification (Zhivotovsky 2001). The high indexes Δ and ω in the community of Kobresio–Betuletum fruticosae shows its regressive character and is considered as becoming old.

Thus, human-induced disturbances on the of demographic structure of coenopopulation *B. fruticosa* in birch-shrublands on the Vitimskoye upland promote development of various geocryological processes. When the disturbances of demographic structure are slight, fast restoration of coenopopulation and ecological conditions occurred.

References

Harper, J.L. 1992. *Population of Plants.* Oxford: The Alden Press, 892 pp.

Rabotnov, T.A. 1978. On coenopopulations of plants reproducing by seeds. In: *Structure and Functioning of Plant Populations.* Amsterdam, 1-26.

Rabotnov, T.A. 1985. Dynamics of plant coenotic populations. In: J. White (ed.), *The Population Structure of Vegetation.* Dordrecht, Boston, & Lancaster: Dr. W. Junk Publ., 121-142.

Smirnova, O.V. 1987. *Struktura travjanogo pokrova shirokolistnyh lesov* (*The Grass Layers Structure of Broad-leaved Forests*). Moscow: Nauka, 207 pp. (in Russian).

Uranov, A.A. 1960. Zhyznennoe sostoyanye vyda v rastytel'nom soobshestve (The life state of species in a plant community). *Bulleten' Moskovskogo obshestva ispytatelei pryrody, otdel biologicheskyi* (*Bulletin of Moscow Society of Naturalists, Biological Series*) 67(3): 77-92 (in Russian).

Uranov, A.A. 1975. Vozrastnoi spektr fytocenopopuljacyi kak funkcija vremeny I energetycheskih volnovyh processov (The age spectrum of phytocoenopopulation as a function of time and power wave of processes). *Biologycheskye nauki* (*Biological Sciences*) 2: 7-34 (in Russian).

Vtorushin, V.A. & Pigareva, N.N. 1996. *Kryomorfnye pochvy: perspektivy ich effektivnogo ispol'zovaniya* (*Criomorphic Soils: Prospects of their Effective Utilization*). Ulan-Ude: BSC SB RAS, 295 pp. (in Russian).

Zhivotovsky, L.A. 2001. Ontogeneticheskie sostojanija, effectivnaja plotnost' i klassifikacija populjacyi rastenyi (Ontogenetic states, effective density, and classification of plant populations). *Ecologija* (*Russian Journal of Ecology*) 1: 3-7 (in Russian).

Rock Glacier Distribution in the Absaroka/Beartooth Wilderness, Montana, USA

Zach M. Seligman, Anna E. Klene
Department of Geography, University of Montana, Missoula, 59812, USA

Introduction

Rock glaciers are relatively understudied glacial features found in many alpine environments around the world. Because they are rock-covered and often similar in appearance to talus fields and moraines, their presence and hydrologic significance has gone widely unnoticed (Millar & Westfall 2007). However, they play an important role in alpine environments. Rock glaciers provide a mechanism for transport of headwall debris (Humlum 2000) and, similar to glaciers, can act as a source of year-round water in high alpine catchments where late summer precipitation is minimal (Johnson 2007). Schrott (1996) determined that these features can contribute up to 30% of river discharge during summer months in the Andes.

Additionally, rock glaciers potentially contain significant climatic information within their spatial distribution (Humlum 1998). While a number of studies have focused on these relationships (Kerschner 1978, Brazier et al. 1998, Humlum 1998), a paucity of relevant climate stations often limits such efforts (Brazier et al. 1998). Other research has examined characteristics of rock glacier age (Aoyama 2005), movement (Chueca & Julian 2005), structure (Arenson et al. 2002), and geomorphology (Berthling & Etzelmuller 2007).

In the Absaroka/Beartooth wilderness, rock glaciers number in the hundreds (unpublished data), existing simultaneously with cirque glaciers and permanent snowfields, yet general information about them is sparse, and hydrological research is non-existent. This study will examine the spatial distribution of rock glaciers to understand the relative local importance of topoclimatic and geologic factors. This understanding will allow further investigations into the relationships between rock glacier distribution, ice volume, and downstream ecology. The interplay of these factors has important implications in light of recent and ongoing climatic changes.

Research will be performed in two phases. Phase one includes analysis through GIS and remote imagery, which will explore trends in rock glacier distribution relative to topoclimatic factors. The second phase will be field verification of the digital data, which will subsequently investigate the link between spatial characteristics of rock glaciers and water availability in alpine catchments.

Background

Topoclimatic and geologic controls

Previous research in New Zealand shows that active rock glaciers tend to favor relatively higher elevations and more southerly aspects (Brazier et al. 1998). In the same study, modern distribution of relict rock glaciers favored lower elevations on all aspects. Similarly, Humlum (1998) describes rock glacier presence to be "a complex function of responses to air temperature, insolation, wind, and seasonal precipitation over a considerable period." Just as topoclimatic factors play a major role in ice formation and retention of rock glaciers, lithology has also been shown to be an important component of rock glacier initiation (Johnson et al. 2007). This study will use GIS to compare topoclimatic and geologic controls on rock glacier distribution.

Ice volume and distributional controls

Rock glacier ice volume may also correlate strongly with topographical distribution in the same ways that rock glacier activity is linked to topographical and altitudinal controls (Humlum 1988). As rock glacier activity is dependent on ice volume for its classification, it should follow that ice volume is subject to the same variables that affect rock glacier activity. This study will explore topographical and altitudinal controls on rock glacier ice volume.

Ice volume and vegetation

Investigations of relationships which may exist between rock glacier distribution, ice volume, and downstream ecology can be based upon the relationships currently known to exist between glacial systems and ecological succession in the region. Previous research has looked at vegetative advancement in response to glacial recession in Africa (e.g., Kazuheru 2003). Locally, Hall and Fagre (2003) used models to project vegetation succession patterns of glacial forelands in Glacier National Park, Montana. Perhaps a similar relationship exists for alpine catchments where rock glaciers, instead of ice glaciers, are the dominant glacial feature. This study will estimate rock glacier ice volume in comparison with percentage per area of appropriate vegetation types downhill of the rock glacier terminus.

Implications for climate

Topological and altitudinal distribution of rock glaciers, in itself, has the potential to contain unique climatic information (Humlum 1998). By comparing ages and elevations of active and relict rock glaciers and interpreting changes in equilibrium line altitudes, timing of glaciations and temperature differences have been determined (Millar & Westfall 2007). Regionally, results of vegetative patterns associated with spatial distribution of rock glaciers may also harbor additional climatic information.

Study Area

This study will focus, in the first phase, on the distribution of rock glaciers within Absaroka/Beartooth wilderness area in southwest Montana. Phase two will look at approximately 30 representative rock glaciers within the wilderness area.

Methodology

Rock glaciers were initially identified in the study areas using GoogleEarth software and then were plotted on a printed map. Digital elevation models (10 × 10 m) for each rock glacier of interest will be obtained from the Montana Natural Resource Information System (NRIS). Digital aerial photos will also be obtained from NRIS for the Absaroka/Beartooth Wilderness. Feature Analyst and ArcGIS software will be used with spectral and pattern-recognition techniques to extract rock glaciers from the imagery. Elevation, slope, aspect, vegetation, and insolation estimates will be computed.

Field component

Ground verification will be needed to assess the predictions from the remote imagery. Elevation, slope, and aspect will be recorded in the field. Rock glacier activity, as described by Johnson et al. (2007), will be classified as Class 1 (active), Class 2 (inactive), or Class 3 (relict). Total rock glacier volume and total cirque glacier volume will be estimated by taking GPS coordinates of the perimeters and estimating depth from surrounding topography. Rock glacier mantle volume will be estimated by multiplying the perimeter with the depth of the mantle. Mantle depth will be estimated by making exposures of the ice core and looking for natural ice exposure in the mantle. Total ice volume will be predicted by subtracting the rock glacier mantle volume from the total rock glacier volume.

Vegetation composition will be determined by techniques from Kimball and Weihrauch (2000). Using 100 m^2 plots, percentage per area of several vegetation communities will be determined. Plot information will be gathered below the rock glacier terminus. Elevations of prominent vegetation regimes will be recorded.

Discussion

In phase one, GIS data will be used to analyze trends in rock glacier distribution relative to topographical, altitudinal, and climatic characteristics. Anticipated results of this phase include a tendency toward active rock glacier presence at higher elevations on north-facing slopes. Additionally, estimated rock glacier size, presence of an uphill cirque glacier, and annual insolation will also be examined with relation to altitudinal data, slope, and aspect. It is expected that distribution will represent a complex correlation based on many factors.

Phase two will focus on the field verification of the GIS data and will also look at rock glaciers as elements of water storage in alpine regions. The presence of ice in a rock glacier may act as the only late-summer water available to downslope vegetation. For example, a discrepancy in elevation and percent composition of more xeric species below active rock glaciers might differ relative to relict rock glaciers, which, in effect, do not release late-summer glacial melt.

References

Aoyama, M. 2005. Rock glaciers in the northern Japanese Alps: Palaeoenvironmental implications since the Late Glacial. *J. Quaternary Science* 20(5): 471-484.

Arenson, L., Hoelzle, M. & Springman, S. 2002. Borehole deformation measurements and internal structure of some rock glaciers in Switzerland. *Permafrost and Periglacial Processes* 13: 117-135.

Berthling, I. & Etzelmuller, B. 2007. Holocene rockwall retreat and the estimation of rock glacier age, Prins Karls Forland, Svalbard. *Geografiska Annaler* 89A(1): 83-93.

Brazier, V. et al. 1998. The relationship between climate and rock glacier distribution in the Ben Ohau Range, New Zealand. *Geografiska Annaler* 80A: 3-4.

Chueca, J. & Julian, A. 2005. Movement of Besiberris rock glacier, central Pyrenees, Spain: Data from a 10-year geodetic survey. *Arctic, Antarctic, & Alpine Res.* 37(2): 163-170.

Hall, M. & Fagre, D.B. In press. Where have all the glaciers gone? Modeling climate-induced glacier change in Glacier National Park. *Bioscience*: 1850-2100.

Hughes, P.D., Gibbard, P.L. & Woodward, C. 2003. Relict rock glaciers as indicators of Mediterranean palaeoclimate during the Last Glacial Maximum (Late Wurmian) in northwest Greece. *J. Quaternary Sci.* 18(5): 431-440.

Humlum, O. 1998. The climatic significance of rock glaciers. *Permafrost and Periglacial Processes* 9: 375-395.

Humlum, O. 2000. The geomorphic significance of rock glaciers: Estimates of rock glacier debris volumes and headwall recession rates in west Greenland. *Geomorphology* 35: 41-67.

Johnson, B.G. 2007. The effect of topography, latitude, and lithology on rock glacier distribution in the Lemhi Range, central Idaho, USA. 91: 38-50.

Kazuheru, M. 2003. Vegetation succession in response to glacial recession from 1997–2002 on Mt. Kenya. *J. of Geography* 473(2): 608-619.

Kerschner, H. 1978. Palaeoclimatic inferences from Late Wurm rock glaciers, Eastern Central Alps, Western Tirol, Austria. *Arctic & Alpine Research* 10: 635-644.

Kimball, K.D. & Weihrauch, D.M. 2000. Alpine vegetation communities and the alpine-treeline ecotone boundary in New England as biomonitors of climate change. *USDA Forest Service Proc*. RMRS 15(3).

Krainer, K. & Mostler, W. 2002. Hydrology of active rock glaciers: Examples from the Austrian Alps. *Arctic, Antarctic, & Alpine Res.* 34(2): 142-149.

Millar, C. & Westfall, R.D. Rock glaciers and related periglacial landforms in the Sierra Nevada, CA, USA: Inventory, distribution and climatic relationships. *Quaternary Internatl.*: doi:10.1016/j.quaint.2007.06.004.

Potter, N., Jr. et al. 1998. Galena Creek rock glacier revisited: New observations on an old controversy. *Geografiska Annaler* 80A: 251-265.

Schrott, L. 1996. Some geomorphological-hydrological aspects of rock glaciers in the Andes (San Juan, Argentina). *Z. Geomorph N.F.* 104: 161-173.

Dynamics of the Cryosphere of Northern Tien Shan as a Reaction to Climate Change

Igor V. Severskiy
Kazakh Institute of Geography,
Eduard V. Severskiy
Permafrost Institute of Russian, Academy of Sciences.

On the basis of analysis of long-term observation, data changes of snowiness, glaciation, and thermal regime of seasonally and perennially frozen grounds in the mountains of southeast Kazakhstan (Northern Tien Shan, Dzhunghar Alatau) for last decades are considered.

According to analysis in the testified region, for the last decades the average maximum snow water equivalent (the main component of snow resources) has not changed. Similar results were found for western Tien Shan and Gissar-Alai.

Glacial systems of Central Asia mountains develop in the same direction and have similar rates of modern changes; so for the last decades, the area of glaciers in different regions of Tien Shan, Gissar-Alai, Pamirs and Dzhunghar Alatau has decreased at the average rate 0.8–1.0% per year.

The dimensions and temperatures of the glacier degradation have been determined on the basis of comparison of data of the unified Glacier Inventories, composed by aero-photograph materials and by satellite images for 6 years within the period of 1955 to 1999.

Mean maximum glacial retreat rates at the Northern Tien Shan characteristic of the mid-1970s by the mid-1980s slowed down.

Glacier retreat rate depends to a great extent on its size. A glacier area F = 13–14 km^2 is the threshold. In case of its excess, the self-regulation mechanism of the glacier is so vivid that it neutralizes evidence of all local factors, and its regime is defined by microclimatic conditions of the region.

The regime of each glacier is unique and can differ from not only average data for this type of glacier system, but also from that of a nearby glacier. The differences can be not only significant but also can have a different negative/positive trend. Glacier retreat rate does not depend on its exposition and morphological type. Territorial differences in the retreat rates are defined by the orientation of slopes in reference to the sides of the horizon and the prevailing direction of humid air mass movements, and the location of the region in the mountainous system.

Predominating opinion about the inevitability of glaciers disappearance in Central Asia mountains cannot be accepted as an axiom. Taking into account stability in the rate of precipitation and especially in the rate of snow resources, one can suppose that glaciers in this region will not disappear during this century. Based on our analysis, which takes into account current global warming trends, the glacier area of Balkhash Basin may shrink by about one-third, but will not disappear completely.

Most scientific publications support an opinion that the glacier runoff must increase with glacier retreat due to global warming. Our research shows that the result of modern climate warming is glacier runoff decrease. But despite the reduction of glaciers, annual runoff volumes and the interannual distribution remained unchanged during the last decades. During the same period, norms of atmospheric precipitation and maximum snow water equivalent in the zone of runoff formation remained stable also. All these allow the proposal of the existence of a certain compensation mechanism. Research, based on data analysis of repeated photogrammetric surveys of a group of glaciers and temperature regime of permafrost in Zailiyskiy Alatau, suggests that such mechanism can be an increased (with climate warming) participation of melting waters of ground ice (buried glaciers, rock glaciers, permafrost) in the river runoff.

Taking into consideration, also, the fact that reserves of ground ice in high mountains of Central Asia and Kazakhstan are equivalent to present-day glacier resources and in the Chinese mountains they are two times greater, and also considering that the rates of melting ground ice are much lower than those of the open glaciers, we believe that even if the present-day trends in climate warming are preserved, the above-mentioned compensating mechanism may work during several coming decades as minimum. Hence it can be predicted that the ongoing degradation of glaciers will not cause considerable reduction in the runoff and regional water resources, at least up to the next decades.

Materials from 33 years of geothermal monitoring testify to the ambiguous reaction of perennial and seasonal permafrost to climate changes in the Northern Tien Shan. Regularities of perennially frozen ground distribution and features of spatial changes of depth and character of seasonal freezing of soils in the Northern Tien Shan are reflected in the regional structure of altitudinal geocryological zonality

The total area of perennial permafrost tracts in the subzone with sporadic spreading amounts to not more than 1–2%, it comes up to 30% at insular spreading, it rises up to 70% at intermittent distribution, and at dense one, it is not less than 90% of the total subzone area. There are not any conditions for formation of local masses of permafrost on a southern macro-slope; therefore the subzone of sporadic spreading is absent there. Altitude borders of other subzones are located there on 300–400 m above in comparison with the position on a northern slope.

During the period of 1974–1995, ground temperature in layer of perennial permafrost had increased 0.2–0.5°C, but after that, has been retained at -0.2°C during the last 11 years.

Reaction of strata of seasonal permafrost to climate changes remains ambiguous in different landscape conditions. Seasonal thawing depth increased from 3.2 m in 1974 up to 6.0 in 2001, but then that process stopped. In 2002, the mentioned figure decreased to 4.6 m., and for the last 5 years, it has remained stable, with small interannual oscillations within the limits of 4.6–4.9 m

Since 1975 to 1998, in high mountains (at an altitude of 3000 m), the changing of seasonal freezing depth on slopes on different expositions has not been supervised, but its increase was marked during the last 4 years: by 1.0 m at northern and 0.3 m at southern slopes.

A steady trend of reduction of seasonal freezing depth has been observed in mid-hill terrain up to the top forest border (from 1400–1500 to 2700 m) for the period 1974–1998. Data relating the value of mentioned characteristic on two opposite, but equal by construction, slopes of the central part of the Zailiyskiy Alatau Range at absolute altitude of 2570 m can be viewed here. So during mentioned period, on loamy-detritus soils of the northern slope, the seasonal freezing depth decreased by 25 cm, and on idem ground of the southern one, it reduced by 21 cm.

The tendency in changing of frost penetration depth on northern and southern slopes was not shown for the period since 1975 up to 1998 at absolute height of 3000 m. However, the increasing tendency of seasonal freezing depth on slopes with different expositions has been marked for the last 3 years. That is connected with the reduction of snowiness. Thus, it has increased for 1 m on northern and for 0.3 m on southern slopes.

The revealed tendency of reduction of seasonal frost penetration depth for mid-hill terrains continued till 2002. It has been stable since 2003 to present time, and has been changing just slightly during the years.

Under all other equal conditions, interannual fluctuations of freezing intensity and its depth depend on two factors: distinctions of soils temperatures before frost penetration, and terms ratio between the beginning of ground freezing and snow cover formation.

General glacier recession in the Tien Shan conducts to an output of moraine sediments up to the surface. They are transferring from subglacial status to a subaerial one. This process essentially changes an orientation of cryogenic and post-cryogenic processes on fresh moraines. When small glaciers recede, permafrost moraine layers are released. In subaerial conditions, they are subjected to thawing on 1–2 m depth from the surface during summer seasons; that is, the layer of seasonal thawing appears.

During large glacier receding, long-term frost penetration of the transparent and blind talik systems occurs alongside with the mentioned process. Transformation of the moraines from subglacial to subaerial condition generates a modification of character of relief formation; new processes and effects appear. There is an especially distinguishing thermokarst among them and different modifications.

The thawing of buried ice, accompanied with partial thawing of accommodating permafrost moraines, conducts to subsidence formation, which is filled usually with the water from melted snow. In such a way, thermokarst lakes are forming. Some of the subglacial lakes originate from water-current ponding by the sediments of cryogenic landslips. Thus, fresh moraines are the same kind of arena for intensive formation of lakes of various genesis, sizes, and configurations. There were only 10 lakes, (with the capacity of each one over 10,000 cubic meters) in the middle of 1960 on the northern slope of the Zailiyskiy Alatau. In 1980, that number has increased to 41, and by 1990, to 60. The last 10 years of aero-visual supervision of the glacial belt testify that their quantity significantly increased.

In addition to the lakes, soliflucton processes are developing on fresh moraines, and also active subglacial rock glaciers are forming. Loose, fragmental deposits of fresh moraines increase the supply area of subglacial rock glaciers that had been formed earlier, in that way stimulating the moving of the last ones. Icings are emerged and destroyed; structural grounds are formed; and frost weathering processes are activated on fresh moraines.

Phase Changes of Water as a Basis of the Water and Energy Exchange Function of the Cryosphere

V.V. Shepelev
Melnikov Permafrost Institute, SB RAS, Yakutsk, Russia

Water exists on our planet in all three of its phases within the temperature and pressure ranges found on Earth, resulting in very high activity and extent of phase transitions of water. This involves intensive phase interaction of water, that is, water transfer from the liquid state to the gaseous state and back, from the solid state to the gaseous or liquid state, etc.

Many authors emphasized the importance of the interphase form of water movement. Priklonsky (1958), in his general characterization of groundwater formation, considered such phase changes as evaporation and freezing to be the main types of water movement in the ground. Khodkov & Valukonis (1968), in their discussion of the main types of movement of natural waters, ranked the phase transition of water above other forms of water movement or migration. It is this form of water movement that Vernadsky (1960) had in mind, suggesting the existence of the phase field of the Earth, which encompasses the upper lithosphere and the near-surface atmosphere. The necessity of applying the theoretical knowledge on water physics to investigations of global water cycles was underlined by Sokolov (1966). He noted, in particular, that the role of the cryosphere as a water-exchange system is very high, though remains little studied.

Research on interphase interactions of water is complicated by the fact that all the basic states of water are not phase-homogeneous, but phase-heterogeneous. In other words, the phase mixing effect is inherent in water. In the atmosphere, water is present in liquid, solid, and gaseous states. Similarly, surface ice and ice-rich permafrost contain some amounts of the liquid and gas forms of water. The phase heterogeneity of the basic states of water can be explained by the fact that in nature, there exists no absolutely pure water in either of the states—liquid, solid, or gas. Water in any macroscopic volume is, above all, a dispersion medium in which various microscopic impurities, such as mineral, organic and other solid particles and compounds, are dispersed. The high surface energy of these microscopic particles causes the formation of water microphases on their surface, which intensively exchange water with the surrounding macroscopic medium, determining to a large measure its water- and energy-exchange function.

In the ground, the microscopic phase dispersion of water is boosted, so to say, by the mechanical dispersion of the soil. For example, pellicular water in the zone of aeration is a liquid microphase of water, which actively exchanges water and interacts with the surrounding pore air medium. Similarly, unfrozen interfacial water in ice-rich permafrost can be considered a liquid microphase of water which is in dynamic equilibrium with the pore ice medium. This explains, among other factors, the well-known concept of equilibrium unfrozen water content in frozen ground (Tsytovich 1945, 1959). This concept implies that the unfrozen water content in frozen ground varies with changes in temperature and external pressure of soil or rock. Phase changes of unfrozen water to ice and back occur even under very slight changes in ground temperature or external pressure.

Hence the basic physical states of water reflect only its macroscopic phase homogeneity, characterizing one or another phase of bulk water as a continuum. From the microscopic point of view, the main physical states of water are phase heterogeneous, and this drives the water and energy exchange and other important processes in the Earth's atmosphere, hydrosphere, lithosphere, and, certainly, cryosphere.

Considering the crucial role the phase changes and phase interactions of water play in the cryosphere, and in order to quantify the water and energy exchange function of the cryosphere, it is proposed that the global cycles in climatic circulation of water are distinguished as follows: cryoatmogenic, cryohydrogenic, atmolithogenic, glaciogenic, and cryolithogenic (Table 1).

The *cryoatmogenic cycle* is related to sublimation of water vapour in the atmosphere, that is, the phase changes of water from gas to solid and back, and subsequent falling on the earth surface as large snow and ice formations.

The *cryohydrogenic cycle* is driven by the formation of seasonal river ice, lake ice, icings, and ground ice in the active layer of permafrost and the subsequent melting of these seasonal ice forms, as well as snow cover.

The *atmolithogenic cycle* involves evaporation, condensation and sublimation of water in the zone of aeration, which can be viewed as subsurface atmosphere and where intensive moisture transfer occurs, linking the atmosphere and the lithosphere.

The *glaciogenic and cryolithogenic cycles* are caused by long-term, rather than seasonal, climatic fluctuations. In cold periods, the solid phase of water in glaciers and permafrost increases in volume and mass. Conversely, in warm periods, liquid water resources increase due to melting of glaciers and ground ice. Hence the glaciogenic and cryolithogenic cycles

Table 1. Characteristics of the cryosphere as a water and energy exchange system.

Main water and energy cycles	Mass of water involved in annual water cycle, kg	Energy released (+) or taken up (-), Wt
Cryoatmogenic	$1.0 \cdot 10^{13}$	$\pm 0.9 \cdot 10^{12}$
Cryohydrogenic	$2.6 \cdot 10^{16}$	$\pm 2.75 \cdot 10^{14}$
Atmolithogenic	$0.2 \cdot 10^{11}$	$\pm 0.18 \cdot 10^{10}$
Glaciogenic	$0.25 \cdot 10^{16}$	$- 2.6 \cdot 10^{14}$
Cryolithogenic	$2.5 \cdot 10^{13}$	$- 0.26 \cdot 10^{12}$

have a trend effect on the annual balance of the liquid phase of natural waters, causing a long-term decrease or increase in their volume and sea level.

For quantitative comparison of the cycles identified above, the mass of water involved annually in each water-exchange cycle and the thermal energy released or taken up during the changes in state of water have been estimated based on available information (see Table 1). It should be noted that the water-exchange functions of some of these cycles are as yet little understood and poorly quantified. This is particularly true for the cryoatmogenic and atmolithogenic cycles, thus requiring the establishment of special-purpose research and observation programs to obtain more reliable estimates. As for the rest of the cycles, the quantitative characterization of their water- and energy-exchange function has been based on the analysis of relatively representative data.

The values presented in the table indicate the crucial role of the cryosphere in the global water and energy budget, allowing us to call it a fluctuating cryogenic phase shell of our planet. Further investigations of the water- and energy exchange function of the cryosphere in this perspective will contribute to a better understanding of the role of the cryosphere in total global exchange of energy and matter, and help detect the changes in these processes due to natural factors and human impacts.

Acknowledgments

The author would like to thank Larisa Fedorova and Lilia Prokopieva, Melnikov Permafrost Institute, for assistance in preparation of this manuscript.

References

Khodkov, A.E. & Valukonis, G.Y. 1968. *The Formation and Geological Role of Groundwater.* Leningrad: Izd-vo Leningradskogo Universiteta, 216 pp.

Priklonsky, V.A. 1958. Basic experimental issues in groundwater formation research. In: *Transactions of the Laboratory of Hydrogeological Problems*, Vol. XVI. Moscow: Izd-vo AN SSSR, 86-105.

Sokolov, B.L. 1996. New results of experimental investigation on the lithogenic component of river runoff. *Vodnye Resursy* 23(3): 278-287.

Tsytovich, N.A. 1945. On the theory of equilibrium state of water in frozen ground. *Izvestia AN SSSR, Seria Geograficheskaya* 5–6: 61-67.

Tsytovich, N.A. 1959. Physical processes and phenomena in freezing, frozen and thawing soils. In: *The Principles of Geocryology (Permafrost Studies). Part I. Permafrost Science*. Moscow: Izd-vo AN SSSR, 108-152.

Vernadsky, V.I. 1960. *Selected Papers*. Vol. 4, Book 2. Moscow: Izd-vo AN SSSR, 651 pp.

Near-Surface Stress and Displacement Measurements from Vehicle Passage Over Frozen Ground

S. Shoop
USA-CRREL, Hanover, NH

Introduction

The freezing and thawing process creates extreme strength changes in frost-affected soils. These seasonal changes in strength both benefit and decrement performance of engineered structures and have a particularly severe effect on transportation systems and horizontal construction. We have developed modeling capability for simulating the complicated impact of freeze-thaw layering on transportation systems. These models have been used in several applications: vehicle operations on freezing/thawing ground, seasonal deterioration of unsurfaced roads, freeze-thaw effects on pavement structures, and aircraft operations on frozen ground (Shoop et al. 2006, Haehnel et al. 2005, Parker et al. 2006). An additional challenge occurs in obtaining data for the development and validation of these models. The measurement of stress and strain in soils is problematic even in unfrozen ground, but to use these instruments in frozen ground, they must also be able to sustain the hardships of prolonged cold temperatures on fluid, sensor, and electronic components.

The objective of this project was to build an instrumented test section where we could observe the changes in vehicle-induced stress and displacement at different frost depths. Three test cells, consisting of two feet of sand (SM), silt (ML), and clay (CL) soils were constructed over a well-compacted sand roadbed. The test cells were instrumented for stress or pressure and for displacements, as well as for temperature and moisture profiles. Trafficking of the test sections was done periodically at various frost depths ranging from no frost to over 20 inches of frost.

Instrumentation

Based on a survey of the limited instruments available for stress and strain measurements in soils, few of which had been used within frozen ground, three types of instruments were chosen. For stress measurement, we chose two methods: the National Soil Dynamics Laboratory (NSDL) Soil Stress State Transducer (SST) and a pressure pad by Sensor Products LLC. Soil displacements were measured using extensometers designed by Geokon.

The SSTs are designed by the engineers at NDSL to measure total stress state (Nicols et al. 1987). Three SSTs were obtained on-loan from NSDL. The SST consists of 6 semiconductor pressure sensor transducers installed in a small sphere to measure stress in 3 perpendicular directions and in 3 additional offsets as shown in Figure 1. The sensors are installed with the z direction upward and the x and y directions facing rearward to the left and right side of the approaching vehicle. The six pressure measurements

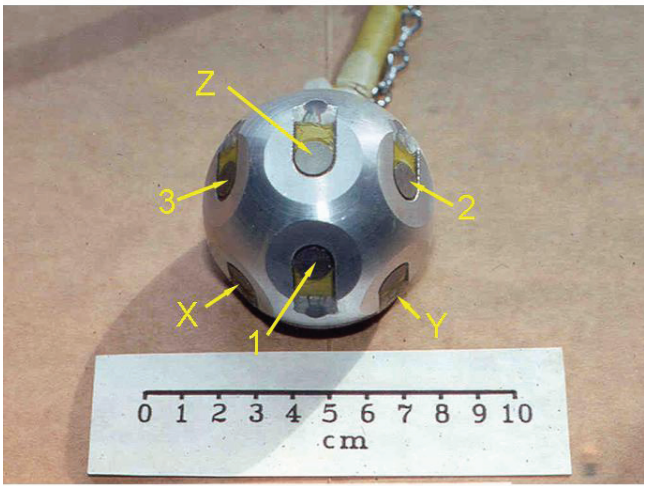

Figure 1. The National Soil Dynamics Laboratory Soil State Transducer (SST) showing the directions of the six pressure sensors.

can be used individually as a measure of pressure in the specific direction, or they can be used in combination and converted to principle stresses with direction cosines or stress invariants. The SST transducers were coated with Teflon to reduce shear on the sensor surface, and the entire sensor was wrapped in plastic and carefully oriented in the soil. The SSTs were installed at five-inch depth within each of the three test soils.

The second stress measurement system was the pressure pads. The pressure pad is a matrix of piezoelectric sensors 19.2 by 19.2 inches with 0.6-inch grid spacing. The sensors are protected with a urethane rubber cover and measure the pressure normal to the pad surface. The pad can capture the tire contact stress distribution as it rolls over the surface, and was specifically designed for use on deformable surfaces, although not to be buried in soil or frozen. Prior to installation in the soil, the pressure pads were tested under vehicle loading while on a hard surface. Two pads were then buried at two inches within the sand and the silt test sections.

The displacement of the soil was measured by installing extensometers modified to measure near-surface displacements. The base of the extensometers was placed below the test soils. Four to six rods of different lengths were fixed to each base, and an anchor plate was attached to the top of each rod as the extensometer was buried. The anchor plates were designed to move with the soil and independent of the other rods in the cluster. Three clusters of extensometers were installed in each test soil: one 6-anchor cluster was placed on the center line of the target wheel path, and two 4-anchor clusters were placed 6 inches to either side of the wheel path center line.

Experiments

The experiments consisted of trafficking vehicles across the test sections during freezing. After several baseline tests were done to make sure all of the instrumentation was working correctly, the ground was allowed to freeze to different depths either naturally or with assistance from freezing panels. At specific frost levels, a vehicle and trailer assembly was driven across the test section and the soil stresses and displacements were measured. Prior to trafficking, the test section was fully characterized by temperature and moisture profiles, density, and various strength measurements.

Results

Even though these instruments had never been used in frozen ground, we were pleased with the performance of all of the instrumentation. The SSTs performed flawlessly during the course of all of the experiments. Although a final reduction of the data into principle stress components has not yet been done, the direction stress data shows the stress from the bow wave in front of each tire, and then the large vertical pressure spike as each tire passes over the sensor. The stress magnitudes clearly diminish as the ground freezes above the sensor and then diminish further as the frost envelopes the entire sensor.

The pressure pads were perhaps the most finicky of the instruments and several of the fine wires within each pad were broken during the course of installation and testing. The configuration of the pads and their calibration were also not entirely suitable for the test conditions so that absolute values of the contact stresses are not reliable. Nonetheless, the trends show the tire contact stresses decreasing and the contact area increasing when the pad is buried, and slight decrease in contact stresses and increases in area as the ground freezes.

As a perfect compliment to the stress measurements, the soil extensometers also show the bow wave prior to each wheel as well as the strong vertical displacement when each wheel passes over the sensor, as shown in Fig. 2. In addition to the displacements measured during trafficking, the extensometers also measure the plastic deformation from the vehicle compacting the soil and the frost heave during freezing.

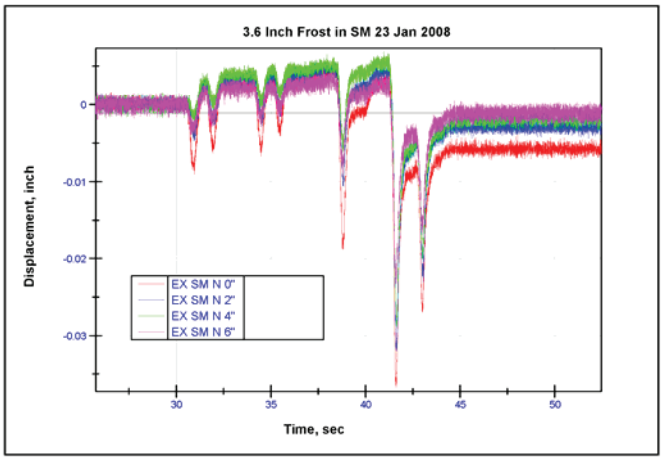

Figure 2. Extensometer data for a four-axle vehicle pulling a multi-axle trailer on sand with 3.6 inch frost (bottom).

Acknowledgments

This project benefited from many engineers and technicians that assisted with design, calibration, and installation of these instruments including Thomas Way and Dexter LaGrand of NSDL, Jason Blume at Sensor Products LLC, Tony Simmonds and Jim McCrae at Geokon, and Glenn Durrell, Chris Williams, Mike Parker, Barry Coutermarsh, Lynette Barna, and Rosa Affleck at CRREL.

References

Haehnel, R., Shoop, S., Affleck, R. & Janoo, V. 2005. Finite element modeling of a thawing pavement structure. *Proceedings, 7th International Conference on the Bearing Capacity of Roads, Railways and Airfields, Trondheim, Norway, 27–29 June.*

Nichols, T.A., Bailey, A.C., Johnson, C.E. & Grisso, R.D. 1987. A stress state transducer for soil. *Transactions of the ASAE* 30(5): 1337-1341.

Parker, M., Barna, L., Shoop, S. & Haehnel, R. 2006. Comparison of Finite Element Model (FEM) data and Single Point Layered Elastic Model (SPLEM) data of a C130 operating on a frozen runway structure. *13th International Cold Regions Conference, Orono, Maine, July*.

Shoop, S., Haehnel, R., Janoo, V., Harjes, D. & Liston, R. 2006. Seasonal deterioration of unsurfaced roads. *ASCE J. of Geotechnical and Environmental Engineering* 132(7): 852-860.

Formation of Frost Boils and Earth Hummocks

Yuri Shur
University of Alaska Fairbanks Department of Civil and Environmental Engineering, Fairbanks, Alaska, USA
Torre Jorgenson
ABR – Environmental Research and Services, Inc., Fairbanks, Alaska, USA
Mikhail Kanevskiy
University of Alaska Fairbanks Institute of Northern Engineering, Fairbanks, Alaska, USA
Chien-Lu Ping
University of Alaska Fairbanks Agriculture and Forestry Experiment Station, Palmer, Alaska, USA

Existing hypotheses of frost boils and earth hummocks formation generally are limited to climatic and active layer processes within a simple two-component system. Based on our field studies and literature review, we have identified two other important factors: vegetation, which affects active layer depth and organic-matter accumulation, and permafrost aggradation, which affects heave and thaw settlement. Accordingly, we have developed a conceptual model of a four-component system involving climate, vegetation, active layer, and permafrost.

A model consists of five stages in the development of frost boils and earth hummocks (Fig. 1). The first three stages describe formation of frost boils, which generally occur in high- to mid-arctic tundra ecosystems. The last two stages depict the evolution of frost boils into earth hummocks, which typically occurs under the slightly warmer climates of the low arctic and taiga regions, or in response to warming climatic conditions.

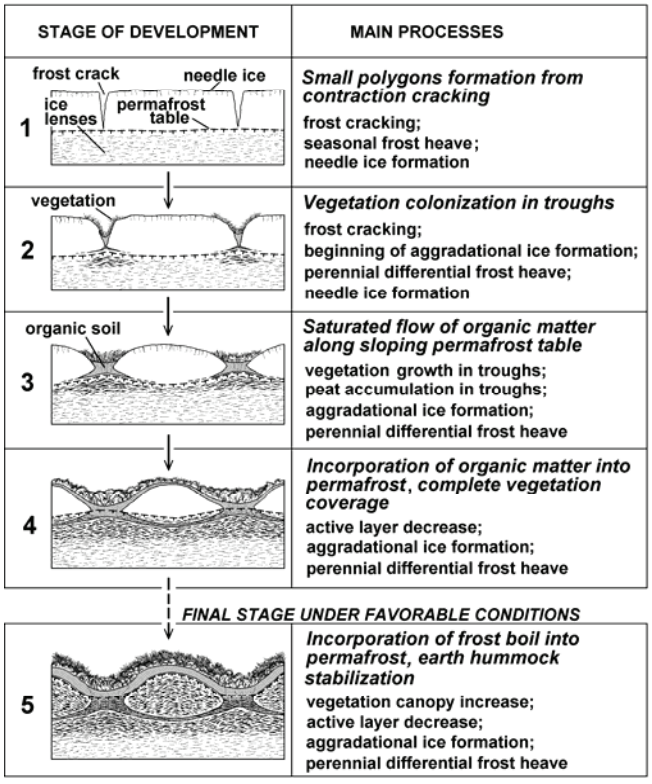

Figure 1. Stages of frost boils and earth hummocks formation. Seasonal segregated ice within the active layer is not shown.

First, small (0.5–3 m) polygons form under a bare soil surface due to frost cracking. This process is typically limited to the high- to mid-arctic, where the low temperatures and thin snow allow sufficient contraction cracking. The contraction cracking generally is limited by the thickness of the active layer because of the small-scale of the features, as opposed to the deeper cracking associated with the larger-scale contraction associated with development of ice-wedge polygons. These small polygonal forms are widespread in the Arctic as noted by ecologists, pedologists and permafrost scientists.

Second, vegetation colonizes the protected microsites of the shallow troughs that develop over the cracks. The surface of frost-boils is usually elevated above the surrounding inter-boil areas, and therefore, is susceptible to wind erosion, especially during winter freeze when the surface becomes elevated by seasonal frost heave. Needle ice prevents vegetation colonization of polygon centers.

Third, further vegetation growth and organic-matter accumulation in troughs change the thermal properties of the soil, causing the depth of the active layer to steadily decrease. In response, segregated ice forms at the top of the aggrading permafrost table, creating an intermediate layer with distinctly different soil and ice morphology (Shur 1988). Gravimetric moisture content in this layer often exceeds 100%. The aggrading ice causes the ground surface to heave. This perennial frost heave differs from seasonal frost heave in the active layer, because it is cumulative and leads to formation of long-term existing features. Features formed by perennial frost heave exist for tens to thousands of years. The differential relief caused by perennial frost heave in frost-boil systems varies from centimeters to decimeters.

At this stage, movement of organic matter from troughs under frost boils becomes important. The permafrost table develops ridges beneath the vegetated areas and concave depressions, or "bowls," beneath the frost boils. Because the permafrost table slopes at the margins of the bowls, organic matter formed in inter-boil areas creeps or flows under saturated conditions into the voids and cracks. There are two possible mechanisms for this gravitational movement of saturated organic matter down to the permafrost table. First, contraction cracks continue to develop, particularly at the interface of the organic matter and the mineral soil. During summer thaw, saturated organic matter, which tends to be moderately or highly decomposed, flows down the cracks.

Second, the thawing of segregated ice, which is formed during fall freeze-back at the top of the permafrost table, leaves voids that are filled with mobile organic matter. Over time, a concave layer of organic matter mixed with mineral soil accumulates at the permafrost table underneath the mineral frost boil. In some boils the organic matter can be discontinuous, but can be traced to its source—the vegetated inter-boil area.

Penetration of organic matter along the bottom of the active layer leads to further decrease in the active layer, aggradation of ice, and incorporation of organic matter in the upper permafrost. This in turn further raises the surface of the frost boil and increases differentiation in seasonal frost heave between boils and inter-boil areas. At this stage, a mature frost boil has developed, and can become the climax stage in the Arctic. While this downward movement of organic matter around frost boils is similar to elements of circulation as described by Mackay's model (1980), there are important differences. In our model, organic moved downward accumulates in the aggrading permafrost. There is no upward movement of solid material, and only dissolved organic can move to the freezing front in winter or desiccated surface in summer.

Fourth, frost boils evolve into earth hummocks when vegetation and organic-rich soil eventually expand to cover the entire surface. This spread may occur over a long time and may be assisted by climate warming. The spread leads to further decreases in depth of the active layer and additional accumulation of aggradational ice above the layer of organic matter, with more accumulation of aggradational ice and more perennial frost heave.

Fifth, sufficient vegetation develops, peat accumulates, and seasonal thaw no longer reaches the base of the former frost boil. Eventually, the thawing front can become limited to the surface peat and no longer penetrates the mineral frost boil. Our previous studies (Shur & Ping 2003, Shur et al. 2005, 2006) explained evolution of the earth hummocks from the frost boils due to growth of vegetation at the surface of frost boil and subsequent accumulation of aggradational ice. Recent observations by Kokelj et al. (2007) support such an explanation.

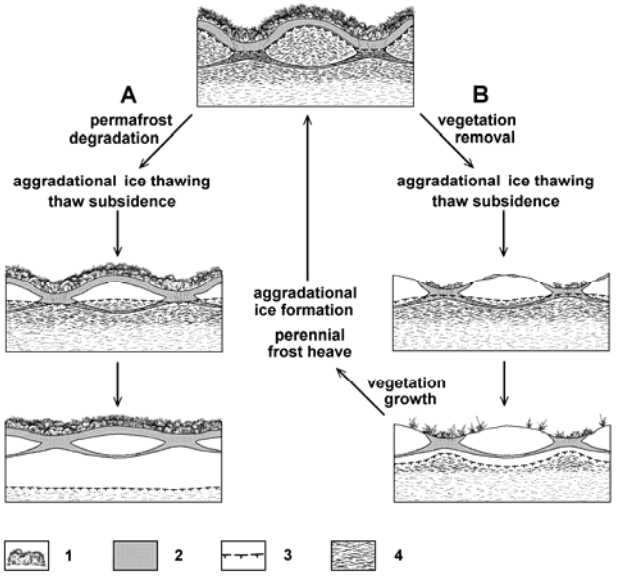

Figure 2. Degradation of earth hummocks due to (A) permafrost degradation and (B) denudation of vegetation, resulting in the regressive frost boils formation. 1 – vegetation; 2 – peat, organic matter; 3 – permafrost table; 4 – ice lenses.

Earth hummocks once fully developed are very sensitive to environmental changes because they evolved in conjunction with ice aggradation below the active layer. Disturbance to the surface, such as by fire, or climate warming can lead to degradation of the extremely ice-rich soil beneath the active layer. In a time scale of hundreds to thousands of years, climate change is the most important process leading to the degradation of the permafrost and earth hummocks (Fig. 2A). In a time scale of years, denudation of vegetation is the leading process in the formation of regressive frost boils. Vegetation recovery, however, can reverse the process and stabilize or restore the earth hummocks (Fig. 2B). Such processes were evident in field observations by Kokelj et al. (2007).

Acknowledgments

Work was supported by NSF grants ARC-0454939 (to YS), ARC-0454985 (to MTJ), EPS-0346770 (to MZK), and OPP-0120736 (to CLP).

References

Kokelj, S.V., Burn, C.R. & Tarnocai, C. 2007. The structure and dynamics of earth hummocks in the subarctic forest near Inuvik, Northwest Territories, Canada. *Arctic, Antarctic and Alpine Research* 39: 99-109.

Mackay, J.R. 1980. The origin of hummocks, western Arctic coast, Canada. *Canadian Journal of Earth Science* 17: 996-1006.

Shur, Y.L. 1988. The upper horizon of permafrost soils. *Proceedings of the Fifth International Conference on Permafrost*, *Trondheim, Norway, August 2–5, 1988*: 867-871.

Shur, Y., Ping, C.L. & Jorgenson, M.T. 2006. Soil formation in frost-boil environment. *Proceedings of 18th World Congress of Soil Science, Philadelphia, Pennsylvania, USA. July 9–15, 2006*. Abstract 106-8.

Shur, Y.L., Ping, C.L. & Walker, D.A. 2005. Comprehensive model of frost boils and earth hummocks formation. *Proceedings of the Second European Conference on Permafrost, Potsdam, Germany, June 12–16, 2005*: 79.

Shur, Y. & Ping, C. 2003. The driving force of frost boils and hummocks formation. *Eos Trans. AGU* 84(46), Fall Meet. Suppl., Abstract C21B-0823.

The Role of Lakes in Carbon Transfers from Permafrost to the Atmosphere: Eight Mile Lake, Alaska

James O. Sickman, Guntram Von Kiparski, William Vicars
Department of Environmental Sciences, University of California, Riverside, Riverside, CA 92521, USA
Edward A.G. Schuur, Jason G. Vogel
Department of Botany, University of Florida, Gainesville, FL 32601-8526, USA

Introduction

In the permafrost-affected watersheds of the arctic and subarctic, dissolved carbon losses can be considerable, accounting for over 37% of net ecosystem production (NEP) in some regions (Judd & Kling 2002). Therefore, dissolved carbon flux may be an important determinant of regional carbon balance in the arctic and subarctic, but more research is needed to understand how these fluxes will respond to warming and whether downstream lacustrine systems can attenuate losses of terrestrial carbon.

The main objectives of our study were to quantify hydrologic losses of carbon along a gradient of permafrost thaw in the Eight Mile Lake watershed and assess the effect of in-lake processes on watershed carbon losses.

Materials and Methods

Field site

The Eight Mile Lake Watershed (EMLW) is located near Healy, Alaska, near Denali National Park. Elevation range in the watershed ranges from 656 to 1057 m, and the drainage area is 1108 hectares. The maximum depth and area of the lake are 3 m and 69 hectares. Within the catchment, plot studies have been initiated across a gradient of permafrost thaw: severely thawed (Old Karst), moderately thawed (New Karst), and not thawed. (Tussock)

Field and laboratory measurements

During 2006, we measured concentrations and estimated fluxes of dissolved organic carbon (DOC) and dissolved inorganic carbon (DIC) at both plot (<5 ha) and watershed (>1000 ha) scales. Stream samples were collected every two-days using ISCO automated samplers during snowmelt (May and June) and manually every week during July through September (surface streams freeze in late September). Soil water was sampled at multiple depths within the tundra active layer using specialized lysimeters called Multisamplers (Martin et al. 2003). Inlet stage was measured in a culvert to a road that bisects the watershed and used to weight lake inlet and outlet chemistry for computation of C fluxes to the lake. Annual runoff was estimated as the difference between watershed precipitation and evaporation.

DOC was measured by high-temperature catalyzed combustion on a Shimadzu TOC 5000. Dissolved CO_2 (the dominant form of DIC in these low pH (<5.6) waters) was determined using headspace equilibration followed by measurement of CO_2 partial-pressure using a LICOR LI820.

Results

Controls on hydrologic carbon fluxes

Soil water DOC concentrations increased significantly along the natural gradient of permafrost thaw in the Eight Mile Lake watershed. (Fig. 1A). In severely thawed soils, concentrations typically ranged from 40 to 60 mg L^{-1}. In moderately thawed soils, DOC concentrations were ca. 30–40 mg L^{-1}, and in unthawed soils, usually 20–25 mg L^{-1}. We observed no strong seasonal trend in soil water DOC. DOC concentrations in the lake inlet responded strongly to hydrology; pulses of DOC were observed during snowmelt runoff (30 mg L^{-1}) and summer rain events. DOC concentrations in the lake outlet were lower and more constant (~10–16 mg L^{-1}) (Fig. 1B).

Dissolved CO_2 in soil water increased with active layer depth with concentrations between 10 to 27 mg C L^{-1} below a depth of 30 cm (Fig. 2C). Dissolved CO_2 concentrations in

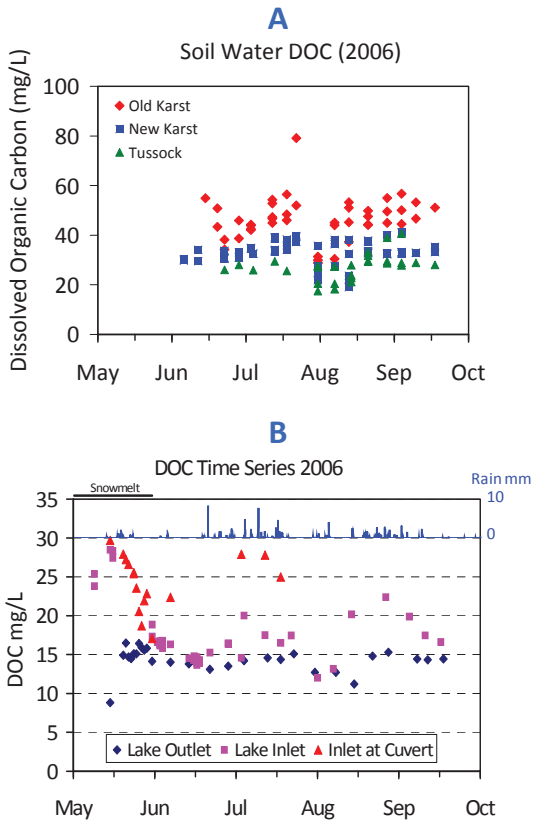

Figure 1. Patterns of DOC concentrations at Eight Mile Lake Watershed during 2006.

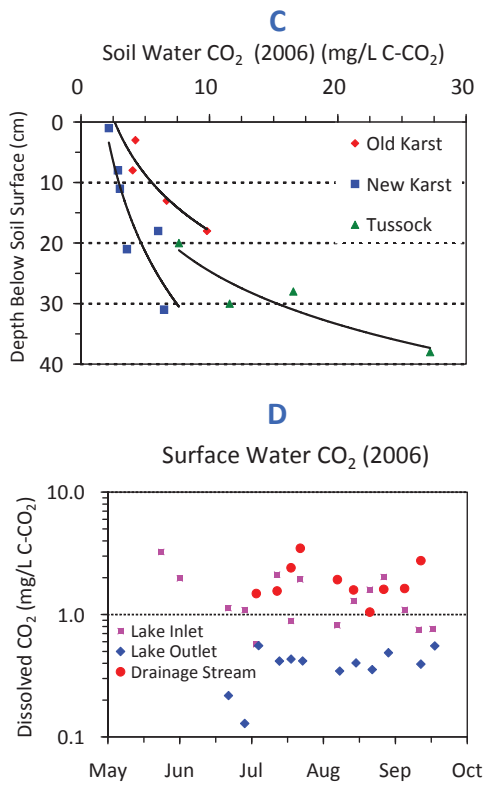

Figure 2. Patterns of DIC concentration at Eight Mile Lake Watershed during 2006.

surface inflows to the lake ranged from ca. 1–4 mg C L^{-1}; at the lake outlet concentrations were <0.5 mg C L^{-1} (Fig. 2D).

Watershed fluxes of water and carbon

During water year 2006, summer rainfall contributed the majority of annual precipitation and runoff (Table 1). Total runoff was estimated to be 19.4 cm. Using lake bathymetry measurements, we computed a lake volume of 1.73 x 10^6 m^3, yielding a mean lake residence time of 0.80 years.

Using stage-weighted inlet and outlet chemistry and estimates of annual runoff, we made a first approximation of the carbon budget for the lake (Table 2). The lake was a strong sink for DOC and CO_2 produced in terrestrial portions of the watershed and was a small net source for POC. Overall, in-lake processing of C accounted for a 50% reduction in watershed yield of C.

Conclusions

At Eight Mile Lake, permafrost thawing, hydrology, and in-lake processes had strong effects on watershed yield of carbon. Concentrations of DOC in soil waters in severely thawed plots were double those in intact tundra. The depth of the seasonal active layer was positively related to dissolved CO_2 concentrations in soil water. Hydrologic flushing (snowmelt and summer rain events) produced spikes in DOC concentration. Waters entering the lake had higher DOC and CO_2 concentrations than waters exiting the lake. Outgassing of CO_2 took place rapidly, while losses of DOC occurred over the course of weeks to months. Preliminary input/output estimates show that the lake consumes about 50% of the carbon entering via runoff.

Table 1. Water balance for the Eight Mile Lake watershed.

Component	Winter/Snowmelt	Summer
Snow/Precipitation Depth (cm)	10.0	22.7
Runoff Coefficient	0.80	0.50
Runoff Depth (cm)	8.0	11.35
Runoff Volume (m^3)	8.86 x 10^5	1.26 x 10^6
Lake Volume/Residence Time	1.73 x 10^6 m^3 / 0.80 years	

Table 2. Dissolved C input/output for Eight Mile Lake. Terrestrial yield is watershed yield at the inlet of the lake. Catchment yield is yield at the outlet of the lake.

Carbon-Flux	Terrestrial Yield (g/m^2)	Watershed Yield (g/m^2)	Net Change Due to In-lake Processes (g/m^2) / % of input
DOC	5.2	2.3	-2.9 / -56%
Dissolved CO_2	0.40	0.07	-0.33 / -83%
POC	0.38	0.59	+0.21 / +55%
DOC + CO_2 + POC	6.0	3.0	-3.0 / -50%

Acknowledgments

We thank Christian Trucco for field assistance. Funding was provided by the National Science Foundation, Division of Environmental Biology.

References

Judd, K.E. & Kling, G.W. 2002. Production and export of dissolved C in arctic tundra mesocosms: The roles of vegetation and water flow. *Biogeochemistry* 60: 213-234.

Martin, J.B., Hartl, K.M., Corbett, D.R., Swarzenski, P.W. & Cable, J.E. 2003. A multi-level pore-water sampler for permeable sediments. *Journal of Sedimentary Research* 73: 128-1325.

Recent Climatic Changes in Yakutia

Yu.B. Skachkov
Melnikov Permafrost Institute, SB RAS, Yakutsk, Russia

Introduction

Yakutia is the largest administrative region of the Russian Federation, occupying an area of 3.1 million square kilometers. Most of the region is underlain by continuous permafrost. Being the product of climate, permafrost is a sensitive indicator of its long-term changes. In view of the predicted permafrost degradation due to global warming and its negative consequences, it is extremely important to gain complete information on recent air temperature variations in the region.

During the past years, several works have been published on the general assessing of climate changes in Siberia and the Far East over different periods of time (Ippolitov et al. 2007, Izrael et al. 2006, Pavlov & Malkova 2005, and others). The present paper continues the previous research made by the author over the period 1966–1995 (Skachkov 2001), and using the new data of the last decade, informs on the current rate of climate warming in Yakutia.

Data and Calculation Technique

To assess trends of the changes of the annual average air temperature (T_{air}) over the period 1966–2005 throughout Yakutia the following actions have been carried out:

1. selection of 29 weather stations with accurate unceasing observation data (Fig. 1).
2. calculation of the linear trend of the air temperature and annual air temperature amplitude and their variance.
3. assessment of the linear trends.

The linear trends significance was estimated with the student criteria by the determination coefficient squared value R^2. The determination coefficient shows the linear trend deposit in the general variation of the analyzed parameter. The parameter variation trend would be considered significant if its confidence level equaled or surpassed 95% ($P \geq 0.95$). With the sample size of 30 years, it conforms to $R^2 \geq 14\%$, and of 40 years, $R^2 \geq 12\%$.

Figure 1. The plan of location of the stations selected for analysis.

The temporal series data of the mean monthly air temperature were used in the analysis. The meteorological observation data were obtained from the climatologic handbook and monthly magazines and also from the USA National Ocean and Atmosphere Agency database (http:www.ncdc.noaa.gov). Trend parameter calculations were performed with Microsoft Excel 97.

Results and Discussion

The mean annual air temperature field analysis shows that T_{air} over the observed area widely varies from -16.7°C (Oymyakon) to -5.6°C (Vitim). High interannual variability of the mean annual air temperature is the peculiarity of extreme continental climate endemic for the major territory of Yakutia. The fluctuations of T_{air} over the observed period in the mean from all stations amount to 4–5°C. The lowest fluctuations of T_{air} (-3.4°C) were noticed in Batamaya, and the highest (-5.6°C), in Tiksi and Chulman.

The global warming started in the end of 1960s over the majority of the Northern Hemisphere including Yakutia. From 1966 to 1989, the warming in this area passed on rather smoothly and had almost zonational increment of the air temperature. The highest increment values (1°C and more) are noticed in central and south Yakutia. Toward the north, there is noticed the decrease of temperature increment. The air temperature trend values of the Laptev Sea shore, island stations and northwest of Yakutia are subzero at this time (Skachkov 2001).

The early 1990s saw spatially variegated temperature increase appear sharply throughout Yakutia. Southward of the latitude 64°N, the air temperature increment amounted to 1.5–2°C and more; northwest and northeast Yakutia was 0.5–1°C. It is significant that the major contribution to the

mean annual air temperature increase pertains to winters that became warmer, especially in central and south Yakutia.

Turning to the data-processing analysis over the period 1966–2005, the trend analysis shows a warming tendency throughout Yakutia, though it is spatially variegated. The trend speed over the area varies from 0.16°C/decade to 0.63°C/decade. The highest trend speed was noticed in central Yakutia, and the lowest, in the regions northward of latitude 64°N. In the arctic regions of Yakutia, the warming is irreducible. The annual air temperature increment appeared mostly due to a rise in the number of warm winters.

The trends comparison for the period 1966–1995 and 1966–2005 shows that the warming rate has decreased and, in some regions, paused during the past decade.

As before (Skachkov 2001), no latitudinal or submeredianal allocation regularity is noticed.

Apart from linear trend parameters assessing the relative contribution of the trend component in the general temperature dispersion, the air temperature increment trends of Yakutia proved to be reliable in 12 points (the annual and winter period values). The reliable trends for the summer period were noticed only in 3 points.

Recently in the scientific literature, there have emerged reports that the current warming in the regions of the Northern Hemisphere is accompanied by a decrease of annual air temperature amplitudes. At the same time, it is noticed that the lowest temperatures grow faster than the highest ones.

Interannual variability is inherent for both mean annual and mean seasonal air temperatures. Therefore the amplitude T_{air}, being one of the most important parameters of the continentality, changes from year to year. The amplitude T_{air} is defined as the difference of the mean warm (T_{sum}) and cold seasons of year (T_{win}). The cold period includes the whole period with subzero temperatures at each station, while the warm period, the period with the above-zero temperatures. At the island Kotelnyi, the most northern station in Yakutia, the warm period lasts only 2 months; at the stations Tiksi, Kjusjur, Jubilejnaja, Cokurdah, and Olenek, the warm period lasts 4 months. At the other stations of the region, summer lasts for 5 months.

The winter air temperature increasing faster then the summer one, the difference (T_{sum} - T_{win}) falls. The most significant and noticeable decrease (to 1.5–2.5°C) descended in central Yakutia.

Conclusion

Significant warming has been noticed in Yakutia during the past decades. The highest air temperature rise in the region occurred in the 1980s. Warming has obviously paused since the mid 1990s in some of the Yakutia regions. There are some points showing a trend of temperature decrease. In general, the 1966–2005 trends notably decrease compared with those of 1966–1995. There has been noticed a fall in continentality over the last decades in central Yakutia.

The insignificant summer period warming almost throughout the republic territory shows minimal cryolitozone reaction to the climate changes that should not cause much alarm. This thesis is also proved with longstanding research (Skachkov et al. 2007).

References

Ippolitov, I.I., Kabanov, M.V. & Loginov, S.V. 2007. Spatial and Temporal Scale of the Observed Warming in Siberia. *DAN* 412 (6): 814-817.

Izrael, Yu.A., Pavlov, A.V., Anokhin, Yu.A., Myach, L.T. & Sherstyukov, B.G. 2006. Estimators of Climate Elements Changes in Permafrost Regions of Russian Federation. *Hydrology and Meteorology* 5: 27-38.

Pavlov, A.V. & Malkova, G.V. 2005. *Recent Climate Changes of the North of Russia: the Album of Small-Scale Maps*. Novosibirsk: Academic Press Geo, 54 pp.

Skachkov, Yu.B. 2001. Present-day variations of air temperature in Yakutia. *Proceedings The Fifth International Study Conference on GEWEX in Asia and GAME, Aichi Trade Center, Nagoya, Japan, October 3-5, 2001*.3: 758-761.

Skachkov, Yu.B., Skryabin, P.N. & Varlamov, S.P. 2007. The Results of 25-years Monitoring Research of Cryolitozone at the Chabyda Station (Central Yakutia). *Proceedings of International Conference Cryogenic Resources of the Polar Regions, Salekhard, June 17-20, 2007*. Puschino, ONTI PNC RAN, 1: 167-170.

Permafrost, Parameters, Climate Change, and Uncertainty

Andrew G. Slater
NSIDC, University of Colorado, Boulder, CO, USA
David M. Lawrence
National Center for Atmospheric Research, Boulder, CO, USA

Introduction

Recently observed changes in the state of permafrost are many and varied. Appearance and disappearance of lakes, degradation of ice wedges, and changes in river channel morphology are several of the processes that have been linked to thawing of permafrost and warming of soil temperatures. Osterkamp (2007) suggests that permafrost at West Dock, Alaska, has warmed about 3.7°C since 1976 and may have warmed greater than 6°C since 1900. While most modeling efforts to assess the effects of future climate change on permafrost and frozen ground indicate that there will be substantial change, the magnitude and extent of the change is still uncertain (e.g., Lawrence & Slater 2005; Zhang et al. 2008). Part of the uncertainty in permafrost simulations can be associated with somewhat external factors such as simulation of snow or specification of soil and vegetation parameters. Here we present a sensitivity study of such inputs and parameters.

Methods

Model

A simple analytic model following the method of Kudryavtsev (Sazonova & Romanovsky 2003) was applied to estimate the current and future state of permafrost. The model produces a steady-state solution under the assumption of constant sinusoidal temperature forcing. The model also accounts for the presence of snow, vegetation, and the organic matter above the mineral soil. The primary inputs to the model are the mean annual air temperature, annual amplitude of air temperature, and the mean snow depth over the winter period. Parameters required by the model include soil texture, so as to compute thermal conductivity and heat capacity as well as estimates of snow thermal conductivity. The model is applied on a 100 x 100 km EASE equal-area grid for the region covered by the pan-arctic drainage basins; this region extends down to 45°N in places.

Data

Temperature data was derived from the ECMWF 40-year reanalysis project. This data has been shown to produce. Average snow depth and density was obtained as the ensemble average from five land surface models (CHASM, CLM, ECMWF, NOAH, and VIC) that had performed 23-year simulations over the region (Slater et al. 2007). The estimates from the models are more consistent with station-based measurements than the available passive microwave satellite data; this is particularly so in the eastern Siberian uplands, where satellite products have known biases. Parameter data for soil texture properties is based on the map of Zobler (1986) and has been used extensively in large-scale modeling experiments. To simplify matters and maintain a conservative estimate of change, soil moisture was prescribed at 99% of saturation.

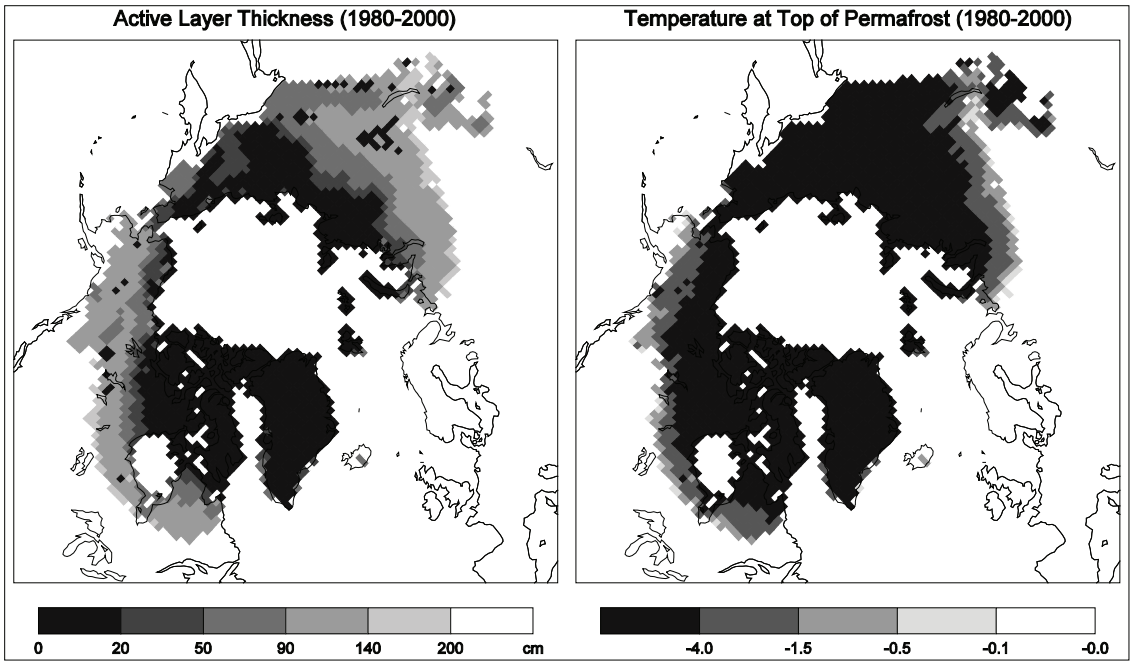

Figure 1. Analytic model simulation of present-day permafrost. Temperature is in degrees Celsius. Disregard results for Greenland.

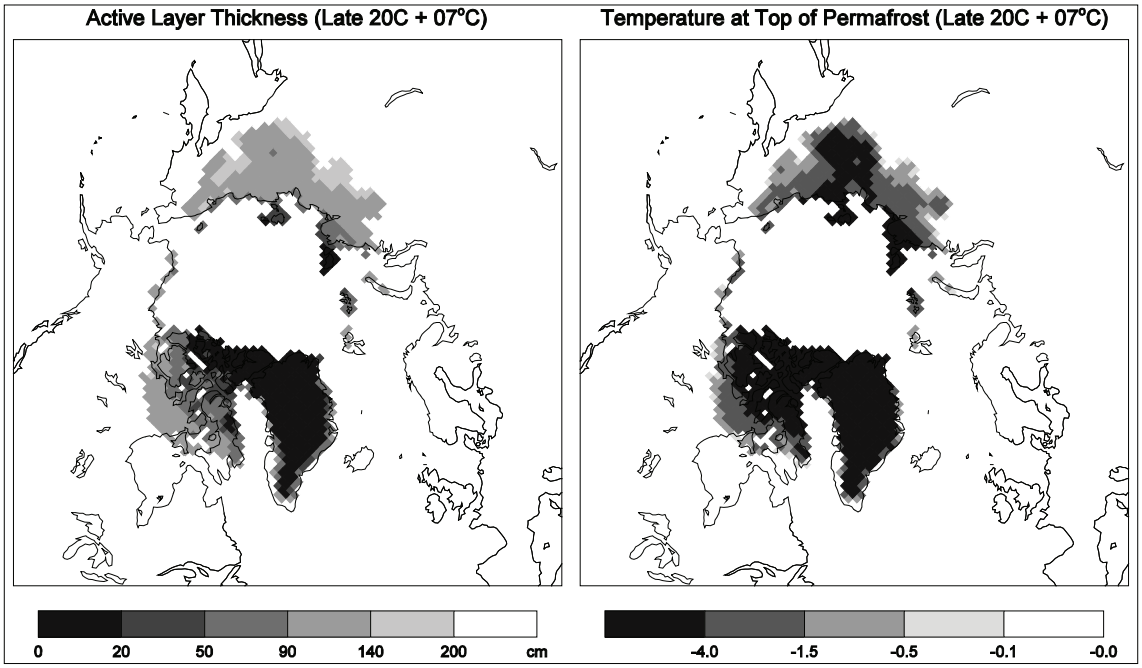

Figure 2. Analytic model simulation of permafrost with a simple climate change scenario of 7°C increase in annual mean temperature.

Results and Summary

Figure 1 shows the results from the analytic model for the late 20th century. Estimates of the active layer depth as well as the mean annual temperature at the top of the permafrost are shown. These results compare favorably to the estimated distribution of permafrost as given by the International Permafrost Association map. Temperature at the top of the permafrost is shown in four ranges that are roughly considered to compare to permafrost zones of continuous, discontinuous, sporadic, and isolated.

Some initial simple experiments were performed in which mean annual temperature was raised by 7°C, which is within the range of changes expected to be seen over the Arctic in the coming century according to IPCC estimates (Fig. 2). Snow depth and cover for these preliminary simulations was kept the same as present day. Estimates of changes in snow depth and cover vary widely, but Räisänen (2008) suggests that there is a likelihood of deeper snow over mid-winter in the high latitudes, as the increased precipitation will still fall in solid phase. This will no doubt have an impact on the future state of permafrost. Further simulations assessing sensitivity to snow and soil will be carried out and presented at the NICOP meeting.

Acknowledgments

This work was partially funded by NSF grants ARC-0229769 and ARC-0531040.

References

Osterkamp, T.E. 2007. Characteristics of the recent warming of permafrost in Alaska, *J. Geophys. Res.* 112: F02S02, doi:10.1029/2006JF000578.

Räisänen, J. 2008. Warmer climate: Less or more snow? *Clim. Dynamics* 30(2–3): 307-319.

Sazonova, T.S. & Romanovsky, V.E. 2003, A model for regional-scale estimation of temporal and spatial variability of active layer thickness and mean annual ground temperatures. *Permafrost Periglac. Process.* 14: 125-139.

Slater, A.G., Bohn, T.J., McCreight, J.L., Serreze, M.C. & Lettenmaier, D.P. 2007. A multimodel simulation of pan-Arctic hydrology, *J. Geophys. Res.* 112: G04S45, doi:10.1029/2006JG000303.

Zhang, Y., Chen, W. & Riseborough, D.W. 2008. Disequilibrium response of permafrost thaw to climate warming in Canada over 1850–2100. *Geophys. Res. Lett.* 35: L02502, doi:10.1029/ 2007GL032117.

Zobler, L. 1986. *A World Soil File for Global Climate Modeling.* NASA Tech. Memo 87802, Natl. Aeronaut. and Space Admin., Goddard Inst. for Space Stud., New York.

Thermal State of Permafrost in Canada: A Contribution to the International Polar Year

Sharon L. Smith
Geological Survey of Canada, Natural Resources Canada, Ottawa, Canada
Antoni G. Lewkowicz
Department of Geography, University of Ottawa, Ottawa, Canada
Christopher R. Burn
Department of Geography and Environmental Studies, Carleton University, Ottawa, Canada

Introduction

Over the past two to three decades, Canadian researchers have established and maintained a permafrost monitoring network consisting of boreholes in which ground temperatures are measured. Data collected from these sites have facilitated documentation of recent trends in permafrost thermal state (e.g., ACIA 2005, Smith et al. 2005, Lemke et al. 2007). The monitoring network is also a key contribution to the Global Terrestrial Network for Permafrost (GTN-P).

The International Polar Year (IPY) provides the opportunity for the Canadian permafrost community and the International Permafrost Association (IPA) to conduct a well-designed global and coordinated multinational programme of permafrost observations in order to explore present conditions and their spatial and temporal variability. It also provides the opportunity to fill gaps identified in the Arctic Climate Impact Assessment (ACIA 2005), such as improved characterization of permafrost-soil-vegetation interactions and the upgrade and maintenance of long-term monitoring networks. Canada is a key contributor to the IPA-led IPY project, the Thermal State of Permafrost (TSP).

In 2007, a collaborative proposal from the Geological Survey of Canada, University of Ottawa, and Carleton University was successful in acquiring funding from the Canadian Government's IPY program for TSP-Canada. This funding along with additional support acquired by the principal investigators and collaborators has facilitated the establishment of new monitoring sites both prior to and during IPY. This paper provides an overview of the TSP-Canada project and summarizes the establishment of new monitoring sites

Objectives of TSP-Canada

Canada's contribution to the Thermal State of Permafrost project will examine the ongoing impacts of climate change on permafrost conditions and meet the following objectives: (1) obtain a set of standardized temperature measurements for all Canadian monitoring sites (snapshot); (2) produce a dataset and map of contemporary permafrost ground temperatures contributing to a global effort; (3) increase the number of monitoring sites prior to and during the IPY; (4) provide data to verify models to improve prediction of future permafrost conditions; (5) examine permafrost-climate linkages and feedbacks to explain observed change and variability in permafrost conditions; and (6) develop outreach products on permafrost change for northerners and present results in scientific papers.

The project builds on an existing network of approximately 100 thermal monitoring sites established over the last two to three decades (see Smith et al. 2003). A key objective of the project is enhancement of the network to fill thematic and regional gaps.

Network Enhancement

New sites

Over the last two to three years, new monitoring sites have been established that contribute to TSP-Canada and GTN-P. Most of these new boreholes are less than 20 m deep, but some extend to depths of 50 m. These new sites consist of cased boreholes in which permanent thermistor cables have been installed.

More than 50 new boreholes have been established in the western Arctic (Fig. 1). The majority of these are located in the Mackenzie Valley and Delta region and were established to provide baseline information essential for design and environmental impact assessment of hydrocarbon development projects. In particular, an important gap north of Norman Wells (north of ~65°N) has been addressed. Sites were also established in collaboration with communities in the NWT and Yukon Territory. Several new boreholes have been established in the central and southern Yukon.

Through collaboration with Parks Canada, seven new boreholes were established in northern Manitoba. These sites are located in Wapusk National Park and York Factory and represent a variety of terrain conditions. They provide better coverage in the area to the west of Hudson Bay.

Dataloggers have been connected to most of the thermistor cables to provide a continuous record of ground temperatures. For sites established prior to summer 2007, preliminary ground temperature data have been collected that provide a baseline against which to measure change. All new sites will be visited in 2008, and this should provide a record of ground temperatures for the first year of IPY.

Plans for additional site establishment

During 2008, further site establishment is planned. Additional sites will be established in the central and southern Yukon. Deep boreholes to depths of 50 to 100 m are proposed with a number of them to be established in collaboration with a mineral exploration company. Efforts

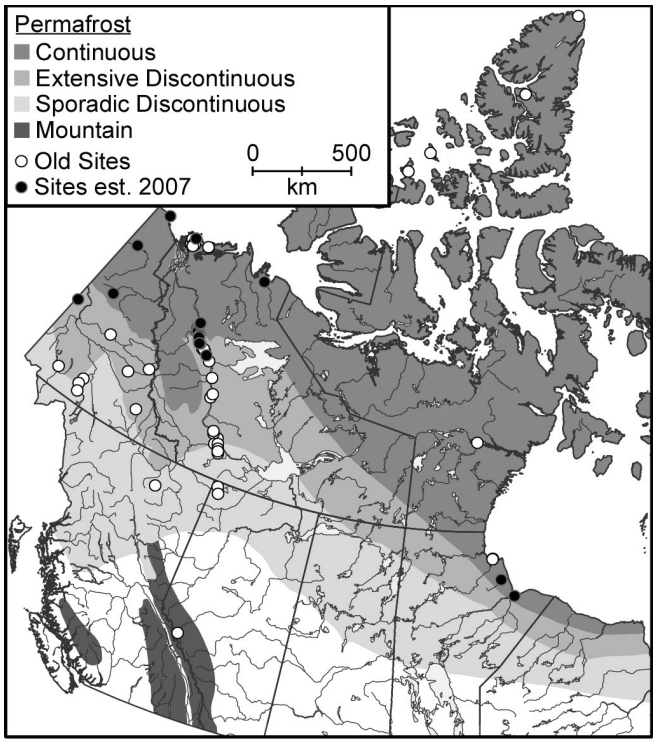

Figure 1. Location of new monitoring sites established in 2007 and older monitoring sites established over the last 30 years in the central and western Arctic. Note: for clarity not all new sites established in the Mackenzie Valley and Delta are shown.

will also be made to locate and re-occupy some boreholes which were drilled in the 1980s by an engineering consulting company and for which historic data are available.

A significant gap still exists in Nunavut. Through collaboration with communities and the territorial government, attempts will be made to establish five to ten monitoring sites to fill gaps in the central and eastern Arctic. Data generated from these sites will also be utilized by the communities for land use planning and development of strategies to adapt to climate change impacts on infrastructure.

Summary

TSP-Canada is the main Canadian contribution to the IPA led IPY project on the thermal state of permafrost. Over the last two to three years, progress has been made towards the objective to establish new monitoring sites in advance of and during IPY. Additional new sites are planned to increase coverage in the central and southern Yukon Territory and the central and eastern Arctic. Preliminary data have been collected from the first IPY year, with further data collection planned between 2008 and 2009. These data provide new baseline information on permafrost thermal state for the Canadian permafrost region and will be utilized to meet the objectives of TSP-Canada.

Acknowledgments

Support for network enhancement has been provided by the Canadian government's IPY program, Natural Resources Canada, Northern Energy Development Memorandum to Cabinet, Canadian Foundation for Climate and Atmospheric Sciences, University of Ottawa, Carleton University, Polar Continental Shelf Project, and NSERC. Sites in the western Arctic were established in collaboration with Indian and Northern Affairs Canada.

References

ACIA 2005. *Arctic Climate Impact Assessment.* Cambridge University Press, 1042 pp.

Lemke, P., Ren, J., Alley, R.B., Allison, I., Carrasco, J., Flato, G., Fujii, Y, Kaser, G., Mote, P., Thomas, R.H. & Zhang, T. 2007. Chapter 4, Observations: changes in snow, ice and frozen ground. In: *Climate Change 2007: The Physical Basis. Contribution of Working Group I to the Fourth Assessment Report of the Intergovernmental Panel on Climate Change,* 337-383.

Smith, S.L., Burgess, M.M., Riseborough, D. & Nixon, F.M. 2005. Recent trends from Canadian permafrost thermal monitoring network sites. *Permafrost and Periglacial Processes* 16: 19-30.

Smith, S.L., Burgess, M.M., Romanovsky, V. & Brown, J. 2003. The Global Terrestrial Network for Permafrost (GTN-P): Status and preliminary results of the thermal monitoring component. Extended Abstracts Reporting Current Research and New Information. In: W. Haeberli & D. Brandova (eds.), *Proceedings of the Eighth International Conference on Permafrost*, *Zurich, Switzerland, July 2003*: 153-154.

Tides as a Possible Reason for Massive Ice Beds Formation

Sergey A. Sokratov, German A. Rzhanitsyn
Faculty of Geography, Moscow State University, GSP–1, Moscow, 119991, Russia

Introduction

The argumentations on the genesis of massive ice beds discovered on wide territories of the Arctic and Subarctic have special meaning for the Russian permafrost scientific community. The critical point of the ongoing discussions turns out to be either marine or glacier origin of the massive ice beds, since this affects in whole the interpretation of the paleo-history of Northern Eurasia (Solomatin 2005). It should be emphasized that the massive ice beds of interest (*plastovye l'dy*) neither are a part of the Russian ground ice classification (Popov et al. 1985) nor a singled-out type of ground ice in the IPA glossary (van Everdingen 2005). From a terminology viewpoint, different genesis of the massive ice beds at different sites is the natural expectation. Recently, these massive ice beds are being classified by expected genetic types (Shpolyanskaya & Streletskaya 2004). However, the disagreement on either buried or in-site origin of seaside massive ice beds, especially, still exists due to uncertainties in explanations of the existence of saline-free massive ice lenses incorporated into salted marine sediments, the isotopic difference between the sea water and the massive ice lenses, and particularly the morphology interpreted as the deformation markings on some of the massive ice beds (Solomatin 2005).

Leaving aside the fundamental question of ice sheet existence over Northern Eurasia, the paleo-climate signal enclosed into the massive ice beds and their bearing strata is the product of the processes responsible for the formation, growth, and melt of an ice body. Since most of the known massive ice beds are found in the former or present coastal zones (Shpolyanskaya & Streletskaya 2004), it is worth considering coastal zones-specific processes as the possible participants in the massive ice beds formation and maintenance. The background of the reported investigation was to test the possibility that periodic natural fluctuations of groundwater level due to upthrust of groundwater runoff by tides play a part in ice lens formation. Such a mechanism, with favorable groundwater freezing climate conditions, allows for formation of saline-free ice lenses from groundwater with close to the atmospheric precipitations isotopic content in the saline marine sediments.

Tides and Groundwater Runoff

The result of field investigations at the White Sea coast (Pon'goma) was the confirmation of the dependence of groundwater level variation on the tidal regime, at least in the case of sandy ground and tides up to 2 m (Fig. 1).

The dependence observed by measurements in dug pits by automatic water level sensors was pronounced up to tens of meters from the shoreline. Figure 1 shows the results of

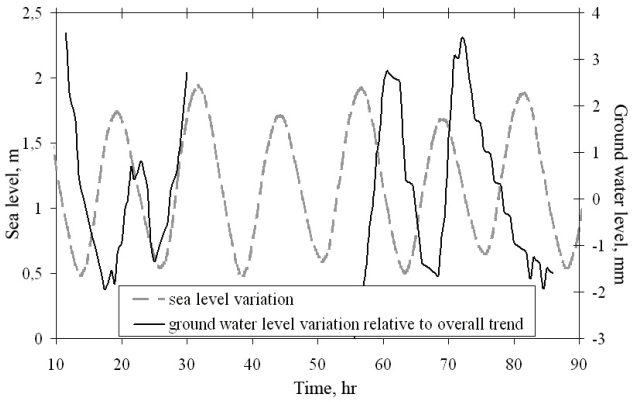

Figure 1. The correlation between sea level variation and groundwater level variation.

the groundwater level measurements in a dug pit 7 m from water's edge at maximal tide, 1 m above the maximal sea level. The variation is extracted from the overall change of groundwater level due to variability in precipitation and snowmelt, and represents about 10% of the overall variability. The delay between the extremums of sea and groundwater level variations is approximately 4 hr. Such dependence was not observed in another area of the coastal zone with clayey and peat grounds, despite high (up to 9 m) tides (Mezenskaya Bay, White Sea).

The field observations also demonstrated strong seasonal variability of the dependence of the groundwater level variability on tides up to disappearance of the propagation of the tides' signal at distance from the shoreline, caused by the amount and unevenness of the groundwater runoff. An important role in the tides' signal propagation was found to belong to the formation of an impermeable seasonally-frozen ground layer near the soil surface. Therefore, it was concluded that the relation between the tides and the groundwater level variation is different for territories with different texture of soil, is determined by the amount of the groundwater runoff and by the activity of tides, and varies considerably in dependence on the soil freezing conditions.

A study of thick deposits of ground ice in exposure at the Ural coast of Baidaratskaya Bay revealed their polygenetic origin. The analysis of the structural characteristics of the ice, however, suggested the possibility of participation of the proposed mechanism in ice lenses formation.

Groundwater Level Variation and Ice Lens Growth

The laboratory studies included modeling of the groundwater level change, periodically introduced upward into two-layer samples with unidirectional frost penetration

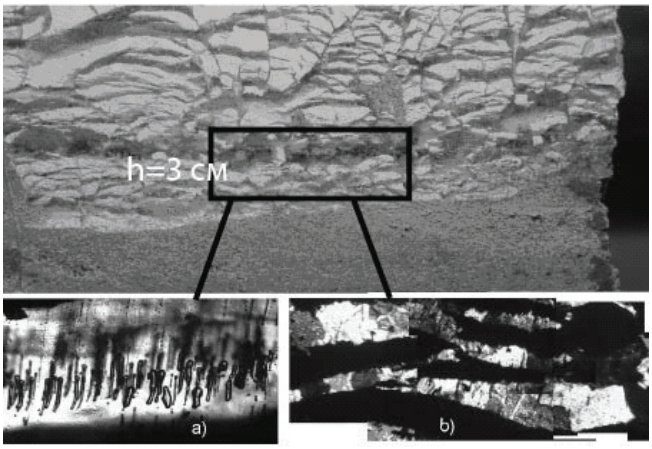

Figure 2. Structure of the ice schlieren near the boundary of the two layers of a sample. The top layer is montmorillonite; the bottom layer is fine sand.

from top downward. The top layers were made from different clay and the bottom layer, from sand (Fig. 2).

The ice-rich horizon and ice lens (up to 1.5 cm thick) were formed near the boundary between the layers during several tens of cycles of the alternating groundwater level variation. The microstructure of the ice filling the fractures in the clay is characterized by subparallel to the schlieren layering related to several stages of ice crystal formation and growth inside the fractures. The ice crystals normally had a columnar structure with the long axes in the heat flux direction regardless of the variation in orientation of the schlieren (Fig. 2a). The gas inclusions in central parts of the schlieren were mainly represented by large elongated allocations, and at the peripheral parts, by chains of small bubbles. Large elongated bubbles were usually oriented subperpendicular to the schlieren's boundaries. Large multilayered schlieren also contained thin chain-like gas inclusions parallel to the schlieren's strike which, together with microcracks, confirm rupturing of already existent ice schlieren and repetitive water freezing inside them (Fig. 2b). The arrangement and form of ice crystals and gas inclusions corresponds to the structural specific of the intrusive ice formed from small amounts of inlet water and is alike to those of the natural massive ice lenses.

Conclusions

The results of the studies verified the possibility of the formation of ice-saturated ground horizons by periodic variation of the groundwater level, with the tides as a possible reason of such periodic variation. A considerable number of conditions required for realization of such a mechanism determines spatial limitations of its manifestation at each time interval. However, long-term variation of sea level against the background of climate change concedes action of the mechanism in past and allows explanation of recent-time distribution of the massive ice deposits over wide territories and at considerable distances from the recent-time Arctic shoreline (Golubev 2007a, 2007b).

Acknowledgments

The project was supported by the Russian Foundation of Basic Research, grant No. 05-05-65115.

References

van Everdingen, R.O. (ed.). 2005. *Multi-Language Glossary of Permafrost and Related Ground-Ice Terms*. International Permafrost Association, 278 pp.

Golubev, V.N. 2007a. Periodicheskie izmeneniya urovnya morya kak faktor formirovaniya plastovykh zalezhei l'da. (Periodic variations of sea level as a factor of the tabular ice formation.) *Kriosfera Zemli* (*Earth Cryosphere*) XI(1): 52-61

Golubev, V.N. 2007b. Rol' morskikh gidrodinamicheskikh protsessov v formirovanii zalezhei plastovykh l'dov na arkticheskom poberezh'e. (The role of sea hydrodynamic processes in formation of the massive ice beds deposits at Arctic shore.) *Materialy Glyatsiologicheskikh Issledovanii* (*Data of Glaciological Studies*) 102: 32-40.

Popov, A.I., Rozenbaum, G.E. & Tumel', N.V. 1985. *Kriolitologiya.* (*Cryolithology*). Moscow: Moscow State University, 239 pp.

Shpolyanskaya, A.N. & Streletskaya, I.D. 2004. Geneticheskie tipy plastovykh l'dov i osobennosti ikh rasprostraneniya v Rossiiskoi Subarktike. (Genetic types of massive ice beds and specific of their distribution in Russian Subarctic.) *Kriosfera Zemli* (*Earth Cryosphere*) VIII(4): 56-71.

Solomatin, V.I. 2005. Gletchernyi led v kriolitozone. (Glacier ice in cryolithozone.) *Kriosfera Zemli* (*Earth Cryosphere*) IX(2): 78-84.

Preservation of the Alaska Highway

Eva Stephani
Department of Geology and Geological Engineering, Université Laval, Québec, Québec, Canada
Daniel Fortier
Institute of Northern Engineering, University of Alaska Fairbanks, Alaska, USA
Yuri Shur
Department of Civil and Environmental Engineering, University of Alaska Fairbanks, Alaska, USA
Guy Doré
Department of Civil Engineering, Université Laval, Québec, Canada
Bill Stanley
Yukon Highway and Public Works, Yukon Government, Whitehorse, Yukon, Canada

Introduction

Road construction in permafrost areas affects the thermal regime of frozen soils via removal of the vegetation, compaction of the soil, road cut, and use of black asphalt pavement, for instance. The thermal degradation of the permafrost causes the ground ice to melt and results in permafrost thaw settlement, as well as subsidence and cracking of pavement. In many northern areas, roads are now showing signs of instability as a result of permafrost degradation, which could be partly due to recent climate warming. According to the IPCC projection of climate warming, this situation will undoubtedly be exacerbated in the future (IPCC 2007).

The Alaska Highway is an essential and widely used communication link between Alaska, Canada, and the southern United States. The highway has a poor driving surface, and some sections of the embankments have experienced substantial settlement. Severe pavement subsidence, longitudinal cracking, and potholes could eventually threaten the structural integrity of the infrastructure. Sections of the Alaska Highway built on ice-rich permafrost might eventually require relocation or replacement with a different design, and sections built on permafrost with a lower volume of ice will require at least rehabilitation. Alternative designs and mitigation measures should be adopted in order to reduce maintenance costs. The Yukon Government has decided to implement a test section at Beaver Creek, Yukon Territory, Canada (62°20′N, 140°50′W). Engineering mitigation measures will be tested to control the degradation of the permafrost. Six techniques will be implemented at the Beaver Creek experimental road site: (1) Air convection embankment (ACE); (2) heat drain; (3) air duct cooling system; (4) thermo-reflective snow shed; (5) grass-covered embankment; and (6) light-colored aggregate bituminous surface treatments (BST).

The Alaska University Transportation Center is responsible for characterizing the stratigraphy at the test site and for determining the geotechnical properties of the permafrost prior to the construction of the road test section. The objectives of this paper are to outline the thaw-susceptible nature of the permafrost at the test site and to illustrate the challenges related to rehabilitation of degraded permafrost under the road embankment.

Methodology

Field methods

Thermal conditions at the Beaver Creek experimental site have been monitored since 1998 by means of thermistor cables. One cable is installed under the center line of the road, one cable is installed in the side slope of the embankment, and one cable is in the natural ground adjacent to the road. Air temperatures also have been monitored.

Drilling and coring operations at the test site were realized during summer 2007 in the natural ground adjacent to the road and in the berms. Permafrost cores from 17 boreholes were collected, sampled, and brought back in a freezer to the University of Alaska Fairbanks for laboratory analyses.

Laboratory methods

The cryostructure and sediment types of soil were identified. Each stratigraphic unit was identified by its pH, electrical conductivity, gravimetric and volumetric ice content, grain-size distribution, and thaw-settlement potential.

Preliminary Results and Discussion

The mean annual air temperature (1971–2000) at Beaver Creek is -5.5°C (Environment Canada 2008). The local extreme maximum was 32.8°C in 1982, while the local extreme minimum was -55°C in 1971 (Environment Canada 2008). The mean annual precipitation is 416.3 mm, of which 123.1 mm water equivalent falls as snow (Environment Canada 2008). Monthly mean air temperatures are 11.9°C, 14°C, and 11.2°C for June, July, and August, respectively. Air temperatures above and below freezing represent an average (1971–2000) of 1532.6 thawing degree-days and 3534.2 freezing degree-days, respectively (Environment Canada 2008).

The coring operations in the natural ground revealed the presence of very ice-rich syngenetic permafrost with buried inactive ice wedges. Three main stratigraphic units were identified: Unit 1 (0–0.5 m) is ice-rich peat. Unit 2 (0.5–6.5 m) is silt, which is ice-rich at the top (>2.0 m), ice-poor below (2.0–3.5 m), and ice-rich in the lower portion (3.5–6.5 m). The top of the ice wedge is located in the ice-poor layer around 2.5 m depth and extends down to at least 6.5 m. Unit 3 (6.5–10 m) is an ice-rich diamicton.

Figure 1. Longitudinal cracking along the shoulder of the Alaska Highway due to degradation of the underlying permafrost. The 1-m shovel (arrow) gives the scale.

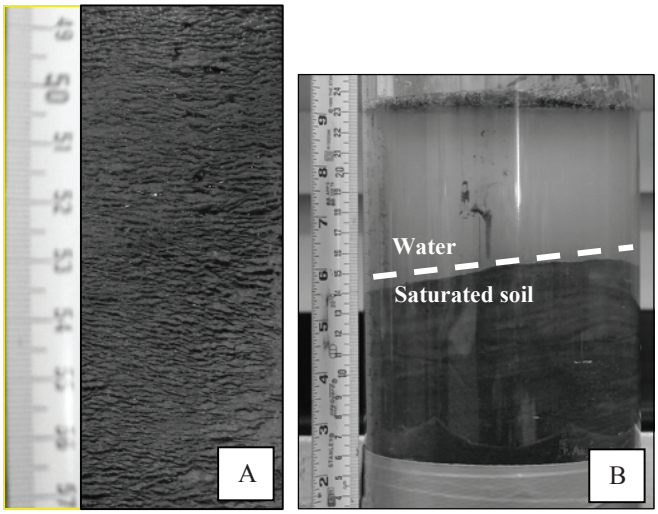

Figure 2. (A) Very ice-rich microlenticular cryostructure typical of syngenetic permafrost. (B) Thaw-settlement-potential test showing excess water upon thawing in the thaw-settlement cell.

In 2004, the maximum thaw depth in the natural ground was 70 cm. The maximum thaw depth under the center line of the road was located in the embankment material. However the mean annual ground temperature just below the embankment was close to the melting point (-0.3°C), and numerous observations (in 2007) of cracks and depressions affecting the central part of the road suggest that the thaw depth now reaches the natural ground where the embankment is thinner. In the side slope of the embankment, the thaw depth was located in the natural ground. Deepening of the active layer in the natural ground under the road creates thaw settlement and subsidence of the embankment (Fig. 1) Drilling realized in 2007 from the berm adjacent to the side slope of the embankment revealed that, locally, the maximum thaw depth can be located as deep as 2.5 m in the natural ground below the base of the embankment. If submitted to warming, these large unfrozen zones will progressively extend towards the center line of the road. The water content measured in the thawed layer under the embankment varied between 221% and 357%. This indicates that these zones are supersaturated due to the melting of ground ice and restricted drainage.

Table 1. Thaw strain values of the stratigraphic units.

Unit	Ice content	Thaw strain
1	Ice-rich	0.35
2 (0.5–2 m)	Ice-rich	0.41–0.61
2 (2–3.5 m)	Ice-poor	0.05
2 (3.5–6.5 m)	Ice-rich	0.43–0.54

The high water content can be explained by the prevalence of permafrost with an extremely ice-rich micro-lenticular cryostructure. This type of cryostructure is typical of syngenetic permafrost and usually has very high settlement potential (Fig. 2). Thaw-settlement tests indicate that the upper part of the permafrost (Units 1 & 2) is highly susceptible to thermal degradation (Table 1). A thaw-settlement test realized on the ice-poor layer of Unit 2 revealed that it is thaw-stable (Table 1). However this layer comprises a widespread network of ice wedges extending in the underlying ice-rich units. Ice wedges are highly thaw-susceptible and their geometric patterns make them prone to thermo-erosion and deep linear subsidence.

Conclusions

Drilling operations revealed the presence of large, unfrozen supersaturated zones under the road embankment. Rehabilitation of thawed permafrost under the road embankment will necessitate refreezing of the sediments. This could be long, due to the large amount of latent heat to extract from the water trapped in these unfrozen zones. Our study indicates that syngenetic ice-rich permafrost is highly susceptible to thermal degradation, especially where ice wedges are present.

Our preliminary results indicate that a detailed spatial geotechnical characterization of the permafrost (e.g., cryostructure, volumetric ice content, grain-size distribution, thaw-settlement potential, thaw-consolidation potential, ground thermal regime) is needed to determine the potential thaw susceptibility of the permafrost to climate warming and to find the proper engineering solutions to control permafrost degradation.

References

IPCC. 2007. *Climate Change 2007: The Physical Science Basis. Contribution of Working Group 1 to the Fourth Assessment Report of the Intergovernmental Panel on Climate Change,* S. Solomon, D. Qin, M. Manning, Z. Chen, M. Marquis, K.B. Averyt, M. Tignor, & H.L. Miller (eds.). Cambridge, UK & New York, USA: Cambridge University Press,

Specific Features of Dynamic Modeling of Processes in the South Siberian Permafrost

V.A. Stetjukha
State University, Chita, Russia

Introduction

The southern Siberian permafrost is unstable because of natural and climatic features of the region. First of all, the condition of soil stability due to external influences results from their high temperature (from -0.1 up to -2°C). Degradation of warm permafrost, even due to small external influences, occurs much more quickly than in other environments. Anthropogenic impacts can easily contribute to this environmental balance.

There are features of soil development due to physical processes in warm permafrost to consider. Traditional models for forecasting the impact on the environment do not give realistic results. They do not adequately model the physical processes in soils, as they do not take into account a number of processes that have an influence on soils. The cumulative impact of these neglected processes is significant. Anthropogenic factors are also not taken into account.

Modeling of Processes

The methods of heat-mass transfer and stress-strain modeling of unstable geocryological systems is presented. The method takes into consideration the adaptation of the model to natural and climatic conditions, and incorporation of technological influences like mining and building. Within a modeling framework, the advanced equations of heat-mass transfer and a technique for their use are developed. The publication is devoted to a process-modeling approach.

The basic process equations are given in an article by Stetjukha (2003a). The model includes the following components: thermo-gradient streams of moisture, the distributed sources and convective streams of thermal energy, a gravitational component for moisture streams, electro-osmotic streams of moisture, and thermal streams caused by electro-osmotic moisture streams. The equations of thermal and water balance on a surface of soil column takes into consideration evaporation, steepness and exposure of slopes, and anthropogenic influences. At the surface boundary, the temperature and moisture balances of a near-surface layer are carried out. The equations are solved in finite difference form.

In conditions of warm permafrost, the total influence of the neglected processes on depth of thawing and freezing that are not taken into account in the majority of traditional models, reaches 75%. Results are confirmed by calculations and comparison with observations.

To determine stresses and strains in soils, the finite element method is again used. In this case, the variable characteristics of loading in time, changeability of soil properties, changing boundary conditions, and temperature deformations are simultaneously taken into consideration.

The proposed technique of forecasting is based on the consideration of several interactions of soil properties and their change with time. This modeling technique differs from others in that it considers mining influences, the cumulative impact of several processes, the application of a system analysis approach, and a new way of considering factors that change with time. The offered model is exposed to continuous change and regulation owing to continuously changing conditions. The mathematical model is exposed to a continuous readjustment in connection with degradation of frozen soils.

The distinctive features of the dynamic model are:

- the coupling of the tasks of heat-mass transfer and geo-mechanics on the basis of developed mathematical models. Thus, researched soils are broken into elements of finite size by grids with common junctions;
- increase in quantity of factors (variables);
- the consideration of complex geometry to capture human-caused changes;
- transformation of impacts in time, caused by the presence of two fronts of freezing, by migration of moisture, by degradation of permafrost;
- ability to adjust, in time, physical-technical parameters of soils: porosity, density, deformation modulus, Poisson's coefficient, an angle of internal friction, coupling forces, tensile and compressive strengths based on change of temperature, humidity and pressure in various points of space. During periods of compression of soils, the thermal capacity, thermal conductivity, coefficient of linear expansion are corrected;
- the consideration of changes in soil properties due to changes in density as a function of their position in the soil profile;
- the consideration of temperature deformations;
- use of the method of combined influences on soil column (Stetjukha 2003b), which provides a determination of extreme values, adverse combinations, and the periods and sequence of loading of separate factors of influences;
- a determination of optimum accommodation of influences in time and space and definition of their optimum quantitative characteristics;
- application of imitating modeling (Stetjukha 2003b) for perfection of preliminary generated mathematical models.

The developed algorithm has the distinctive features shown in Figure 1.

The block model diagram is characterized by an extensive quantity of initial factors. The incorporation of the quantity of the initial data has required statistical processing. Within the framework of the block, the double-step process of correction

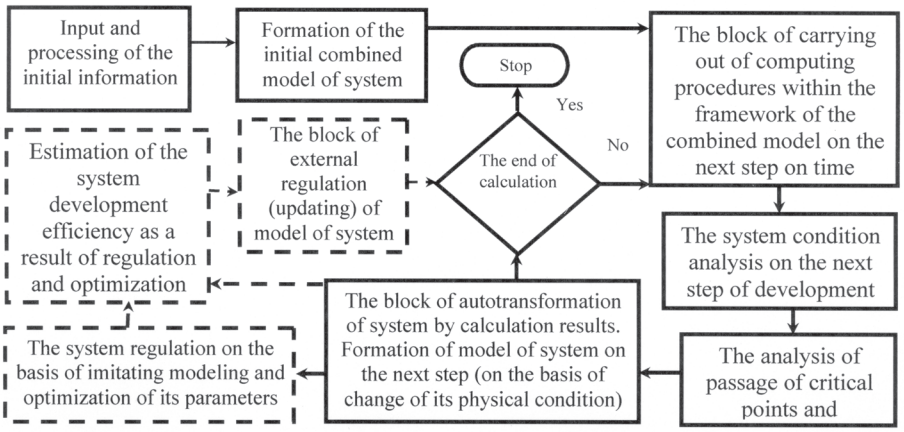

Figure 1. The integrated circuit of calculations with change of model in time.
□ = the common modules of system; ⬚ = the modules used at regulation.

of the complex model is carried out. Preliminary selection of parameters is carried out by generating alternative variants. The correlation analysis of factors provides a procedure of parameter selection on the degree of their importance. From initial analysis results, some parts of the complex model can be removed. Those factors staying are divided into two groups. First, those used in the performance of numerical experiments; second, those used for forming regression equations (Stetjukha 2003b). The second stage of model correction consists in quantitative correction of separate parameters. The algorithm of imitating modeling and optimization of system lays in the basis of this stage.

Computing procedures are carried out under the obvious circuit. It allows tracing the development of processes and inserting corrective changes.

The analysis of the system at each step of calculations takes into account changes of borders between thawed and frozen zones, achievement by soil of a condition of saturation by moisture, etc. The control points are analyzed. Control points are established on restrictions in the use of materials, on design factors, on restrictions of technological process, etc.

The major elements of the model are mechanisms of system adaptation to changed conditions. Thus two stages are allocated. One of them is updating of the model at the next step on the basis of change of a physical condition of system components. New dependences between factors are determined here. The second stage of adaptation of the combined model is its regulation on the basis of results of imitation modeling and optimization. The procedure of imitation modeling and optimization of processes includes performance of numerical experiments on a considered circle of tasks. As a result of regulation, a planned correction of physical-mechanical properties and other parameters of the system on the next step of external forcing are carried out.

Results of Calculation

The described modeling was carried out in an area of construction of a federal motorway, "Amur." Thawing of permafrost imbedded with ice on a slope with an inclination of 34° was predicted. Opening of frozen soils was carried out in the middle of April. The site with an open cut on a slope with the weak soils on 726 km of the motorway was considered. Up to a depth of 1.5 m on a slope, loam is encountered (layer 1); up to a depth of 2.5 m, fine loamy sand (layer 2); up to 4.4 m, loamy sand containing ice (layer 3); up to 5.6 m, fine sand containing ice (a layer 4); up to 6.5 m, loam, including rubble (layer 5); finally, a diorite. The depth and speed of thawing of separate layers during the warm period of the year were determined. Calculations established loss of stability of a slope in the middle of July. The predicted results are confirmed with observation.

The author carried out the forecast of results of impacts on other environments, such as where the soil/vegetation cover has been disturbed, preservation of frozen soils with use of heat insulating materials, shading screens, waterproof screens, and frozen veils (Stetjukha 2003b).

Depth of permafrost thawing under the bottom of the projected channel on a deposit of brown coal on a coal pit was determined. Predicted depth of thaw in 5 years was 5.5 m; in 10 years, 7.8 m. The threat of destruction of the channel is confirmed.

On the basis of the described method, a model of anthropogenic ices mound forecasting (Stetjukha 2003b) is developed.

The offered model of dynamic development of a natural-technological system allows objective estimation of temperature distribution, humidity, pressure, and deformation fields in conditions of changing influences on soil. Forecasting of processes in frozen soil has allowed the development of recommendations on optimum technological circuits of work during various seasons of the year.

References

Stetjukha, V.A. 2003a. Complex analytical modeling of processes in the south Siberian permafrost. *Permafrost*. Zurich, Switzerland: Swets and Zeitlinger Publishers: 1103-1106.

Stetjukha, V.A. 2003b. *Forecasting of a Mining Processes Influence for a Condition of a Permafrost Region Soils*. Chita: Publishing of Chita State University, 192 pp.

Understanding the Filling Process in Ice Wedges Using Crystallography, Isotopes, and Molar Gas Ratios

Mélanie St-Jean
University of Ottawa, Ottawa, Canada
Ian D. Clark
University of Ottawa, Ottawa, Canada
Bernard Lauriol
University of Ottawa, Ottawa, Canada
Paul Middlestead
University of Ottawa, Ottawa, Canada

Introduction

Much still remains unclear about ice wedge formation and filling process. Some researchers have indicated that the primary source of water for ice wedge growth is derived from snow meltwater (Washburn 1980, Lauriol et al. 1995). Other researchers suggest ice wedge growth by hoar-frost accretion in some cases rather than by the traditionally accepted process of water trickling into the wedge during the spring thaw prior to closure of the fissure.

Literature Review and Methodology

In Canada, the discussion concerning the identification of massive ground ice bodies is mostly focused on whether the ice is a remnant of the Laurentide ice sheet, or whether it is derived from segregation/injection processes. The majority of research in this field has been focused on the stratigraphic and petrographic characteristics of massive ground ice. The concentration and molar ratios of CO_2, O_2, N_2, and Ar gases entrapped in the ice, offer an innovative tool that allows differentiation between ground ice of glacial (firnified glacier ice), non-glacial intrasedimental, and surface origin. The principle behind this technique is that molar gas ratios of gases (O_2/Ar and N_2/Ar) entrapped in glacier ice tend to preserve an atmospheric signature modified by firn diffusion and gravitational settling, whereas the molar gas ratios of segregated-intrusive ice are significantly different from those found in the atmosphere and glacier ice due to the different solubilities of the gases in water (Lacelle et al. 2007, Cardyn et al. 2007).

This new extraction technique, modified from Sowers et al. (1997) and Cardyn et al. (2007) could also be useful in better understanding the filling process in ice wedges. The concentrations and molar ratios of atmospheric gases change during dissolution in water. Therefore, ice bubbles will have a gas composition closer to atmospheric air if the filling process involves hoar-frost accretion or snow, while ice bubbles resulting from snow meltwater filling will have a composition closer to gases exsolved from freezing water. An extraction line was built to isolate gases from ice, and a mass spectrometry technique was used to analyze the gas ratios (O_2/Ar and N_2/Ar).

Study Area

Ice samples used in this analysis were collected in northwestern Canada. What distinguishes these sites from others in the Canadian Arctic is that they are located outside and inside the limits of the last Pleistocene Cordilleran glaciation and could represent modern, Holocene, and Pleistocene ice bodies of different origin (see Fig. 1). They are ideal sites to have an extensive range of values of gas ratios. Here we present results that should enable us to distinguish the two different ice wedge-filling processes.

Old Crow, Yukon

A series of ice wedges along the Eagle, Bell, and Porcupine Rivers (Yukon) were sampled on the Holocene terrace to identify their period of growth and source of infiltrating water. Preliminary results from one ice wedge near Old Crow indicate ratios similar to gases dissolved in water, but

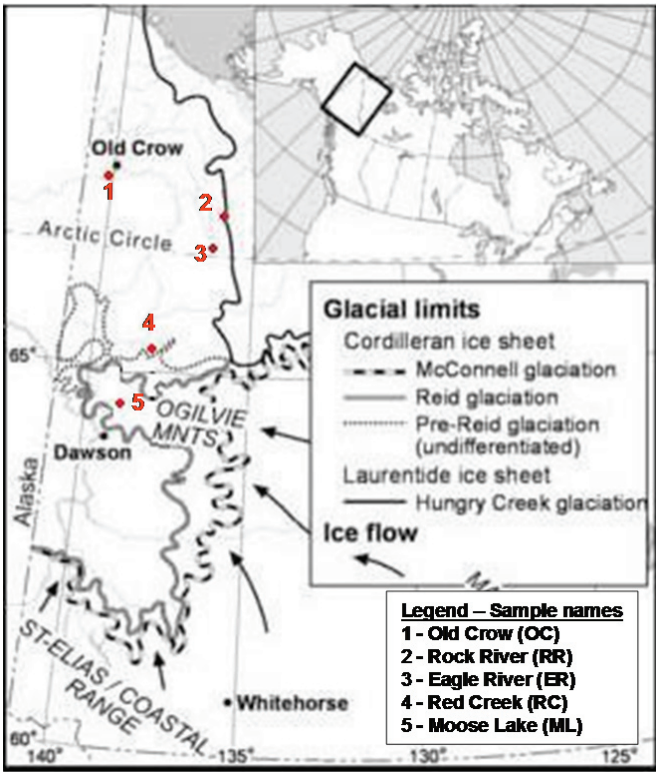

Figure 1. Study area (modified from Lacelle et al. 2007).

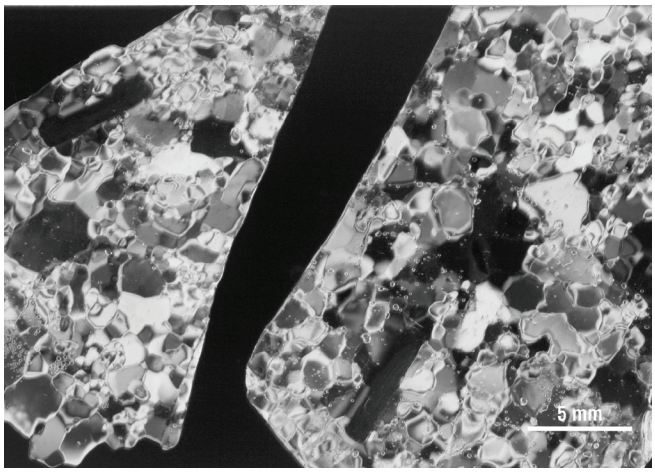

Figure 2. Thin sections from an ice wedge under crossed polaroids.

with significantly less oxygen than usual. Preliminary results of stable isotopes show homogeneity between ice wedge centers and exteriors, indicating climatic stability over this time. The range in $\delta^{18}O$ values of waters (from -24‰ to -26‰) agrees well with the range of modern ice wedges (-27 ‰ to -23 ‰) in the Old Crow area (Lauriol et al. 1995) and in the Richardson Mountains (-29 ‰ to -22 ‰) (Lacelle 2002). The $\delta^{18}O/\delta^{2}H$ signatures are plot below the meteoric waterline, indicating that ice wedges are filled during the later stages of snowmelt.

Ice crystal size (see Fig. 2) ranges from 0.5 to 6 mm in diameter, and the average size is about 2 mm in diameter. *C*-axes show a dispersed pattern. Ice wedge crystal size seems to be constrained by the width of the thermal contraction cracks. Elongated and spherical bubbles follow the foliated structure produced by repeated infilling of vertical thermal contraction cracks. Spherical bubble size ranges from 0.5 to 1 mm in diameter, and elongated bubble size ranges from 0.5 to 5 mm long.

Eagle River, Yukon

Samples of ice and soil were taken on top of the banks of the Eagle River at 372 m. Preliminary results for this site indicate molar gas ratios closer to atmospheric air ratios. The bubbles are bigger than Holocene ice wedge bubbles, and the crystals are similar to those found in glacier ice. Isotopic composition of the water coming from the ice indicates that these ice wedges are possibly older, dating from the Pleistocene ($\delta^{18}O_{water} \approx$ -30‰). A possible explanation for those results could be that the ice found at the Eagle River site is Pleistocene ice wedge ice, filled by snow or hoarfrost accretion. A silty sample between ice wedges is possibly carbonated loess coming from the Mackenzie, because loess coming from Old Crow Flats is not carbonated, and Mackenzie loess is highly carbonated. We can possibly make a connection with big ice wedge remnants of the Arctida loess bridges that can be found in the Laptev Sea (Tomirdiaro 1996). Tomirdiaro describes them as polygonally-veined ice formations developed to incredible size, but in form rather typical ice wedge polygons. These deep cracks were formed by infilling with sublimated and congealed ice, forming ice wedges.

Conclusion

These results should provide a better interpretation of ice wedge formation and filling process, and should be significant to palaeoclimatic interpretation of ground ice in permafrost areas.

Acknowledgments

We wish to thank the G.G Hatch Isotope Laboratory for their support and expertise. Financial support was provided by Natural Science and Engineering Research Council of Canada (NSERC) and by Northern Scientific Training Program (NSTP).

References

Cardyn, R., Clark, I.D., Lacelle, D., Lauriol, B., Zdanowicz, C. & Calmels, F. 2007. Molar gas ratios of air entrapped in ice: A new tool to determine the nature and origin of relict massive ground ice bodies in permafrost. *Quaternary Research* 68(2): 239-248.

Lacelle, D., Lauriol, B., Clark, I.D., Cardyn, R. & Zdanowicz, C. 2007. Middle Pleistocene glacier ice exposed in the headwall of a retrogressive thaw flow near Chapman Lake, central Yukon Territory, Canada, *Quaternary Research* 68(2): 249-260.

Lacelle, D. 2002. *Ground Ice Investigation in the Far Northwest of Canada.* Thesis (M.Sc.). Ottawa: University of Ottawa, 101 pp.

Lauriol, B., Duchesne, C. & Clark, I.D. 1995. Systématique du remplissage en eau des fentes de gel: les résultats d'une étude oxygène-18 et deutérium. *Permafrost and Periglacial Processes* 16: 47-55.

Sowers, T., Brook, E., Etheridge, D., Blunier, T., Fuchs, A., Leuenberger, M., Chappellaz, J., Barnola, J.M., Wahlen, M., Deck, B. & Weyhenmeyer, C. 1997. An interlaboratory comparison of techniques for extracting and analyzing trapped gases in ice cores. *Journal of Geophysical Research* 102: 26527-26538.

Tomirdiaro, S.V. 1996. Palaeogeography of Beringia and Arctida, In: F.W. West (ed.), *American Beginning: the Prehistory and Palaecology of Beringia*. Chicago: University of Chicago Press, 58-69.

Washburn, A.L. 1980. *Geocryology: A Survey of Periglacial Processes and Environments*. New York: Wiley.

Snowmelt in an Arctic Catchment: Application of the Hydrological Model WATFLOOD in a Small Arctic Basin with Different Land Cover Classes

A. Strutzke
Philipps-University Marburg, Germany
Ch. Opp
Philipps-University Marburg, Germany

Introduction

The world's climate change affects arctic areas in many ways. Climate models predict considerable warming for most northern regions, especially the Western Canadian Arctic. As a result, the western Arctic faces a shortened snow-covered season, changes in winter snow cover properties, and changes in timing and volume of snowmelt water runoff. Furthermore, the fragile ecosystem of the Canadian Arctic has to face a huge impact on its vegetation and animal species. Shrubs and trees will expand northwards and to higher elevations, replacing existing plants. Animals dependent on cold temperatures such as polar bears, seals, caribou, and reindeer are forced to move further north.

The objective of this research project is to examine the capability of the Canadian model WATFLOOD to simulate the runoff in Arctic environments. WATFLOOD was developed for and, so far, is mainly used in southern Canadian river systems and large drainage basins. In arctic areas the physical conditions are very different from those in the south: rivers freeze over completely in winter, the soil is permanently frozen (permafrost), and the watersheds in most cases are untouched by human influences. One of the most important aspects of arctic watersheds is that over the long winter, the precipitation falls almost exclusively as snow, which accumulates in the watershed. At the end of winter, snowmelt occurs, and most of the meltwater is released within days out of the basin. The end-of-winter snowmelt creates the highest yearly runoff peak in spring, with little runoff in the short summer that follows.

Modeling small watersheds in the Canadian Arctic is still a young science. The Arctic itself is a data-poor area compared to other well-researched areas in Canada or the world. Applying a hydrological model to arctic areas relies on having measurement stations in the Arctic as well as doing fieldwork to compare the modeled results with the measured data in evaluating the model's ability. The hope with modeling in the Arctic is that scientists will be able to come up with generalized parameter sets that can be used elsewhere in the Arctic where observation stations do not exist.

Results

Considering that WATFLOOD was developed for more temperate regions than the Arctic, the validation runs showed that WATFLOOD was able to simulate runoff in Hans Creek fairly accurately. WATFLOOD produced reasonable meltwater hydrographs in most years by only using WATFLOOD's relatively simple air temperature index algorithm to simulate snowmelt, together with the calibrated soil and channel parameters for Hans Creek. The aspect that WATFLOOD consistently estimates the days of first runoff too early can be explained by two naturally occurring processes that are not specifically addressed in the WATFLOOD model: snow meltwater percolation through the snow cover and snow damming. Both of these processes delay runoff by several days and are not accounted for by the model, leading to the problems in simulating the first day of runoff. Another major problem is the existence of many lakes in the Hans Creek watershed, where the outflow of the basin is located. This plays a huge role in the hydrology of the study basin, slowing runoff considerably. The lake-rich environment might also be an explanation for why WATFLOOD was not able to simulate any runoff from rainstorm events at the end of the summer, even though they were clearly visible in the gauging station.

The water storage in lakes and their particularly complex freezing and melting patterns clearly were a problem for WATFLOOD. One reason for this could be that the land cover class "water," as used for lakes in Hans Creek, was based on snow survey data from the generally very small lakes in the neighboring Trail Valley Creek. Hans Creek, however, holds lakes in a huge variety of sizes, which were all initiated in spring with the same amount of snow water equivalent. This may lead to large modeling errors because of the extensive redistribution of snow during blowing-snow events, which happen especially over lakes. Responsible is a lack of vegetation and the absence of melt/freeze cycles that could stabilize the snow cover. Additionally high wind speed events happen often over the long winter period in this area leading to frequent periods of blowing snow and high sublimation losses.

In a subsequent model series, the model performance was tested using climate data from a long-term observation station in Inuvik, 60 km south of the Hans Creek watershed. While the overall average of total and peak runoff volumes was fairly good, the individual hydrographs for the 15 years used in this series as well as the NSC clearly showed that WATFLOOD could not simulate the runoff accurately for most of the years. Since WATFLOOD was able to predict the runoff of the neighboring watershed Trail Valley Creek (Pohl et al. 2007) using Inuvik climate data, the reason must be sought in the differences between both watersheds. Likely reasons seem to be the bigger size of Hans Creek and

the existence of many lakes and wetland areas in the basin, which considerably slow the runoff because of their storage capacity. The modeling of runoff through lakes and arctic wetland areas could not be processed by WATFLOOD with satisfying accuracy.

Recent Rise of Water Level in Lake Hovsgol in the Permafrost Zone of Northern Mongolia: Trends and Causal Factors

Kazuo Takeda
Obihiro University of Agriculture and Veterinary Medicine, Obihiro, Japan
Hiroji Fushimi
University of Shiga Prefecture, Hikone, Japan
Tatuo Kira
Lake Biwa Environmental Research Institute, Ohtsu, Japan

Introduction

Lake Hovsgol is the largest freshwater lake in Mongolia (Table 1), located on the southern fringe of the east Siberian permafrost zone that supports the so-called "light taiga," or the deciduous conifer forests dominated by larch (*Larix spp.*). Once the larch vegetation is destroyed due to increasing forest fires and the outbreak of pest insects, direct sunshine raises ground surface temperature, resulting in deeper thawing of permafrost in summer.

According to observations at the station of the National Agency for Meteorological (1940–2006) in Hatgal village (on the southernmost shore of Lake Hovsgol) during 67 years, the annual mean temperature has gone up at the rate of 3°C per century with mean annual precipitation of only 200~400 mm/yr. Also noticed is that the water level of the lake has risen by 100 cm during the latest 37 years (Murun Meteorological Station 1970–2006).

As for the cause of such recent rise in water level, it is sometimes suggested that global climate change might be responsible (Kumagai 1998, Kumagai et al. 2006). Namely, the inflow of thawed fossil water from permafrost layers and glaciers brought about by global warming is supposed to be the main source of increasing lake water. This hypothesis, however, lacks concrete evidence because of the absence of continuous reliable records of groundwater supply into the lake.

This paper deals mainly with another causal factor relevant to the lake water level rise, viz. the bottleneck structure at the head of the Egiyn Gol (= river), the sole outlet of the lake. Environmental information related to the water budget of the lake is presented based on field survey around the lake.

Study Methods

Field surveys were conducted at 12 sites (Fig. 1), including 57 observation points during 3 years since 2000. Items observed were depth of active later (at most sites), soil properties such as moisture content, and grain size composition (at some limited number of sites). To find the depth of the active layer, a temperature profile was measured along a vertical hole made by striking an iron rod into the ground. The 0°C isotherm depth was then estimated by extrapolating the profile curve downward. This procedure was done after late August, when the active layer depth approached the seasonal maximum.

About 1.5 km southward from Hatgal at Site L (Fig. 1), the Egiyn River starts draining lake water through a very narrow and shallow bottleneck route, produced by the deposits carried by a tributary river. The structure of riverbeds of the two joining streams, so important for the control of the lake's water budget, was carefully surveyed. Further, as some of groundwater, the flow rate of an inflow stream originating from Har usnii Spring about 700 m from the lake (Site C, Fig. 1) was measured.

Results

On most alluvial beds deposited around the lake, ground surface soil layers generally consisted of silt and clay, fairly rich in mixed round gravel, and relatively dry with a volumetric water content of 10–20%. The estimated maximum depth of the active layer in late summer mainly amounted to 1.5–4.0 m under grasslands (pasture), while it was mainly 1.4–2.0 m under larch forests. The water content of surface soil under larch forests on north-facing slopes was around 22%, whereas it was only 13% on slopes facing the other three directions. However, once such a forest stand had been burned or clear-felled, the depth of active layer increased up to 1.9–5.4 m, owing to increased solar irradiation on the exposed ground.

At Site L, a large tributary river, Ulgen Sair, joins the uppermost stream of Egiyn River (Fig. 2). The stream bed of Ulgen Sair is far larger than the Egiyn stream, about 400 m wide at the confluence, and is entirely filled with fully eroded round gravel. Surface water flow does not exist under normal weather, but in case of concentrated heavy rainfall, vast mounts of debris are carried down by flood water and deposited on and around the confluence with the Egiyn River. For instance, in July 1971, the debris deposits following a heavy rainfall of 71 mm/day (at Hatgal) entirely buried the Egiyn stream, completely cutting off the outflow from the lake (Batsukh et al. 1976). Similar events took place twice in 2003

Table 1. Physical dimensions of Lake Hovsgol (Kurata 1993).

Location	50°27′–51°37′N, 100°51′–101°47′E
Altitude (m)	1,645
Surface area (km^2)	2,770
Maximum depth (m)	267
Mean depth (m)	138
Volume (km^3)*	383
Length of shoreline (km)	414
Drainage basin area (km^2)	4,940
Forest (km^2)**	(2,365)
Pasture (km^2)**	(1,559)
Mountain (km^2)**	(1,016)

* Data (Kumagai 1998); ** Values measured in map.

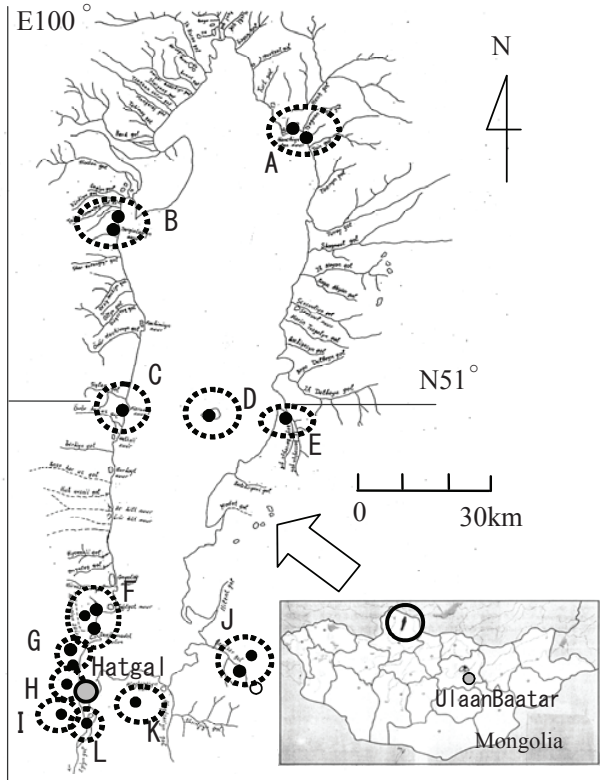

Figure 1. Distribution of the study sites around L. Hovsgol.

and 2006. Owing to such repeated flood disasters, it is difficult for Egiyn River at Site L to maintain a clearly open channel. The outflowing rate at Site L calculated from the current speed measured at stream surface (1.89 m/sec) and the cross-sectional area water channel (26.44 m^2) amounted to 1.58 km^3/yr.

At Site C, the inflowing rate of stream to originate from Har usnii Spring, where the water keeping 4.3~6.2°C flows throughout the year, was measured as 6.05 m^3/s and amounted to 0.19 km^3/yr.

Discussion

Based on the survey results, a depth of active layer was determined, and thereby estimated the increase of water inflow to the lake caused by additional thawing of permafrost due to climate warming. For example, the additional increase of the active layer in the forest area was determined to be 3.5 m, assuming that the forest vanishes and it becomes deeper from 1.9 m to 5.4 m. Using *Vw* 40% as the volumetric water content in permafrost and *Vw* 20% after thawing, the amount of fossilized water to outflow to the lake was estimated to be 1.66 km^3, using the area of forest given in Table 1.

However, such water does not flow out at the same time, but does so gradually for a long time. For example, it is known that the fossilized water keeps flowing out due to thawing of permafrost for several years after a forest fire. If it takes a century for the forest to vanish and the fossilized water flows out by the thawing of permafrost, the outflow of the water is estimated to be only 0.02 km^3/yr. The estimated amount is not even so much in the forest area larger than the pasture or the mountain (Table 1), because of the thin surface soil and abundance of gravel and rocks.

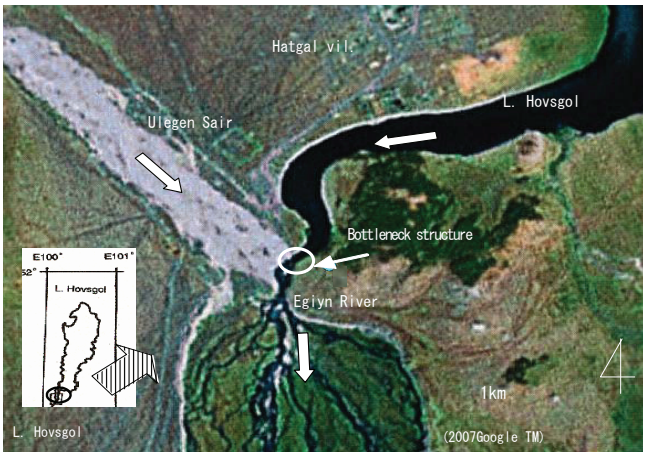

Figure 2. Outflow River, Egiyn River, at the confluence with the tributary river, Ulgen Sair.

The total amount of fossilized water in the drainage basin area is considered to be too small to cause a significant rise in water level, because the amount in the forest area is negligibly small compared with the outflow 1.58 km^3/yr through Egiyn River. Therefore, it is difficult to regard as the main causal factor that the increase of water inflow to the lake caused by additional thawing of permafrost due to climate warming induces the rise in water level.

On the other hand, the draining capacity of the sole outflowing river—Egiyn River—is very unstable, since its uppermost course suffers from vast amounts of sediment carried down by a large tributary stream at times of heavy rainfall, filling the river channel either partly or completely. A close negative correlation was found between the lake's water level and the rate of outflow through this bottleneck in the uppermost part of the Egiyn River.

References

Batsyk, N., Schymeev, V.P. et al. 1976. Surface water and water balance of Lake Khubusgul. In: N. Sodnom & N.E. Losev (eds.), *Natural Conditions and Resources of the Khubusgul Region in the Mongolian Peoples Republic.* Moscow: Nedra, 185-206 (in Russian and Japanese, translated by Dr. Naganawa).

Kumagai, M. 1998. Lake Hovsgol in Mongolia. In: Lake Biwa Research Institute (ed.), *Record of the 16th IBRI Symposium*. Otsu: LBRI, 89-104 (in Japanese).

Kumagai, M., Urabe, J. et al. 2006. Recent rise in water level at Lake Hovsgol in Mongolia. In: C.E. Goulden, T. Sitnikova et al. (eds.), *The Geology, Biodiversity and Ecology of Lake Hovsgol (Mongolia)*. Leiden: Backhuys, 77-91.

Kurata, A. (ed.), 1993. *Data Book of World Lake Environments: Compact-size Ed 1: Asia and Oceania.* Kusatsu: ILEC & UNEP.

Murun Meteorological Station 1970-2006. *Meteorological Data Observed at Lake Hovsgol during 1970–2006.*

National Agency for Meteorology 1940–2006. *Meteorological Data observed at Moron and Hatgal during 1940–2006.*

Effects of Increased Snow Depth on Ecosystem CO_2 Fluxes in Arctic Tundra

Lina Taneva
Environment and Natural Resources Institute, University of Alaska Anchorage
Patrick F. Sullivan
Department of Biology, University of Alaska Anchorage
Bjartmar Sveinbjornsson
Department of Biology, University of Alaska Anchorage
Jeffrey M. Welker
Environment and Natural Resources Institute, University of Alaska Anchorage

Introduction

Shrub expansion into arctic tundra has been documented (Tape et al. 2006) and climate warming and altered precipitation regime have been proposed as possible drivers of plant community composition changes (Sturm et al. 2005). Increases in winter precipitation and deeper snowpack can alter the soil microclimate, leading to warmer soils and deeper active layer, potentially resulting in changes in the carbon, water, and nutrient cycles of arctic ecosystems. Associated changes in plant community composition in tundra ecosystems can further lead to altered ecosystem function. The Arctic represents a large carbon reservoir in the global carbon cycle, and changes in the cycling of carbon in tundra ecosystems with observed changes in biotic and abiotic conditions could have important implications for atmospheric CO_2 accumulation.

The objective of this study was to evaluate the short-term and long-term effects of deeper winter snow depth on ecosystem carbon cycling during the growing season.

Methods

This research was conducted during the 2007 growing season at three moist tussock tundra sites near Toolik Lake, in the northern foothills of the Brooks Range, Alaska, USA. Plant community composition is dominated by the tussock grass *Eriophorum vaginatum,* the shrubs *Betula nana,* and *Salix pulchra*, as well as other short-stature vegetation, mosses and lichens. Snow fences were constructed in 1994 (n = 1) and 2006 (n = 3), in order to increase snow depth in the treatment plots during winter/spring. A naturally occurring shrub patch was used as a reference.

Ecosystem CO_2 flux measurements were taken using a clear plexiglass chamber, connected to a Licor 6200 infrared gas analyzer.

Results

No significant changes in ecosystem C uptake or respiration after one year of snow depth increase were observed, with the ecosystem representing a C source for part of the growing season (Fig. 1). Long-term (13 yr) snow depth increase resulted in greater C uptake rates in treatment plots, whereas no significant changes in ecosystem respiration rates were observed, and both treatment and control plots were a C sink during the growing season (Fig. 1). Ecosystem C fluxes in a nearby naturally occurring shrub patch were lower than those in tussock tundra under ambient or increased winter snow depth, and NEE was near zero (Fig. 1).

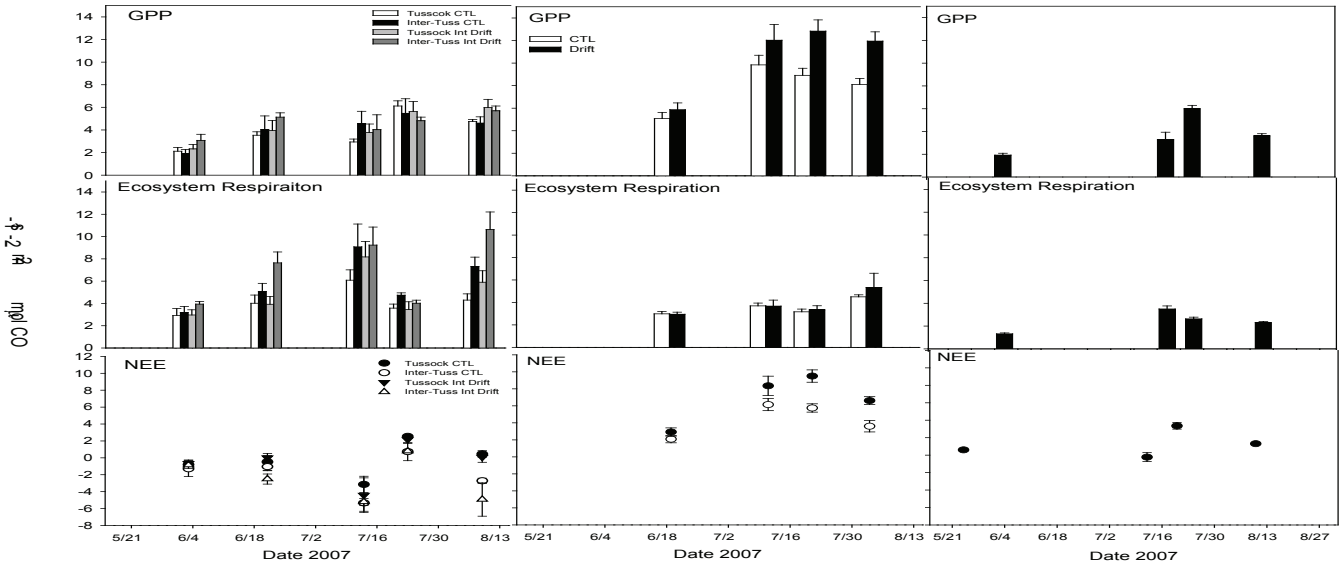

Figure 1. Ecosystem CO_2 fluxes (gross ecosystem productivity [GEP], ecosystem respiration, and net ecosystem CO_2 exchange [NEE]) in tussock tundra after 1 and 13 years of snow accumulation increase, and in a site dominated by shrub (*B. nana*) vegetation without any snow treatments.

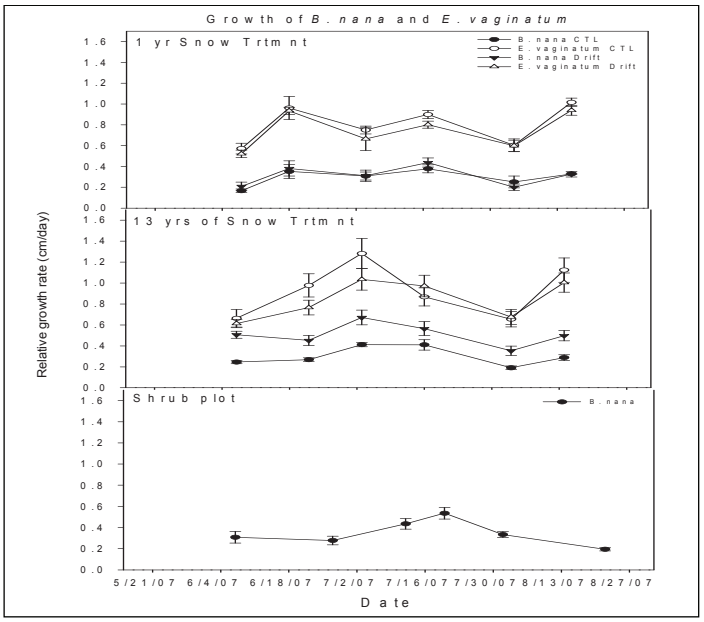

Figure 2. Growing season growth rate of *B. nana* and *E. vaginatum* in a tussock tundra ecosystem after 1 and 13 years of snow accumulation increase, and in a shrub-dominated plot with no snow depth manipulation.

The growth rate of *E. vaginatum* was higher than that of *B. nana*, with no significant changes in growth rates after 1 yr of snow depth increase (Fig. 2). Long-term snow depth manipulation led to a stimulation in *B. nana* growth rate and a trend towards lower *E. vaginatum* growth rates, relative to ambient snow plots (Fig. 2). Rates of *B. nana* growth in the long-term treatment plots were higher than those in the shrub-dominated plot, while growth rates at ambient snow were comparable at tussock tundra and shrub sites (Fig. 2).

Conclusions

Long-term increases (13 yr) in winter snow cover and associated changes in plant community composition (i.e., increases in shrub abundance; Wahren et al. 2005) converted this tundra ecosystem from a source of C to the atmosphere (as reported in Jones et al. 1998 and Oberbauer et al. 2007 after 2, 3, and 4 years of treatment) to a C sink.

Enhanced GEP with deeper snow cannot be explained by increases in shrub abundance alone and suggests altered winter soil processes under deeper snow that may alleviate ecosystem nutrient limitation.

Changes in plant community composition in tundra ecosystems can potentially translate to altered C inputs, storage, and turnover rates in these C-rich and warming-sensitive ecosystems, with subsequent implications for the global C cycle.

Acknowledgments

This research was funded by an International Polar Year grant #0612534 through the Office of Polar Programs at the National Science Foundation. We gratefully acknowledge the staff at Toolik Field Station for camp maintenance and operation. We thank Jeremy Chignell for his help in the field.

References

Jones, M.H., Fahnestock, J.T., Walker, D.A., Walker, M.D. & Welker, J.M. 1998. Carbon dioxide fluxes in moist and dry Arctic tundra during the snow-free season: Responses to increases in summer temperature and winter snow accumulation. *Arctic and Alpine Research* 30(4): 373-380.

Oberbauer, S.F., Tweedie, C.E., Welker, J.M., Fahnestock, J.T., Henry, G.H., Webber, P.J., Hollister, R.D., Walker, M.D., Kuchy, A., Elmore, E. & Starr, G. 2007. Tundra CO_2 fluxes in response to experimental warming across latitudinal and moisture gradients. *Ecological Monographs* 77(2): 221-238.

Sturm, M., Schimel, J., Michaelson, G., Welker, J.M., Oberbauer, S.F., Liston, G.E., Fahnestock, J. & Romanovsky, V.E. 2005. Winter biological processes could help convert Arctic tundra to shrubland. *Bioscience* 55(1): 17-26.

Tape, K., Sturm, M. & Racine, C. 2006. The evidence for shrub expansion in northern Alaska and the Pan-Arctic. *Global Change Biology* 12(4): 686-702.

Wahren, C-H.A., Walker, M.D. & Bret-Harte, M.S. 2005. Vegetation responses in Alaskan arctic tundra after 8 years of a summer warming and winter snow manipulation experiment. *Global Change Biology* 11: 537-552.

Modeling Permafrost Evolution and Impact on Hydrogeology at the Meuse/Haute-Marne Sedimentary Site (Northeast France) During the Last 120,000 Years

Vanessa Teles, Emmanuel Mouche, Christophe Grenier, Damien Regnier
Laboratoire des Sciences du Climat et de l'Environnement, UMR CEA-CNRS-UVSQ, France
Jacques Brulhet, Hakim Benaberrahmane
Andra, Agence nationale pour la gestion des déchets radioactifs, France

Introduction

The Callovo-Oxfordian layer in the eastern part of the Parisian Basin (France) was recognized as a potential nuclear waste repository layer. To evaluate transfers from the host formation to the biosphere, it is important to understand the temporal evolution of the hydraulic boundary conditions of the clayey layer, which means to understand the evolution of the whole hydrogeological system. The Callovo-Oxfordian unit is part of the Parisian Basin consisting of piled up sedimentary units ranging over thousands of meters in depth at maximum and covering the northern half of France. Besides this specific sedimentary geological structure, past permafrost extension differs from Nordic situations, because ice cover remained here very limited in time and depth soon followed by a cold and dry steppic landscape.

A few years ago, Andra (National Agency for Nuclear Waste Management) launched a research program on the geoprospective of the MHM (Meuse/Haute-Marne) site, including the study of the impact of glacial cycles on the underground flow patterns (Andra 2005, Andra 2004, Brulhet 2004).

Recent efforts to study the impact of permafrost on underground flow patterns, modeling of permafrost extension through geological times as well as on going activities, are reported here involving the LSCE (Laboratoire des Sciences du Climat et de l'Environnement) team. This work follows a former phase of pure hydrological modeling of the MHM site.

The studies conducted at LSCE are presented here along 3 major issues: (1) impact of permafrost reconstruction on hydrogeology during the last 120,000 years; (2) 3D thermal modeling of permafrost extensions based on solar radiation evolution (120,000-year period); and (3) coupled thermo-hydrological modeling and role of small-scale surface and subsurface units (valley vs. hill, river, lake, aquifer).

The thermal and hydrodynamic simulations have been performed with the Cast3M code, developed and implemented by the CEA (Atomic Energy Commission), using finite-element or mixed hybrid finite-element formulations.

The extension of the modeled zone is 75 km x 80 km, involving the actual present-time topography and rivers, as well as geological layers (from bottom to surface: Dogger, Callovo-Oxfordien, Oxfordien-Calcaire, Kimmérigien, Cretacé-Barrois) corresponding for the latter to roughly a 500 m depth.

Impact of Permafrost Reconstruction on Hydrogeology During the Last 120,000 Years

The idea behind this first modeling phase (refer to Teles & Mouche 2005) consists in taking reconstructions of permafrost extensions over the last 100,000 years, transfer it into permeability information, and simulate transient flow on the MHM domain with adequate boundary conditions. More precisely, reconstructions from Van Vliet (2004) concerning the MHM region were considered. They involve five development stages with associated time periods: present conditions for 10,000 years BP, installation of a thin permafrost (starting 95 BP), permafrost on hills with free valleys (from 75,000 years BP on), thick continuous permafrost (starting 20,000 years BP), relict permafrost (from 13,000 years BP). Three-dimensional simulations of transient flow were conducted starting from initial conditions close to present state. Freezing causes a stop in the infiltration as permafrost develops, so surface boundary conditions are changed from imposed heads assumed close to the local altitude to no flow conditions. Furthermore, the 3D permeability field is modified to account for the presence of permafrost. Practically speaking, permeability tensors are associated with each mesh element corresponding vertically to harmonic mean between permafrost permeability (arbitrary put at 10^{-13} m/s) and actual geological formation permeability; horizontally, arithmetic mean was considered. Consequently, vertical flow is limited, whereas horizontal flow is directly a function of the vertical fraction of unfrozen formation thickness.

Results show that the flow velocities are reduced as compared with present-state conditions in all geological formations during permafrost phases. This is the result of the stop in the recharge as well as reduction in the permeability. Flow velocity in the aquifers not directly concerned themselves by freezing is roughly reduced by a factor of two.

It should be stressed here, nevertheless, that conditions inferred at the MHM site for the last glacial cycle are very different from conditions reconstructed for more Nordic locations, where the ice thickness was large and lead to a mechanical load onto the geological units. Consequently, increased pressure boosted access of water to deeper zones, though recharge from the surface was actually stopped. The situation at the MHM site is considered best represented as a mere stop in recharge, leading to a pure aquifer drainage situation for deeper units.

3D Thermal Modeling of Permafrost Extensions from Solar Radiation Evolution (Last 120,000 Years)

In a second step (refer to Teles & Mouche 2006), focus was put on the modeling of transient evolution of permafrost extension. Former 3D geometrical features were retained for a thermal modeling approach and identical 100,000-year time period. A purely conductive model was considered with actual geological formation thermal properties, imposed bottom geothermal flux, and transient imposed surface temperature. The latter followed the normalized variation in solar radiation over the time period according to Berger (1978). The modeling of permafrost extension was attempted considering the following refined points: (1) Imposed surface temperature was made dependant from the actual altitude and incident solar radiation (Šafanda 1999). (2) Ground level solar radiation was considered dependant on incident solar radiation, topographic slope and surface orientation (Senkova & Rontu 2003). (3) Imposed surface temperature was affected a positive correction when corresponding to a river mesh to account for heat exchange resulting in the reduction of permafrost development under rivers (the coefficient was chosen constant and its value assessed based on model sensitivity analysis). Simulation results were finally compared to a vertical reconstruction of 0°C isotherm for a deep borehole location. These reference values correspond to a best expert view resulting from in situ analysis, naturalistic considerations, as well as 1D vertical thermal modeling including phase change effects (cf. Courbouleix et al. 1998).

This study remains preliminary in the sense that the 3D model was not further complexified to account for phase-change phenomena and heat advection due to water flow. This is attempted in the third modeling phase. Nevertheless, results show that qualitative evolution of the 0°C isotherm could be well simulated, although quantitative fit requires better constraints on the solar radiation forcing history. This is a critical point, since literature shows that uncertainties in solar radiation histories resulting from existing scenarios remain large, whereas the sensitivity of the thermal model to this input data is very large. For two models considered in the study only differing roughly by a factor of two, permafrost extensions were very different. Consequently, care should be put in the future in increasing the robustness of this forcing term.

Coupled Thermo-Hydrological Modeling of Small-Scale Units

Ongoing efforts consist in (1) developing a coupled TH (Thermo-Hydro) numerical model within our Cast3M code including thermal conduction, convection, and phase change; (2) answering the issue of the level of heat flux actually transmitted to the underground while considering various surface- and subsurface-specific units leading to heat exchange like water bodies (river, lake, aquifer), or including topographic variability (valleys vs. hills); and (3) addressing the issue of spatial and temporal upscaling (e.g., periodic thermal stress, daily, yearly, cycles) to achieve regional modeling for a 120,000-year time period.

These efforts will serve to organize the various mechanisms into a hierarchy, and finally improve the physical and numerical modeling of the impact of glacial cycles on the hydrogeology at the MHM site over geological time scales.

References

Andra. 2005. Dossier 2005. Argile, Référentiel du site de Meuse / Haute-Marne, Tome 3. *Document Andra* n° C.RP.ADS.04.0022.B.

Andra. 2004. *Site Meuse/Haute-Marne, Géothermie*. Inventaire des nouvelles données. *Note Technique Andra* n° C.NT.ASMG.04.0001.

Berger, A. 1978. Long-term variations of daily insolation and Quaternary climatic changes. *Journal of the Atmospheric Sciences* 35(12): 2362-2367.

Brulhet, J. 2004. L'évolution géodynamique (tectonique et climatique) et son impact sur l'hydrogéologie et l'environnement de surface. Site MHM. *Note Technique Andra* n° C.NT.ASMG.03.106.B: 84 pp.

Courbouleix, S., Gros, Y., Clet, M., Coutard, J.P., Lautridou, J.P., Van Vliet-Lanoe, B., Dupas, A. & Cames-Pintaux, A.M. 1998. Simulation de la profondeur du pergélisol au cours du dernier cycle climatique. Utilisation des échantillons du sondage EST106, *Rapport Andra* n° D.RP.0ANT.98.011.

Šafanda, J, 1999. Groundwater surface temperature as a function of slope angle and slope orientation. *Tectonophysics* 306: 367-375.

Senkova, A.V. & Rontu, L. 2003. *A Study of the Radiation Parametrization for Sloping Surfaces*. St. Petersburg: Baltic HIRLAM Worshop, 79-82.

Teles, V. & Mouche, E. 2005. Analyse de sensibilité de la présence d'un pergélisol continu et discontinu sur l'hydrogéologie du secteur, Site MHM. *Rapport Andra* n° C.RP.12CEA.05.001.

Teles, V. & Mouche, E. 2006. Site MHM, Modélisation tridimensionnelle de la distribution du pergélisol au cours d'un cycle climatique. *Rapport Andra* n° C.RP.12CEA.06.001.

Van Vliet-Lanoë, B. 2004. Modèle conceptuel du pergélisol, Site MHM. *Rapport Andra* n° C.RP.0UST.04.002.

Effect of a Snow Fence on the Shallow Ground Thermal Regime, Baker Lake, Nunavut, Canada

Jennifer L. Throop
Department of Geography, University of Ottawa, Ottawa, Canada
Sharon L. Smith
Geological Survey of Canada, Natural Resources Canada, Ottawa, Canada
Antoni G. Lewkowicz
Department of Geography, University of Ottawa, Ottawa, Canada

Introduction

Snow depths on the tundra can be highly variable due to snow redistribution by high winds in relation to topography and vegetation. These differences are an important factor in the spatial variability of the ground thermal regime (Smith & Riseborough 2002). Variations in snow depths substantially affect the heat exchange between the air and ground surface, thereby influencing the surface offset. Changes in amounts of snow cover are expected to accompany a warming climate (ACIA 2005) and may be an important factor in influencing future permafrost conditions.

An instrumented arctic tundra site at Baker Lake, Nunavut, (64°19.6′N, 96°2.5′W) provides the opportunity to investigate the impact of variable snow depths on the shallow ground thermal regime. Baker Lake is in a region of continuous permafrost with thicknesses of up to 200 m (Smith et al. 2005). The site consists of a transect of four shallow boreholes reaching depths of 3 m along a gentle south-facing slope. The installation of a 4 m tall snow fence in 1981 has prevented snow from drifting into the community. This has resulted in a large snowdrift developing downwind of the fence that persists into late July. Our goal is to assess the impact of the snow fence by examining the thermal data collected from two of the boreholes: the site least affected by the snow fence (BH4, representing natural conditions) and the site most affected by the snow fence (BH2, beneath the snowdrift).

Site Description and Methods

The boreholes were drilled in 1997. BH4 is located 400 m upwind of the snow fence, and BH2 is located 45 m downwind, where the large snowdrift forms. These boreholes were instrumented with temperature cables that have thermistors at 50 cm intervals down to 3 m. Manual readings were taken monthly or semi-monthly from 1997 until 2005 and less frequently since 2005. A datalogger was attached at BH4 in 2002 to record temperatures three times daily. A weather station was installed near BH4 in 2002 to obtain air temperature, wind speed, and the natural snow depth for the area. Temperature sensors were installed in 2002 at 2–5 cm depth to provide an indication of the surface temperature.

Surface offsets were calculated for both sites from 2002–2006 by subtracting the mean annual air temperature (MAAT) from the mean annual ground surface temperature (MAGST). The maximum and minimum values at each depth to 3 m were taken from the manual data collected between 1997 and 2005.

Maximum thaw depths were calculated for each year at both boreholes using linear interpolation between sensors located above and below the 0°C isotherm. Thawing and freezing degree-days (TDD and FDD) were calculated using the air temperature data from the weather station at BH4.

Results

The MAAT varied between -8.8 and -12.2°C over the 4 years of continuous records (Table 1). For the same period, the MAGST at BH4 ranged from -5.2 to -8.6°C, giving surface offsets of 2.4 to 4.7°C. At BH2, MAGST was higher, ranging from -0.1 to -2.0°C, producing very large surface offsets of 7.8 to 10.6°C. The difference between the two sites indicates that the ground surface warmed beneath the snowbank by 4-8°C over the 16-year period.

The temperature envelopes (Fig. 1) illustrate that the snowdrift at BH2 has strongly affected minimum ground temperatures down to 3 m. At BH4, these range between -16 and -22°C, whereas at BH2 the range is between -5 and -7°C. There is a difference of approximately 15°C near the surface, and 11°C at 3 m depth. Maximum temperatures on the other hand, are quite similar.

Calculated maximum thaw depths at BH4 averaged 1.84 m for 1997–2005 with a standard deviation of 0.28 m (Fig. 2). The minimum value of 1.25 m occurred in September 1997, and the maximum of 2.17 m in September 2005, giving a range of 0.9 m. Although the results suggest a trend towards increasing thaw depths, the dataset is too short to reach a definitive conclusion. A comparison between thaw depths and the square root of TDD from the nearby Baker

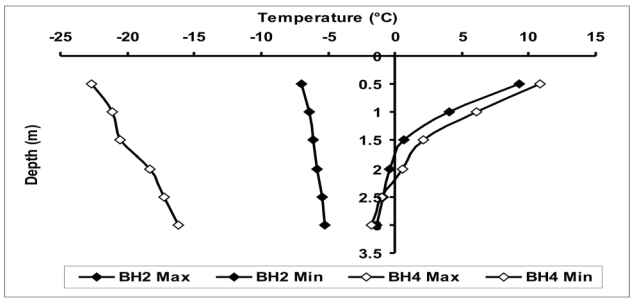

Figure 1. Temperature envelopes (maximum and minimum values) at BH2 and BH4 from the 1997–2005 manual readings.

Table 1. Summary table of data values at BH4 and BH2.

Year (Sept-Aug)	MAAT	Snow Depth Average (cm)	Snow Depth Maximum (cm)	MAGST BH4	MAGST BH2	Surface Offset BH4	Surface Offset BH2
2002–2003	-10.5	18.0	33.2	-8.1	-0.1	2.4	10.4
2003–2004	-12.2	14.6	24.8	-7.6	-2.0	4.7	10.2
2004–2005	-11.5	12.6	36.3	-8.6	-0.9	2.9	10.6
2005–2006	-8.8	28.1	56.1	-5.2	-1.0	3.6	7.8

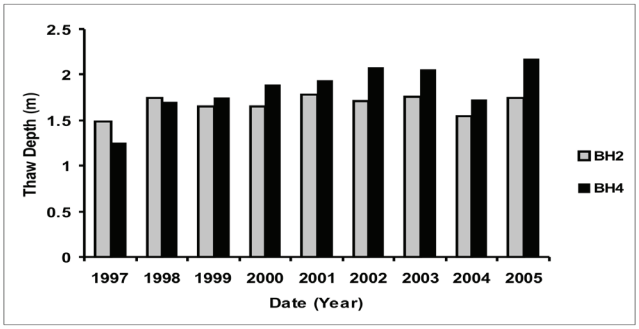

Figure 2. Maximum calculated thaw depths for BH2 and BH4 from 1997 to 2005 using manual data taken approximately three times per month during maximum thaw season.

Lake weather station did not produce a significant linear fit (results not shown).

Calculated maximum thaw depths at BH2 beneath the snowbank averaged 1.67 m with a standard deviation of 0.10 m, and range from a minimum of 1.48 m in September 1997 to a maximum of 1.78 m in September 2001 (Fig. 2). Interannual variability in the thaw depth at this borehole, therefore, was only about 0.3 m, substantially less than at BH4.

The average snow depth at BH4 from 2002–2006 ranged from 13 to 28 cm. The highest value occurred in the winter of 2005–2006, when the maximum depth reached 56 cm at the end of April, at least 20 cm deeper than any of the other three years (Table 1).

The year 2004 had the lowest TDD in the four years of continuous monitoring at the site with a value of 843, whereas 2003, 2005, and 2006 ranged between 947 and 1051.

Discussion

The effect of the snowdrift can be seen clearly in the temperature envelopes in Figure 1. The amplitude of the envelope is much greater at BH4, reaching much lower minimum temperatures showing a more direct link to changes in air temperature. The small amplitude of the envelope and the milder temperatures at BH2 illustrate the muting effect of the snowdrift, dampening the effect of air temperature changes.

The decrease in thaw depth in 2004 reflects the low value of thawing degree-days that year (843) compared to other years. There was not a clear link between interannual differences in snow depths measured at BH4 and surface offsets. The 2005–2006 winter at BH4 had more snow than other years along with the highest MAGST and MAAT. Even though this year had the most snow, the greatest surface offset was in 2003–2004, and that at BH2 was noticeably less than in the other years in 2005–2006.

The result that the deep snowbank produces very large surface offsets and substantially warms the ground surface on an annual basis was also found beneath a snow fence induced snowbank in Barrow, Alaska (Hinkel & Hurd 2006). Similarly, the shallower thaw depths produced by the late-lying snow were observed in Alaska, where in one year their snowbank failed to melt completely.

Conclusion

The long-lasting snow fence induced snowbank at Baker Lake results in the ground surface beneath being warmer than the surrounding area by 4–8°C on an annual basis. However, the snow is so deep that thaw is retarded significantly, and thaw depths average 17 cm less beneath its deepest section than at the control site (BH4). Variability in depths of thaw over 9 years was greater at the control site than beneath the snowbank. There is no evidence from the ground temperature data that warming by the snowbank is causing thermokarst at the site.

Acknowledgments

Support for this project has been provided by Natural Resources Canada, the Canadian Government's Climate Change Action Plan 2000, and International Polar Year Program. Orin Durey, a Baker Lake resident, maintains the site and collects the temperature data.

References

ACIA 2005. *Arctic Climate Impact Assessment*. Cambridge University Press.

Hinkel, K.M. & Hurd, J.K. Jr. 2006. Permafrost destabilization and thermokarst following snow fence installation, Barrow, Alaska, U.S.A. *Arctic, Antarctic and Alpine Research* 38: 530-539.

Smith, M.W. & Riseborough, D.W. 2002. Climate and the limits of permafrost: a zonal analysis. *Permafrost and Periglacial Processes* 13: 1-15.

Smith, S.L., Burgess, M.M., Riseborough, D.W. & Nixon, F.M. 2005. Recent trends from Canadian permafrost thermal monitoring network sites. *Permafrost and Periglacial Processes* 16: 19-30.

Examining the Temporal Variation in Headwater Drainage Networks and Potential for Thermokarst Using Remote Sensing in the Imnavait Basin

Erin D. Trochim
University of Alaska Fairbanks
Douglas L. Kane
University of Alaska Fairbanks
Anupma Prakash
University of Alaska Fairbanks

Introduction

Surficial drainage networks underlain by a confining layer such as permafrost are characterized by significant amounts of overland flow, manifesting features such as water tracks and incised channels as the dominant complex. Variations in routing can occur in the Arctic fresh water hydrological cycle as feedback mechanisms between vegetation and permafrost distribution. Predicting and characterizing potential response is an important component for engineering infrastructure appropriate for the climatic conditions. The Imnavait basin north of the Brooks Range in Alaska is part of a long-term monitoring effort, and provides an opportunity to pair hydrological studies and high-resolution topography models with remotely sensed data, to create a qualitative, spatially distributed perspective.

Water tracks are saturated areas mantled with organic soils which may or may not connect to the channel network (McNamara et al. 1999). Flows are perpendicular to elevation contours, and they often develop a parallel distribution with spacing of approximately tens of meters. The vegetation associated with water tracks is proportional to quantity of water typically present within the channel (Walker et al. 1994). Well-developed water tracks contain the *Eriophorum angustifolium-Salix pulchra* willow community while water tracks of intermittent flow, which are poorly defined, contain shrub facies of the *Sphagno-Eriophoretum vaginati*. subass. *typicum*.

Thawing of ice-rich permafrost or thermokarsting (van Everdingen 1998) in foothills or mountainous areas typically occurs along water tracks; determining the thermal regime of the water tracks will allow the prediction of (if) when a thermokarst may occur. Assessment of whether the water tracks are experiencing shrub expansion, one of the strongest indicators of ecosystem change due to climate change measured to date (Stow et al. 2004), is important for prediction of the future thermal state. Changes in vegetation can result in feedbacks to the thermal state of the associated permafrost, as an increase in density and spatial expansion lower the albedo and allow more energy to be absorbed into the ground (Callaghan et al. 2004). Coupling this effect with potential alterations to landscape as a result of thermokarst activity, including changes in groundwater flow and storage, relief, and discharge patterns and amounts (Grosse et al. 2006), results in the potential to significantly alter the landscape.

Figure 1. Water tracks in the Kuparuk River basin.

The Imnavait basin covers an area of 2.2 km^2. Till from a glacial advance in the middle Pleistocene covers the slopes (Hamilton 1989). Thick permafrost reaching 300 m deep (Osterkamp & Payne 1981), and lack of springs in the basin effectively isolate the basin from deep groundwater sources. Maximum depths of thaw are typically 25 to 50 cm, but can extend to 100 cm with variation in environmental factors including soil type, slope, aspect, and soil moisture (Hinzman et al. 1991).

Aerial photographs from July of 1956, 1978, and 2007 were georeferenced and used to digitize water tracks into three classes to examine the temporal variation in both area and texture over this 61-year period. Water tracks that were least, moderately, and well developed were buffered by 2, 5, and 7.5 m, respectively, to approximate area. Zonal GIS analysis using a 5 m digital elevation model acquired in 2001 was used to examine the variations in slope, aspect, and elevation.

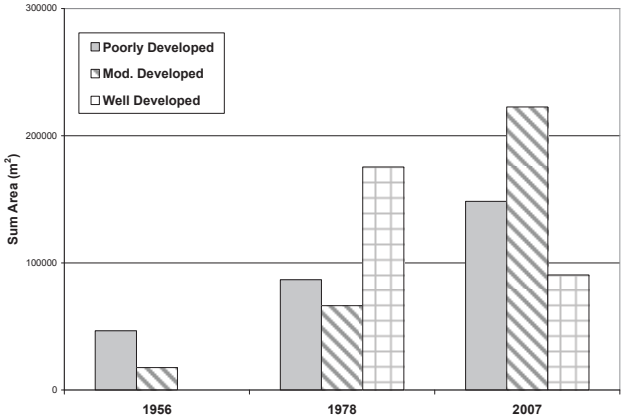

Figure 2. Imnavait Basin water track distribution: 1956, 1978, and 2007.

Table 1. Zonal GIS analysis of water track distribution.

		Elevation (m)			Aspect (°)	Slope (°)
Develop. of WT		*Mean*	*Min*	*Max*	*Mean*	*Mean*
Poorly	*1956*	900.64	874.75	951.13	235.43	4.71
	1978	906.91	878.74	946.2	226.46	4.94
	2007	903.19	873.67	946.72	204.72	4.34
Mod.	*1956*	895.52	873.88	905.44	229.88	3.98
	1978	907.72	897.01	943.24	256.73	5.23
	2007	899.71	871.83	943.55	224.89	4.86
Well	*1956*	0	0	0	0	0
	1978	899.1	872.01	930.11	206.99	4.78
	2007	901.25	874.1	932.03	222.98	5.71

Changes in the distribution of the poorly and moderately developed water tracks both exhibited significant positive linear trends with R^2 values >0.90. The well-developed water tracks show an initial increase from 1956 to 1978 and then a decrease from 1976 to 2007. This may be due to changes in precipitation and soil moisture, which negatively affected species distribution or gradual channel incision which restricted saturated flow to a smaller area.

The mean elevation of water tracks varies with time, climbing initially in 1978 and then decreasing in 2007. This suggests that water tracks initially extend in distribution up the slope, and then expand in density in the lower elevations by 2007. Overall, water tracks in the Imnavait show a southwest (202.5–247.5°) aspect with significant variation only in the moderately developed classes with a shift in 1978 to west (247.5–292.5°). Well-developed water tracks show an increase in mean slope angle with time, supporting the notion that a decrease in overall precipitation or deeper active layer permitting more infiltration would restrict overland flow to the steeper areas.

Analysis of water track distribution and density from 1956 through 2007 showed an increase in both poorly and moderately defined tracks, while the well-developed water tracks decreased in area. This trend corroborates climate warming and may indicate increased amounts of solid precipitation as snow which leave the ground more saturated in the early growing season and, coupled with warming weather, provide ideal conditions for shrub expansion. The effect of the change in climatic conditions and the corresponding shrub expansion in this area on the permafrost will be examined in future work.

Acknowledgments

Many thanks to Matt Sprau for field assistance and Jason Stuckey of the Toolik Field Station GIS program. Funding was provided by a student research grant awarded by the Center for Global Change & Arctic System Research, University of Alaska Fairbanks.

References

Callaghan, T.V., Bjorn, L.O., Chernov, Y., Chapin, T., Christensen, T.R., Huntley, B., Ima, R.A., Johansson, M., Jolly, D., Jonasson, S., Matveyeva, N., Panikov, N., Oechel, W., Shaver, G., Schaphoff, S. & Sitch, S. 2004. Effects of changes in climate on landscape and regional processes, and feedbacks to the climate system. *Ambio* 33(7): 10.

Grosse, G., Schirrmeister, L. & Malthus, T.J. 2006. Application of Landsat-7 satellite data and a DEM for the quantification of thermokarst-affected terrain types in the periglacial Lena-Anabar coastal lowland. *Polar Research* 25(1): 51-67.

Hamilton, T.D. 1989. *Late* Cenezoic glaciation of the Central Brooks Range. In: T.D. Hamilton, K.M. Reed & R.M. Thorson (eds.), *Glaciation in Alaska: The Geologic Record,* Vol. 99. Anchorage, AK: Alaska Geol. Soc., 9-49.

Hinzman, L.D. & Kane, D.L. 1991. Snow hydrology of a headwater arctic basin. 2. Conceptual analysis and computer modeling. *Water Resources Research* 27(6): 1111-1121.

McNamara, J.P., Kane, D.L. & Hinzman, L.D. 1999. An analysis of an arctic channel network using a digital elevation model. *Geomorphology* 29: 339-353.

Osterkamp, T.E. & Payne, M.W. 1981. Estimates of permafrost thickness from well logs in Northern Alaska. *Cold Regions Science and Technology* 5(1): 13-27.

Stow, D.A., Hope, A., McGuire, D., Verbyla, D., Gamon, J., Huemmrich, F., Houston, S., Racine, C., Sturm, M., Tape, K., Hinzman, L., Yoshikawa, K., Tweedie, C., Noyle, B., Silapaswan, C., Douglas, D., Griffith, B., Jia, G., Epstein, H., Walker, D., Daeschner, S., Petersen, A., Zhou, L. & Myneni, R. 2004. Remote sensing of vegetation and land-cover change in Arctic Tundra Ecosystems. *Remote Sensing of Environment* 89: 281-308.

Van Everdingen, R. (ed.) 1998. *Multilanguage Glossary of Permafrost and Related Ground-Ice Terms*. Boulder, CO: National Snow and Ice Data Center for Glaciology.

Walker, M.D., Walker, D.A. & Auerbach, N.A. 1994. Plant communities of a tussock tundra landscape in the Brooks Range Foothills, Alaska. *Journal of Vegetation Science* 5: 843-866.

Detection of Degraded Mountain Permafrost with the Help of GPR Profiling at Mesón San Juan, Mendoza, Argentina

Dario Trombotto Liaudat
Geocryology Ianigla-Cricyt-Conicet, Casilla de Correo 330, 5500 Mendoza, Argentina
Jandyr Menezes Travassos
Observatório Nacional, Rua General José Cristino, 77, 20921-400, Rio de Janeiro, Brazil
Giovanni Chaves Stael
Observatório Nacional, Rua General José Cristino, 77, 20921-400, Rio de Janeiro, Brazil

This work shows the use of ground penetration radar (GPR) for detection of superficial structures of degradation in mountain permafrost imaging in an area of the Central Andes. Andean permafrost can be classified on the basis of topography, hydrology (or estimated ice content), and climate (global warming) (Trombotto 2003). Continuous or quasi continuous Andean permafrost still appears at -2 to -4°C, found on the mountain summits or as "island permafrost" if it appears as an isolated body. Permafrost types could be also subclassified on the basis of more or less than 10% of ground ice content (Brown et al. 1998).

The study area was a permafrost plateau at Mesón San Juan (Fig. 1, 6012 m, 33°30′S and 69°49′W), located on the foot of the glacier and bordering recent moraines at a height of 4400 m a result of the glaciation retreat of the Mesón San Juan summit and the consequent cryoweathering and erosion of the sediments produced by cryogenic phenomena. The Cenozoic volcanic Mesón San Juan with 6012 m are located on the Argentinean-Chilean border, south of Tupungato volcano (6570 m) and Cerro Aconcagua (6962 m), the highest mountain of the Western Hemisphere, in the province Mendoza.

The permafrost plateau at Mesón San Juan is related to the highest parts of the mountain and represents a type of

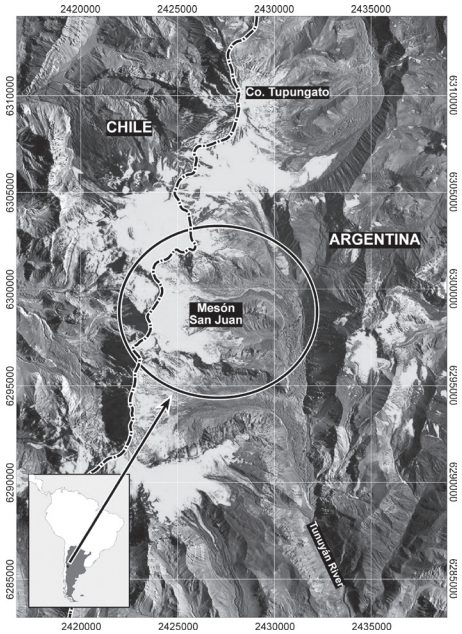

Figure 1. Study area.

cryoplanation surface of polygenetic origin on the foot of the glacier and bordering recent moraines at a height of 4400 m. It falls as glacier-shaped rocky slopes reaching down to 3600 m in the area. The plateau is a result of the glaciation retreat of the Mesón San Juan summit and the consequent cryoweathering and erosion of the sediments produced by cryogenic phenomena.

The GPR data were collected with PULSE EKKO IV equipment with a time window of 2048 ns, a sampling interval of 800 ps, a 1000 V transmitter, and 50 MHz antennae. The antennae were moved along fixed-offset profiles with a constant step size of 0.20 m and kept 2 m apart from each other. We kept the same step size for the central mid-point (CMP) profiles, where each antenna was moved away from another symmetrically in fixed steps of 0.10 m. We concentrate here on two profiles: one fixed-offset that is the result of merging two 51 m long profiles with directions 96º MN and 134º MN, the former along the largest dimension of the plateau; and two CMP profiles. The two mutually perpendicular CMP profiles were deployed crossing at the center point of the first fixed-offset profile. Each CMP profile was 31 m long, one of them having the same direction of the first fixed-offset profile. We also restricted the time-window to 1024 ns, where the signal-to-noise ratio is higher. We adopted a basic processing flux in our data set. After some editing, the time window was chopped off to earlier times, dewowed, low-pass filtered to reduce high-frequency noise, and gained with an automatic gain control.

The periglacial sedimentary cover on the plateau displays an open permeable structure. The thickness of the active layer and the depth to the permafrost table was obtained with 3 superficial holes reaching a depth of 1.20 m. One hole was drilled at the edge of the glaciation in an ice-covered area with transitional sediments from the SE wall of the glacier of the Mesón San Juan, thus correlating with the morainic area. Two holes were drilled further away on cryoplanation surfaces bordering the present glaciation and did not reach a permafrost table, but revealed the presence of a freezing level without any visible ice, which was interpreted as dry permafrost. Temperatures were obtained with Weston thermometers.

The CMP profiles yielded an average velocity of 0.09 m/ns, and a very interesting indication of lower velocity at two-way travel time ≥ 200 ns was discovered. There was a clear transition at 270 ns from a more conductive and inhomogeneous horizon to a less conductive, albeit still

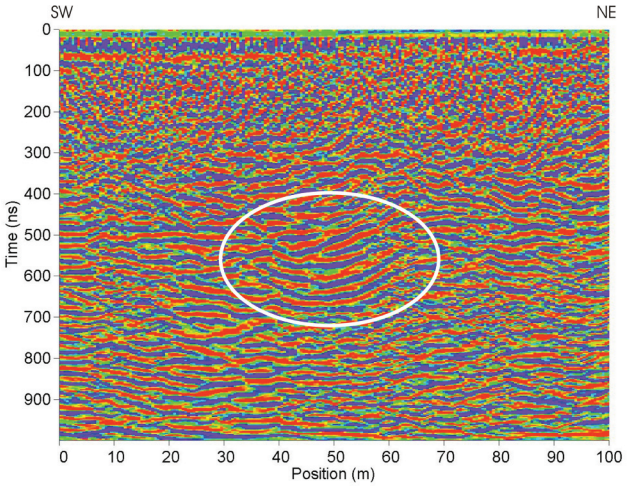

Figure 2. Migrated section with the I-zone.

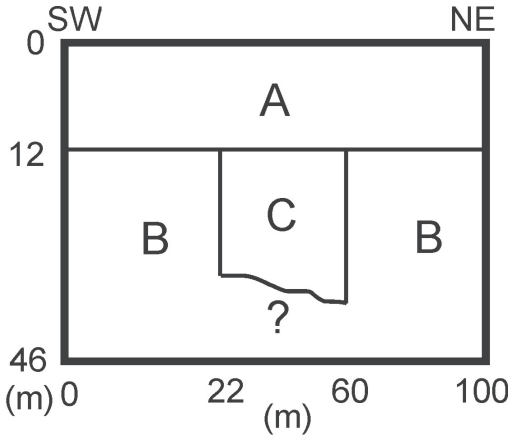

Figure 3. Interpretation of the subsoil at Mesón San Juan.

cluttered, subsurface. Another important characteristic of the section was relatively higher amplitudes seen at later times between 22 and 60 m of reflectors that do not display lateral continuity.

A migrated section, which has conspicuous smiles at later times inside a so-called vertical I-shaped zone located between 22 and 60 m, indicated a significantly smaller phase velocity within it (Fig. 2). The lower velocity I-zone is surrounded laterally by two zones of phase velocity, v = 0.09 m/ns. Moreover the tails of the diffractions in the I-zone indicate that the conductivity is lower compared to the remainder of the section. We found that the I-zone is correctly migrated only with very low velocities like the water velocity, v = 0.03 m/ns for migrating the section. We supposed by weight and low ion contents that it is a region of liquid water probably due to the degradation of permafrost. The I-zone is topped by a cluttered, more conductive horizon, reaching 270 ns or 12 m, that encompasses the active zone formed probably mainly by till and cryogenic sediments.

One explanation for the I-zone is that the segment is a discharge channel linking a suprapermafrost—a laterally discontinuous near-surface system not seen in this work—to a subpermafrost aquifer (Lawson et al. 1996). Most probably the source of that water is the retreating glacier above the plateau that finds its way through the morainic till, which composes the active layer. Figure 3 expresses the interpretation of the frozen and unfrozen subsoil. We expected to find the basement at 45–50 m, but that is beyond the limit of our data.

As already described for other areas (Trombotto et al. 1998), with gradual disappearance of snow patches, the retreat of the Andean glacier fronts generates a considerable input of melting water in the open structure of the Andean cryolithozone, which enhances erosion of suprapermafrost but also allows the water to penetrate through the discontinuities of the frozen soil, thus contributing to the degradation of its internal structure.

Acknowledgments

We would like to thank Dr. Alberto Aristarain (LEGAN) for his financial and logistical support, and José Hernández, José Corvalán, and Rafael Bottero for their technical support. JMT acknowledges a grant from the CNPq.

References

Brown, J., Ferrians Jr., O.J., Heginbottom, J.A. & Melnikov, E.S. 1998. *Cicum-Artic map of permafrost and ground-ice conditions.* U.S. Geological Survey.

Lawson, D.E., Strasser, J.C., Strasser, J.D., Arcone, S.A., Delaney, A.J. & Williams, C. 1996. *Geological and Geophysical Investigations of the Hydrogeology of Fort Wainwright, Alaska, Part I: Canol Road Area*. CRREL Report 96-4, 32.

Trombotto, D. 2003. Mapping of permafrost and the periglacial environment, Cordón del Plata, Argentina. *Proceedings of the Eighth International Conference on Permafrost, Zurich,* Extended Abstracts: Reporting Current Research and New Information, W. Haeberli & D. Brandová (eds.): 161-162.

Trombotto, D., Buk, E., Corvalán, J. & Hernández, J. 1998. Present state of measurements of cryogenic processes in the "Lagunita del Plata," Mendoza, Argentina, Report Nr. II. *Proceedings of the Seventh International Conference on Permafrost, Yellowknife, Canada*. Program, Abstracts, and IPA Reports, Extended Abstracts: 200-201.

Pleistocene and Holocene Periglacial Forms in the Cantabrian Mountains (Northwest Spain)

Dario Trombotto Liaudat
IANIGLA, CONICET, 5500 Mendoza, Argentina
V. Alonso
Departamento de Geología. Universidad de Oviedo. 33005, Oviedo, Spain

Detailed geomorphological mapping of a deglaciated area in the Cantabrian Mountains (CM) has revealed a great variety of periglacial forms that have been ascribed to different cryomeres during and following deglaciation.

The CM, with frequent altitudes around 2000 m, show erosional and depositional glacial features related to the Pleistocene last glacial cycle; distribution of till, erratic blocks and glacially abraded surfaces indicate ice thicknesses up to 400 m in some areas (Alonso & Suárez Rodríguez, 2004), while glacier fronts reached altitudes around 900 m a.s.l. in many of the valleys.

A geomorphological map, at a 1:5000 scale, was made for a sector to the south of the main watershed characterized by a homogeneous bedrock. The map has been analyzed in a regional context.

This zone around El Miro peak, 1985 m, shows a strong asymmetry in processes and forms. Most of them are fossil features. Rock glaciers (Fig. 1), felsenmeer, protalus, boulder lobes, solifluction forms, and talus deposits were developed, from glacially derived material or from cryosediment, on cold slopes.

Warm slopes, slighter or even nonglaciated, developed giant sorted stone stripes (Fig. 2), boulder lobes and stone-banked lobes from cryosediment.

In relation to deglaciation, gravitational slope readjustments took place in cirque zones and mixed landslides partially modified warm slopes; paraglacial alluvial fans were formed in adjacent valleys.

Deglaciation in this zone of the CM was dated to be before 34,000 ± 1400 ^{14}C yr BP in Laguna de Villaseca, at 1305 m a.s.l. (Jalut et al. 2004). But terminal moraine complexes at lower altitudes, formed when glaciers still were 11 km in length in areas with calculated previous ice thicknesses up to 260 m, suggest a long evolution between the beginning of deglaciation and stabilization phases during retreat. Other data worth mentioning (Pallàs et al. 2006) about the close region of the Pyrenees, where an early maximum glacier extent during the last glacial cycle is not excluded, indicate an extensive glaciation at ca. 18–20 ka (MIS 2), coinciding with the global LGM.

Altitude, aspect, preservation degree, and soil development of cryogenic forms around El Miro indicate more than one cryomere, although the lack of datable material has not allowed us to determine a precise time for these cryomeres. A tongue-shaped rock glacier in a cold and low position and giant sorted stripes on warm slopes, both proposed to be coeval with cirque glaciers, suggest continuous mountain permafrost in ice-free areas during deglaciation, when the most important indicators were cryogenic periglacial and not glacigenic. We propose that conditions during deglaciation were probably similar to those of the Pyrenees, where continuous permafrost and important cryogenic landforms with glacier ice at the same time are represented in the *Climex Map of 2002* for the Last Glacial Maximum.

The peak of the periglacial environment in the CM, however, must have occurred after the LGM, with predominantly much drier climatic conditions and benefitting from vaster areas uncovered by ice; discontinuous permafrost, expressed by rock glaciers during the Late Pleistocene or Early Holocene, is likely to have reached 1540 m a.s.l.

Figure 1. Fossil rock glacier.

Figure 2. Giant sorted stone stripes.

At higher altitudes, sparsely vegetated small forms with scarce or no development of soil—lobate rock glaciers, protalus, and boulder lobes—would correspond to more recent times; some of these landforms were probably active during the LIA. The rock glacier fronts end at approximately 1730 m a.s.l.

References

Alonso, V. & Suárez Rodríguez, A. 2004. Evidencias geomorfológicas de la existencia de un pequeño casquete glaciar en la Comarca de Babia Alta (Cordillera Cantábrica). *Revista de la Sociedad Geológica de España* 17: 61-70.

CLIMEX World Maps. 2002. Cartes des Envionnements du Monde pendant les deux derniers extremes climatiques. N. Petit-Maire, Ph. Bouysse (Scientific editors), CCGM, CGMW & ANDRA, France.

Jalut, G., Belet, J.M., García De Celis, A., Redondo Vega, J.M., Bonnet, L., Valero-Garcés, J.M., Moreno, A., Villar Pérez, L., Fontugne, M., Dedoubat, J.J., González-Sampériz, B.L., Santos Hidalgo, L. & Vidal Romaní, J.R. 2004. Reconstrucción paleoambiental de los últimos 35 000 años en el Noroeste de la Península Ibérica: La Laguna de Villaseca (León). *Geo-Temas* 6: 105-108.

Pallàs, R., Rodés, A., Braucher, R., Carcaillet, J., Ortuño, M., Bordonau, J., Bourlès, D., Vilaplana, J.M., Masana, E. & Santanach, P. 2006. Late Pleistocene and Holocene glaciation in the Pyrenees: a critical review and new evidence from ^{10}Be exposure ages, south-central Pyrenees. *Quaternary Science Reviews* 25: 2937-2963.

Permafrost Response to Dynamics of External Heat Exchange: Comparison of Observed and Modeled Data (Nadym-Pur-Taz Region)

Julia Ukhova
Institute of Environmental Geoscience, Russian Academy of Sciences, Moscow, Russia
Alexey Osokin
NadymGazProm, Nadym, Russia
Dmitry Sergeev
Institute of Environmental Geoscience, Russian Academy of Sciences, Moscow, Russia
Julia Stanilovskaya
Institute of Environmental Geoscience, Russian Academy of Sciences, Moscow, Russia

Introduction

The study of thermal state permafrost dynamics in connection with climate conditions has became topical in recent years.

Besides the air temperature, the amount of precipitation and the temperature of permafrost have increased in some areas since the 1960s (Israel et al. 2006, Pavlov et al. 2005). The problem of permafrost state forecast became significant for industrial companies. It requires the organizing of temperature permafrost monitoring. Most measured boreholes are located near industrial and civic constructions that disturb the ground temperature regime dynamics. It is difficult to consider the climatic role in permafrost temperature dynamics by using this data because the influence of construction and business activities is greatly powerful in local aspect. This problem impedes efficient permafrost forecasting because of the difficulty of model accuracy estimation.

Methods

The authors used mathematical modeling for the diagnosis of the man-caused disturbances factor that influences the permafrost temperature regime. We supposed that the codirectionality of modeled and observed temperature trends at low depths proves the weakness of anthropogenic influences in a short time period.

The forecast was done for the Nadym-Pyr-Taz region where climate warming is evident. The air temperatures have been increasing 0.05°C per year in the observed period 1960–1995. We modeled the ground temperature for a one-dimensional system, using the one-layer loamy silt configuration and observed mean monthly values of air temperature and snow cover depth (Fig. 1). We used the meteorological data from the Salekhard met-station, adding constant monthly average corrections in considering microclimatic features of the investigation site. Other climate characteristics were used as long-term average monthly values.

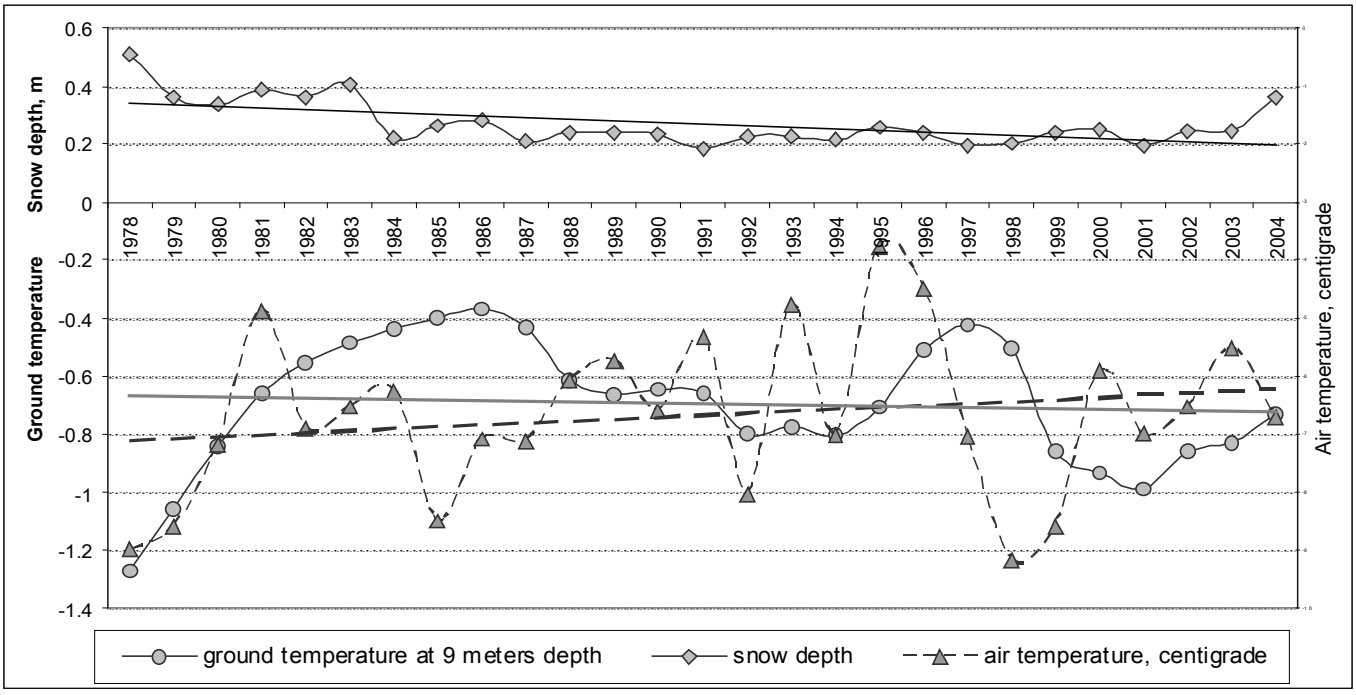

Figure 1. Long-term course of climate characteristics (air temperature and thickness of snow cover) and calculated ground temperature at 9 m depth.

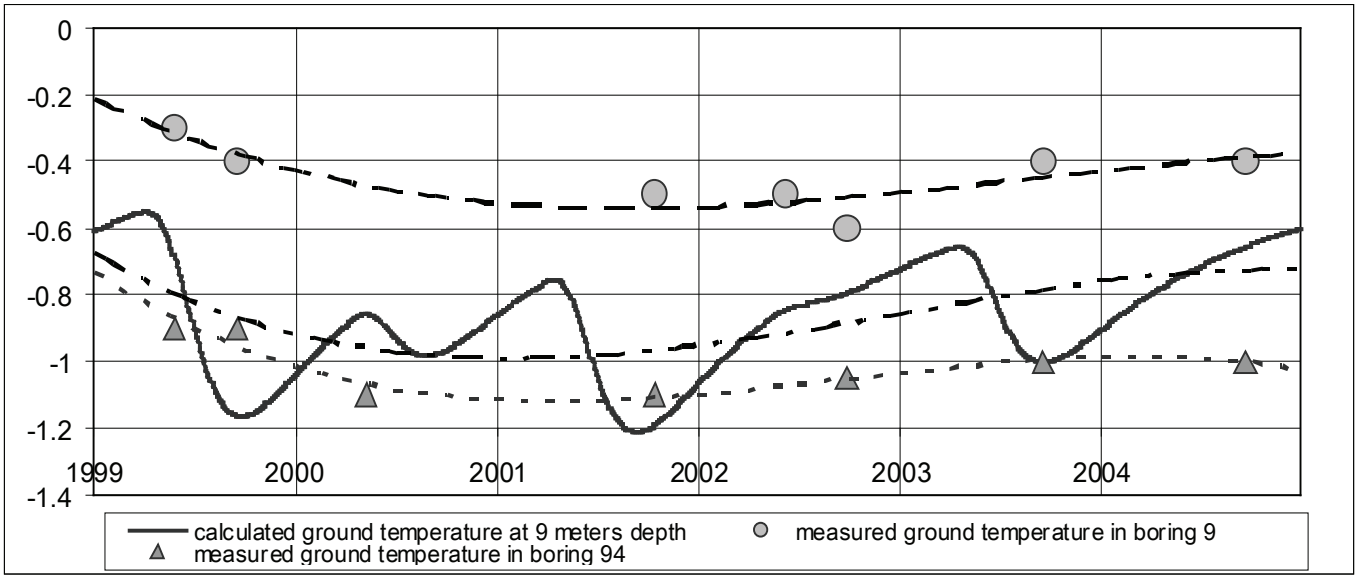

Figure 2. Comparison of measured and modeled ground temperature at 9 m depth.

The mathematical realization of the model was determined by G.S. Tipenko. The calculated values of ground temperature at 9 m depth was obtained and compared with the climate trend.

Results

The course of the modeled ground temperature is conformable to the measured temperature trend in boreholes #9 and #94.

We supposed that boreholes #9 and #94 are located in undisturbed conditions in the industrial area. The disagreement in the absolute value of the ground temperature in these boreholes is determined by the variability of snow cover. The data in detail of snow cover are not available; however, the interannual course of ground temperature at low depths is probably defined by climate dynamics, especially by the snow cover trend.

It is seen that the course of snow cover dynamics in long-range aspect has a stronger influence on ground temperature at low depth when compared with the course of air temperature.

To generalize, the framed and calibrated model of dynamic ground temperature allowed us to forecast the permafrost dynamics, depending not only on air temperature change but also on other factors of surface heat exchange. The model calibration criterion was the agreement fact of the trends rather than the desired accuracy of model parameter. Comparing the model of boreholes in undisturbed and disturbed conditions, the influence of technogenesis cannot be allowed. Thus, the data of climate contribution in the dynamics of permafrost temperature can be obtained. The boreholes that have the different tendency are strongly influenced by building and other man-caused factors.

References

Israel, J.A., Pavlov, A.V., Anokhin, J.A., Myach, L.T. & Chertyukov, B.G. 2006. Statistical estimation of climate components change in permafrost area in Russia. *Meteorology and Hydrology* 5: 27-38 (in Russian).

Pavlov, A.V. 2002. Century anomalies of the air temperature on the Russian North. *Earth Cryosphere* 6(2): 75–81 (in Russian).

Pavlov, A.V. & Malkova, G.V. 2005. *Actual Climate Change on the Russian North: Album of Low-Scale Maps*. Novosibirsk: GEO, 54 (in Russian).

Application of DC Resistivity Tomography in the Alpine Area of the Southern Carpathians (Romania)

Petru Urdea, Florina Ardelean, Alexandru Onaca, Mircea Ardelean, Marcel Török-Oance
West University of Timişoara, Department of Geography, B-dul. V. Parvan, Nr. 4, 300223, Timişoara, Romania

Introduction

During the last decade, the use of geophysical techniques has become increasingly important in geomorphological study and for many geomorphologists, new and exciting tools (Schrott & Sass 2008).

The acquisition of a complex geophysical system, PASI 16GS24, opens new possibilities for performance investigations of some landforms and deposits of the alpine area of the Southern Carpathians—for first time in Romanian geomorphology—and, accordingly, the aim of this paper is to present some results of the application of DC resistivity tomography in alpine area of the Southern Carpathians (Romania). By application of geophysical techniques on different geomorphic deposits, we have the possibility to gain insight into their overall thickness and inner structures, as well as the aspect of the contact surfaces with bedrock (Milmson 1996).

Study area

The Southern Carpathians, or Transylvanian Alps, are the most massive and the highest part of the Romanian Carpathians, having 11 peaks above 2500 m and a maximum elevation of 2544 m in Moldoveanu Peak (Făgăraş Mountains). In the high area of the Southern Carpathians, the geomorphological landscape is dominated by glacial landforms, the detailed characteristics being due to periglacial forms, like rock glaciers, talus cones, and scree slopes, block fields, rock streams, cryoplanation terraces, patterned ground, solifluction forms, etc. (Urdea et al. 2004).

Geophysical investigations were carried out in numerous study areas of the Southern Carpathians in the Făgăraş, Retezat, and Şureanu Mountains (Fig. 1), representative units for the main geomorphological landscapes of Romanian Carpathians. Our investigation focused on rock glaciers, scree slope deposits, late glacial stadial moraines, post-glacial in-filled glacial depressions, solifluction lobes, and fossil patterned grounds (Table 1).

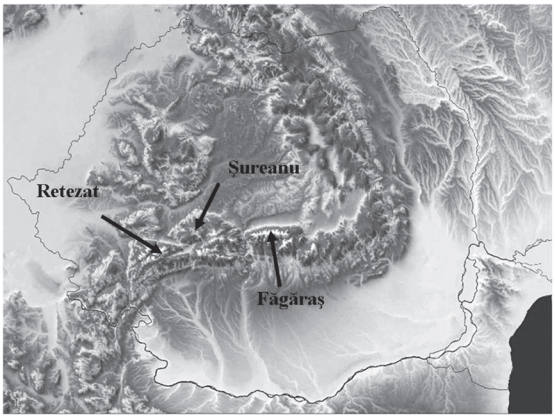

Figure 1. Location of the investigated areas.

Methodology

The PASI system consisted of 32 electrodes with a standard spacing of 5 m. In function of deposits and landforms dipole-dipole, Wenner and Wenner-Schlumberger arrays was used, with a maximum penetration depth of 30 m. The longitudinal profiles were carried, and for rock glaciers were carried also longitudinal and transversal profiles. Due

Table 1. Location of DC resisitivity investigations.

Area & date	Altitude (m)	Latitude Longitude
Scree slopes		
Bâlea Lake (Făgăraş Mts.) 03.07.2007	2088	45°36′06″ N 24°37′10″ E
Văiuga (Făgăraş Mts.) 11.09.2007	2270	45°35′17″ N 24°37′22″ E
Stadial moraines		
Doamnei Valley (Făgăraş Mts.) 04.07.2007	1903	45°36′19″ N 24°35′51″ E
Rock glaciers		
Ana (Retezat Mts.) 22.08.2007	1989	45°21′13″ N 22°52′04″ E
Pietrele (Retezat Mts.) 23.08.2007	2043	45°22′13″ N 22°52′16″ E
Capra (Făgăraş Mts.) 10.09.2007	1928	45°35′20″ N 24°37′19″ E
Postglacial in-filled glacial depression		
Valea Doamnei (Făgăraş Mts.) 04.07.2007	1879 m	45°36′21″ N 24°35′49″ E
Căldarea Berbecilor (Făgăraş Mts. 03.07.2007	1907	45°36′33″ N 24°37′07″ E
Şureanu (Şureanu Mts.) 26.08.2007	1769	45°34′51″ N 23°30′33″ E
Solifluction lobes		
Paltinu (Făgăraş Mts.) 06.07.2007	2372	45°35′52″ N 24°36′25″ E
Patterned grounds (fossil)		
Paltinu – Piscu Negru (Făgăraş Mts.) 06.07.2007	2338	45°35′48″ N 24°36′26″ E

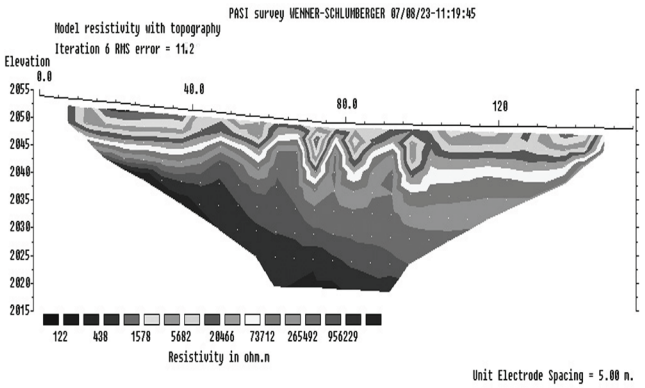

Figure 2. 2-D resistivity longitudinal section at Pietrele rock glaciers.

to the special characteristics, in the case of solifluction lobe and fossil patterned ground, the electrodes were arranged in a different configuration, on equal distance of 1 m, which permits a differentiation of distinct layers of 40–50 cm. Two-dimensional model interpretation was undertaken using the software package RES2DINV (Loke 1999). This software package produces a two-dimensional subsurface model from the apparent resistivity pseudosection.

Results and Interpretation

Application of 2-D electrical resistivity tomography began with measurements in Făgăraş, Retezat, and Şureanu Mountains on different geomorphic landforms, such as rock glaciers, scree slopes, solifluction lobes, fossil patterned ground, and glacial overdeepening depression filled with postglacial sediments. In all cases the results show varying resistivity. Starting with this design, we can know and interpret the structure of different deposits and, importantly, the depth and configuration of the surface contact with bedrock. In the case of scree deposits is the evidence of the presence of quasi-layered structure and some different bodies of rock blocks and/or fines—made by downwash and debris flow processes—with contrasting resistivity (more than 10 kΩ/m and, respectively, less than 2 kΩ/m). For fossil-patterned grounds are revealed undulating layers and elipsoidal bodies of fines, more humid and with low resistivity (500–800 Ω/m). In the case of Ana and Pietrele rock glaciers, electrical tomography reveals typical structures, and, important for permafrost scientists, the presence of ice-rich bodies in the Ana rock glaciers or ice-rich layer on Pietrele rock glaciers, revealed by high resistivities, on the order of more than 900 k Ω/m (Fig. 2).

We must mention that the presence of permafrost in the reported area was indicated by BTS measurements and by the low temperatures (<2°C) of the spring situated on the base of the front of rock glaciers Pietrele (Urdea 1993).

Acknowledgments

The authors are grateful to numerous students from West University of Timişoara for their committed help in carrying and installing the heavy equipment in the field. Financial expenses was supported by National Council for University Research (grant CEEX 738/2006).

References

Farbrot, H., Isaksen, K., Eiken, T., Kääb, A. & Sollid, J. 2005. Composition and internal structures of a rock glacier on the strandflat of western Spitsbergen, Svalbard. *Norwegian Journal of Geography* 59: 139-148.

Loke, M.H. 1999. Electrical imaging suurvey for environ-*mental and engineering studies – a practical guide to 2-D and 3-D surveys*. Copyright by M.H. Loke, Penang, Malaysia.

Milmson, J. 1996. *Field Geophysics*. Chichester: Wiley, 187 pp.

Sass, O. 2006. Determination of the internal structure of alpine talus deposits using different geophysical methods (Lechtaler Alps, Austria). *Geomorphology* 80: 45-58.

Schrott, L., Sass, O. 2007. Application of field geophysics in geomorphology: Advances and limitations exemplified by case studies. *Geomorphology* 93: 55-73.

Urdea, P. 1993. Permafrost and periglacial forms in the Romanian Carpathians. *Proceedings of the Sixth International Conference on Permafrost.* South China University of Technology Press, I: 631-637.

Urdea, P., Vuia, F., Ardelean, M., Voiculescu, M. & Török-Oance, M. 2004. Investigations of some present-day geomorphological processes in the alpine area of the Southern Carpathians (Transylvanian Alps). *Geomorphologia Slovaca* 4(1): 5-11.

Repeated Mapping of the Northern Taiga Ecosystems in West Siberia, Disturbed by Pipeline Construction

E.V. Ustinova
Earth Cryosphere Institute, Tyumen, Russia

Engineering construction in the north of West Siberia leads to disturbances of vegetation cover and changing permafrost conditions. The scale of changes is in direct relation to the degree of human-induced disturbance and landscape properties. Many natural features can be lost under increasing anthropogenic pressure; therefore, solving the problem of rational land usage and wildlife management becomes extremely difficult. The information presented here results from ecosystem monitoring.

Monitoring of disturbed ecosystems has been carried out for 35 years along a gas pipeline located in the subzone of northern taiga at the Nadym field station. Terrain changes are studied every 3–5 years by large-scale repeated mapping of the territory, using contemporary air photos and fieldwork. The last analyses were made in 2006. The greatest environmental disturbances occurred during pipeline construction in 1971–1972 and pipeline replacement in 2004. Smaller changes took place in 1974 in relation to electrical line construction, and in 1983, in adding new fill to the embankment. The service road along the pipeline is reconstructed every year.

Disturbance of natural conditions triggered activation of thermokarst and frost heave. Bog formation in areas ponded by embankments and wind erosion of sand on dry sites also take place. Observations show that in disturbed areas the occurrence of lakes has increased 22%.

The landscape hierarchy was described according to Melnikov (1983) using information on permafrost distribution, topography, and vegetation. A series of digital maps shows natural terrain units (ecosytems) as well as terrain units affected by construction over the time period from 1970 to 2006. These maps are based on air photography of different years and on field surveys. The location of monitoring sites, temperature boreholes, and features related to cryogenic processes are shown as well. The database of boreholes is linked to the maps.

The analysis of the maps compiled for different years revealed changes in the area of human-induced disturbances and trends in ecosystem development under the impact of climatic changes and disturbances (Fig. 1). After construction, the width of the disturbance zone increased differently in the various terrains. The increase in boggy areas due to swamping of the forest ecosystems was determined by comparing the maps of 1970 with those of 1988 (Fig. 1).

During 2004 pipeline reconstruction, pipes were replaced. The histogram (Fig. 2) is based on comparison of the terrain map of 1970, which was prepared prior to construction of a gas pipeline, and the map of 2005. Figure 2 shows that human-induced disturbance has caused an increase of 2.9%

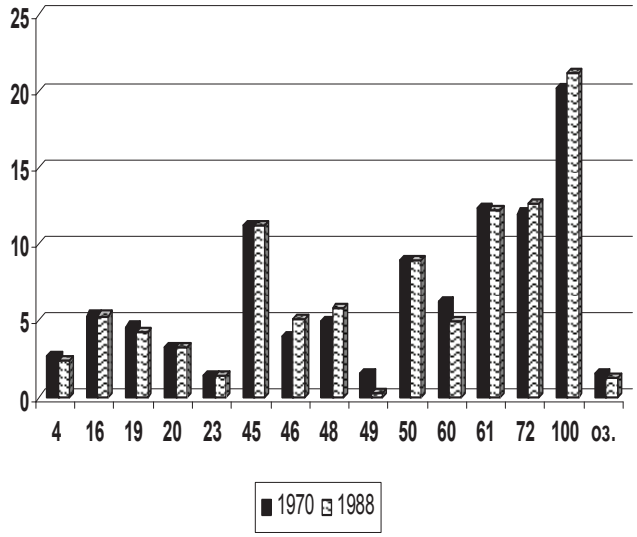

Figure1: Frequency of ecosystems at the Nadym site in 1970 and 1988 years.
4 - dry gentle slopes with birch-pine-cowberry-lichen sparse forests; 16 - flat slightly drained sites with birch-pine-wild rosemary-lichen–moss sparse forests; 19 - flat boggy sites with larch-wild rosemary-moss open forests; 20 - flat boggy sites with hummocky larch-wild rosemary-lichen-moss open forests; 23 - peat-mineral frost mounds with sedge-shrub lichen-moss open larch-pine woodland; 45 - hollows with sedge-moss mires; 46 - hollows and flat sites with tussocky sedge-moss mires; 48 - flat sites with hummocky sedge-peat moss bogs; 49 - flat sites with dwarf shrub-sedge-peat moss bogs; 50 - hollows occupied bogs with dwarf shrub-sedge-peat moss ridges and sedge-moss pools; 60 - flat sites with cloudberry-wild rosemary-moss- peatlands, 61 - flat sites with cloudberry-wild rosemary-moss-lichen peatlands; 72 - palsa peatland with sedge-shrub-moss-lichen cover on palsa and sedge-peat moss on pools between palsa; 100 - flat sites with hummocky tundras with sedge-shrub-moss-lichen cover on hummocks and sedge-peat moss on pools and rare frost boils; 03 - lakes.

in the area of hummocky sites (ecosystem 100), 1.8% in the areas of bogs (ecosystems 45, 46, 48), and 1.5% in the area of palsa peatland (ecosystem 72). Some flat areas (ecosystems 60 and 61) have partly recovered, however, and disturbance decreased by 2.8%.

Most disturbance relates to the removal of vegetation, modification of a microrelief, removal of 10 to 20 cm of peat during clearing of the right-of-way, and partial destruction of vegetation as a result of road transportation. The smaller areas occupy the sites disturbed as a result of caterpillar transport travel, where vegetation, soil cover, and microrelief have been broken only in part. The areas occupied by sites

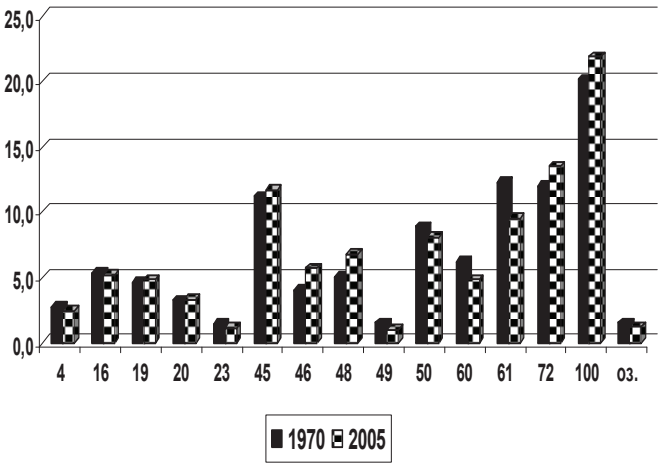

Figure 2. Frequency of ecosystems at the Nadym site in the years 1970–2005.

which have undergone other kinds of disturbance (burial and destruction of vegetative cover as a result of formation leading the removed vegetation), do not exceed 15%.

More often because of various human-induced loadings and various degrees of stability of covers, mosaic groupings are formed, including simultaneously 3–4 types of disturbance. Most all disturbance of all types was in 2004, during reconstruction of a gas pipeline.

Construction of service roads led to sufficient change in the regime of surface water and swamping of the surrounding territory and appearance of new lakes. With time, areas of lakes decrease as a result of swamping. Small frost mounds and palsas up to 1 m in height appeared in the surrounding areas.

Vegetation recovery is on sandy, well-drained sites. Natural recovery on the wet clayey soils is much faster. The highest rate of recovery of the disturbed vegetation takes place on boggy sites, where almost continuous vegetation cover was observed 3–4 years after disturbance. Lack of moisture on well-drained sites is one of the major factors that slow down vegetation recovery.

The degree of ecosystem resistance to recovery can be used for classification and mapping of geoecological hazards. Maps can be used for planning purposes. Maps of ecosystem conditions prepared for different years are a good tool for studying changes in ecosystems; for example, to find the occurrence of new frost mounds on bogs.

Repeated landscape mapping enables us to locate a zone of natural ecosystem disturbance and to trace its changes at the time of observation. Compiled landscape maps can form a basis for geoecological maps and for forecast maps of ecosystems impacted by pipelines and roads construction.

References

Mann, R.E. 1973. *Global Environmental Monitoring System (GEMS). Action Plan for Phase 1.* SCOPE, rep. 3. Toronto, 130 pp.

Melnikov E.S. (ed.) 1983. *Terrain Units of Permafrost Zone of the West Siberian Gas Province*. Novosibirsk: Nauka, 165 pp.

Moskalenko N.G. (ed.) 2006. *Anthropogenic Changes of Ecosystems in West Siberian Gas Province.* M., RASHN, 358 pp.

Forcing Factors of Permafrost Retreat: A Comparison Between LGM and Present-Day Permafrost Extent in Eurasia

Jef Vandenberghe
Institute of Earth Sciences, VU University Amsterdam, The Netherlands
Andrei Velichko
Laboratory of Evolutionary Geography, RAS, Moscow, Russia
Aldar Gorbunov
Permafrost Institute, SD RAS, Almaty, Kazakhstan

In recent years, it has been shown that growth and especially decay of permafrost may have tremendous effects on the environmental conditions of the concerned region. Attributing the cause for changes in permafrost occurrence only to global temperature changes is apparently too simple. There are a number of feedback mechanisms that potentially may induce regional differences in permafrost extension or reduction. In this short note, we expand on the factors that have contributed to the northward displacement of the southern permafrost limit on the Eurasian continent since the last glacial maximum (LGM) and which role potentially may be enhanced in the near future.

For that purpose we have constructed the southernmost extent of the permafrost during the LGM by combining different sources of research, and compared that with the present-day permafrost extent. Mapping the southern limit of permafrost is not as simple as it may look because of several reasons:

- LGM permafrost maps are not always distinctive in describing whether the permafrost is continuous, discontinuous, or sporadic.
- Even when this distinction is made, the definitions of those terms are not always the same in the different papers.
- The age of permafrost indicators of the LGM has often not precisely been defined.
- The altitude plays a decisive role in permafrost distribution, and the distinction between latitudinal and mountainous permafrost may be diffusive (French 1996).
- High altitudes may shift the latitudinal permafrost limit substantially southward.

With these restrictions in mind we (re)constructed for both periods the location of the position of the southern limit of permafrost (including sporadic, island, and discontinuous permafrost) and that of continuous permafrost (Fig. 1).

For the present-day situation, we based us essentially on the Arctic Permafrost Map as compiled by Brown et al. (1998). In the zone of continuous permafrost, regions with mountainous permafrost are included (e.g., in the Ural Mountains and especially in eastern Siberia). The LGM reconstruction is more complicated. For western and central Europe, we used data published by Van Vliet (1996), Renssen & Vandenberghe (2003), Vandenberghe et

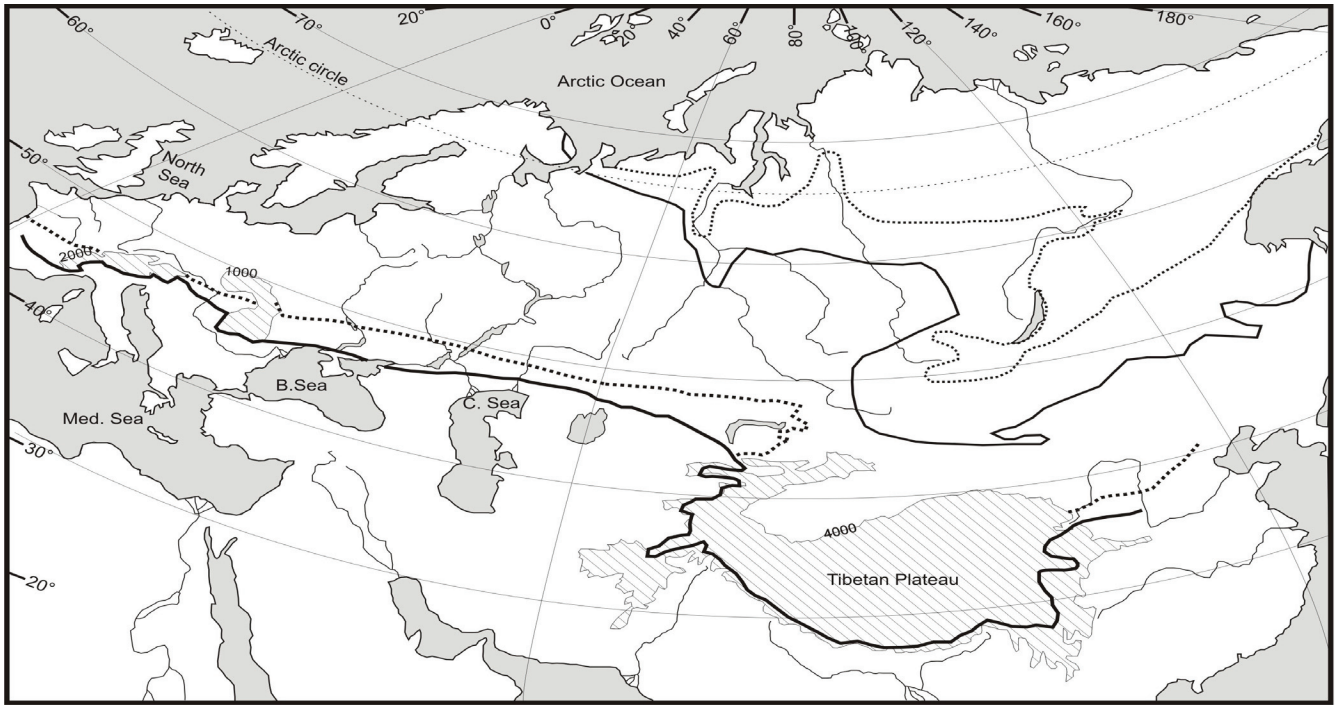

Figure 1. Southern limits of modern permafrost (upper full line) and continuous permafrost (upper stippled line), and LGM permafrost (lower full line) and continuous permafrost (lower stippled line), largely based on Aubekerov & Gorbunov (1999), Vandenberghe et al. (2004a,b) and Velichko (2002).

al. (2004b); for Russia, maps provided by Velichko (2002); for Kazakhstan, a map by Aubekerov & Gorbunov (1999); and for China, data compiled from different sources (e.g., Vandenberghe et al. 2004a). Especially in regions where the boundary between discontinuous and continuous permafrost is crossing mountainous areas, the zone of discontinuous and sporadic permafrost may be very limited in extent and, as such, not exactly defined in the published literature. For the LGM situation, this is the case, for instance, in the southern Central Massif (France), the southern Carpathians, and the southern margin of the Tibetan Plateau.

A few striking results appear from the comparison between LGM and present-day permafrost extension limits. We derive a general, extremely constant west–east orientation of the permafrost boundary during the LGM at around 52°N latitude in lowlands, apart from minor expulsions to the south in upland regions (e.g., Central Massif, Carpathians) and a major southward expulsion due to the mountain permafrost of the Tibetan Plateau. This is in line with the zonal extension of permafrost reported by Huijzer and Vandenberghe (1998) for west and central Europe and by Velichko (1973) for southern Russia. It may be explained by the combined cold sources of sea ice and ice sheets in the North Atlantic Ocean, Arctic Sea, northern Europe, and Siberia. Tracks of westerly winds were shifted towards the south and, in any case, were not able to induce maritime influences on the continent at the latitude of permafrost occurrence (Isarin & Renssen 1999, Renssen & Vandenberghe 2003).

The present-day situation shows a distribution pattern that significantly differs from the LGM pattern. The southern limit of permafrost shows a clear shift to the south from c. 69°N latitude south of Nova Zembla to 66° in west Siberia and 61° in east Siberia (around the Lena River). The latitudinal permafrost occurrence in easternmost Siberia is difficult to determine because of the interference with altitudinal permafrost. This Eurasian permafrost extension is obviously directed by the cold Arctic Sea, while there is no steering at all by North Atlantic sea ice. Maritime influences, through westerlies that transport temperate air from the North Atlantic waters, are diminishing towards the east. On the contrary, warm equatorial waters are entering the North Atlantic Ocean at present by the Gulf Stream.

Thus, both the temperatures over the North Atlantic and the Arctic Sea determine the extent of permafrost over Eurasia. During the LGM the cold (frozen) North Atlantic Ocean and Arctic Sea induced the regular zonal pattern with overall west–east oriented permafrost limit. By now the North Atlantic Ocean change to warmer conditions induced a northward shift of the permafrost limit over Europe, which is gradually disappearing eastward over Siberia.

References

Aubekerov, B. & Gorbunov, A. 1999. Quaternary permafrost and mountain glaciation in Kazakhstan. *Permafrost and Periglacial Processes* 10: 65-80.

Brown, J., Ferrians, O.J., Jr., Heginbottom, J.A. & Melnikov. E.S. 1998. Revised February 2001. *Circum-Arctic Map of Permafrost and Ground-Ice Conditions*. Boulder, CO: National Snow and Ice Data Center/ World Data Center for Glaciology. Digital Media.

French, H.M. 1996. *The Periglacial Environment,* 2nd ed.), Edinburgh Gate: Addison Wesley Longman.

Huijzer, A.S. & Vandenberghe, J. 1998. Climatic reconstruction of the Weichselian Pleniglacial in north-western and central Europe. *Journal of Quaternary Science* 13: 391-417.

Isarin, R.F.B. & Renssen, H. 1999. Reconstructing and modelling Late Weichselian climates: the Younger Dryas in Europe as a case study. *Earth Sci. Rev*. 48: 1-38.

Renssen, H. & Vandenberghe, J. 2003. Investigation of the relationship between permafrost distribution in NW Europe and extensive winter sea-ice cover in the North Atlantic Ocean during the cold phases of the Last Glaciation. *Quaternary Science Reviews* 22: 209-223.

Vandenberghe, J., Cui, Z.J., Zhao, L. & Zhang W. 2004a. Thermal contraction crack networks as evidence for Late-Pleistocene permafrost in Inner Mongolia. *Permafrost and Periglacial Processes* 15: 21-29.

Vandenberghe, J., Lowe, J., Coope, G.R., Litt, T. & Zöller, L. 2004b. Climatic and environmental variability in the Mid-Latitude Europe sector during the last interglacial-glacial cycle. In: R. Battarbee, F. Gasse, & C. Stickley (eds.), *Past Climate Variability through Europe and Africa: PEPIII Conference Proceedings.* Dordrecht: Kluwer, 393-416.

Van Vliet-Lanoë, B. 1996. Relations entre la contraction thermique des sols en Europe du Nord-Ouest et la dynamique de l'ínlandsis Weichsélien. *Comptes Rendus Académie des Sciences de Paris* 322, série IIa: 461-468.

Velichko, A.A. 1973. Paragenesis of a cryogenic (periglacial) zone. *Biuletyn Peryglacjalny* 7: 89-110.

Velichko, A.A. 2002. *Dynamics of terrestrial landscape components and inner marine basins of Northern Eurasia during the last 130,000 years*. A.A. Velichko (ed.-in-chief). Moscow: GEOS Publishing House, 231 pp. (in Russian).

Application of Georadar in the Cryosphere for the Study of Engineering Constructions

Sergey Velikin
Viluy Permafrost Station of the Permafrost Institute, RAS Siberian Branch, Chernishevskii
Rudolf Czhan
Permafrost Institute, RAS Siberian Branch, Yakutsk

The ground-penetrating radar (GPR) method is very useful for the study and monitoring of different engineering constructions foundation beds. The advantages of GPR are mobility, compactness, and possibility of continuous observation. The results of a GPR survey with different day surface preparations—cleaning, surfacing, wettings—are presented. Seasonal peculiarities of the state of ground sections were also taken into consideration for GPR data interpretation. This approach, in some cases, improves the effectiveness of GPR surveys performed in Western Yakutia.

The effectiveness of the GPR method for the study and diagnosis of engineering constructions foundation beds can be improved as a result of special day surface preparation (cleaning**,** surfacing**,** and wetting) before survey. The other factor of GPR data improvement is seasonal observations (Judge at al. 1991). A priori information about lithology of sections, changes of temperature condition in basement soils, and temperatures of the beginning of thawing-freezing gives a key to the effective use of GPR technologies for the study and control of engineering constructions, buildings, and road coverings. Use of georadar sections difference observable in winter and summer time, before and after precipitations, that is, in various temperature-moisture conditions, is very informative (Velikin at al. 2000).

Figure 1 shows the result of a GPR survey along a road with a concrete covering. Measurements were carried out with the same equipment at a present small air-gap (4 cm) between the bottom of the antenna and road (measurements on a support with wheels) and without it (shooting without a support). As shown in Figure 1, in the case of measurements, an antenna radarogramma raised above the road is considerably noisy in comparison with the results of observation without a support that complicates section study.

After clearing road dirt from along the top of Sitikan reservoir dam, GPR data revealed rather detailed elements of the dam structure. Knowledge of the positions of the revealed elements allows supervision of the state of Sitikan dam while conducting building actions (strengthening of a road cloth, cementation of embanked sections weakened during object exploitation). Figure 2 shows the result on GPR data quality of cleaning the Sitikan reservoir ice sheet. After cleaning, the noise level becomes much lower. These data were used for proper determination of the thickness of the underwater part of bank slope anti-seepage filling.

It is important to note that cleaning and smoothing of sounding surfaces sharply improves radarogramm quality due to reduction of the influence of microrelief and a non-uniform covering of study sites with dirt and sleet, which can considerably deform and attenuate signals.

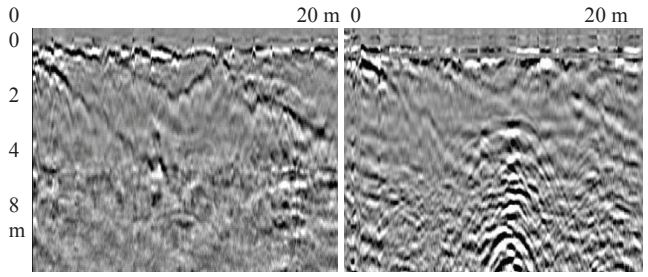

a) b) noise from air electric main

Figure 1. An example of a small air stratum effect (4 cm) between the bottom of antenna (facility SIR2000 antenna FGMOD5106, f = 200 MHz) and probing surface (concrete-surfaced road on frozen foundation): a) georadarogramm with antenna without air-gap (no support); b) georadarogramm with uplifted antenna (4 cm air-gap due to support on wheels).

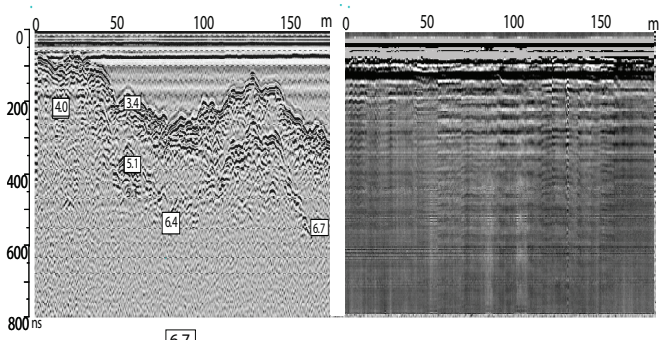

6.7 Depth of reflectors in meters

Figure 2. Georadar observation from the ice sheet of Sitikan reservoir (bottom sediments study). On the left: GPR observation after ice cleaning from sleet mixed with road dust.

Figure 3 presents GPR mapping of the productive horizon basement and reveals details of its structure. This becomes possible only after removal of the soil-vegetative layer, which was a strong screen because of high humidity and presence of a clay sheet.

Among other measures on preparation of probing surfaces, it is necessary to note filling with a fine-grained material and smoothing of a surface of studied structures. In particular at one of the dams in western Yakutia, it revealed with high resolution a weakened zone and a filtration window in the body of the dam (Fig. 4).

During a georadar survey, good effect gives the use of seasonal and weather factors; that is, sounding in freezing and thawing conditions of investigated sections, before and after surface wetting by rainfall.

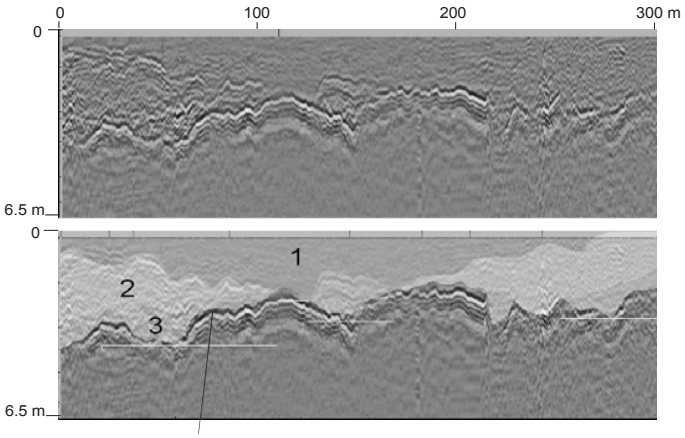

Figure 3. Georadar plot of diamond alluvial deposit from diamond-field in Western Yakutia: a) radarogramm after preliminary processing; b) radarogramm with picked geoelectric horizons corresponding to different soils of terrace sediments.

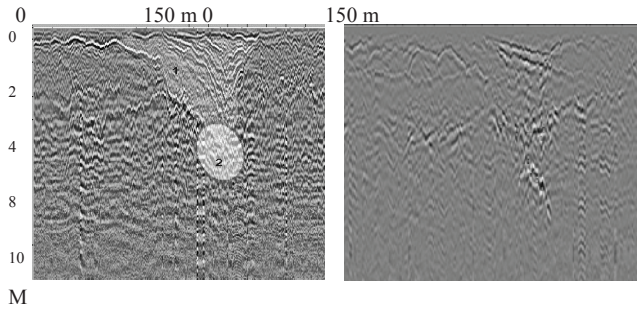

Figure 4. Radarogramm along coping of settling pound. Detecting seepage zone in the body of dam. 1: outline of deconsolidation sink; 2: seepage zone. On the right, road-covered wet mud with broken stone. On the left, road after preparation.

In December 2005 and February 2006, GPR seasonal surveys were performed on a diamond alluvial deposit during winter frost penetration time. It appeared that, in December, the maximum frost penetration and summer maximum thaw depth rather precisely marked out, which has proved to be true by temperature observations. Further in January–February, during further freezing of a section, lithological borders, including the roof and bottom of the productive horizon, distinctly stand out on the radarogramm, which proves to be true by the geological data on cores and description of a prospecting shaft. During processing, the account of a relief of a daytime surface has been carried out, and it has revealed confidently the bottom of the productive horizon, to define its depth and thickness for the moment of the beginning dragging works. Consequently, it was possible to predict the state of soils developed section (time of thawing of productive horizon after filling dragging a foundation trench).

Conclusion

The results presented in our work show that during georadar survey, application of different types of preparation of studied surfaces (cleaning, filling, smoothing, wetting, etc.), as well as using and accounting seasonal- climatic and weather factors, allows productivity increase of GPR survey in many cases.

In spite of that, in a basis of georadar survey is difference of rocks and soils in dielectric permittivity and electro conductivity, the basic character of georadar sections lays, as a rule, reflects mainly lithological boundaries (Finkelshtein et al. 1977, Vladov & Starovoitov 2005). Boundaries associated with the geocryological state frequently have a secondary character and come to light on a radarogramm less precisely. In many cases, basic elements of geocryological structure come to light more brightly during the periods which are not corresponding seasonal geocryological state. In particular, it concerns the boundary of maximal seasonal thawing during intensive freezing.

References

Finkelshtein, M.I., Mendelson, V.L. & Kuteev, V.A. 1977. *Radar-Location of Layered Terrestrial Covers*. Moscow: Soviet Radio, 176 pp. (in Russian).

Judge, A.S., Tucker, C.M., Pilon, J.A. & Moorman, B.J. 1991. Remote Sensing of Permafrost by Ground-Penetrating Radar at Two Airports in Arctic Canada. *Arctic* 44 Supp. 1: 4-48.

Velikin, S.A., Vladov, M.M. & Makcheeva, I.V. 2000. Application georadiolocation method for the study of hydro units in permafrost conditions. In: *Georadar in Russia-2000*. Moscow, MGU: 36-38.

Vladov, M.M. & Starovoitov, A.V. 2005. Introduction to georadiolocation. Moscow: MGU, 165 pp. (in Russian).

A Role of Description of Thaw/Freeze Processes in the Permafrost Zone for Quantifying Fire Weather

Sergey Venevsky
School of Geography, University of Leeds, Leeds, UK
Met Office – Hadley Centre for Climate Prediction and Research, Exeter, UK
Alexey Rubtsov
School of Geography, University of Leeds, Leeds, UK

Introduction

Wild fires happen frequently over northeastern Eurasia. The occurrence of these fires can be monitored from satellite data and shows a large seasonal cycle, together with a strong interannual variation. Several indices are available in the literature and aim at a quantification of fire risk based on various meteorological and soil moisture parameters. In this paper, we evaluate the ability of three such indices at quantifying the occurrence of fires over large areas of Siberia (60°E–140°E, 48°N–72°N). We compare the ability of Reg-FIRM fire weather danger index (Venevsky et.al. 2002) at quantifying the occurrence of fires over large areas of Siberia (60°E–140°E, 48°N–72°N) and estimate a role of thaw-freeze processes for correct description of fires with this index.

Methods

The Reg-FIRM fire danger model was developed by Venevsky et al. (2002) for introducing fire processes in the LPJ and SEVER dynamic global vegetation models (Sitch et al. 2003, Venevsky & Maksyutov 2007). This index is evolved from the Nesterov index, according to Equation (3). The increase in fire risk caused by drier fuel loads is explicitly accounted for in the Reg-FIRM WFDI by an exponentially decreasing function of the soil moisture, *S*. The driving input variables of the Reg-FIRM WFDI are the maximum and minimum daily air temperature ($T_{air}^{\max}$ and $T_{air}^{\min}$ in °C) and the daily soil moisture *S* in the upper soil layer, expressed in relative volumetric units.

We used as input the weather parameters from the ECMWF operational data and the GLC-2000 vegetation classification. We compare these indices to the number of fires detected by the MODIS spaceborne instrument at 8-day time scales over a 4.5-year period.

The Reg-FIRM WFDI would be unrealistic over Siberia, in particular during the spring season, without distinguishing between the liquid and the frozen components of the soil moisture *S*. We replaced *S* in Equation (4) by the liquid fraction of soil moisture S_{liq} , defined by $S_{liq} = (1-\alpha) \times S$, where α is the frozen fraction of soil moisture diagnosed each month from a global run of the HadGEM1 Atmospheric General Circulation Model of the Hadley Center

The frozen fraction of soil moisture, used in the Reg-FIRM WFDI was diagnosed from the output of the HadGEM1 general circulation model (Johns et al. 2006) with a monthly time step. However, the HadGEM1 has a "warm bias" 2°–7°C in the Siberian region so that the predicted thaw is too early by 2–10 days compared to the observed values (Legates & Willmot 1990). This warm bias depends upon latitude, and it is caused by an underestimate of the low cloud fraction, which results in an overestimate of the downward short-wave radiation at the surface. A rough-and-ready correction of the thaw date is given by:

$$d_{mid-month}^{corr} = d_{mid-month}^{old} - (l - 62) \quad (1)$$

where $d_{mid-month}^{old}$ is a mid-month thawing date in a given grid point, $d_{mid-month}^{corr}$ is the mid-month thawing-date day corrected for the warm bias, and *l* is the latitude in degrees. Equation (1) was empirically obtained and accounts for delay in thaw and shift forward of freeze of roughly one day per degree of increasing latitude north of 62°N.

Results

With the frozen water correction, spring fires that are detected by MODIS, are well captured by the Reg-FIRM WFDI. The improvement is quantified by both the averaged correlation coefficients (% of grid cells with positive correlation increased from 55 to 73) and their spatial distributions. This finding confirms the importance of thaw and freeze processes for predicting the occurrence of fires in boreal forests as suggested in previous studies (Venevsky 2006).

References

Johns, T.C., Durman, C.F., Banks, H.T. et al. 2006. The new Hadley Centre climate model HadGEM1: Evaluation of coupled simulations. *Journal of Climate* 19(7): 1327-1353.

Legates, D.S. & Wilmott, C.J. 1990. Mean seasonal and spatial variability in gauge-corrected, global precipitation. *International Journal of Climatology* 10: 111-127.

Sitch, S., Smith, B., Prentice, I.C. et al. 2003. Evaluation of ecosystem dynamics, plant geography and terrestrial carbon cycling in the LPJ dynamic global vegetation model. *Global Change Biology* 9(2): 161–185, doi:10.1046/j.1365-2486.2003.00569.x.

Venevsky, S., Thonicke, K., Sitch, S., et al. 2002. Simulating fire regimes in human dominated ecosystems: Iberian Peninsula case study. *Global change Biology* 8: 984-998.

Venevsky, S. 2006. Estimate of global carbon emissions to the atmosphere from lightning and human induced fires. Integrated Land Ecosystem-Atmosphere Process Study. In: A. Reissell & A. Aarflot (eds.), *Proceedings of the 1st iLEAPS Science Conference, Boulder, Colorado, USA. Report Series in Aerosol Science*. Helsinki, 109-110.

Venevsky, S. & Maksyutov, S. 2007. SEVER: A modification of the LPJ global dynamic vegetation model for daily time step and parallel computation. *Environmental Modelling and Software* 22: 104-109.

Hydrogen and Oxygen Isotope Studies from an Ice Wedge in Svalbard

Helle Vittinghus
Institute of Geography, University of Copenhagen, Denmark and
Department of Geology, The University Centre in Svalbard, UNIS, Norway
Hanne H. Christiansen
Department of Geology, The University Centre in Svalbard, UNIS
Hanno Meyer
The Alfred Wegener Institute, Potsdam, Germany
Bo Elberling
Institute of Geography, University of Copenhagen

Introduction

Svalbard is located in an area of great sensitivity to climate change. Palaeo-climate archives from glaciers have been investigated; however, the longest record analysed dates back 800 years. Ice wedges in Adventdalen are believed to be up to 3500 years old (Jeppesen 2001) and, therefore, possibly contain mid to late Holocene palaeo-environmental information.

Field Site

The Adventdalen Valley is located in central Svalbard. The valley trends east–west and is 3.5 km wide and 27 km long. The permafrost in Adventdalen is continuous, with widespread ice wedges. Polygonal networks are found on the flat terraces along the riverbed and on the gentle valley slopes up to 25° and up to 500 m a.s.l. (Sørbel & Tolgensbakk 2002). They are of variable sizes reaching 10–20 m in diameter. Distinct troughs range from 0.5–5 m across with adjacent ramparts, clearly delimiting the ice wedges below. The oldest age of an ice wedge in Adventdalen is 3685–3640 cal. yr BP (Jeppesen 2001). At the northernmost edge of the terrace at the south side of Adventdalen, thermal erosion of gullies into ice wedges have developed in the river bank cliff. In other places ice wedges are exposed due to river erosion.

Methods

An ice wedge was first exposed in the terrace river cliff in 2003 during stratigraphical studies in outer Adventdalen. This ice wedge was 1.6 m wide, with the top 145 cm exposed. It is a syngenetic ice wedge, reflected by an elevated upper part of the top 10 cm of the ice wedge being only 60 cm wide. Leaves of *Salix* twigs found in the outer part of this ice wedge were ^{14}C AMS dated to 1980–2150 cal. yr BP (Christiansen et al. in prep).

The ice wedge was sampled, cutting horizontally across by chainsaw in winter, to avoid any thawing during cutting and transportation. Ice wedge sampling was designed to capture the isotopic chronology of the vein accumulation and to study vein orientation and/or reactivation event. Since the ice wedge exposure was assumed syngenetic, two sets of samples were taken: one across the widest part of the ice wedge, sampling 107 cm, and one 60 cm above, across the smaller top of the ice wedge, sampling 12 cm.

To capture the horizontal variation in as much detail as possible preferably representing each vein, only a few mm wide samples were necessary. This was achieved by vertical sampling with a microtome from the ice wedge sample blocs in the freezing laboratory at UNIS. Several microtome slices representing 2–3 mm of ice wedge were collected in one sample. The wide ice wedge sample was sampled only in 1–1.5 cm slices, using a standing band saw for ice in the freezing laboratory. This method offered a good opportunity to cut along the vein orientation, since skew cutting was manageable.

The water stable isotopic compositions of $\delta^{18}O$ and δD from the ice wedge samples were determined using a Finnigan MAT Delta-S mass spectrometer by the equilibrium technique at the AWI laboratory. δD and δO^{18} values were calculated by the commercial software ISODAT (version 5.2) and displayed as per mille differences relative to Vienna Standard Mean Ocean Water (V-SMOW) with an internal 1 σ error of better than 0.8‰ and 0.1‰ for δD and δO^{18}, respectively (Meyer et al. 2000).

Results

Results from the ice wedge studies are shown in Figure 1a–d. The grey line in Figure 1b–d represents results from high-resolution sampling from the upper, smaller ice- wedge part. The black line represents the samples from the wider part of the ice wedge. Figure1a shows the general vertical veins, with some veins displaced and some crossings. This shows that, to some extent, a complete horizontal vein pattern could not be assumed to reflect a perfect chronological evolution across the ice wedge, but we believe the overall pattern reflects a symmetrical growth.

Discussion

The horizontal distribution of $\delta^{18}O$ (Fig. 1b) and δD (Fig. 1c) values from the wider part shows, respectively, a peak and a low towards the middle, with descending and ascending values going towards the sides. An overall symmetrical pattern is thus visible, but the values from the smaller part show a more detailed picture, with significantly different values to the samples from the wider part. Thus,

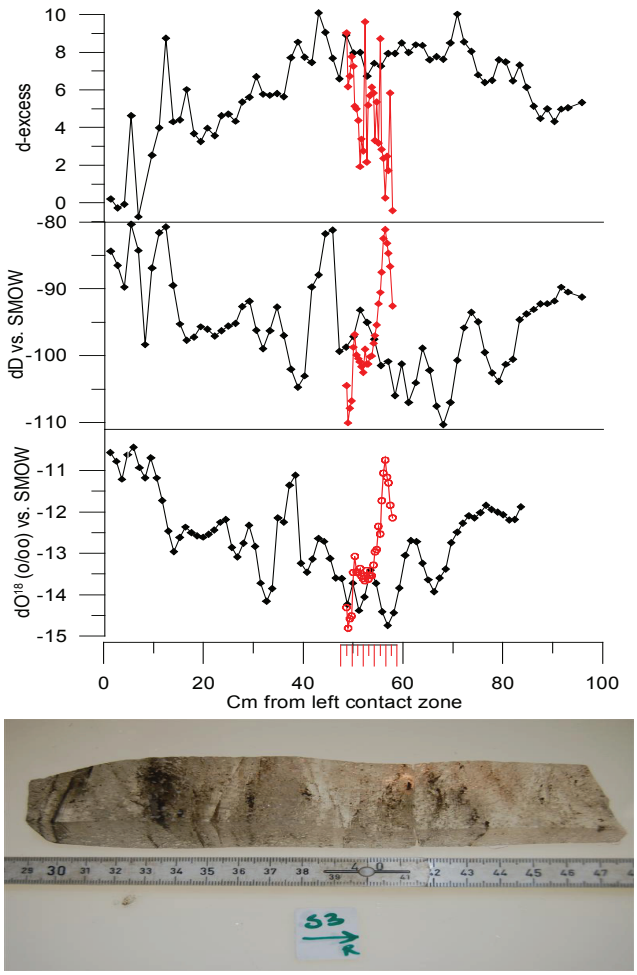

Figure 1. 1a represents the ice wedge part from 28–43 cm from the left contact zone and shows the general vertical vein structure. 1b–d shows the horizontal distribution of $\delta^{18}O$, δD and *d*-excess with the black line representing the wider ice wedge part and the grey line representing the upper, smaller ice wedge part.

the higher resolution samples reveal a more detailed isotopic pattern, and the lower resolution samples from the wider part reflect a mean value of the veins represented in the respective samples. The small vertical distance of 60 cm between the two set of samples is not enough, in this case, to detect a vertical climatic trend, and could account for the similarity (from a climatic point of view) in the isotopic values.

The horizontal *d*-excess signal (Fig. 1d) shows that values from the side sections are too low for a genetic relation with an oceanic moisture source. *D*-excess values in the smaller part range from -0.7‰ to 10‰, with decreasing values towards the sides. The mean value of winter precipitation collected in 2006 in Adventdalen was 7.5‰. Since mean values of winter precipitation should be found in the veins, another moisture source or an altered signal from potential fractionation processes since deposition must be assumed towards the ice wedge sides.

Conclusion

While an overall symmetrical pattern could be interpreted from the horizontal $\delta^{18}O$ and δD variations, a climatic trend during the period of activity was considered detectable. Since a more detailed isotopic pattern was revealed from the higher resolution samples, the lower resolution samples are believed to reflect a mean value of the veins represented in the respective samples. No vertical climatic trend could be seen between the two cores. The veins of the investigated ice wedge are seen to crossing, which most likely complicates palaeo-environmental reconstructions.

References

Christiansen, H.H., Hormes, A. & Snowball, I. (in prep). *High Resolution Late Holocene Loess Record with Syngenetic Ice-Wedges in Adventdalen, Svalbard*.

Jeppesen 2001. *Palæoklimatiske Indicatorer for Central Spitsbergen, Svalbard. Eksemplificeret ved Studier af Iskiler og Deres Værtssedimenter*. M.Sc. Thesis. Svalbard: The University Centre in Svalbard.

Meyer, H., Schönicke, L., Wand, U., Hubberten, H.W. & Frederichsen, H. 2000. Isotopes studies of hydrogen and oxygen in ground ice. Experiences with the equilibration technique. *Isotopes in Environmental and Health Studies* 36: 133-149.

Sørbel, L. & Tolgensbakk, J. 2002. Ice wedge polygons and solifluction in the Adventdalen area, Spitsbergen, Svalbard. *Norsk Geografisk Tidskrift* 56: 62-66.

Vegetation Change and Thermokarst Development: Effects on Ecosystem Carbon Exchange in Upland Tussock Tundra

Jason G. Vogel, Hanna Lee, Christian Trucco, Edward A.G. Schuur
Department of Botany, University of Florida, Gainesville, FL 32601-8526, USA
James Sickman
Department of Environmental Sciences, University of California Riverside, Riverside, CA 92521, USA

Introduction

Thermokarst development generally alters the vegetation composition of an area because of changes in soil temperature and moisture (Camill et al. 2001). In upland tussock tundra, thermokarst depressions are wetter and warmer than undisturbed areas, while areas along the sides of thermokarst are drier due to drainage (Schuur et al. 2007). The changes in soil climate and vegetation composition that occur with thermokarst could affect ecosystem C cycling. Plant growth, or net primary productivity (NPP) and microbial respiration (Rm) of organic matter are both affected by soil climate, and it is the balance between these two processes that determines net ecosystem exchange (NEE). Vegetation composition can directly affect NPP because plant species differ in growth potential, and can indirectly affect Rm because tissue chemistry strongly influences decomposition rates (Chapin & Shaver 1996). Potential C loss from permafrost soils is important to the global C budget because these soils store ~1.6 times more C than is currently in the atmosphere (Schuur et al., in press).

The objective of this study was to examine how vegetation composition and NPP, and thermokarst development may be affecting ecosystem C cycling. In a previous study, we reported that thermokarst depressions in upland tussock tundra apparently caused the loss of tussock-forming species (*Eriophorum vaginatum, Carex bigelowii*) and a gain in deciduous shrubs and mesophilic *Sphagnum* species (Schuur et al. 2007). In this study, we relate these changes in vegetation composition, mortality, and NPP to measurements of seasonal change in ecosystem respiration (Reco), gross primary productivity (GPP), and net ecosystem exchange (NEE).

Materials and Methods

Field site

The study area was in the Eight Mile Lake (EML) watershed in central Alaska. The EML watershed is located 7 miles west of the town of Healy, and is near the north end of Denali National Park and Preserve. Osterkamp and Romanovsky (1999) have monitored permafrost temperatures to 27 m since 1985. Between 1990 and 1998 the permafrost profile warmed by ~0.7–1.2°C, warming that coincided with thermokarst development (Osterkamp 2007). Since 1999, permafrost temperatures have stabilized or slightly decreased (~0.2°C).

A natural gradient study was established within 400 m of the permafrost monitoring borehole. Three sites were located: "Minimal Thaw," where surface topography and tussock tundra vegetation appeared little changed by thermokarst; "Moderate Thaw," where thermokarst development began about 15 years ago; and "Extensive Thaw," where surface depressions are wider and deeper than Moderate Thaw due to a prolonged period (minimum of 50 years) of thermokarst development (Schuur et al. 2007).

Vegetation sampling

Vegetation composition and NPP were sampled in twelve 0.7 x 0.7 m quadrats (chamber base) per site that were distributed in pairs across a 40 m transect The "point frame" method was used to estimate vegetation characteristics, where a thin metal rod is passed vertically through the canopy and the number of interception points with vegetation used to estimate biomass. Site-specific relationships between the number of point intercepts and vegetation biomass were developed in 2004 (Schuur et al. 2007) and applied to surveys in 2004 and 2006. We estimated ground coverage of live and dead mosses and *Eriophorum vaginatum* using the line-intercept method. The five dominant moss groups within the quadrats were identified, including the area coverage of dead *Sphagnum spp*.

Ecosystem carbon exchange

NEE and Reco were estimated with both an automatic and manually operated closed chamber system. The chambers were 0.4 m high and were placed on the same 0.7 x 0.7 areas or chamber bases where NPP and plant species composition were measured. The air inside a chamber was circulated to an infrared gas analyzer (LI-820) and the rate change in CO_2 concentration recorded on either a Campbell CR10x (automatic chamber) or Palm Tungsten C palm pilot (manual chambers). Measurements began in the first few weeks of May and continued until the end of September. Response curves of NEE to light and Reco to temperature were developed and growing season estimates constructed with these response equations. Gross primary productivity was estimated as the difference between growing season NEE and Reco.

Analyses

Multiple regression analysis was used to determine if vegetation characteristics of a chamber base (proportion of dead moss and NPP of functional groups) covaried with chamber level variation in growing season NEE, GPP, and Reco. The best parameters for the regression model were selected based on the maximum coefficient of variation

(adjusted R^2) and Mallow's CP statistics. When a minimum CP statistic and maximum R^2 are selection criteria, the result is the best fit model with the minimum number of parameters.

Results

NPP and ecosystem C exchange

In both 2004 and 2006, NEE, GPP, and Reco measured with the closed chambers were significantly correlated with NPP measured with the point-framing method (Fig. 1a, b, c). These same ecosystem C exchange variables were significantly correlated with active layer thickness, but NPP better described overall variation (not shown). The slope and intercepts of the NPP vs. Reco and GPP relationships were not significantly different between years, but the slope of the NEE lines did differ significantly between years.

Relationship between carbon exchange and specific plant functional groups

We previously reported that across this upland tussock tundra landscape, thermokarst corresponded to a relative decrease in the NPP of graminoids while moss and deciduous shrub NPP increased (Schuur et al. 2007). Here we use multiple regression analysis to examine whether the NPP of individual functional groups corresponded to a change in NEE, Reco or GPP. For NEE, the regression procedure selected a different combination of plant functional types in different years. In 2004, the variance in NEE was best explained with evergreen shrub NPP (+ effect in model) and the coverage of dead moss (- effect in model). In 2006, the variance in NEE was best explained by moss, evergreen shrub, and graminoid NPP. Interestingly, in neither year were deciduous shrubs a component of the NEE model despite the NPP of this functional group generally increasing with active layer thickness (Schuur et al. 2007). Indeed, for GPP deciduous shrubs were also removed from the overall model in both years. This suggests that additional C uptake by deciduous shrubs was effectively replacing the C uptake of the different functional groups that were lost.

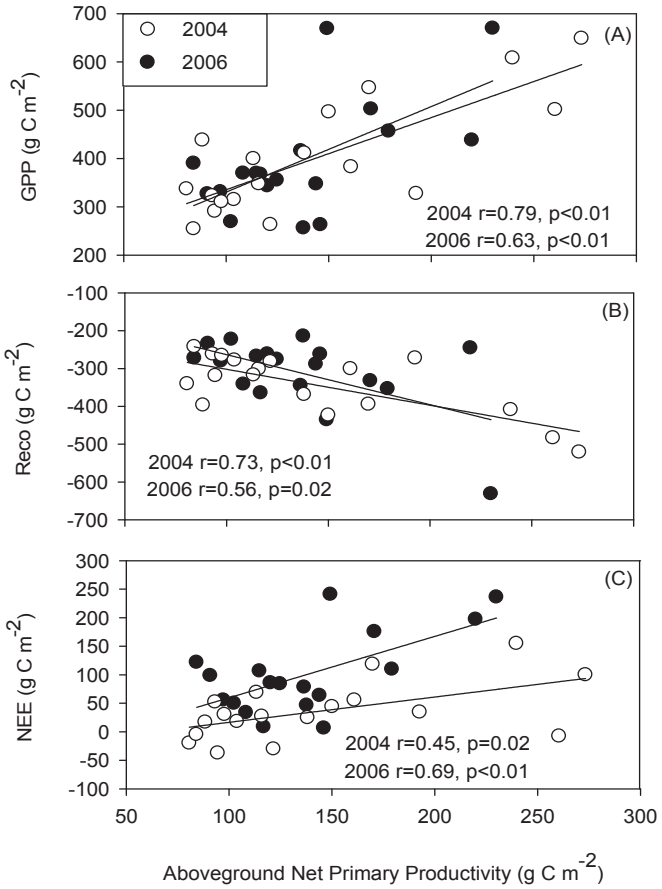

Figure 1. Relationships between growing season aboveground net primary productivity (NPP) and NEE, GPP and Reco across three sites that varied in the degree of permafrost thaw and thermokarst development.

Acknowledgments

We thank Michelle Mack for assistance in processing vegetation samples. Terry Chapin provided laboratory resources. Emily Tissier, Jamie Hollingsworth, and Brian Charlton provided logistical support. Tom Osterkamp undertook the early research that made this project possible, and Guy Adema and Larissa Yocum of Denali National Park and Preserve provided logistical support.

References

Camill, P., Lynch, J.A., Clark, J.S., Adams, J.B. & Jordan B. 2001. Changes in biomass, aboveground net primary production, and peat accumulation following permafrost thaw in the boreal peatlands of Manitoba, Canada. *Ecosystems* 4: 461-478.

Chapin, F.S. & Shaver G.R. 1996. Physiological and growth responses of arctic plants to a field experiment simulating climatic change. *Ecology* 77: 822-840.

Osterkamp, T.E. & Romanovsky, V.E. 1999. Evidence for warming and thawing of discontinuous permafrost in Alaska. *Permafrost and Perigl. Process* 10: 17-37.

Osterkamp, T.E. 2007. Characteristics of the recent warming of permafrost in Alaska. *Journal of Geophysical Research* 112: F02S02, doi:10.1029.

Schuur, E.A.G., Crummer, K.G., Vogel, J.G. & Mack, M.C. 2007. Plant species composition and productivity following permafrost thaw and thermokarst in Alaskan tundra. *Ecosystems* 10: 280-292.

Preliminary Analysis of Anthropogenic Landscape Fragmentation: Tazovsky Peninsula, Russia

Jesse S. Wallace
Department of Geography, University of Montana, Missoula, 59812, USA
Anna E. Klene
Department of Geography, University of Montana, Missoula, 59812, USA

Introduction

As part of the IPA 2007 International Polar Year activities, Moscow State University offered a "Technogenic and Environmental Permafrost Observatories" field course in west Siberia. During this course, students were granted access to three natural gas fields owned by regional subsidiaries of the Russian energy company, Gazprom. The fieldwork addressed the impact of industrial development in permafrost regions, with an emphasis on the evolution of technologies designed to mitigate the problems associated with engineering in arctic environments.

The fragmentation analysis performed as a result of this field course examines these issues by quantifying the degree to which recent industrial development has affected the tundra. Anthropogenic impacts on this region have been discussed at length with regard to ecological consequences (Vilchek & Bykova 1992, Kryuchkov 1993). Ramifications of climate change on both the tundra and an ageing infrastructure have also been examined (Mazhitova et al. 2004). This fragmentation analysis provides additional quantitative information for future environmental assessments of the region.

Study Area

The Tazovsky Peninsula occupies the central north of the Tyumen oblast, surrounded by the Gulf of Ob' as it enters the Kara Sea (Fig. 1). This region lies within the West Siberian Basin, the largest petroleum and natural gas basin in the world (Ulmishek 1998). Underlain by continuous permafrost, the landscape is primarily peat tundra, characterized by mosses, lichens, grasses, and shrub-level bushes (*sphagnum balticum, ledum palustre, carex, betula nana, larix siberica*). Tree growth is restricted to river banks, where increased active layer depths allow more substantial root systems. Average temperatures range from -22°C to -26°C in January, and 4°C to 15°C in July (Russian Climate Server 2007).

History of industrialization

The Yamburg gas-oil condensate field is the largest proven field in the world, accounting for 15% of Russia's total natural gas and condensate reserves (Yamburggazdobycha 2007). Natural gas deposits on the Tazovsky Peninsula were discovered in 1969. In 1982, construction on the settlement of Yamburg began in order to house workers for the developing gas field. Located on the west coast of the peninsula, Yamburg is currently the only urban area in the region. Though there are no permanent residents, the town

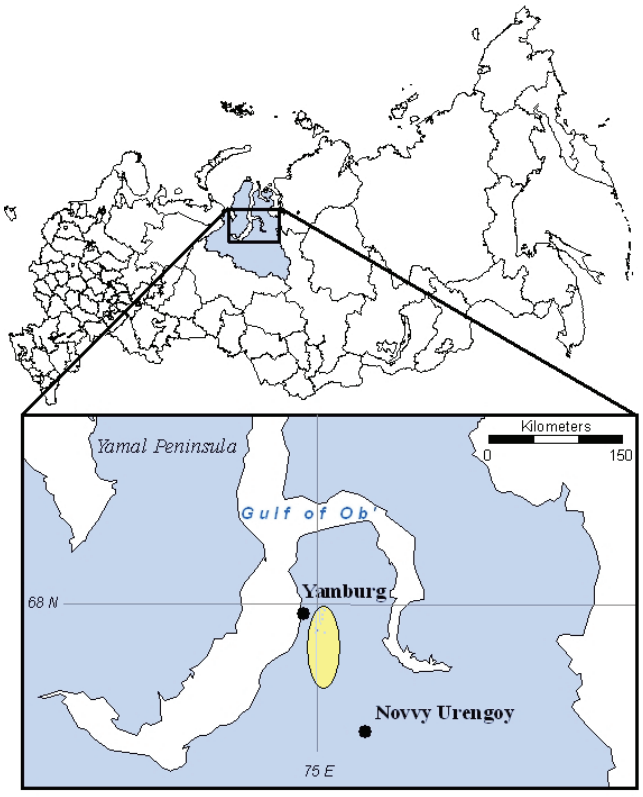

Figure 1. A detail map of the Tazovsky Peninsula shows the towns of Yamburg and Novvy Urengoy. The area to the southeast of Yamburg shows the approximate location of the Yamburg gas-condensate field.

is capable of housing up to 10,000 workers. The natural gas field and related industrial complex spreads to the south and east of the town, covering an approximate area of 8,500 km². In 2007, the estimated annual output of the Yamburg gas field was 10 bln m³, with a maximum capacity of 40 bln m³ (Yamburggazdobycha 2007).

Methodology

Satellite imagery of the study area was collected across a 23-year period corresponding to the inception and growth of the Yamburg natural gas field. Imagery from 1984, 1987, and 1999 were collected by the LANDSAT MSS, TM, and ETM+ sensors respectively. Imagery of 2007 is from the TERRA ASTER sensor.

The imagery was classified according to land-cover, with an emphasis on identifying all areas of anthropogenic impact, including drill pads, processing complexes, roads,

and pipelines. Data collected in the field were used as a validation set for the resulting classification. The areas classified as "industrial" were then used as the basis for the fragmentation analysis.

The FRAGSTATS statistical program has the ability to calculate over 200 fragmentation metrics (McGarrigal & Marks 1995). Each of the classified images of the study region was analyzed within this program to determine quantitative changes as measured by a set of established metrics. Of these, patch count, mean patch size, and edge density are the most efficient in evaluating fragmentation of a region over time (Ritters et al. 1995). While these metrics provide discrete values for each image, it is the change in these values over time that provides the basis for comprehensive fragmentation understanding. In order to put these changes in perspective, the results will be compared to other areas that have undergone similar development. Recent technological advances employed in the construction of the natural gas complex at Zapalyrnoe, to the southeast of the study area, have allowed similar production levels with significantly less infrastructure (Yamburggazdobycha 2007). Correlating fragmentation metrics to production levels at each site provides one avenue of comparative analysis.

Discussion

The ability to trace quantified changes across the study area, from the introduction of industrialization to the present day, offers a unique opportunity to assess the comprehensive impact of anthropogenic development in permafrost regions. Increases in patch count, and decreases in mean patch size, nearest neighbor, and diversity indices at each temporal analysis point provide quantitative evidence of the degree to which the region has been affected. Extension of the analysis potentially allows investigation of a correlation between annual natural gas production at the Yamburg field and key fragmentation metrics. Verification of this correlation offers the possibility of predicting the impacts that future resource development will have on other areas of west Siberia that have yet to be developed. The fragmentation correlation template additionally introduces a vehicle for analyzing the mediating effects of new extraction technologies on regional landscape fragmentation.

Acknowledgments

The field course was made possible through Moscow State University as part of the International University Courses on Permafrost offerings for the International Polar Year. Gazprom and its regional subsidiaries, NadymGasprom and Yamburggazdobycha, granted special access to their fields, and provided generous hospitality throughout the course. The University of Montana provided financial assistance to Dr. Klene through grants and startup funding.

References

Kryuchkov, V. 1993. Anthropogenic loads and the northern ecosystem condition. *Ecological Applications* 3(4): 622-630.

Li, X., Cheng, G. & Xiao, H. 2001. Quantifying landscape structure of the Heihe River basin, northwest China using FRAGSTATS. *Journal of Arid Environments* 48: 521-535.

Mazhitova, G., Karstkarel, N., Oberman, N., Romanovsky, V. & Kuhry, P. 2004. Permafrost and Infrastructure in the Usa Basin: Possible impacts of global warming. *Ambio* 33(6): 289-294.

McGarigal, K. & Marks, B. 1995. *FRAGSTATS: Spatial Pattern Analysis Program for Quantifying Landscape Structure*. Reference manual. Forest Science Department, Oregon State University, Corvallis, Oregon.

North, R. 1972. Soviet northern development: The case of NW Siberia. *Soviet Studies* 24(2): 171-199.

O'Neill, R.V., Krummel, J.R., Gardner, R.H., Sugihara, G., Jackson, B., Deangelis, D.L., Milne, B.T., Turner, M.G., Zygmunt, B., Christensen, S.W., Dale, V.H. & Graham, R.L. 1988. Indices of landscape pattern. *Landscape Ecology* 1: 153-162.

Russian Climate Server. 2007 URL: http://meteo.infospace.ru/climate/html/index.ssi

Ulmishek, G. 2003. *Petroleum Geology and Resources of the West Siberian Basin.* USGS Bulletin 2201-G.

Vilchek, G.E. & Bykova, O. 1992. The origin of regional ecological problems within the northern Tyumen Oblast, Russia. *Arctic and Alpine Research* 24(2): 99-107.

Weller, C., Thomson, J., Morton, P. & Aplet, G. 2002. *Fragmenting Our Lands: The Ecological Footprint from Oil and Gas Development*. Seattle, WA, & Denver, CO: The Wilderness Society.

Yamburggazdobycha, LTD. 2007. Promotional CD-ROM.

Engineering Effect on the Thermal Status of Shallow Ground in Permafrost Regions

Zhi Wen
State Key Laboratory of Frozen Soil Engineering, CAREERI, CAS, Lanzhou Gansu 730000
Yu Sheng
State Key Laboratory of Frozen Soil Engineering, CAREERI, CAS, Lanzhou Gansu 730000
Wei Ma
State Key Laboratory of Frozen Soil Engineering, CAREERI, CAS, Lanzhou Gansu 730000
Qingbai Wu
State Key Laboratory of Frozen Soil Engineering, CAREERI, CAS, Lanzhou Gansu 730000
Bo Huang
Qinghai Provincial Highway Research and Survey Institute, Xining Qinghai 810008, China

Introduction

The construction of an embankment in permafrost regions may induce substantial disturbance on the heat and mass transfer balance between the ground surface and atmosphere, which results in more heat absorption in the embankment. The temperature of the permafrost underneath increases even if permafrost thaws, causing serious problems for embankment due to thaw settlement on the Qinghai-Tibetan Plateau (Wen & Sheng 2003). The thermal status of the embankment affects directly the thermal status of permafrost under the railway embankment, which determines the embankment stability in the permafrost regions, especially ice-rich permafrost regions (Yu & Lai 2002).

Owing to important signification of the thermal regime of the upper soil layer on permafrost stability, many researchers have studied the thermal regime of the natural ground on the Qinghai-Tibetan Plateau (Xu & Ma 1984, Zhang & Zhu 1998). However, there is scarce research on heat balance and annual heat incomes and expenses of railway embankments. To know about the influence of engineering activities on the thermal regime of the natural ground, dynamic monitoring using dataloggers made in Compbell Company for temperature and heat flux in the upper active layer was carried out during August 2002, making it possible to use quantificational method analyses of the influence of engineering activities.

General Situation of the Test Sites

The test site is situated between Kekexili and Fenghuoshan along the Qinghai-Tibetan Railway on the Qinghai-Tibetan Plateau. Dynamic monitor sections of railway embankment and natural ground were set up on August 2002. Each section may measure heat flux and temperature of shallow ground simultaneously. Instruments used in two sections were self-calibrating heat flux sensor, temperature sensor, and datalogger and the readings were taken once half hour. The temperature probe may measure the temperature at the depth of 2.0 cm, 5.0 cm, 10.0 cm, 20.0 cm, and 50.0 cm from ground surface. The depth of heat flux placed was 20.0 cm from ground surface. Taking the difference of heat flux at two sides of the embankment into consideration, there was one self-calibrating heat flux sensor at each side of two sections and the data of heat flux were the even value of two sensors.

Variation Character of Soil Temperature

After railway embankment construction, many conditions were changed compared to natural ground, such as surface conditions (vegetation, albedo, etc.), soil moisture content, and soil component, which affected radiation absorption of surface and its transfer process downwards certainly. As seen in Figure 1, the soil temperature under the embankment surface at a depth of 50.0 cm was 2°C higher than that of the natural ground and had same phase location under similar climatic conditions (embankment testing site was close to natural ground site). Apparently, the phase and variation current of soil temperature was similar between two sites, which was due to some same conditions for two sites, such as climatic conditions, etc., that had nothing to do with engineering activities. However, the soil temperature at the embankment site was 2°C higher than that of the natural ground site if other conditions stayed the same, which was affected by engineering activities distinctly. After engineering construction, vegetation in the natural ground was destroyed, and the soils type, soils component, and its moisture content were changed, which increased the radiation absorption and decreased the evaporation water content. In a word, a high temperature boundary was brought to bear on the surface, which augmented the heat exchange and accelerated the permafrost degradation. Due to engineering activities, thawed core below embankment came into being and thawing settlement began.

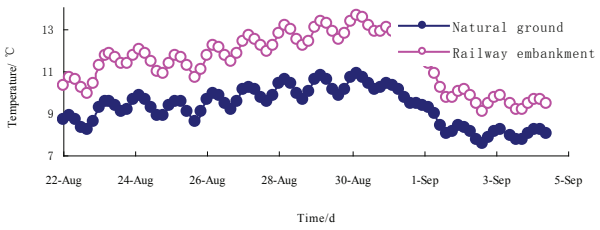

Figure 1. The contrastive temperature curves between the railway foundation and the natural ground at 50 cm depth.

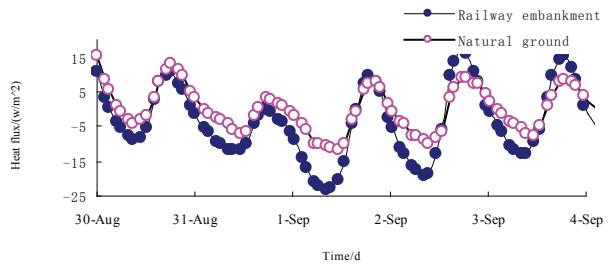

Figure 2. The contrastive heat flux curves between the railway foundation and the natural ground at 50 cm depth in the warm season.

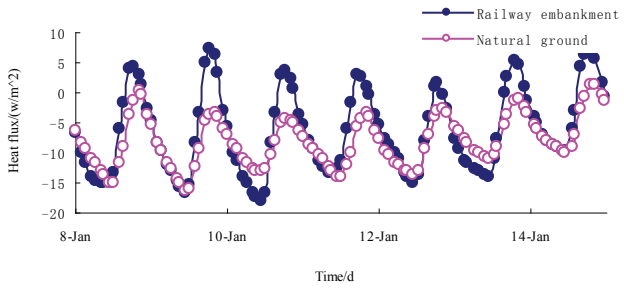

Figure 3. The contrastive heat flux curves between the railway foundation and the natural ground at 50 cm depth in the cold season.

The Variation Character of Soil Heat Flux

Figures 2 and 3 show the soil heat fluxes of two sites at a depth of 20 cm in the warm season and the cold season, respectively. The observed results of soil heat fluxes at two sites showed that there were distinct differences between the embankment site and the natural ground site (Figs. 2 and 3). The soil heat flux at the natural ground site varied mild, while the soil heat flux at the same depth of the embankment site varied great. In addition, the daily amplitude of heat flux at the natural section was smaller than that of the embankment section at the same depth.

It can also be seen from Figures 2 and 3 that there were two processes (heat release state and heat absorption state) for the soil heat flux at a depth of 20 cm in the warm season, whatever under embankment and under natural ground. As for the cold season, the soil heat flux at the natural ground site was in the heat release state invariably. In addition, we also found that the daily variation amplitude of soil heat flux in the cold season was smaller than that in the warm season, and the daily variation amplitude of soil heat flux in the cold season was approximately one-half to two-thirds of that in warm season.

Conclusion

Due to railway construction and instrument fault, long-term observation data were not obtained. Additionally, the moisture content was not monitored. To realize the heat-moisture process of the active layer in permafrost regions, a heat-moisture observation plan will be performed in 2007, when the temperature and the moisture probes will be installed simultaneously. Based on testing results and foregoing analyses, some useful conclusions can be drawn. The soil temperature under the embankment surface at a depth of 50 cm was 2°C higher than that of natural ground, and they had the same phase location under similar climatic conditions, which was affected by engineering activities distinctly. The daily variation amplitude of soil heat flux at the natural ground site was smaller than that of the embankment site, and the variation at the natural ground site was even more. In addition, the soil heat flux at the embankment site was more sensitive to the change of air temperature and tended more to be disturbed by the environment. There were two processes (heat release state and heat absorption state) for soil heat flux at a depth of 20 cm in the warm season, whatever under embankment and under natural ground. The daily variation amplitude of soil heat flux in the cold season was smaller than that in the warm season, and the daily variation amplitude of soil heat flux in the cold season was approximately one-half to two thirds of that in the warm season.

Acknowledgments

The research was supported by a grant of the Western Project Program of the CAS (Grant No. KZCX2-XB2-10), by the Graduate Student Innovation Program of the CAS granted to Dr. Zhi Wen, and by Opening Foundation of State Key Laboratory of Frozen Soil Engineering.

References

Wen, Z., Sheng, Y. & Wu, Q. 2003. Dynamic monitoring of thermal state for shallow ground in Qinghai-Tibetan Railway embankment. *China Journal of Rock Mechanics and Engineering* 22(2): 2664-2668.

Xu, Z. & Ma, Y. 1986. Calculation of soil heat flux on Qinghai-Tibetan plateau and analysis of stability of climate generalization method. Scientific testing paper volume on Qinghai-Tibetan plateau climate. Beijing: Science Press, 35-45.

Yu, W., Lai, Y. & Niu F. 2002. Temperature field features in the laboratory experiment of the ventilated railway embankment in permafrost regions. *Journal of Glaciology and Geocryology* 22(5): 601-607.

Zhang, J., Zhu, B. et. al. 1998. *Process in Climate Science of Qinghai-Tibetan Plateau*. Beijing: Science Press, 78-88.

Long-Term Monitoring of Sensible and Latent Heat Fluxes Using Eddy Covariance at a High Arctic Permafrost Site in Svalbard, Norway

S. Westermann
Alfred-Wegener-Institute for Polar and Marine Research, Potsdam, Germany
J. Boike
Alfred-Wegener-Institute for Polar and Marine Research, Potsdam, Germany
K. Piel
Alfred-Wegener-Institute for Polar and Marine Research, Potsdam, Germany
J. Lüers
Univ. of Bayreuth, Germany, Dept. of Micrometeorology

Introduction

Land-atmosphere interactions are an important element in the energy and water budgets in permafrost regions. The eddy covariance method has proven to be the most reliable way to directly measure sensible and latent heat fluxes (Foken 2006). However, due to the difficult logistics and the extreme environment, very few long-term eddy covariance studies exist in arctic regions (Grachev et al. 2007). Previous measurements on Svalbard, Norway, were limited to the summer season (Lloyd et al. 2001). Here we present long-term eddy covariance measurements of sensible and latent heat fluxes at a High Arctic continuous permafrost site on Svalbard.

Methods

The eddy covariance measurements were performed near Leirhaugen hill, located approximately 2 km southwest of the village of Ny-Ålesund. The site is situated in hilly tundra at the foot of two major glaciers, and is characterized by sparse vegetation alternating with exposed soil and rock fields.

The eddy covariance system consisted of a Campbell CSAT 3D sonic anemometer and a LiCor LI-7500 CO_2 and H_2O gas analyzer, which were sampled at 20 Hz using a CR3000 Campbell Scientific datalogger. The evaluation of the raw data was performed with the software "TK2" (Mauder & Foken 2004) from the University of Bayreuth, Germany. The quality assessment scheme of Foken & Wichura 1996 (see also Foken 2006), which is based on tests for stationarity and integral turbulence characteristics, was used to assess the quality of the flux measurements.

Measurements were collected from April to September 2007, covering a period from late winter until the end of the summer season. To account for the changing height above ground of the flux sensors due to accumulation or melting of snow, the snow depth directly at the EC-site was recorded using a Campbell Scientific SR50 distance sensor. The measured heights above ground ranged from a minimum of 2.0 m to 3.2 m at the end of the snow ablation period. After a complete snow melt, the EC-instruments were lowered to a height of 2.5 m above ground.

The net radiation was recorded at a climate station in the vicinity of the eddy covariance site, so that it is possible to compare the magnitude of the sensible and latent heat fluxes with the radiation balance.

Results

During the entire snow-covered period, either a stable or a neutral near surface atmospheric stratification was recorded, corresponding to z/L (measurement height over Obukhov length) significantly greater than zero or approx. zero, respectively. Hereby, a stable stratification was associated with low horizontal wind speeds of less than 5 m/s, while a neutral stratification was found predominantly for higher wind speeds. Particularly at stable conditions, the use of the eddy covariance method, which depends upon a fully developed turbulence field, is questionable. This was also reflected applying the Foken & Wichura quality assessment: a significant part of the data measured during the snow-covered period was classified as "only for orientation purposes" or "to be discarded" both for the sensible and latent heat flux. The data, which withstood the quality assessment, typically yielded low fluxes of less than 20 W m^{-2}. Hereby, the sensible heat flux was usually negative, corresponding to a sensible flux directed from the atmosphere to the ground (longwave radiation forcing), while the latent heat flux was positive, corresponding to weak but still existing sublimation and/or evaporation processes of snow or melt water.

The appearance of large snow-free patches around June 26 triggered a strong increase of both sensible and latent heat fluxes, with now both fluxes being positive, corresponding to a warming of the tundra surface forced by shortwave radiation. During this period the latent heat flux, with a maximum of 90 W m^{-2}, was more than twice as large as the sensible heat flux, likely due to very wet soil conditions directly after snowmelt. This situation reversed during July, when the tundra increasingly dried up throughout most of the potential fetch area of the eddy covariance site. Around the middle of July, both heat fluxes were approximately equal, the sum of both peaked at values of more than 200 W m^{-2}. Towards the end of July, the sensible heat flux subsequently became dominant over the latent heat flux by approximately a factor of two. The immediate surrounding of the measurement site could then be characterized as moderately damp tundra. From mid of August onwards, both

fluxes decreased steadily. At this time, the latent heat flux with peak values around 50 W m^{-2} was found to dominate once again over the sensible heat flux.

During the polar day season, the sensible and latent heat flux displayed a strong diurnal course with peak fluxes associated with maxima of solar radiation around midday. At the lowest sun angles, around midnight, both fluxes usually decreased to close to zero, but remained positive.

From the completion of snowmelt through the middle of August, the atmospheric stratification (according to the z/L ratio) was found to be either unstable or neutral, resulting in a good data-quality assessment. Towards and after the end (approximately middle of August to September) of the polar day season the general pattern could be characterized as neutral to weak unstable atmospheric stratification during the day and stable atmospheric stratification during the night. The quality assessment still indicated a good data quality during the day, with an increasingly poor data quality during the night.

Discussion

The highest amount of the net radiation was observed around beginning of July to be around 300 W m^{-2}, corresponding with a total of sensible and latent heat fluxes reaching values around 200 W m^{-2}. This clearly shows the importance of the sensible and latent heat fluxes regarding their parts in the whole energy budget of permafrost soils around Ny-Ålesund. Thus, eddy covariance measurements must be regarded as an essential tool in obtaining a complete picture of the energy budget and the allocation of the available energy during the summer period.

At snow-covered times, that is, for approximately two-thirds of a year, the situation is yet more difficult to assess. On the one hand, the quality of a significant portion of the data is questionable according to quality assessment (Foken & Wichura 1996), and only low fluxes were observed. On the other hand, such quality assessment schemes were developed in and for temperate zones, and are therefore not necessarily well suited for conditions found in the Arctic. Furthermore, low but sustained sensible and latent heat fluxes might have to be taken into account in the energy budget of the snow-covered ground. It is of great importance to critically review and possibly modify the evaluation and quality assessment for eddy covariance data for these circumstances.

References

Grachev, A.A., Andreas, E.L., Fairall, C.W., Guest, P.S. & Persson, P.O.G. 2007. SHEBA flux–profile relationships in the stable atmospheric boundary layer. *Boundary Layer Meteorol.* 124: 315-333.

Foken, T. 2006. *Angewandte Meteorologie, Mikrometeorologische Methoden*, (2 and extended edition). Heidelberg: Springer, 326 pp.

Foken, T. & Wichura, B. 1996. Tools for quality assessment of surface-based flux measurements. *Agric Forest Meteorol*. 78: 83-105.

Lloyed, C.R., Harding, R.J., Friborg, T. & Aurela, M. 2001. Surface fluxes of heat and water vapour from sites in the European Arctic. *Theor. Appl. Climatol.* 70: 19-33.

Mauder, M. & Foken T. 2004. Documentation and instruction manual of the eddy covariance software package TK2. *Work Report University of Bayreuth, Dept. of Micrometeorology* Vol. 26, ISSN 1614-8916.

Scientific Opportunities and Environmental Impacts Related to Ski Run Construction, Zermatt, Swiss Alps

Oliver Wild
Department of Geography, University of Giessen, Germany
Isabelle Roer, Stephan Gruber
Department of Physical Geography, University of Zurich, Switzerland
Barbara May, Dietmar Wagenbach
Institute for Environmental Physics, University of Heidelberg, Germany

Background

The building of ski runs and their associated installations are likely to influence the alpine environment and the permafrost present at many of those sites. Therefore, it is important to have a good understanding of the impacts of this construction. As it is impossible to restore the normal environment once the work is finished, the present state should be documented, and information about how the formation of the area and its periglacial landforms took place in the past (e.g., with ice samples) should be gained. During the years after the construction, further research must be conducted to evaluate the degree of change. The research within this article contributes to this knowledge, and preliminary results are presented.

Study Site

During construction for a new ski run at the Gornergrat (Zermatt, Swiss Alps), diverse exposures of ground-ice were created. The site (3135 m a.s.l) is located in the southern Swiss Alps and is part of the Matter Valley. The Zermatt region has a continental climate with 610 mm annual precipitation (MeteoSwiss 30-year average 1961–1990) and strong direct solar radiation.

Located on the northern slopes of the east–west running crest between Gornergrat and Hohtälli (3286 m a.s.l.) is the area called "Kelle" (Fig. 1). Here, the ski run is constructed within the discontinous permafrost zone, which can be expected between 2600 and 3500 m a.s.l., according to King (1996). Regarding permafrost distribution, measurements of the ground surface temperature (GST) and the basal temperature of the snow (BTS), as well as permafrost models have contributed to knowledge about this area (Gruber 2000, Herz 2006).

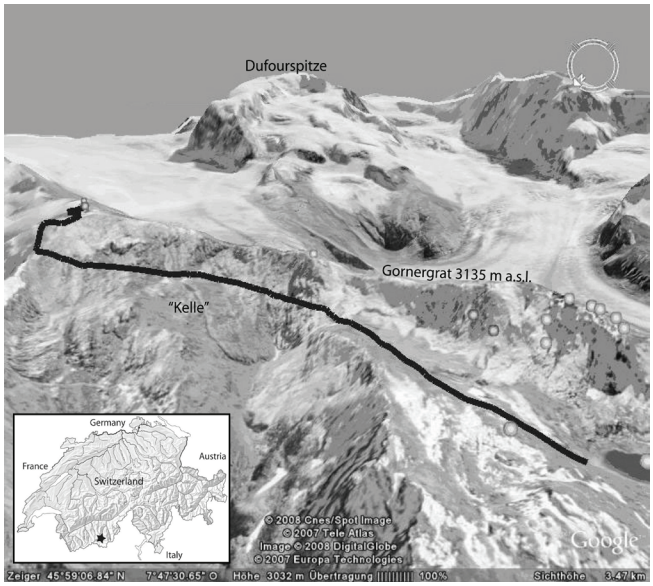

Figure 1. The study site with its new ski run (black line).

Environmental Impacts

During the construction in summer 2007, ground-ice was exposed at various spots in the "Kelle" area. The building of a new ski run with a snowmaking system, commissioned by Zermatt Bergbahnen, was the reason for that. With a length of approximately 2.5 km and an altitudinal difference of 350 m, the track leads through a steep cirque where large masses of rock and sediments had to be moved. Various geomorphological features were affected by these actions. The uppermost part of the track leads through the remaining ice of a small glacier (Fig. 2a), the middle part cuts through a rock glacier (Fig. 2b & 2c), and rock glacier-like features (polygenetic landforms) were influenced in the lowest part (Fig. 2d).

The maximum depth reached is approximately 8 m below the former surface. Due to the removal of the active layer and

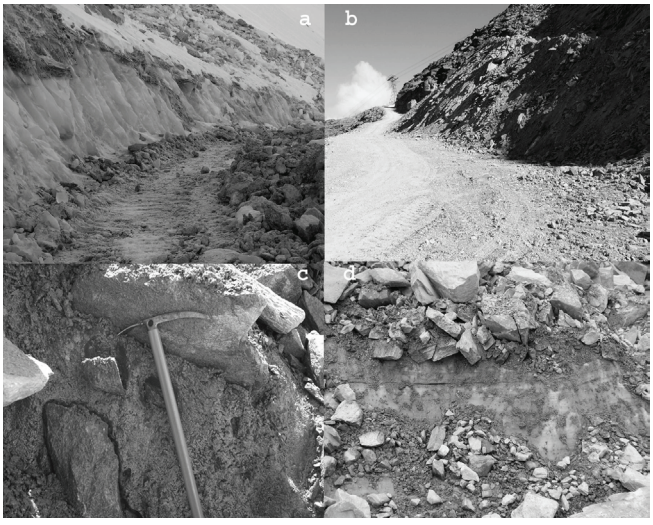

Figure 2. The ice of the remaining glacier (a), the ski track cutting through the rock glacier (b), rocks and ice (c), and an ice core of a polygenetic landform (d).

the exposure of ground-ice, the thermal regime is disturbed. Increased melting during the summer and the formation of a new active layer is expected.

Unique Scientific Opportunities

Even if the interferences with the periglacial system of "Kelle" have negative consequences, it offers great opportunities for permafrost research, which can rarely be found elsewhere. Due to the excavations it was possible to document and map the inside of rock glaciers and other geomorphological features. On the rock glacier, stratigraphy was mapped and compared to geophysical soundings (Hilbich et al. 2008).

Considering the expected effects of a disturbed thermal regime and increased melting, repeated geodetic surveys will be conducted. A geodetic survey of the whole area at the beginning of summer 2008 gives the opportunity to quantify the amount of sediments that has moved in 2007. A second survey in autumn 2008 will show if thaw settlement has occurred. The observed landforms may show different reaction times and degrees of change. It is known that the preparation of ski runs is leading to decreasing temperature in the ground, compared with non-prepared places in the surrounding area (Rixen et al. 2004); however, the removal of a coarse blocky surface layer, which exerts a strong cooling influence, can lead to significant ground warming and permafrost degradation (cf. Herz 2006).

In addition, ice samples were taken at different locations and are currently being investigated (Fig. 3). Three ice samples are inspected for visual features such as air bubbles and grain size prior to first sub-sampling for ice density, total ion content (conductivity), and stable water isotope ($\delta^{18}O$ and δD) measurements. This is expected to lead to information about the dominating processes of ice formation and exchange. Here, tritium analyses are envisaged as well, allowing for estimating any influence of recent water. ^{14}C analysis of organic impurities might help to infer an upper age limit, in case the ice would date back over several centuries.

Preliminary Results

In 2007, this unique opportunity was used to map the permafrost landforms, which is the basis for observation of future changes. Because of the disturbed thermal regime and thawing permafrost, rebuilding of the ski run must be expected for future years.

The pilot analyses of the ice, performed so far, indicate:

- An ice texture broadly similar to non-temperate ice found in Alpine ice caves, as characterized by centimeter-size grains, an ice density close, but still significantly below 0.9 g/cm^3, and few but relatively large bubbles.
- A surprisingly low ion and dissolved impurity content likely due to post depositional snow cover elution and $\delta^{18}O$ values clearly pointing to freeze on of mainly winter precipitation.

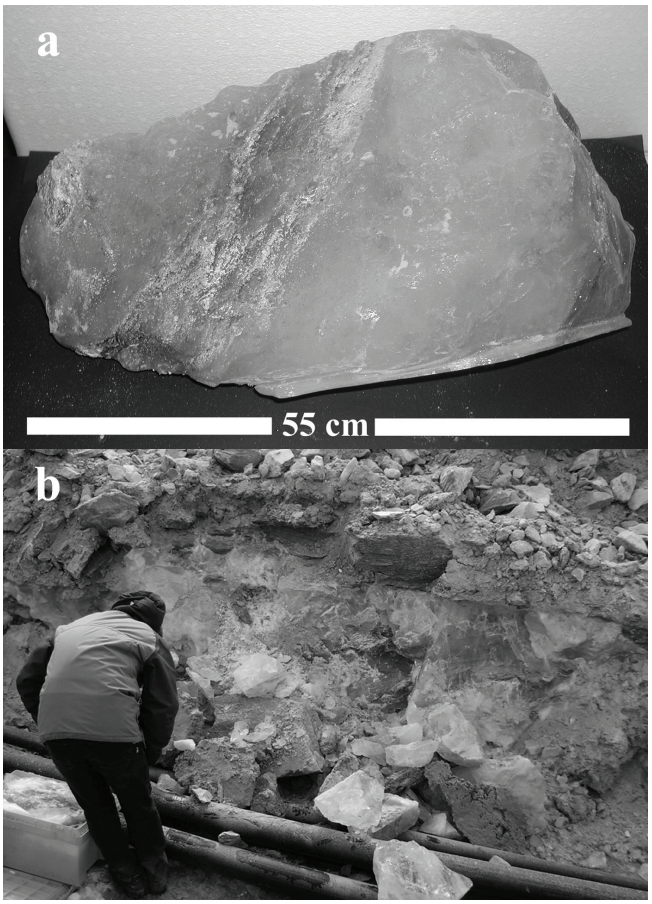

Figure 3. The biggest ice sample (a), which was taken in the ditch for the snowmaking system (b).

References

Gruber, S. 2000. *Slope instability and permafrost: A spatial analysis in the Matter Valley, Switzerland*. Unpublished Master Thesis. Giessen, Germany: Institute of Geography, Justus Liebig University.

Herz, T. 2006. *Das Mikroklima grobblockiger Schutthalden der alpinen Periglazialstufe und seine Auswirkungen auf Energieaustauschprozesse zwischen Atmosphäre und Lithosphäre.* Institute of Geography, Justus Liebig University Giessen, Germany. URL: http://geb.uni-giessen.de/geb/volltexte/2006/3837/

Hilbich, C., Roer, I. & Hauck C. 2008. Ground truth observations of the interior of a rock glacier as validation for geophysical monitoring datasets. *Extended Abstracts, Ninth International Conference on Permafrost, Fairbanks, Alaska, 29 June–3 July 2008.*

King, L. 1996. Dauerfrostboden im Gebiet Zermatt–Gornergrat–Stockhorn: Verbreitung und permafrostbezogene Erschließungsarbeiten. *Z. Geomorph. N.F., Suppl. Bd.* 104: 73-93.

Rixen, C., Haeberli, W. & Stoeckli, V. 2004. Ground temperatures under ski pistes with artificial and natural snow. *Arctic, Antarctic, and Alpine Research* 36(4): 419 – 427.

The Effect of Climate and Permafrost on Tree Line Dynamics in Northwest Russia: A Preliminary Analysis

Martin Wilmking
Saskia Kenter
Jens Ibendorf
University Greifswald, 17487 Greifswald, Germany

Introduction

Tree line dynamics provide important feedback mechanisms to the global climate system by altering albedo and carbon storage at high latitudes. A northward movement of the northern tree line is generally assumed to decrease albedo (Chapin et al. 2005), but increase above-ground carbon storage. However, ecosystem carbon storage might be reduced during tree line advance due to the respiration of (old) soil carbon and thus result in a positive feedback to warming (Wilmking et al. 2006).

Establishment of trees north of tree line requires on the one hand favorable climatic conditions (climate driver) and on the other hand suitable microsite conditions (microsite driver) (Lloyd & Fastie 2002). Suitable microsites are often hampered by the existence of permafrost, and thus ultimately may depend on permafrost degradation. Thus, one main factor controlling carbon storage and tree line advance in many regions is permafrost.

The EU Project "CarboNorth" aims at quantifying the carbon budget in northwest Russia, and as part of this project, the consortium is studying tree line dynamics. This paper reports preliminary results from the dendroecological part of the investigation. Particularly, we were interested in the climate sensitivity of established trees at tree line (climate driver) and in the age structure of seedlings extending beyond tree line from mostly permafrost-free soils to permafrost-influenced soils (microsite driver).

Methods

Field sites were located at northern tree line in northwest Russia at 67.4°N, 62.3°E (R1), 67.2°N, 62.1°E (R2), 67.1°N, 59.5°E (Kho). Each site consisted of a gradient from tree islands on well-drained soil with permafrost pockets, through woodland to treeless tundra underlain by permafrost (conceptional permafrost degradation). Each transect consisted of 3–4 plots (15 x 15 m): (1) forest, (2) dense woodland, (3) open woodland, and (4) tundra. Permafrost depth was measured with a 120 cm long probe (July/August 2007). We collected penetrating tree cores or disks (at root collar level) from every *Picea obovata* tree or seedling within each plot in 7/2007. Samples were prepared according to dendrochronological standards. Age of samples was determined by ring counts and adjusted for sample height. We measured ring-width (LINTAB 5, 1/1000 mm) from all R2 samples including other well-established trees close by and crossdated visually and with COFECHA. We used the program ARSTAN (negative exponential, straight line fits, Huggershoff) to standardize the tree ring series, to remove the biological age trend, and to build site chronologies. We calculated climate-growth relationships of chronologies only, if EPS (expressed population signal) exceeded 0.85. We used mean monthly temperature and precipitation data (1901–2002) from the closest grid point of the gridded CRU-dataset, because the temperature record correlated very well ($r > 0.98$) with the closest station (Khoseda Hard) and records of Pecora ($r > 0.90$) and Nar Jan Mar ($r > 0.87$). Correlation and response functions over time were analyzed with the program DENDROCLIM2002 (Biondi & Waikul 2004); moving window length was 50 years.

Results

Microsite conditions

The active layer depth was generally significantly shallower in the tundra plots compared to woodland and forest plots, which showed similar thaw depths (Fig. 1), often exceeding the depth of the probe. While forest plots were generally well drained, woodland and especially tundra plots were often waterlogged, and trees and seedlings had often established on slightly higher terrain (hummocks).

Age structure

The age structure revealed a striking similarity at all plots at all three study sites, where most individuals had established between 1950 and 1960, and none had after 1982.

Climate-growth relationships at R2

Only one chronology (Forest) exceeded an EPS value of 0.85 during the 20th century and, subsequently, was used for the calculation of climate-growth relationships. The standard chronology showed some significant correlation and responses to temperature, but none was very strong or stable over time. No significant correlation existed with precipitation. The residual chronology showed significant

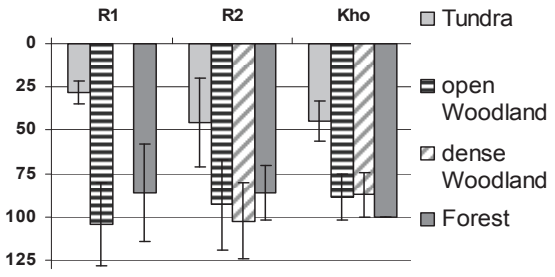

Figure 1. Minimum thaw depth (in cm) across the forest–tundra transect; error bars are standard deviation.

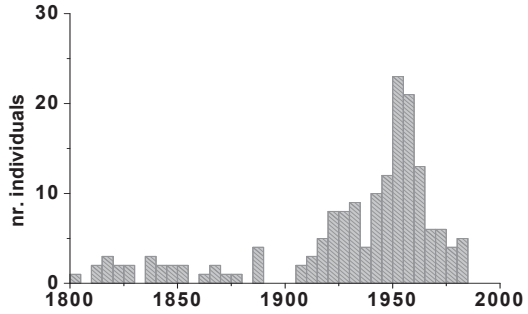

Figure 2. Establishment date of trees and seedlings on all plots since 1800. Note distinct peak between 1950 and 1960.

strong negative correlation and response functions to previous July (mostly consistent over time) and also partly to previous June and August temperatures; and significant strong positive correlation and response functions to current June and July temperatures (inconsistent over time).

All other chronologies did not exceed the 0.85 EPS threshold. Preliminary analyses of individual trees and seedling groups revealed differing growth responses, with increasing influence of precipitation closer to tundra areas.

Discussion and Conclusions

Tree line advance not only depends on favorable climatic conditions, but also on suitable microsites (Lloyd & Fastie 2002). In northwest Russia, where recent warming has not been pronounced and concentrated on spring and summer, no recent establishment in forest or woodland has occurred. In fact, most seedlings established 50–60 years ago in a period of winters warmer than and summers slightly cooler than today. No seedlings have established after 1982, the period of strongest warming in spring and summer. While established trees show positive correlations with warmer summers (growth year), they also show a drought stress-like signal of negative correlations to previous July temperatures, as reported from boreal forest and tree line areas in Alaska (Barber et al. 2000, Wilmking et al. 2004). More analysis is necessary to confirm these results.

The possible influence of precipitation on growth of seedlings in the woodland plots seems to point to the additional influence of microsite conditions on growth. Active layer depth (and thus the distance to the local water table) varies on very small scales, partly following the microtopography, and seedlings often establish on top of hummocks. There, soil temperatures are higher, and no waterlogging occurs. However, the top of hummocks are prone to drying. Preliminary analysis revealed strong, mostly positive correlations of seedling growth with summer precipitation. Higher precipitation might be counteracting drought during the warmest part of the year.

Our preliminary investigation points to a complex interaction between climate (temperature and precipitation) and microsite drivers (active layer depth) for the establishment of trees in the tundra areas of northwest Russia, warranting further investigations. Our plans include the inclusion of two additional sites in the calculation of the climate growth relationships of established trees and seedlings, and a more sophisticated analysis of the actual microsite conditions of each sampled individual.

Acknowledgments

This study was supported by a Sofja Kovalevskaja Award from the Alexander von Humboldt Foundation (M. Wilmking), the German National Scholarship Foundation (S. Kenter), and the EU-Project CARBO-North (6th FP, Contract No. 036993).

References

Barber, V., Juday, G. & Finney, B. 2000. Reduced growth of Alaska white spruce in the 20th century from temperature-induced drought stress. *Nature* 405: 668-72.

Biondi, F. & Waikul, K. 2004. DENDROCLIM2002. A C++ program for statistical calibration of climate signals in tree ring chronologies. *Computers & Geosciences* 30: 303-11.

Chapin, F.S. et al. 2005. Role of land-surface changes in Arctic summer warming. *Science* 310: 657-660.

Lloyd, A.H. & Fastie, C.L. 2002. Spatial and temporal variability in the growth and climate response of treeline trees in Alaska, *Climatic Change* 52: 418-509.

Wilmking, M., Juday, G.P., Barber, V.A. & Zald, H.S.J. 2004. Recent climate warming forces opposite growth responses of white spruce at treeline in Alaska through temperature thresholds. *Global Change Biology* 10: 1724-36.

Wilmking, M., Harden, J. & Tape, K. 2006. Effect of tree line advance on carbon storage in NW Alaska. *JGR* 111: G02023, doi:10.1029/2005JG000074.

Bathymetric Mapping of Lakes in the Western Arctic Coastal Plain, Alaska

Barry Winston
University of Cincinnati, Cincinnati, USA
Kenneth Hinkel
Department of Geography, University of Cincinnati, Cincinnati, USA
Richard Beck
Department of Geography, University of Cincinnati, Cincinnati, USA

Introduction

The Arctic Coastal Plain (ACP) of northern Alaska is characterized by thousands of lakes developed atop continuous permafrost. This region can be subdivided into the Younger Outer Coastal Plain (YOCP), the Outer Coastal Plain (OCP), and the Inner Coastal Plain (ICP) (Hinkel et al. 2005), which are demarcated by ancient shorelines at 23–29 m. a.s.l. and 7 m a.s.l. (Hopkins 1973, Péwé 1975). These subregions can be further differentiated by surficial sediments that reflect the effects of recent geomorphic processes, with fine-grained marine sediments associated with the OCP and YOCP and eolian sand characteristic of the ICP (O'Sullivan 1961, Williams et al. 1978, Williams 1983). Lakes are significantly different among these three subregions with respect to lake surface area, depth, and lake density (Hinkel et al. 2005).

Many lakes on the ACP have depths of less than 2 m (Carson & Hussey 1962). Such lakes are shallow enough that water freezes to the lake bottom during winter and is continuous with the underlying permafrost. However, in the case of deeper lakes, water at depth remains unfrozen. With water temperature above freezing, the underlying permafrost begins to thaw, thereby creating a thaw bulb. The thaw bulb expands and the substrate slowly subsides as it loses volume when pore ice is converted to water. As the lake grows larger and deeper over time, the thaw bulb beneath the lake expands, the underlying permafrost thaws, and the ground subsides further. It is possible for the thaw bulb to reach the maximum depth of permafrost (>300 m) in large, deep lakes, resulting in the formation of an open talik (French 2007).

Several models for lakes on the ACP suggest that these features develop, expand, and drain as part of a cyclical process (Cabot 1947, Carson & Hussey 1962, Everett 1980, Billings & Peterson 1980). However, recent research suggests that lake evolution is more complex and may not be applicable across the entire ACP (Jorgenson & Shur 2007). The goal of this study is to gather basic bathymetric and sedimentological information from these small, deep lakes. They appear to be fundamentally different from the well-studied lakes of the OCP that were used to develop the thaw-lake cyclical model.

Study Area and Methodology

The lakes reported on here are all with 32 km of our base camp at 70°0′N and 153°5′W. They are located within the ICP and are characterized by deep central basins and prominent shelves composed of sand deposits. Bathymetric data were collected along transects from 17 lakes during late summer 2007 to determine general basin depth, slope, and morphological characteristics.

Depth measurements from the lakes were recorded with an Eagle SeaCharter 502c DF iGPS sonar mounted to the stern of the vessel. The sonar was equipped with a 50/200 kHz dual-frequency transducer that was positioned approximately 15 cm below the water surface. The GPS was calibrated to UTM Zone 5 North, NAD-1983 and had a locational accuracy better than 3 m. The data were collected by making a series of transect passes across the lakes, recording both depth and location once every second. The distance between each sample was estimated during post-processing of the GPS locations. The slope was calculated between each pair of samples using the depth measurements.

Results and Conclusions

Out of the 17 lakes sampled, 7 lakes contained deep basins that exceed a depth of 10 m; the maximum recorded depth in one lake was 19 m. These 7 lakes contained shallow shelves that declined into deep basins over short distances. However, the deep basins were not always located in the center of the lake, and several lakes contained multiple basins or exhibited discontinuous basins.

The shelves were very shallow (0.3–3 m), with dunes and ripples apparent in the sandy sediment. The basin floors were relatively flat (1–2°), and the shelf-basin transition area averaged 30°. However, for the 2 transects shown in Figures 1 and 2, a slope of 54° was estimated in Lake A, and a slope of 44° was determined in Lake B.

The sandy lake bottom sediments should have an angle of repose no greater than 35° (Stegner & Wesfreid 1999). However, in the case of the 2 observed lakes, the slope was significantly greater. This suggests that the shelf sediments are bonded by permafrost, since unconsolidated sand cannot maintain the observed slope.

It is not known if the permafrost is syngenetic, and aggraded upward with sediment deposition along the lake margin. The association of the deepest lake basins (~18 m) with oversteepened slopes suggests thaw bulb development and subsidence. However, thaw consolidation is typically not very effective in sandy sediments unless significantly enriched in ice. Jorgenson & Shur (2007) indicate that near-surface sediment cores from this region of the ACP have not evidenced ice oversaturation. Subsequent fieldwork on lakes in the ACP will focus on mapping lake bathymetry,

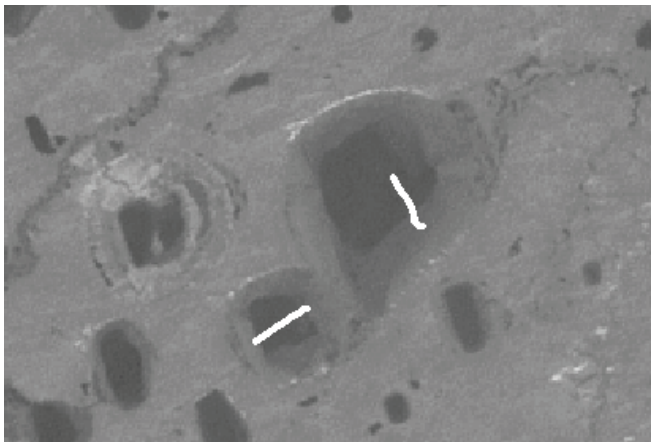

Figure 1. Landsat-7 grayscale image showing two sampled lakes. White lines indicate data acquisition path. For reference, Lake A is on the left; Lake B is on the right.

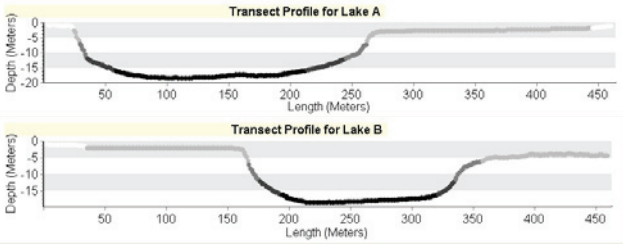

Figure 2. Associated transect profiles. Transect in Lake A is from west to east; transect in Lake B is from south to north.

collecting bottom cores, and conducting ground penetrating radar investigations.

Acknowledgments

This work was supported by the NSF under grants 9732051 & 0094769 to KMH and 0548846 & 0539167 to W. Eisner. Any opinions, findings, or conclusions expressed in this material are those of the authors. We appreciate support from the Barrow Arctic Science Consortium and the Ukpeagvik Inupiat Corporation.

References

Billings, W.D. & Peterson, K.M. 1980. Vegetational change and ice-wedge polygons through the thaw-lake cycle in Arctic Alaska. *Arctic and Alpine Research* 12: 413-432.

Cabot, E.C. 1947. The northern Alaska coastal plain interpreted from aerial photographs. *Geographical Review* 37: 369-648.

Carson, C.E. & Hussey, K.M. 1962. The oriented thaw lakes of northern Alaska. *Journal of Geology* 70: 417-439.

Carter, L.D. 1981. A Pleistocene sand sea on the Alaskan arctic coastal plain. *Science* 211: 381-383.

Everett, K.R. 1980. Landforms. *Geobotanical Atlas of the Prudhoe Bay Region, Alaska.* Hanover, NH: U.S Army Cold Regions Reserve.

French, H.M. 2007. *The Periglacial Environment,* 3rd ed. England: John Wiley and Sons Ltd.

Hinkel, K.M., Frohn, R.C., Nelson, F.E., Eisner, W.R. & Beck, R.A. 2005. Morphometric and spatial analyses of thaw lakes and drained thaw lake basins in the western Arctic coastal plain, Alaska. *Permafrost and Periglacial Processes* 16: 327-341.

Hopkins, D.M. 1973. Sea level history in Beringia during the last 210,000 years. *Quaternary Research* 3: 520-540.

Jorgenson, M.T. & Shur, Y. 2007. Evolution of lakes and basins in northern Alaska and discussion of thaw lake cycle. *Journal of Geophysical Research* (in press).

O'Sullivan, J.B. 1961. *Quaternary geology of the Arctic Coastal Plain, northern Alaska*. Ph.D. Dissertation. Ames: Iowa State University Science and Technology.

Péwé, T.L. 1975. *Quaternary Geology of Alaska*. U.S. Geological Survey Professional Paper 835.

Stegner, A. & Wesfreid, J.E. 1999. Dynamical evolution of sand ripples under water. *Physical Review* 60: 3487-3490.

Williams, J.R. 1983. *Engineering-Geologic Maps of Northern Alaska, Meade River Quadrangle.* U.S. Geological Survey Open File Rep. 83-294.

Williams, J.R., Carter, L.D. & Yeend, W.E. 1978. Coastal Plain Deposits of NPRA, In: K.A. Johnson (ed.), *The U.S. Geological Survey in Alaska: Accomplishments During 1977*. Reston, VA: USGS, Circ. 77-2 B.

Digitizing Regional Permafrost Maps for Central and Eastern Asian Permafrost Mapping

Lizong Wu
Cold and Arid Regions Environmental and Engineering Research Institute, CAS, Lanzhou 730000, China
Xin Li
Cold and Arid Regions Environmental and Engineering Research Institute, CAS, Lanzhou 730000, China
Jerry Brown
International Permafrost Association, P.O. Box 7, Woods Hole, MA 02543, USA

Introduction

Permafrost and seasonally frozen ground regions occupy approximately 24% and 60%, respectively, of the exposed land surface in the Northern Hemisphere. The actual area underlain by permafrost is approximately 12% to 18% of the exposed land area. Accelerated warming of permafrost in mountainous, highland, and plateau regions of Asia will result in disequilibria of the water cycle, increased mass wasting processes, and related sediment transport and slope hazards. Without a unified and verified regional permafrost map, these processes cannot be assessed adequately.

Although national permafrost maps exist for China, Kazakhstan, Mongolia, and Russia, there is no consistent cartographic for mountainous and high altitude regions. The existing classifications based on spatial continuity or percentage distribution and ground ice content have limited application for mountainous or plateau regions. The 2001 International Symposium on Mountain and Arid Land Permafrost held in Mongolia recommends that an international team of experts is required to prepare a uniform map of Central Asia permafrost. A team for central and eastern Asian permafrost mapping was established during the workshop on Permafrost of Central and Eastern Asia held in China (2006). The members agreed to digitize and archive the recent permafrost map, and auxiliary information exists for China, Kazakhstan, Mongolia, and Russia to complete a pilot map with a unified legend. Classification-based temperature and/or thermal stability was recommended to employ in this work (Brown et al. 2006). The WDC for Glaciology and Geocryology at Lanzhou was expected to organize the digitizing of the permafrost maps for the four countries.

Regional Permafrost Maps Resource

China

Permafrost mapping study in China began in the 1960s. After that, regional permafrost distribution maps for Da and Xiao Xing'anling Mountain (1:2,000,000), Tianshan Mountain (10,000,000), and Qilian Mountain (1:10,000,000) were completed in 1980, 1981, and 1983, respectively (Cheng 1999). Permafrost mapping for the plateau regions began in the 1980s; the permafrost map along the Qinghai-Tibetan Highway (1:600,000) was published in 1981, and the permafrost map of the Qinghai-Tibetan Plateau (1:3,000,000) was finished in 1996 (Tong et al. 1983, Li et al. 1996).

Up to now, there are three permafrost maps that exist for all of China's land territory. The first one, entitled "Map of Snow, Ice and Frozen Ground in China" compiled by Yafeng Shi, was published in 1988 (Shi et al. 1988). The "Map of Geocryological Regionalization and Classification in China," at a scale of 1:10,000,000, was published in 2000 (Qiu et al. 2000). The map was digitized by T. Zhang and collected by NSIDC at Boulder. The latest version contained in the "Map of the Glaciers, Frozen Ground and Deserts in China" was published in 2006 at a scale of 1:4,000,000 (Wang et al. 2006). The classification used in these maps is based on spatial continuity or percentage distribution and elevation.

Thermal stability was used to classify permafrost on Tibet by Nan, performed upon the analysis of mean annual ground temperature distribution features from 76 observed data (Nan et al. 2002).

In the last two years, most of these maps have been digitized, and an attempt to merge different sources was carried out at the WDC for Glaciology and Geocryology, Lanzhou to obtain a more detailed permafrost map.

Russian

Beginning in 1995, geocryological maps published in the USSR (former Soviet Union) and Russia were identified and catalogued to form an inventory. This bibliography was compiled in 1998 by Irena Streletskaya and Marina Leibman, Earth Cryosphere Institute Russian Academy of Sciences, Siberian Branch. The detail information can be browsed from the Frozen Ground Data Center of NSIDC (NSIDC).

The "Geocryological Map of Russia and Neighbouring Republics" by Yershov at a scale of 1:2,500,000, with four attached maps at a scale of 1:25,000,000, were published between 1991 and 1996. An English-language description of the map and its compilation procedure are given by Zaitsev et al. (1998).The map divides permafrost zones by both percent of coverage and ground temperatures at the depth of zero amplitude. So the present legends can be used as reference classification in compiling the other permafrost maps.

The map project used is identified only as "conic equidistant projection," and lacks specific information on the projection. After the digitizing of the map, a geometry correction has been conducted.

Kazakhstan

An unpublished map of Kazakhstan was available and presents the distribution of mountain permafrost and legend. Dr. Sergei S. Marchenko from the Geophysical Institute,

University of Alaska Fairbanks, offers the original data of the map. The map divides permafrost zones by both altitudinal belts and ground temperatures (Brown et al. 2006).

A second mapping effort by Marchenko will prepare a modeled map of the four-country Altai Mountain region, showing the computed extent of permafrost and estimated MAGT at 20 m depth.

Mongolia

The "Map of Geocryology and Geocryological Zonation of Mongolia" was derived from the National Atlas of Mongolia and collected by the Frozen Ground Data Center of NSIDC. The Mongolia maps have 14 different terrain classifications determined according to elevation, mean annual air temperature, permafrost thickness and thaw depth, and seasonal frozen ground freeze depth (NSIDC).

Next Step

All of the maps mentioned above have been digitized at the WDC for Glaciology and Geocryology in Lanzhou. The next step is to develop a merged regional permafrost map of central and eastern Asia. A thermal stability-based classification system (Cheng 1984) is proposed to be used.

Acknowledgments

This work is supported by the Ministry of Science and Technology of China project "Data-sharing Network of Earth system" and the NSFC (National Science Foundation of China) project "Environmental and Ecological Science Data Center for West China."

References

Brown J., Marchenko, S., Li, X. et al. 2006. *Report for the Workshop on Classification, Mapping and Monitoring of Permafrost of Central and Eastern Asia*. Lanzhou, China.

Cheng, G.-D. 1984. Problems of zonation of high-altitude permafrost. *ACTA Geographica Sinica* 39(2): 185-193.

Cheng, G. 1999. Glaciology and geocryology of China during the past 40 years: Progress and prospects. *Journal of Glaciology and Geocryology* 21(4): 289-310.

Li, S. & Cheng, G. 1996. *Map of Frozen Ground on Qinghai-Xizang Plateau*. Lanzhou: Gansu Culture Press.

Nan, Z., Li, S. & Liu, Y. 2002. Mean annual ground temperature distribution on the Tibetan Plateau: Permafrost distribution mapping and further application. *Journal of Glaciology and Geocryology.* 24(2): 142-149.

NSIDC. http://nsidc.org/fgdc/

Qiu, G., Zhou Y., Guo, D. et al. 2000. *The Maps of Geocryological Regionalization and Classification in China (1:10,000,000)*. Beijing: Science Press.

Shi, Y. 1988. *Map of Snow, Ice and Frozen Ground in China*. Beijing: China Cartographic Publishing House.

Tong, B., Li, S., Bu, J. et al. 1983. Principle and method of compilation of permafrost map (1:600,000) along Qinghai-Xizang (Tibet) Highway. *Proceedings of the Second International Conference on Permafrost (Selection)*. Lanzhou: Gansu People's Publishing House, 75-80.

Wang T. (ed.) 2006. *Map of the Glaciers, Frozen Ground and Deserts in China (1:4,000,000)*. Beijing: Sino Maps Press.

Challenges of Infrastructure Growth on a University Campus in Discontinuous Permafrost

Frank Wuttig
Shannon & Wilson, Inc.

Introduction

The University of Alaska Fairbanks (UAF) campus is located in a transition zone from the southern edge of a broad upland area down onto lowlands of the Chena and Tanana Rivers (Fig. 1). The campus is underlain by warm discontinuous permafrost.

The main portions of the campus, including Lower Campus and West Ridge, are on a low east–west trending ridge overlooking the lowlands to the south. The distribution and character of the permafrost has affected and continues to affect the development of the campus and surrounding infrastructure.

This abstract describes the geologic and permafrost setting of the campus and surrounding area, and describes some of the effects permafrost has had on design and construction of campus facilities.

The majority of campus development has occurred on the crest or southern slope of the ridge, which is generally free of permafrost and permafrost-related features. Development becomes more challenging in discontinuous permafrost areas north of the ridge crest and on the lowlands south of the ridge. This abstract discusses four campus infrastructure projects impacted by permafrost, as well as challenges and lessons learned from developing the projects.

Geologic and Permafrost Setting

The upland ridge is underlain by loess-covered schist bedrock, and bedrock outcrops are found at the east end of campus. The windblown silt is retransported downslope to the north and south of the ridge crest. The lowlands consist of vegetated floodplains and low benches cut by the Tanana and Chena Rivers. Soils in the lowlands typically consist of interbedded alluvial sands and gravels mantled by silty overbank deposits dissected by filled sloughs and oxbow lakes representing former river channels.

A large, low-angle fan of retransported loess emanating from the nearby Cripple Creek Valley onto the lowland covers the southwest portion of the area. The distal (leading) edge of the silt fan is scalloped where it has been eroded by former channels of the Chena River. Soils along the leading edge of the fan have been mapped as silt-filled meander scars. Terrain units mapped by Pewe (1976) are shown in Figure 1.

The silt fan is generally underlain by continuous permafrost, with a low to moderate ice content, occurring primarily as pore ice with some segregated ice as seams and lenses.

Permafrost on the floodplain is generally discontinuous. Surficial soils on the floodplain have low to moderate ice content. The underlying sands and gravels typically have low moisture contents.

Retransported silt permafrost on the north-facing slopes and in the valley bottoms is typically perennially frozen with moderate to very high ice content in the form of pore ice, segregated ice as seams and lenses, and massive ice associated with ice wedge deposits.

International Arctic Research Center

The International Arctic Research Center (IARC), founded on windblown silt in the West Ridge area of the UAF campus, was originally designed to sit north of Koyukuk Drive in line with the front of the adjacent Elvey building. A portion of the proposed footprint extended into a forested area north of the ridge crest. Exploratory drilling showed the area to be underlain by discontinuous ice-rich silt permafrost. Long-term thaw settlement concerns resulted in a shift of the building footprint to the south into Koyukuk Drive and a reroute of the road south of the structure.

In the first year following construction of the facility, the sidewalk slab in front of the main entry heaved, blocking the front entrance. The slab was constructed on a thin layer of nonfrost-susceptible fill overlying a frost-susceptible silt fill and a silt subgrade. It was postulated that the heaving was likely aggravated by construction water, which was used to compact the silt fill beneath the sidewalk. Heaving has not been a problem in subsequent years.

West Ridge Research Building

The multi-storied West Ridge Research Building (WRRB) is north of the Elvey Building in the West Ridge area of the UAF campus. The structure is north of the east–west trending ridge crest in an area originally developed as a parking area for adjacent buildings. Numerous ground collapses, some more than 7 m deep, have developed along the northern edge of the parking lot, the result of concentrated surface runoff entering thermokarst voids in the subsurface.

Subsurface exploration of the area showed the southern portion of the parking area immediately behind the Elvey Building had suitable conditions for a deep, conventional foundation consisting of thawed and low-moisture-content silt permafrost. The northern portion of the lot was not suitable for construction due to known thermokarst and thaw-unstable silt permafrost. However, the footprint of the structure was extended out into the northern portion of the parking area. During construction, large voids and massive ice representing degrading ice wedges were encountered in the northern portion of the foundation excavation. To reduce the potential for thermokarst collapse beneath the structure

foundation, additional subexcavation to a depth below the anticipated base of thermokarsts and ice wedges was completed and the base of the excavation probed on a tight grid for additional thermokarst voids and ice. The northern foundation wall of the structure was redesigned as a deep grade beam that could span localized settlement in the event undetected thermokarsts were present.

Harper Building

The Harper Building is near the southern edge of the campus along Geist Road. The building is on the floodplain at the leading edge of the silt fan in an area of meander scars. Ice-rich organic silts and inorganic silts were encountered to depths averaging about 3.6 m. Localized peat deposits occurred at the site outside the building footprint. Thaw-unstable sand and silty sands extended to depths averaging 7.3 m; slightly thaw-unstable gravels occurred below this depth. The building is founded on steel pipe adfreeze piles bearing in the underlying gravels. The structure was designed to be elevated to provide a free air space beneath the building and protect the permafrost from thawing.

Since construction, the free air space of the structure was skirted and passively heated, resulting in more than 60 cm of differential settlement beneath the pile and grade-beam-supported floor. Connections to buried utilities, not designed to withstand building settlement, have reportedly failed. Landscaped areas and driveways have experience significant amounts of differential settlement.

Main Entrance Roads

The main entrance to the university at time of the last permafrost conference in Fairbanks in 1983 was along Fairbanks Street off Geist Road. A four-lane overpass was constructed at the railroad tracks along this access. The center span of the three-span bridge is supported on strip footings founded on colluvium and shallow bedrock. The bridge abutments were founded on continuous footings bearing in the embankment fill on either side of the tracks. The north abutment and center piers were founded on thaw-stable soils, whereas the southern approach embankment was constructed on highly thaw-unstable slough deposits at the leading edge of the silt fan. The southern abutment subsequently settled approximately 1 m, rendering the bridge unsafe.

A new access road to the university (Thompson Drive) was constructed across permafrost terrain in 2005 and 2006. The majority of the alignment is located on silt fan deposits, which are perennially frozen and slightly to moderately thaw-unstable. Cleared farm fields were thawed to a depth of 9 m.

Thompson Drive was constructed using experimental passive refrigeration systems in areas underlain by shallow permafrost, including a system of insulation, nonfrost-susceptible fill, and hairpin thermosyphons completely buried in the road bed at the southern end of the project, shoulders ventilated with a layer of coarse rock in the center of the project, and an air convection embankment at the northern end of the project. The bridge over the railroad is founded on permafrost schist bedrock, and alluvial sands and gravels underly the site.

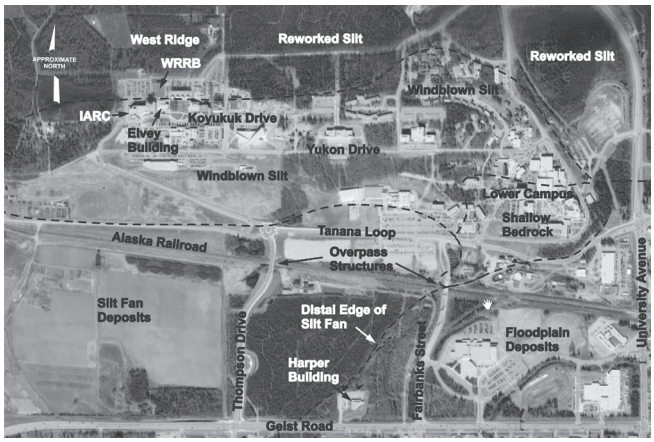

Figure 1. UAF campus and terrain units mapped by Pewe (1976).

References

Pewe, T.L. & Bell, J.W. 1976. Map *Showing Foundation Conditions in the Fairbanks D-2 SW Quadrangle, Alaska*. U.S. Geological Survey Map I-829-E.

Modeling and Monitoring Ecosystem Performance of Boreal Forests in the Yukon River Basin

Bruce K. Wylie
ASRC Research and Technology Solutions, contractor to U.S. Geological Survey (USGS)
Earth Resources Observation and Science (EROS) Center

Li Zhang
SAIC, contractor to USGS EROS

Norman Bliss
ASRC Research and Technology Solutions, contractor to U.S. Geological Survey (USGS)
Earth Resources Observation and Science (EROS) Center

Lei Ji
ASRC Research and Technology Solutions, contractor to U.S. Geological Survey (USGS)
Earth Resources Observation and Science (EROS) Center

Larry Tieszen
U.S. Geological Survey, Earth Resources Observation and Science Center, Sioux Falls, South Dakota

W.M. Jolly
U.S. Department of Agriculture Forest Service, Fire Sciences Laboratory, Missoula, Montana

Introduction

We emphasize the ability to quantify ecosystem processes, not simply changes in land cover, across the entire period of the remote sensing archive (Wylie et al., in press). The method builds upon remotely sensed measurements of vegetation greenness for each growing season. However, a time series of greenness often reflects annual climate variations in temperature and precipitation. Our method seeks to remove the influence of climate so that changes in underlying ecological conditions are identified and quantified. We define an "expected ecosystem performance" to represent the greenness response expected in a particular year given that year's climate. We distinguish "performance anomalies" as cases where the ecosystem response is significantly different from the expected ecosystem performance. Performance anomaly maps and anomaly trends provide valuable information on the ecosystem for land managers and policy makers at 1-km resolution. The results offer a prototype to assess the entire Yukon River Basin, a task slated for completion with our Canadian counterparts for the entire archival period (1984 to current) at 1 km and at 250 m (2000 to current).

Methods

A regression tree model was developed to predict growing season Normalized Difference Vegetation Index (NDVI), or expected ecosystem performance, from nearly 14,000 random pixels, which represents a range of annual climatic conditions and numerous site conditions. We used 1-km Advanced Very High Resolution Radiometer NDVI 7-day composites integrated from April through the first week of October as a proxy for ecosystem performance. Using spatial climatic data and site potential information, annual maps of expected growing season NDVI from 1996 to 2004 were constructed from this model.

Site potential is the historical performance related to elevation, slope, aspect, soils, and other factors. Dry years have lower expected ecosystem performance, and wet years have higher expected ecosystem performance. Areas that do not perform within a normal range determined by the regression tree model's expected error were identified as ecosystem performance anomalies. These anomalies are areas that responded to climatic conditions differently from areas with similar expected ecosystem performance.

The anomalies were validated using Composite Burn Index data from selected fires and Landsat spectral indices across a burned-to-unburned gradient. Linear time series trends in the performance anomaly were mapped based on the significance and sign (positive or negative) of the slope.

Results

Expected ecosystem performance

Regression tree models predicted expected performance from site potential, climate data, and land cover ($R^2 = 0.84$) and showed little bias. Withheld test locations had similar mean standard error of regression values as those of the model development dataset. Regression tree committee models were used, wherein each regression tree model possessed five different regression trees, each trying to improve predictions made by the previous regression tree model. This resulted in over 500 different piecewise multiple regressions being employed.

Ecosystem performance anomaly

Significant ecosystem performance anomalies were determined at 90% confidence intervals of the expected ecosystem performance model. Underperforming anomalies correlated with recent fires. Composite burn index (Epting et al. 2005) from selected fires validated the ecosystem performance results. Landsat spectral indices were also

used to validate performance anomalies across a burned-to-unburned gradient. We investigated trends in post-fire performance anomalies and found that ecosystem performance in burned areas showed varying rates of recovery when compared to climatically-predicted expected ecosystem performance. This indicates that this approach identifies and quantifies post-fire vegetation succession, although ground validation of vegetation and surface cover are needed for further interpretation.

Areas with significant consistent performance anomalies over multiple years are likely boreal forests under environmental stress. Frequency and trend maps of performance anomalies emphasize areas which perhaps experience degrading permafrost, marked by dryness, insect infestations, or disease.

Areas with burn dates prior to the beginning of the study often exhibited positive trends during the study.

Conclusions

Our approach uses climate data to account for interannual variations in ecosystem performance. The ecosystem performance anomalies reflect ecological changes that are caused by factors other than climate or site potential. The underperforming areas documented in this study were strongly associated with burn disturbances. Based on climate, portions of the study reveal that boreal forest performance is declining, and the trend appears more severe with time.

Acknowledgments

The authors would like to thank Barry Baker of the Nature Conservancy for providing domain cluster data (Saxon et al. 2005) used to help map boreal forest site potential. Funding was provided by the USGS Earth Surface Dynamics and Land Remote Sensing programs, with work performed under USGS contract numbers 08HQCN0007 (B.K. Wylie), 03CRCN0001 (L. Zhang), and 08HQCN0007 (N. Bliss and L. Ji).

References

Epting, J., Verbyla, D. & Sorbel, B. 2005. Evaluation of remotely sensed indices for assessing burn severity in interior Alaska using Landsat TM and ETM+. *Remote Sensing of Environment* 96: 328-339.

Saxon, E., Baker, B., Hargrove, W., Hoffman, F. & Zganjar, C. 2005. Mapping environments at risk under different global climate change scenarios. *Ecological Letters* 8: 53-60.

Wylie, B.K., Zhang, L., Bliss, N., Ji, L., Tieszen, L. & Jolly, M. In press. Integrating modeling and remote sensing to identify ecosystem performance anomalies in the boreal forest, Yukon River Basin, Alaska. *Int. J. Digital Earth*.

Impact of Frozen Ground Change on Streamflow Hydrology Over the Lena Watershed in Siberia: A Preliminary Analysis

Daqing Yang, Ipshita Majhi, Doug Kane
Water and Environmental Research Center, University of Alaska Fairbanks
Tingjun Zhang
National Snow and Ice Data Center, University of Colorado

Permafrost limits the amount of subsurface water storage and infiltration that can occur, leading to wet soils and ponded surface waters, unusual for a region with such limited precipitation. Changes in climatic conditions significantly affect the thermal regimes of active layer and permafrost (Pavlov 1994, Kane 1997, Frauenfeld et al. 2004, Zhang et al. 2005). Warming of high latitude regions results in an increase of active layer and permafrost temperatures, a deeper active layer and talik development, lateral thawing of permafrost in discontinuous and sporadic permafrost regions, and finally northward movement of the permafrost boundaries (Serreze et al. 2000, Woo 1986, Zhang et al. 2005).

Studies show that near-surface permafrost temperature in northern Russia has increased by 0.6–0.7°C during the period 1970–1990 owing to higher air temperature and deeper snow cover over Siberia (Pavlov 1994). In some regions of Siberia, permafrost temperature has warmed more than 2°C (Zhang et al. 2005, Pavlov 1996), active layer thickness has increased by up to 20 to 30 cm, and talik over permafrost may have developed over the past several decades. It has been predicted that, under a moderate climatic warming scenario, changes in permafrost temperature and active layer thickness will become more significant in the next few decades in the Russian Arctic and Subarctic (Pavlov 1996, Lawrence & Slater 2005, Saito et al. 2007).

Changes in timing, duration, and thickness of seasonal freeze and thaw, talik development, and permafrost conditions have a significant impact on surface runoff and ground hydrology. Changes in active layer thickness directly affect groundwater storage and river discharge through partitioning surface runoff (Kane 1997). A deeper active layer delays the freeze-up dates of the active layer and allows drainage to occur later in the winter. Analysis of soil moisture data in the upper (1 m) layer in the former Soviet Union over recent decades reveals a long-term increasing trend of soil moisture north of 50°N, mainly due to precipitation increases of 10–30 mm every 10 years (Vinikov & Yeserkepova 1991). Observation records show that the absolute amount of water content increases 10–30 mm in the 1 m soil layer, and groundwater level rose by 50–100 cm in Siberia. This increased groundwater storage may result in underground water recharge to the river system, and consequently, a significant increase of runoff in the winter months.

Recent assessments of the large rivers in the Arctic (i.e., the Lena, Ob, and Yenisei—drainage areas between 2,400,000 and 3,000,000 km^2, and contributing more than 45% of the total freshwater inflow to the Arctic Ocean) identify significant changes in streamflow seasonal cycle (Yang et al. 2002, 2004a,b, Ye et al. 2003). For example, since the mid-1930s, the Lena River summer runoff has not changed significantly, but winter runoff has increased 25–80%. In the Yenisei River basin, summer runoff has decreased by 20–30%, and winter discharge has gone up by 35–110%. The Ob River has also experienced a winter runoff increase of 30–40%, and summer runoff has risen in July by 10%. Base (low) flow increases have been reported over Siberian regions and watersheds. This may indicate hydrologic response to climate and permafrost changes. The linkage between streamflow and permafrost changes is not well understood.

This study applies comprehensive statistical methods to examine the linkage between frozen ground and river streamflow changes. Statistical analyses include the combinations of multiple-correlation, stepwise regression, and linear correlation and regression techniques. These methods have been applied to data of river streamflow, temperature, precipitation, soil moisture, and active layer depth. This allows us to establish statistical relationships useful for identifying important climatic and permafrost factors to regional streamflow changes. Further, it helps to quantify lengths of memory of different variables (temperature, precipitation, snow cover, etc.) and their impact on interannual variation of river discharge.

More specifically, this study examines the relation among ground temperature, active layer depth and base flow changes. The focus of the analysis is placed on the regions/basins with significant changes, such as the Aldan tributary in the upper Lena basin, where ground temperatures and winter flows have increased significantly in the last 40–50 years. The results of this work are useful in assessing the impact of permafrost changes on long-term streamflow variations over large watersheds, and they improve our understanding of the processes and interactions among climate, permafrost, and hydrology systems in the arctic regions.

References

Frauenfeld, O., Zhang, T., Barry, R.G. & Gilichinsky, D.G. 2004. Interdecadal changes in seasonal freeze and thaw depths in Russia. *J. Geophys. Res.* 109: D05101, doi:10.1029/2003JD004245.

Kane, D.L. 1997. The impact of Arctic hydrologic perturbations on Arctic ecosystems induced by climate change. In: W.C. Oechel (ed.), *Global Change and Arctic Terrestrial Ecosystems.* Springer-Verlag Ecological Studies 124, 63-81.

Lawrence, D.M. & Slater, A.G. 2005. A projection of severe near-surface permafrost degradation during the 21st century. *Geophys. Res. Lett.* 32: L24401, doi:10.1029/2005GL025080.

Pavlov, A.V. 1994. Current change of climate and permafrost in the Arctic and Subarctic of Russia. *Permafrost and Periglacial Processes* 5: 101-110.

Saito, K., Kimoto, M., Zhang, T., Takata, K. & Emori, S. 2007. Changes in hydro-thermal regimes in frozen ground regions under global warming scenarios simulated by a high-resolution climate model. *J. Geophys. Res.* 112: F02S11, doi:10.1029/2006JF000577.

Serreze, M.C, Walsh, J.E., Chapin, E.C, Osterkamp, T., Dyugerov, M., Romanovsky, V., Oechel, W.C., Morison, J., Zhang, T. & Barry, R.G. 2000. Observation evidence of recent change in the northern high-latitude environment. *Climate Change* 46: 159-207.

Vinnikov, K.Ya. & Yeserkepova, I.B. 1991. Soil moisture: empirical data and model results. *J. Climate* 4: 66-79.

Woo, M.-K. 1986. Permafrost hydrology in North America. *Atmosphere-Ocean* 24(3): 201-234.

Yang, D., Ye, B. & Shiklomanov, A. 2004. Streamflow characteristics and changes over the Ob river watershed in Siberia. *J. of Hydrometeorology* 5(4): 69-84.

Yang, D., Ye, B. & Kane, D. 2004. Streamflow changes over Siberian Yenisei river basin. *J. of Hydrology* 5(4): 69-84.

Yang, D., Kane, D., Hinzman, L., Zhang, X., Zhang, T. & Ye, H. 2002. Siberian Lena river hydrologic regime and recent change. *J. Geophys. Res.* 107(D23): 4694, doi:10.1029/2002JD002542.

Ye, B., Yang, D. & Kane, D. 2003. Changes in Lena river streamflow hydrology: human impacts vs. natural variations. *Water Resources Research* 39(8): 1200, doi: .10.1029/2003WR001991

Zhang, T. 2005. Influence of the seasonal snow cover on the ground thermal regime: An overview. *Reviews of Geophysics* 43: RG4002, doi:10.1029/2004RG000157.

Zhang, T., Frauenfeld, O.W., Serreze, M.D., Etringer, A., Oelke, C., McCreight, J., Barry, R.G., Gilichinsky, D., Yang, D., Ye, H., Ling, F. & Chudinova, S. 2005. Spatial and temporal variability of active layer thickness over the Russian Arctic drainage basin. *J. Geophys. Res.* 110: D16101, doi:10.1029/2004JD005642.

Simulating the Effects of Wildfire on Permafrost and Soil Carbon Dynamics of Black Spruce Over the Yukon River Basin Using a Terrestrial Ecosystem Model

Shuhua Yi
Institute of Arctic Biology, University of Alaska Fairbanks
A. David McGuire
U.S. Geological Survey, Alaska Cooperative Fish and Wildlife Research Unit
Jennifer Harden
U.S. Geological Survey, Menlo Park, California

Introduction

Wildfire is considered an important disturbance agent in boreal forest ecosystems (Kasischke et al. 2006). It can affect high latitude carbon dynamics directly through combustion emissions, and indirectly through vegetation succession and removal of the surface organic layer, which might accelerate the degradation of permafrost and, hence, the release of soil carbon. At the regional scale, the direct effects of fire have received a lot of attention, but the evaluation of the indirect effects has been more limited because the appropriate tools have not yet been developed for application at the regional scale.

Research objectives and questions

In this study, we implemented a dynamic soil layer module in the Terrestrial Ecosystem Model (hereafter DSL-TEM) to answer the following questions: (1) What is the change of permafrost over the Yukon River Basin for periods before and after year 1976, when there was a shift in the Pacific Decadal Oscillation? (2) What is the effect of fire on permafrost? and (3) What is the effect of fire on carbon fluxes between the land surface and the atmosphere?

Model Description

TEM is a process-based ecosystem model that simulates carbon and nitrogen dynamics of plants and soils for terrestrial ecosystems. TEM has been widely used to investigate the effects of climate, carbon dioxide fertilization, and wildfire disturbances on the carbon dynamics of North America. Research has focused on developing TEM for applications in high latitudes, including incorporation of the Goodrich algorithm for calculation of soil temperatures for permafrost and seasonal frost regions; and incorporation of the hydrological module for methane production and transport for high latitude wetlands. In this study, further improvements have been made to account for the indirect effects of wildfire in developing the DSL-TEM. The DSL-TEM consists of four interaction modules: an environmental module, an ecological module, a fire disturbance module, and a dynamic soil layer module (Fig. 1). The environmental module has been evaluated and presented at previous scientific conferences (Yi et al. 2007).

Environmental module

The processes considered in the environmental module are

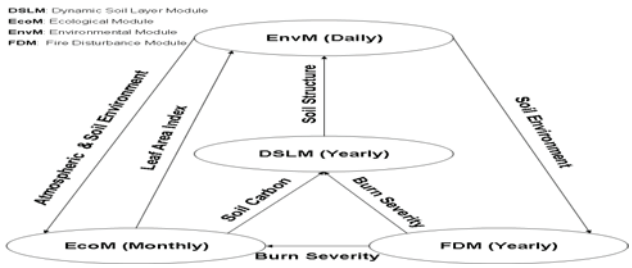

Figure 1. Overall structure of DSL-TEM.

canopy interception of snow and rain; drip and throughfall of snow and rain; canopy transpiration, evaporation, and sublimation; soil evaporation; snow sublimation; melt and accumulation; surface runoff; and subsurface baseflow. A Two-Directional Stefan Algorithm was first applied to simulate the freezing/thawing fronts in soil layers. Temperatures of snow/soil/rock layers were then updated by solving finite difference equations for layers above the first front, layers below the last front, and layers between the first and last fronts. Soil water contents of the unfrozen soil layer were updated by solving Richard's equations.

The above processes are simulated at a daily timestep. The monthly averaged soil temperature and moisture are then passed to the ecological module.

Ecological module

In addition to the carbon and nitrogen dynamics described in previous studies using TEM, a few new features are included in DSL-TEM, including explicit simulation of soil carbon vertical distribution and change of the thicknesses of organic layers based on the soil carbon content.

Soil carbon content of each layer is determined by the litter fall input and carbon decomposition. The above- and below-ground litter fall are assigned to each soil layer according to the fine root distribution. Carbon decomposition is calculated using the soil temperature, moisture, and carbon pool of each soil layer.

The carbon contents of the organic soil layer, including shallow organic and deep organic soil layers, are used to determine the thickness of organic layers, based on the relationship derived from field and laboratory measurements.

The simulated leaf area index is passed to the ecological module; the organic layer thicknesses are passed to the dynamic soil layer module.

Fire disturbance module

The fire disturbance module is run at an annual timestep. When a fire happens, it is used to calculate the fire severity based on the drainage (poorly drained and moderately drained), fire season (early season or late season), and fire size (small, large to ultra-large). The severity is used to calculate the burned organic layer thickness, which is then passed to the dynamic soil layer module.

The above- and below-ground living vegetation is also killed by wildfire. It is assumed that only 1% of above-ground vegetation remains alive, while the fraction of living below-ground vegetation depends on the burned organic layer thickness and the fine root distribution.

Dynamic soil layer module

The dynamic soil layer module is used to manipulate soil layer structures to maintain stability and efficiency of the soil temperature and moisture calculations, when the thickness of the organic layer is changed by wildfire disturbance and ecological processes. There are at most 2 moss layers, 3 shallow organic layers, and 3 deep organic layers. The minimum thickness of a soil layer is set to 2 cm. When an organic layer is too thin, it may be either removed or combined to an adjacent soil layer of the same type. When an organic layer is too thick, it will be divided into two layers.

Datasets

The input datasets include nonspatial datasets (atmospheric CO_2 concentration and fire size), grid-level datasets (0.5° by 0.5°, climate, fire return interval, fire season and soil texture), and pixel-level datasets (1 km by 1 km vegetation type, drainage, and fire history).

Three different cohort-level datasets have been created, based on grid- and pixel-level information. To initialize DSL-TEM, each cohort is run to an equilibrium state using the 1901–1930 mean climate, without disturbances. The equilibrium cohort is a unique combination of drainage, vegetation, and climate. During the next phase of simulation, the spinup stage, each cohort is run using 1901–1930 atmospheric data in a cyclic fashion that considers fire disturbance over the period 1001–1900. Thus the spinup cohort is a unique combination of equilibrium cohort and fire history during period 1001–1900. To save computing time, the fire history has been reclassified into several categories based on the first recorded fire occurrence after 1900. The final phase of the simulation results in a transient cohort that is a unique combination of a spinup cohort and both climate and fire history from 1901–2006.

Overall, for black spruce in the Yukon River Basin, there are 1,167 equilibrium cohorts, 6,858 spinup cohorts, and 40,738 transient cohorts. The total black spruce area in the Yukon River Basin is 213,513 km^2.

Model Experiment

The DSL-TEM was first run to equilibrium state in year 1000 and then through the spinup phase over the period from 1001–1900. A factorial experiment of 8 simulations was then performed over the period from 1901–2006, considering the effects of CO_2 fertilization (constant vs. transient CO_2), climate (constant vs. transient climate), and fire disturbance (with and without fire disturbance).

Results and Discussion

1. The mean annual air temperature increased 0.39 to 1.14°C over the Yukon River Basin (YRB) between 1950–1975 and 1976–2000. Winter precipitation (DJF) increased 4–20 mm at the eastern and western ends of the YRB, and decreased by 7–14 mm in the Tanana River, Eastern Central Yukon, and Koyukuk River sub-basins between the same time periods. The unfrozen column, which is defined as the mean thickness of unfrozen soil layer over a year, increased at both the eastern and westerns ends of the YRB, but decreased in the central YRB. This suggests that winter snowfall plays a more important role than air temperature in affecting permafrost dynamics between the two time periods.

2. For the whole YRB, climate plays a dominant role in determining the thermal state of soil. The effects of fire on soil thermal state are relatively small, in part due to the small fraction of burn area, and in part due to the decrease of winter snowfall in areas with high fire return interval.

3. Fire plays a dominant role in determining the net carbon flux between the land surface and the atmosphere, especially after 1985. The difference between simulations with and without fire can be 140 gC m^{-2}. However, the indirect effect of fire through increasing soil temperature on soil decomposition is relatively small, usually less than 10 gC m^{-2}.

Acknowledgments

We would like to thank other coauthors, including Eric Kasischke, Kristen Manies, Larry Hinzman, Anna Liljedahl, Jim Raderson, Heping Liu, Vladimir Romanovsky, Sergey Marchenko, and Kim Yongwon.

References

Kasischke, E.S. & Turetsky, M.R. 2006. Recent changes in the fire regime across the North American boreal region – Spatial and temporal patterns of burning across Canada and Alaska. *Geophysical Research Letters* 33: doi:10.1029/2006GL025677.

Yi, S., McGuire, A.D., Harden, J., Kasischke, E., Manies, K., Hinzman, L., Liljedahl, A., Randerson, J., Liu, H., Romanovsky, V. & Marchenko, S. 2007. A dynamic soil layer model for assessing the effects of wildfire on high latitude terrestrial ecosystem dynamics. *The 2007 Fall Meeting of American Geophysical Union, December 10–14, 2007, San Francisco, CA*.

Non-Linear Analysis of the Thermal Characteristics of Permafrost Embankment with Crushed-Rock Revetment and Insulation on Qinghai-Tibet Plateau

Mingyi Zhang, Shuangyang Li, Shujuan Zhang, Yuanhong Dong
State Key Laboratory of Frozen Soil Engineering, Cold and Arid Regions Environmental and Engineering Research Institute, Chinese Academy of Sciences, Lanzhou 730000, China

Introduction

The embankment with crushed-rock revetment has been widely used in the construction of the Qinghai-Tibet railway/highway and is an effective measure to ensure the thermal stability of permafrost embankment (Lai et al. 2003, 2004, Sun et al. 2004, Ma et al. 2002); however, because of the influence of global warming, it is difficult to protect the underlying permafrost from warming, even thawing (Wang et al. 1996). Therefore, in order to sufficiently protect the underlying permafrost, a numerical representation of the unsteady two-dimensional continuity, momentum, and energy equations of thermal convection for incompressible fluid in porous media (Nield et al. 1999, Kong et al. 2002) is used to analyze and compare the temperature characteristics of the embankments with crushed-rock revetment, with and without insulation, under the global warming in this study.

Results and Discussions

Based on the temperature and geology conditions on the Qinghai-Tibet Plateau (Cheng et al. 2003, Zhu et al. 1988, Qin, 2002, Lai et al. 2003), the temperature distributions of the three embankment models with crushed-rock revetment, with and without insulation (Fig. 1), constructed on July 15, are simulated and analyzed for 50 years.

Figure 2 is the temperature distribution of the embankment with crushed-rock revetment (1.60 m thick), without insulation on October 15, after 50 years of the construction. It can be seen from this figure that the location of the permafrost table (0°C isotherm) is y = -2.39 m under the natural ground surface, while that is y = -1.79 m in the centerline of the embankment and 0.60 m higher than that under the natural ground surface; furthermore, -0.2°C isotherm is high under the slope foot of the embankment, while low in the middle of embankment.

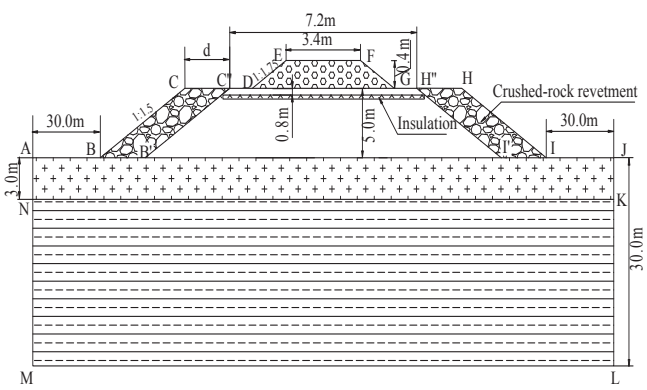

Figure 1. Embankment model with crushed-rock revetment.

Figure 3 shows the temperature distribution of the embankment with crushed-rock revetment (2.0 m thick), without insulation on October 15, after 50 years of the construction. From this figure, we find that the ground temperature distribution is similar to the embankment with crushed-rock revetment (1.60 m thick), without insulation (Fig. 1). In detail, the permafrost table (0°C isotherm) is y = -2.39 m under the ground surface, while that is y = -1.69 m and 0.03 m in the centerline and side slope of the embankment, respectively.

Based on the above the analyses, we can conclude that the embankments with crushed-rock revetment without insulation have an active cooling effect on the underlying permafrost, but cannot effectively reduce the underlying ground temperature. Furthermore, their cooling effects are strongest at the side slope foot, but weak in the middle. We

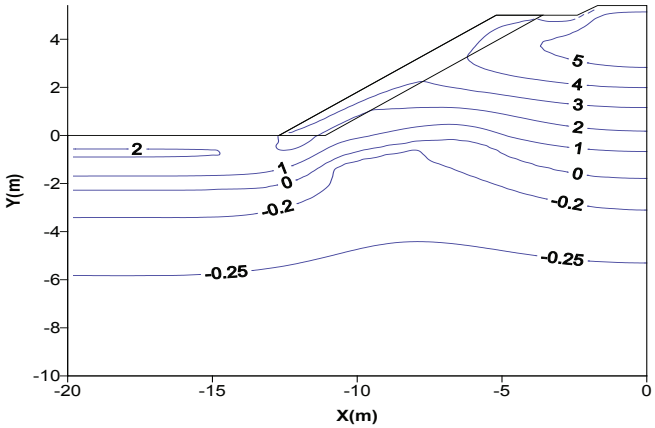

Figure 2. Temperature distribution of the embankment with crushed-rock revetment (1.60 m thick), without insulation on October 15, after 50 years of the construction (Unit: °C)

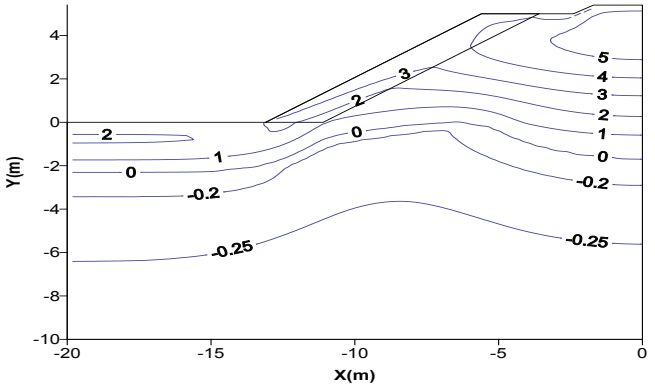

Figure 3. Temperature distribution of the embankment with crushed-rock revetment (2.0 m thick) without insulation on October 15, after 50 years of the construction (Unit: °C).

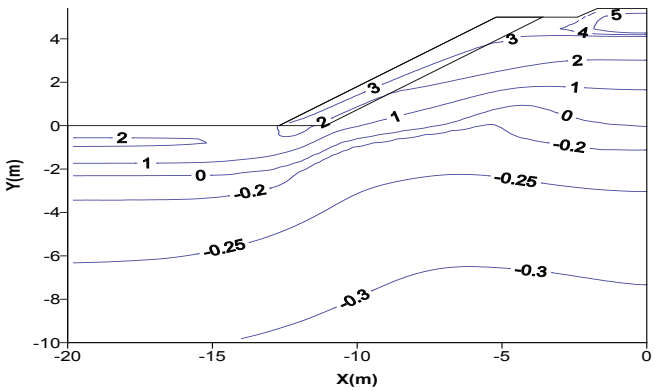

Figure 4. Temperature distribution of the embankment with crushed-rock revetment (1.6 m thick) and insulation on October 15, after 50 years of the construction (Unit: °C).

also find that when the thickness of a crushed-rock revetment reaches a certain value, its cooling effect on the middle part of embankment cannot be effectively increased by adding its thickness only.

Therefore, we propose the embankment with crushed-rock revetment (1.60 m thick) and insulation, namely, add insulation at the upside of the embankment with crushed-rock revetment.

Figure 4 is the temperature distribution of the embankment with crushed-rock revetment (1.6 m thick) and insulation on October 15, after 50 years of the construction. It can be seen from this figure that the permafrost table (0°C isotherm) is y = -2.39 m under the ground surface, while that is y = 0.05 m and 0.92 m in the centerline and side slope of the embankment, respectively. Furthermore, the temperature under the embankment is lower than those under the above two embankments without insulation (Figs. 1, 2), and -0.3°C isotherm still exists under the embankment. This shows that the embankment with crushed-rock revetment and insulation not only can raise the permafrost table, but also reduce the underlying permafrost temperature.

Therefore, it is proposed that, in warm permafrost regions, insulation should be used to increase the cooling effect of embankment with crushed-rock revetment; however, the insulation must be paved in the upper portion of the embankment.

Acknowledgments

This research was supported by the National Natural Science Foundation of China (Grant No. 40601023 and 40730736), the Knowledge Innovation Important Program of the Chinese Academy of Sciences (Grant No. KZCX3-SW-351).

References

Cheng, G.D., Jiang, H., Wang, K.L., et al. 2003. Thawing index and freezing index on the embankment surface in permafrost regions. *Journal of Glaciology and Geocryology* 25(6): 603-607.

Kong, X.Y. & Wu, J.B. 2002. A bifurcation study of non-Darcy free convection in porous media. *Acta Mechanica Sinica* 34(2): 177-185.

Lai, Y.M., Li, J.J., Niu, F.J. et al. 2003. Nonlinear thermal analysis for Qing-Tibet Railway embankments in cold regions. *Journal of Cold Regions Engineering* 17(4): 171-184.

Lai, Y.M., Zhang, S.J., Zhang, L.X. et al. 2004. Adjusting temperature distribution under the south and north slopes of embankment in permafrost regions by the ripped-rock revetment. *Cold Regions Science and Technology* 39(1): 67-79.

Ma, W., Cheng, G.D. & Wu, Q.B. 2002. Preliminary study on technology of cooling foundation in permafrost regions. *Journal of Glaciology and Geocryology* 24(5): 579-587.

Nield, D.A. & Bejan, A. 1999. *Convection in Porous Media,* 2nd ed. New York: Springer-Verlag.

Qin, D.H. 2002. *The Comprehensive Evaluating Report on the Environment Evolvement in West China*. Beijing: Science Press.

Sun, Z.Z., Ma, W. & Li, D.Q. 2004. Experimental study on the cooling effect air convection embankment crushed rock slope protection in permafrost regions. *Journal of Glaciology and Geocryology* 26(4): 435-439.

Wang, S.L., Zhao, X.F., Guo, D.X. et al. 1996. Response of permafrost to climate changes in the Qinghai-Xizang Plateau. *Journal of Glaciology and Geocryology* 18 (suppl): 157-167.

Zhu, L.N. 1988. Study of the adherent layer on different types of ground in permafrost regions on the Qinghai-Xizang Plateau. *Journal of Glaciology and Geocryology* 10(1): 8-14.

Interannual Variability of the Near-Surface Soil Freeze-Thaw Cycle Detected from Passive Microwave Remote Sensing Data in the Northern Hemisphere

Tingjun Zhang
National Snow and Ice Data Center, Cooperative Institute for Research in Environmental Sciences, University of Colorado at Boulder
Richard Armstrong
National Snow and Ice Data Center, Cooperative Institute for Research in Environmental Sciences, University of Colorado at Boulder

Introduction

Better knowledge and understanding of the near-surface freeze-thaw cycle of soils are prerequisite for evaluating the impact of cold season/cold region processes on surface and subsurface hydrology, regional and global climate, carbon exchange between the atmosphere and the land, and the terrestrial ecosystem as a whole. The challenge is to develop new techniques and methodologies to obtain data and information of the near-surface soil freeze-thaw cycle. A combined frozen soil algorithm using passive microwave satellite remote sensing data and numerical modeling was developed and validated to detect the near-surface soil freeze-thaw cycle over snow-free and snow-covered land areas. In this study, we use the NSIDC Frozen Soil Algorithm (Zhang & Armstrong 2001, Zhang et al. 2003) to investigate the interannual variability of the near-surface soil freeze-thaw cycle over the period from 1988 through 2006 in the Northern Hemisphere.

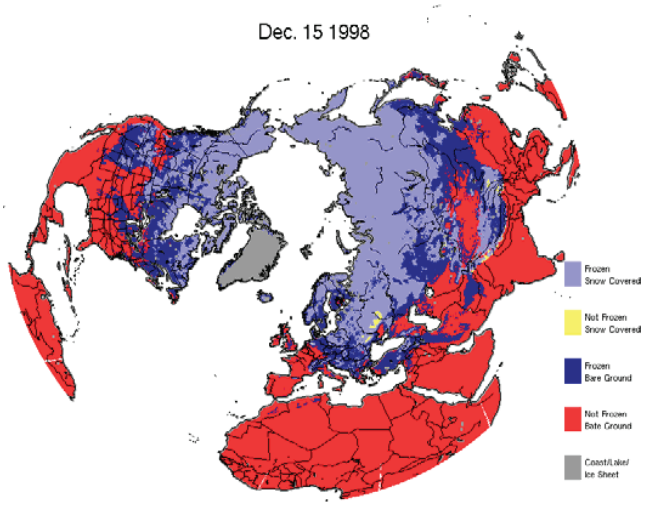

Figure 1. Distribution of the near-surface soil freeze on December 15, 1998, in the Northern Hemisphere.

Data and Methods

The NSIDC Frozen Soil Algorithm consists of two parts: (1) Over snow-free land surface, passive microwave satellite remote sensing algorithm was used to detect the near-surface soil freeze-thaw cycle; (2) Over snow-covered land surface, a one-dimensional heat transfer numerical model with phase change was used to detect soil freeze-thaw status under snow cover (Zhang & Armstrong 2001, Zhang et al. 2003). Using the Defense Meteorological Satellite Program's Special Sensor Microwave Imager (SSM/I) data, the passive microwave algorithm uses a negative spectral gradient between 19 GHz and 37 GHz, vertically polarized brightness temperatures, and a cut-off brightness temperature at 37 GHz with vertical polarization (T_B[37V]). SSM/I data and soil temperature data from 26 stations over the contiguous United States from the two-year period July 1, 1997, through June 30, 1999, were used to calibrate the algorithm (year 1), to validate the algorithm (year 2), and to demonstrate freeze/thaw classification (both years). A cut-off brightness temperature of 258.2 K was obtained based on a linear correlation ($r^2 = 0.84$) between the soil temperature at 5 cm depth and the T_B(37V). The NSIDC Frozen Soil Algorithm provides accuracy for frozen soil detection of about 76% and accuracy for the correct classification of both frozen and unfrozen soils of approximately 83% with a percent error of about 17%. We used the validated NSIDC Frozen Soil Algorithm to investigate the interannual and interdecadal variability of the timing, frequency, duration and number of days, and daily area extent of the near-surface soil freeze-thaw cycle over the period from 1988 through 2006 in the Northern Hemisphere.

Results

In the Northern Hemisphere, the near-surface soil starts to freeze in September, expanding southwards and reaching to maximum extent by January or February, then decreasing in area extent, disappearing in late May or early June. Figure 1 is a snapshot of area extent of snow cover and the near-surface soil freeze on December 15, 1998, detected from the NSIDC Frozen Soil Algorithm. Area extent of the near-surface soil freeze (Fig. 1, dark blue) is larger than that of snow cover (Fig. 1, light blue). Generally speaking, the near-surface soil freeze-thaw or seasonally frozen ground is the largest in extent among all cryospheric components. The timing of snow on ground is very critical for soil freeze/thaw status under snow cover. Snow may not be accumulated when the ground surface temperature is above 0°C, since snow will be melted when it reaches the ground. Soil may be thawed under thick snow cover (Fig. 1, yellow) this is because of the combined impact of geothermal heat flux and snow insulation effect.

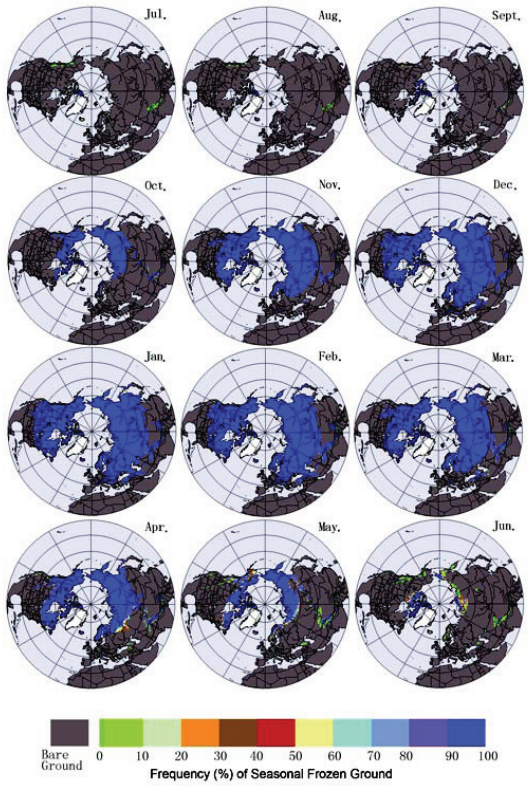

Figure 2. Climatology of monthly area extent of the near-surface soil freeze in the Northern Hemisphere over the period from 1988 through 2006, detected from the NSIDC Frozen Soil Algorithm.

Over the majority of the middle latitude regions and certainly whole high latitude regions, the near-surface soil experiences soil freeze-thaw cycle every year. Near-surface soils occasionally experience freeze in summer months over high elevation mountain areas (Fig. 2). The preliminary results indicate that the long-term average maximum area extent of the near-surface soil freeze-thaw, including permafrost regions, is about 65 x 10^6 km^2 or 68% of the land mass in the Northern Hemisphere (Fig. 2). The absolute maximum area extent can be up to 76 x 10^6 km^2 or 80% of the land mass in the Northern Hemisphere.

The number of days of the near-surface soil freeze varies from a few days in the middle or lower latitude region to several months over high elevation mountain regions and high latitude regions (Fig. 3). For High Arctic regions, such as in Siberia and northern Canada, the near-surface soil experiences up to nine months of freeze per year. As we move southwards, the number of days of soil freeze per year decreases gradually with clear zonal characteristics (Fig. 3).

Another feature is that mean length of a freeze-thaw cycle varies from a few days in middle and low latitude regions, to several months in high elevation mountain and latitude regions. Autumn and spring seasons at high latitude regions are very short, fluctuations of air temperature around 0°C are not as frequent as in the middle latitude regions. When the near-surface soil freezes in autumn at high latitudes, it is expected to be still frozen until next spring thaw.

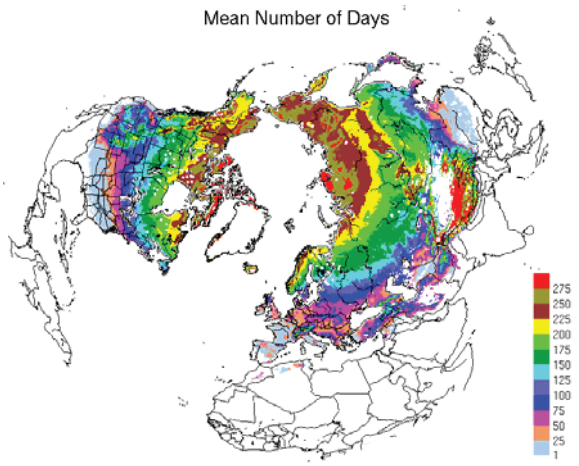

Figure 3. Mean number of days of the near-surface soil freeze in the Northern Hemisphere.

Meanwhile, frequency of the soil freeze-thaw cycle on average varies from more than 20 times in middle and low latitudes to less than 10 times in high mountain and elevation regions.

Based on results from passive microwave satellite remote sensing data, we have not detected any significant trends of changes in timing, duration, and frequency of the near-surface soil freeze-thaw cycle in the Northern Hemisphere from 1988–2006. However, further work is still needed to better validate the NSIDC Frozen Soil Algorithm. The current algorithm is validated using data from the contiguous United States. Data from other parts of the world are needed to further validate the algorithm.

Acknowledgments

We thank Jeff Smith at the National Snow and Ice Data Center (NSIDC), University of Colorado at Boulder, for preparing datasets and graphs. This study was supported by the U.S. National Aeronautics and Space Administration (NASA) grants 13721 and NNX06AE65G.

References

Zhang, T. & Armstrong, R. L. 2001. Soil freeze/thaw cycles over snow-free land detected by passive microwave remote sensing. *Geophysical Research Letters* 28(5): 763-766.

Zhang, T., Armstrong, R.L. & Smith, J. 2003. Investigation of the near-surface soil freeze/thaw cycle in the contiguous United States: Algorithm development and validation. *J. Geophys. Res*. 108(D22): 8860, doi:10.1029/2003JD003530.

Current State and Dynamics of Permafrost in the Siberian Platform

M.N. Zheleznyak
Melnikov Permafrost Institute SB RAS, Yakutsk, Russia
V.T. Balobaev
Melnikov Permafrost Institute SB RAS, Yakutsk, Russia
V.G. Rusakov
Melnikov Permafrost Institute SB RAS, Yakutsk, Russia

The Siberian Platform is a major geological structure in Asia located in the north-central part of the continent. A characteristic feature of the Siberian Platform is the widespread occurrence of permafrost, the thickness and areal distribution of which vary greatly depending on climatic conditions, topography, and the complex interaction of external and internal factors.

The geothermal data collected by the authors during the last 20 years were analyzed to provide a characterization of the geothermal field and permafrost conditions in the region. Heat flow varies across the Siberian Platform from 15 to 65 mW/m^2, and is determined by the structural and tectonic setting of the region. Thermal properties of rocks depend on the age, composition, and moisture content of the material, and vary widely from 1.2 to 7.3 W/m·K. Ground temperatures range from -5.0°C (in the presence of thick permafrost) to 16.0°C (where permafrost is absent) at depths of 500 m and from 0°C to 38.0°C at 1500 m, depending on the heat flow and rock type.

Permafrost occurs in 65% of the Siberian Platform. Its southern boundary is at 63°N latitude over most of the region, rising northwards to the latitude of Igarka in the west. Patches of frozen ground are encountered south of this boundary, where favorable local conditions exist.

The thickness of permafrost in the Siberian Platform varies from a few meters to as much as 1370 m in the Anabar Shield. It is determined by the ground surface temperature, the thermal properties of subsurface materials, and the geothermal heat flow. The latter two factors remain relatively constant over long periods of time, while the ground surface temperatures have changed repeatedly during the permafrost history. The present thermal state of the permafrost is mainly determined by the difference between the present-day temperature and the temperature in the last cold period (the Sartan) (Zheleznyak 2005).

The thermal state of the permafrost is in steady state in some parts of the region and in unsteady state in others.

The steady-state thermal regime is characterized by the constant position of the permafrost base due to the equal heat flows in unfrozen and frozen ground at the phase boundary. Equilibrium permafrost occurs in the areas composed of Early Mesozoic and Paleozoic sedimentary rocks or crystalline and metamorphic rocks. They occupy most of the Siberian Platform, the Verkhoyansk-Chukotka Folded Region, the Aldan-Stanovoy Massif, the Anabar Shield, and some minor uplifted basement blocks. The rocks comprising these structures have low porosity, are poorly fractured, and contain very little water, so their temperatures rise above 0°C rapidly, with minimum heat involved. The high thermal conductivity of these rocks facilitates rapid smoothing of the thermal state and maintains the steady-state regime.

Disequilibrium permafrost is characterized by the difference of heat flows at the lower phase boundary. Since the present epoch is warmer than the previous one, the heat flow in unfrozen ground is greater than in frozen ground, because the internal heat is partially absorbed at the phase boundary during the thawing of ice inclusions. As a result, the lower phase boundary of permafrost rises slowly, and the thickness decreases. In the Siberian Platform, disequilibrium permafrost is confined to the areas of exposed Upper Mesozoic (Jurassic and Cretaceous) and Cenozoic rocks. They occur in the pre-Yenisei zone, the Vilyuisk Basin,

Table 1. Geothermal parameters of permafrost in the Vilyuisk Basin and the Verkhoyansk Trough in Recent Epoch and 200,000 years BP.

Geothermal measurement site	Recent		Sartan		ΔT°C	ΔH, m	Rate of thaw, cm/yr
	H_o, m	T_o, °C	H_s, m	T_s °C			
Bakhynai	650	-5.0	720	-12.4	7.4	-70	-1.7
Balagachi	700	-5.0	760	-13.6	8.6	-60	-1.8
Lindenskaya	400	-2.1	520	-11.6	9.5	-120	-1.9
Srednevilyuisk	485	-1.8	568	-11.8	10.0	-83	-2.2
Vilyuisk	600	-3.0	730	-13.3	10.3	-130	-1.5
Ust-Vilyui	150	-2.8	360	-10.4	7.6	-210	-2.1
Badaran	500	-2.0	610	-11.5	9.5	-110	-1.7
Sobo Khaya	80	-1.7	350	-11.3	9.6	-270	-2.3
Khailakh	600	-5.0	785	-12.5	7.5	-185	-1.4
Namtsy	480	-3.2	580	-10.4	7.2	-100	-1.9
Yakutsk	350	-2.5	578	-10.8	8.3	-228	-1.7

and the Verkhoyansk and Yenisei-Khatanga Troughs. The disequilibrium permafrost is much less in areal extent than the equilibrium permafrost.

The pre-Yenisei zone and the Lena-Vilyui interstream area, located nearly 2000 km apart, have identical temperature fields. In both regions, the heat flow is greater in the unfrozen zone than in the frozen zone, suggesting the thawing of permafrost from below. The only difference is that the present thickness of the permafrost along the lower Yenisei River decreases from north to south under the influence of the maintained relict (Sartan) thickness. In the Vilyuisk Basin, the west–east decreasing trend developed in the Holocene under the influence of the geothermal heat flow increasing in the same direction. This is related to the increasing proximity to the tectonically active Verkhoyansk Range, where the heat flow is greater (60–80 mW/m^2) (Zheleznyak et al. 2007).

Based on the geothermal data and the physical properties of subpermafrost materials, changes in the lower permafrost boundary were estimated for the areas of disequilibrium permafrost. Calculations were made for the Vilyuisk Basin, using the data from key boreholes. The results are given in Table 1. From these values, the average regional rate of bottom thaw during the Holocene and the average difference in heat flow between the unfrozen and frozen zones was calculated, yielding $dH_M/d\tau$ = 1.9 cm/yr and $q_U - q_F$ = 34 mW/m^2. Thus, the permafrost bottom thawed, on average, 140 m during the Holocene in the region.

The geothermal data and information for the region were compiled and synthesized to produce a geothermal database of the Siberian Platform and to construct a series of geothermal sections up to 3000 m in depth and 500 to 2500 km in length.

Acknowledgments

This study was supported by RFBR grant no. 06-05-96126 and INTAS grant no. 06-1000025-9220.

References

Zheleznyak, M.N. 2005. *The Geothermal Field and Permafrost in the South-Eastern Siberian Platform*. Novosibirsk: Nauka, 227 pp.

Zheleznyak, M.N., Gavriliev, R.I., Rusakov, V.G., Shipitsyna, L.I. & Botulu, T.A. 2007. Geothermal field and cryolithozone of Tunguska syneclise and the north-eastern West Siberian Plate. *Proceedings of International Conference on Cryogenic Resources of Polar Regions, Salekhard, June 17–20, 2007*, 2: 143-146.

The Biocomplexity Manipulation Experiment: Effect of Water Table Drop on CH_4 and CO_2 Fluxes in the Alaskan Arctic at the Barrow Environmental Observatory

Donatella Zona
Global Change Research Group, San Diego State University, San Diego, CA
Walter C. Oechel
Global Change Research Group, San Diego State University, San Diego, CA

Introduction

The arctic tundra contains more than 191.8 Pg C as soil organic matter (Post et al. 1982). Increasingly, this carbon is, or is at risk of being, released to the atmosphere as CO_2 (Oechel et al. 1993, Oechel et al. 1994) and/or CH_4 (Vourlitis & Oechel 1993). However, predictions of future rates of release of CO_2 and CH_4 flux, following changes in temperature, moisture, and other variables associated with climate change, are uncertain. To predict with confidence future CO_2 and CH_4 releases to the atmosphere, it is necessary to understand the controls on net CO_2 and CH_4 fluxes. The patterns and controls on net ecosystem CO_2 and CH_4 fluxes are complex and non-linear. Warming and drying of the tundra can result in increased net CO_2 emissions from the Arctic to the atmosphere. However, areas that become warmer and remain wet, or become wetter, may be larger net emitters of CH_4 to the atmosphere.

Results and discussion

According to our study, water table does not have a consistent impact on methane and carbon dioxide flux, and in certain conditions, lower water table is related to higher methane efflux and does not affect carbon dioxide flux. This result is connected to the importance of other factors like thaw depth, soil temperature, and soil moisture more important than water table early in the season. Later in the season, water table depth becomes more important, and we observed higher methane effluxes from the site where the water table was higher. During this period, the CO_2 fluxes appear to be very similar at both sites. This unexpected result is contrary to most of the past studies that showed increased soil respiration and CO_2 release with decrease in water table and increased aeration status of the soil. A possible explanation could be connected to the characteristics of the vegetation in our study site. Even with a water table drop, below surface mosses are able to hold the water and maintain an anaerobic environment. In other words, the two sites with substantially different soil moisture and water table depth are both characterized by largely anaerobic soils. As a consequence, soil respiration is restricted to the shallower soil layers, and it is not influenced by the difference in thaw depth or water table between the two sites. In our study site, mosses are major components of the vegetation representing more than 80% of the biomass.

The differential response of the water table drop on CO_2 and CH_4 fluxes is probably due to the differential importance of shallower aerobic versus deeper anaerobic soil layers on the emission of the two gases. Methanogensis probably occurs in deeper soil layers, so a deeper thaw depth could significantly increase methane production (as we observed in the north site in late season), while shallower soil layers are the ones mainly responsible for the aerobic respiration.

Acknowledgments

We thank Robert Clement, University of Edinburgh for having written the code for the data reduction; Joe Verfaille and Hiroki Ikawa for field and technical assistance; Rob Rhew, Steven Hastings, and Rommel Zulueta for insight and advice; Douglas Deutschman for helpful advice on the statistics analysis; the Barrow Arctic Science Consortium (BASC) and Glenn Sheehan for logistic support. This work was funded by the Biocomplexity Program of the National Science Foundation (award number OPP 0421588).

References

Oechel, W.C., Cowles, S., Grulke, N., Hastings, S.J., Lawrence, B., Prudhomme, T., Riechers, G., Strain, B., Tissue, D. & Vourlitis, G.L. 1994. Transient nature of CO_2 fertilization in Arctic tundra. *Nature* 371: 500-503.

Oechel, W.C., Hastings, S.J., Vourlitis, G.L., Jenkins, M., Riechers, G. & Grulke, N. 1993. Recent Change of Arctic tundra ecosystems from a net carbon dioxide sink to a source. *Nature* 361: 520-523.

Post, W.M., Emanuel, W.R., Zinke, P.J. & Stangenberger, A.G. 1982. Soil carbon pools and world life zones. *Nature* 298: 156-159.

Vourlitis, G.L., Oechel, W.C., Hastings, S.J. & Jenkins, M.A. 1993. The effect of soil moisture and thaw depth on CH_4 flux from wet coastal tundra ecosystem on the north slope of Alaska. *Chemosphere* 26: 329-338.

The Oil Pollution Influence of Frozen Soils on Their Geophysical Characteristics

Yu.D. Zykov
The Moscow State University, Geological Faculty, Geocryology Department
A.V. Koshurnikov
The Moscow State University, Geological Faculty, Geocryology Department
I.V. Anisimova
The Moscow State University, Geological Faculty, Geocryology Department
T.E. Mironova
The Moscow State University, Geological Faculty, Geocryology Department

High rates of oil-extracting development and process industries in the cryolitozone have created a sharp geoenvironmental problem. It is pollution of natural-technical systems by oil and its products. The general losses of oil are estimated within the limits of 2–10% from annual extraction or from 5 to 25 million tons a year (Arens 1994, Masur 1995), in western Siberia approximately 0.7 and 0.4 million tons in the Timano-Pechora region (Permafrost … 2002).

In the Geocryology Department at Moscow State University, a special program on studying moving polluting organic substances (Ershov et al. 1996, Chuvilin et al. 2001) has been carried out. It is found that oil migrates in frozen soil and is present even at negative temperatures (up to -20°C and below). The research is confirmed recently in laboratory (Chuvilin et al. 2001) and field (Biggar et al. 1998).

Hydro carbonic pollution leads to change in the temperature-humid mode of soil thawing due to change in heat conductivity and thermal capacity—properties of frozen disperse soils as the bases of engineering constructions. It can also lead to development of negative geocryological processes and phenomena (Korolev 2001).

Thus, detection of and supervision over the dynamics of the pollution process became one of the serious ecological problems. Geophysical methods can be an important tool if the change in frozen soil properties laws is known. For these purposes laboratory research is executed at some set of values of a pollution degree (Z), from 0 to 10% (to weight of a mineral part) (Zykov et al. 2003).

Specific electric resistance (ρ) and polarizability (η) were measured by peak-phase method on "Spectrum" equipment (Open Company, Moscow State University–Geophysics) with the installation of four-electrodes. Speeds of longitudinal waves (Vp) were measured by ultrasonic equipment UD4-130 (Scientific Industrial Union "LUCH") on frequencies 60 and 100 kHz.

The executed measurements have shown that, in most cases, pollution causes a decrease in ρ (УЭС) [u.e.r.] and V_p. Thus, apparently from the resulting figures, in soils not salted, at negative temperatures, the influence of pollution is shown more strongly (Fig. 1). Except for what is well

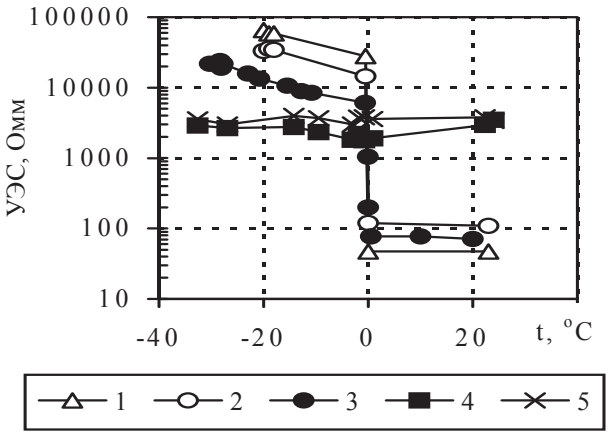

Figure 1. Temperature dependences УЭС [u.e.r.] (ρ) in oil and in not salted polluted sand; a degree of pollution (Z) and humidity (W). 1 – Z = 0, W = 20%; 2 – Z = 0, W = 10%; 3 – Z = 2.5%, W = 10%; 4 – Z = 10%, W = 0; 5 – oil.

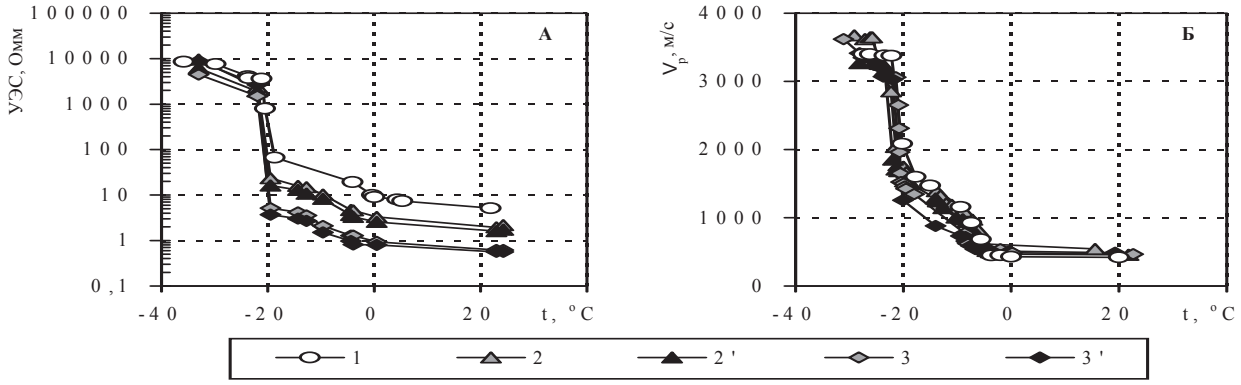

Figure 2. Temperature dependences. A: УЭС [u.e.r.], and B: V_p in the sand salted by solution NaCl of various concentration (C) with various degree of pollution (Z) at the fixed humidity (W = 10%). 1 – C = 0.0476; 2 – Z = 0; 2 – C = 0.0476; Z = 2.5%; 2 ′ – C = 0.0476; Z = 5%; 3 – C = 0.0909; Z = 2.5%; 3 ′ – C = 0.0909; Z = 5%.

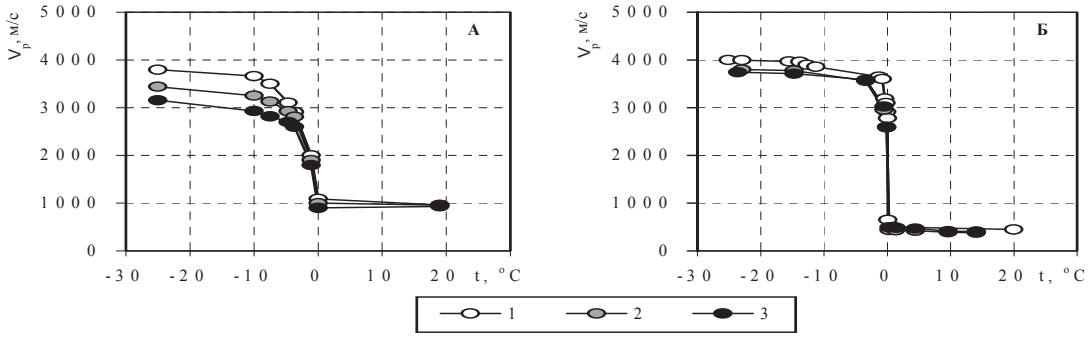

Figure.3. Influence of a degree of oil pollution (Z) for speed of longitudinal waves (V_p). A: in caolin (W = 40%) and sand (W = 20%). 1 – Z = 0; 2 – Z = 2.5%; 3 – Z = 10%.

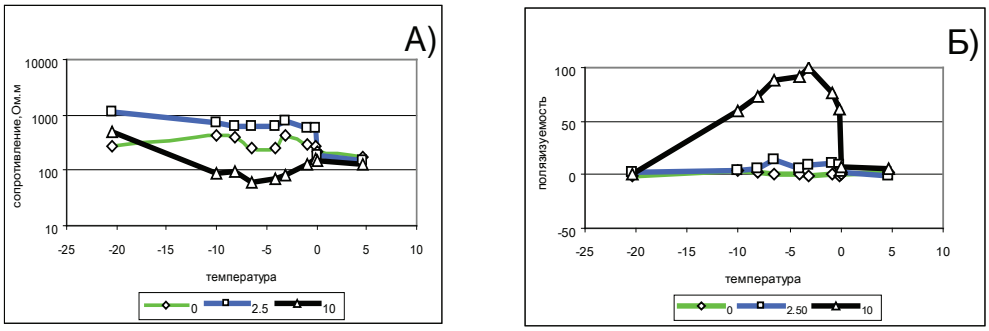

Figure 4. Temperature dependence (ρ) and polarizability (η) on frequency of 4.88 Hz on frequency of 4.88 Hz at various pollution Z (the first cycle).

visible, the initial stages of pollution (from 0 up to 2.5%) affect studied parameters more strongly, than its further increase (from 2.5 up to 10%) (Fig. 2).

Soil research from sand to clay has shown that the influence of pollution increases in the process of increase in dispersiveness (Fig. 3).

The increase in pollution can sometimes result not only in reduction of resistance, but also to its increase (Fig. 4A). In clay, it is connected with various modular conditions at various degrees of pollution. In the first cycle of freezing, data about abnormal high values (to 100%) of the polarizability factor are obtained (Fig. 4B). After thawing and repeated freezing of these polluted soils, an essentially smaller degree of polarizability (to 20%) has been noted. It testifies to the opportunities of using polarizability for studying the degree of pollution.

It is interesting to note the correlation between speed of elastic waves and heat conductivity.

References

Arens, V.Z. et al. 1999. *Clearing of an Environment of Hydrocarbonic Pollution*. Interbook, 371 pp.

Biggar, W., Haider, S., Nahir, M. & Jarrett, P.M. 1998. Site investigations of fuel spill migration into permafrost. *Journal of Cold-Regions Engineering* 12(2): 84-104.

Chuvilin, E.M., Mikljaeva, E.S., Kozlova, E.V. & Instanes, A. 2001. The experimental studying of oil pollution of frozen soils. *Materials of the Second Conference Russia Geocryologist*. I (I): *Physics-Chemistry and Mechanics of Frozen Soils, the Moscow State University,*163-169.

Ershov, E.D., Chuvilin, E., Smirnova, O.G. & Naletova, N.S. 1996. Experimental research of interaction of oil with cryogenic soils. *Materials of the First Conference Russia Geocryologist. Book 2, the Moscow State University,* 153-159.

Geoecological Inspection of the Enterprises Oil Industry. 1999. V.A. Shevnin & I.N. Modin (eds.), RUSSO, 511 pp.

Korolev, V.A. 2001. Clearing soils from pollution. *Interperiodika.* Nauka, 368 pp.

Masur, I.I. 1995. Ekology of objects of the oil and gas industry construction. *NEDRA,* 279 pp.

Permafrost and Development Oil-Gas Areas. 2002. E.S. Melnikov & S.E. Grechishchev (eds.), GEOS, 402 pp.

Zykov, Yu.D., Motenko, R.G., Anisimova, I.V. & Zhuravlyov I.I. 2005. Influence of oil pollution on properties frozen soils. *Earth Cryosphere* IX(3): 28-35.

Author Index